ANALYSIS OF PAPAIN-LIKE PROTEASE MEDIATED PROCESSING AND ROLES OF THE CLEAVAGE PRODUCTS IN CORONAVIRUS REPLICATION

By

Mark Jacob Gadlage

Dissertation

Submitted to the Faculty of the

Graduate School of Vanderbilt University

in partial fulfillment of the requirements

for the degree of

DOCTOR OF PHILOSOPHY

in

Microbiology and Immunology

May 2010

Nashville, Tennessee

Approved:

Christopher Aiken

Jim Chappell

Timothy Cover

Mark Denison

John Williams

To Kristyn,

You are my best friend.

ACKNOWLEDGEMENTS

One of the greatest writers in my opinion, who I will acknowledge below, once wrote, “The truth of the matter is that we are all inspired in some way. Be it by a friend, a book, a daily task; be it the urge to succeed, or the fear of failure; be it the world, the environment, your surroundings. Part of what gives the human race creativity and intellect, is the ability to be influenced.” My graduate school experience was surrounded by inspiring and influential people, who created a scholarly environment and amiable surroundings. It was these people who gave me the urge and willingness to succeed and the strength to never fail. It is with honor and due respect that I express my gratitude to all of the individuals who have made my graduate education a successful and rewarding experience.

First, I would like to send much appreciation and thanks to the Denison Laboratory. Special thanks goes to past members of the Denison Lab: Adam Sperduto, Sunny Lee, Rachel Graham, Jennifer Sparks, and Eric Ward. I am filled with many fond memories, and I truly appreciate your assistance, discussions, and your support throughout our time together. I especially thank you for allowing me to tell jokes and for you laughing at my jokes (if that is what you can call them), even if they weren’t really funny. I would also like to thank the rotating students, Dia Beachboard, Reagan Cox, and Josh Doyle, who helped me with projects in the lab.

Much of my research would not have been possible without the knowledge and assistance of Michelle Becker, Lance Eckerle, Chris Stobart, and Xiaotao Lu. You all are intelligent, hard-working individuals who shared your time and energy to help strengthen

and further my research projects and achieve my goals. You have helped me become the scientist and critical thinker I am today. I know great scientific discoveries are ahead for each and every one you. You all are more than just coworkers. You are spectacular friends.

This dissertation and my advancement and growth as a scientist would not have been possible without my mentor and friend, Mark Denison. Mark, you never discouraged me from performing any experiment, no matter the cost or the time it would take. You have pushed me to become the best scientist I can be, and your encouragement and enthusiasm are second to none. I am forever grateful for the opportunity you gave me when I joined your lab. Outside of the scientific realm, we shared common interests, such as bike riding and enjoy nature. It was relaxing and enjoyable to share previous adventures, as well as new ones that we were about to embark on. But most importantly, you were a great listener, whether it be a scientific or personal discussion. It was very helpful to know that someone else had been through the tough, enduring, and sometimes joyous times of a successful long distance relationship. And for that, I am very thankful.

I would also like to thank Dr. Terry Dermody and his lab. It didn't matter where Terry was going or how busy he was at any particular time. He always greeted me with a smile on his face, and some days I really needed it. Although Terry was not on my committee, he took great interest in my research and made sure I was on the ball. I would also like to thank the Dermody Lab for technical assistance and reagents that I needed throughout my graduate research. I also thank you for allowing me to tag along at ASV and other conferences.

An extended thanks goes to my dissertation committee. I express my gratitude to Chris Aiken, who has been extremely devoted to my growth as a scientist, as well as a person. The input that I have received through our multiple conversations will always be a great memory that I have of my graduate education. The knowledge that he has taught me through courses and committee meetings has been enormous.

I am grateful for the contributions from other committee members. Special thanks goes to Dr. Jim Chappell, who always gave excellent advice on methods and next steps on my research projects. The insight and knowledge of Dr. Timothy Cover aided in my capacity to critically think and analyze results and data. The optimism and enthusiasm expressed by Dr. John Williams increased my desire to learn, perform experiments, and excel as a scientist. Much appreciation and thanks goes to each one of my committee members.

Much gratitude goes to the faculty, staff, and students in the Department of Microbiology and Immunology. I am appreciative of the comments, questions, and suggestions that I have received throughout my multiple Research in Progress presentations. I extend my gratefulness to Dr. Jacek Hawiger for his devotion to graduate education and the Department of Microbiology and Immunology. I also extend thanks to Jean Tidwell, who always made sure I wasn't late on any student fees, signed me up for classes, and aided in the dissertation writing and defense process.

I would like to thank the Division of Pediatric Infectious Diseases. The assistance and support that I have received from the faculty and staff have aided in my development as a scientist.

Much appreciation goes to the Elizabeth B. Lamb Center for Pediatric Research. I would like to give thanks to the George and Patricia Lamb family for their generosity. Their support has influenced my research, both in the lab as well as through the Lamb Center and Pediatric Infectious Diseases Seminar Series.

I would also like to thank Elvin Woodruff and Magnify, Inc for all the help and assistance with my electron microscopy studies.

I gratefully acknowledge Dean Hoover for my support from the Mechanisms of Vascular Diseases Training Grant. I am truly grateful for the opportunity to be funded by this training grant because it helped broaden my knowledge and skills as a scientist. I also would like to thank the National Institute of Allergy and Infectious Diseases at the National Institutes of Health for their financial support.

I want to extend deep appreciation to my colleagues and friends that I met through the IGP experience and graduate school. I enjoyed the intramural sports, night outs, and scientific discussions that we shared. Much appreciation goes to Becca Zuvich for being a wonderful and caring friend. I know we will remain friends for life. Special thanks goes to my previous roommates, Randy Scherer and Blake Branson, for whom I have shared the graduate school experience with these past few years.

I would also like to extend thanks to friends that I have known for a long time. Much thanks goes to John Neukam, Clint Brosmer, Jayme Brosmer, Adam DeKemper, Joni DeKemper, Jarod Vonderheide, Adam Schroeder, Gary Seger, Jason Hulsman, Brad Schroering, Tom Mathias, and Shelley Stein. Thanks for coming and visiting me or housing me during my time in graduate school. Thank you for being my friends.

So much gratitude and love goes to my family. Whether you are still with me on earth or have passed before me, you have all been influential in my life and have shaped me into the person I am today. I will never forget the endless love and support I have received and will receive from each and every one of you.

I would like to extend thanks to my Grandma and Grandpa Gadlage and my Grandma and Grandpa Knies. I could not have asked for better grandparents. The first time that I believe I had ever been stimulated intellectually was learning how to play card games with my grandparents. I believe that this started the great intellectual journey that has not stopped to this day.

I would also like to thank my aunts, uncles, and cousins who have always been wonderful and loving. You all have had a great impact on my life.

Great appreciation goes to Clarence Eilertsen. Your energy and spirit are truly admirable and are such a blessing.

I would also like to extend gratitude to Karolyn Eilertsen. Your vibrant smile and laugh are so calming. Hanging out with you is always a joy because I feel as though I am a teenager again. I will always appreciate the facebook messages that you send me because they light up my day.

Many thanks and much appreciation goes to Justin Eilertsen. The many experiences we have shared through the past few years have been times that I will never forget. Our deep philosophical conversations, which were mainly fueled by your intellect, have taught me the art of critical analysis. Also, I am grateful for our fishing experiences. They take away all worries and make me realize how truly lucky I am.

I would also like to show my appreciation to Susan Eilertsen. Your love of life is just amazing. You never get caught up with the complexitites of life. Your outlook on life has influenced mine forever. Thank you for your support and views these past few years.

This dissertation would not have been possible without the help and support of Ken Eilertsen. I am thankful for the time you took out of your busy day to read and revise my manuscripts and show me how to be a better scientist. I am also thankful for you sharing some of your graduate school and industry experiences with me. The support you have given me the past few years have eased the stress of graduate school. Thank you for showing me how to relax in stressful situations.

I would also like to express my thanks and appreciation to my younger brother, Jason. Your laid-back and casual attitude taught me never to take little matters too seriously. You are always a breath of fresh air, and you can always ease my tensions and worries. It was always comforting to hear about your research experiences and troubles that you were having with some of your experiments, something a graduate student knows all to well.

I must give appreciation and great thanks to my older brother, Matt. It has been a great blessing to be going through the whole graduate school experience with you. We could talk to each other about our research, although it was hard to comprehend some of the things you were doing. I will always cherish the walks to and from campus with you. It didn't matter what we were talking about; it was just nice to have you there. I also want to thank you for helping me get through difficult times the past few years. It would not have been possible without you.

Where would I be without my mother? Mom, you always stressed the importance of education and that I was going to go to college. I did not have a choice. Little did you know I would go to graduate school to further my education. For as long as I can remember, you believed in me, and you supported me. I know that this will continue forever. You have been anything and everything that I needed you to be throughout my life. I am proud and honored to call you my mother. Words cannot express what your love and support have done for me. They have turned me into the person I am today. Thank you for everything.

The fundamental reason that I have pursued an education in science and a love for science is due to my father. Dad, your love of nature and the outdoors was my first exposure to the scientific world. It is because of you that I have chosen this path in science. Along with your love of nature, you have always fought for what is right. You and mom have worked extremely hard to give your sons the best life possible. You have taught me the meaning of hard work and dedication. You have a sense of humor that can make anyone laugh. I am forever grateful for the qualities that you have taught me and all the support that you have given me throughout my life.

Finally, I am forever indebted to my better half, Kristyn Eilertsen. Kristyn, one day while I was writing my dissertation, I came upon an essay written by you while you were in college, and I used part of what you had written to start my acknowledgements. You truly are an excellent writer. But more importantly, you are my inspiration, and you are the greatest influence on my life. Words or actions cannot do justice for what you have done for me. Even through the most difficult times of our relationship, you never put yourself first. You always do what is right, never taking the short route or the easy

road for the sake of convenience. You always stood beside me. You always supported me. You were always there for me. I know, without a doubt, that you will always stand beside me, support me, and be there for me. You have taught me to never settle and to be all that I am capable of being. I am absolutely blessed and so fortunate to be loved by you. Your love has carried me through this part of my life, and it will carry me to the end. Together, we will accomplish many great things. We will be extraordinary.

TABLE OF CONTENTS

Page

LIST OF TABLES

LIST OF FIGURES

LIST OF ABBREVIATIONS

3CLpro, 3 chymotrypsin-like protease

BHK, baby hamster kidney

BSA, bovine serum albumen

CM, convoluted membrane

CPE, cytopathic effect

CS, cleavage site

DBT, delayed brain tumor

DMEM, Dulbecco's modified Eagle medium

DMV, double membrane vesicle

Endo H, endoglycosidase H

ERGIC, endoplasmic reticulum Golgi-intermediate complex

HCoV, human coronavirus

h p.i., hours post-infection

IBV, infectious bronchitis virus

kDa, kilodaltons

MHV, murine hepatitis virus

MOI, multiplicity of infection

nsp, nonstructural protein

ORF, open reading frame

P, position or passage

PBS, phosphate buffered saline

PFU, plaque forming units

PLP, papain-like protease

pp, polyprotein

RdRp, RNA-dependent RNA polymerase

SARS-CoV, severe acute respiratory syndrome coronavirus

sg, subgenomic

TCA, trichloroacetic acid

TEM, transmission electron microscopy

TM, transmembrane

TRS, transcriptional regulatory sequence

UTR, untranslated region

wt, wild-type

CHAPTER I

BACKGROUND AND LITERATURE REVIEW

Introduction

Coronaviruses are a family of enveloped, positive-strand RNA viruses, which are important pathogens of both humans and animals. Coronaviruses are widely dispersed among mammals and birds and can cause a multitude of enteric, gastrointestinal, neurological, and respiratory illnesses. In humans, however, disease is usually limited to the upper respiratory tract, and approximately 5 to 20% of yearly common colds are caused by coronaviruses (Engel, 1995; Makela et al., 1998). Because coronaviruses were previously not associated with severe human disease, these viruses were scientifically and agriculturally important, but not considered medically important pathogens of humans. However, enthusiasm in the coronavirus field intensified in the past few years due to the identification of a newly emerged coronavirus as the causative agent of severe acute respiratory syndrome (SARS).

In late 2002, multiple cases of severe atypical pneumonia were reported in southern China. As additional cases of severe, often fatal respiratory disease began to spread throughout the world in early 2003, worldwide health organizations began a collaborative effort to identify the unknown pathogen. The cooperation of the international organizations led to the identification of a newly emerged coronavirus as the causative agent of SARS within a matter of weeks after its emergence. The newly discovered coronavirus was named after the disease it caused, severe acute respiratory

syndrome coronavirus, or SARS-CoV. Between November 2002 and July 2003, over 8400 individuals in 32 countries were diagnosed with SARS. Over 900 infected individuals succumbed to the disease before the pandemic was controlled in late 2003 (Ksiazek et al., 2003; Kuiken et al., 2003a; Kuiken et al., 2003b; Marra et al., 2003).

The identification of a novel coronavirus as the etiological agent of SARS in 2003 resulted in a new awareness of the potential for severe disease in humans, as well as demonstrating their potential for transspecies movement and pathogenicity. Following the SARS epidemic, increased surveillance led to the discovery of previously unidentified coronaviruses in numerous animals, as well as in archival tissue samples. The SARS epidemic also resulted in increased focus on research aimed at elucidating the mechanisms by which coronaviruses move between species, replicate, and cause disease. The research presented in this dissertation uses the coronavirus murine hepatitis virus (MHV) as a model to gain a more complete understanding of specific events that take place in the coronavirus life cycle.

Proteins encoded within the replicase gene are proposed to mediate coronavirus replication in host cells. The replicase gene is translated as a polyprotein that is co- and post-translationally processed into intermediate and mature replicase nonstructural proteins (nsps) by virus-encoded proteases (Anand et al., 2003; Baker et al., 1993; Bost et al., 2000; Denison et al., 1998; Denison et al., 1992; Dong and Baker, 1994; Kanjanahaluethai and Baker, 2000; Kim et al., 1995; Lu, Sims, and Denison, 1998a; Lu, Lu, and Denison, 1995; Schiller, Kanjanahaluethai, and Baker, 1998; Thiel et al., 2003; Weiss et al., 1994). These proteins localize to virus-induced double membrane vesicles in the cytoplasm of infected cells, which also are sites of viral RNA synthesis (Gosert et

al., 2002; Prentice et al., 2004). While functions of some replicase intermediate and mature proteins have been identified in infected cells, the functions of others remained to be determined. However, the establisment of reverse genetics systems for multiple coronaviruses likely will lead to the discovery of several new functions of these proteins.

When this research began, it was known that protease inhibitors that block overall polyprotein processing abort new viral RNA synthesis when added at any time during MHV infection, demonstrating the overall requirement for ongoing processing of replicase polyproteins in virus replication (Kim et al., 1995). It was also known that the coronavirus-encoded proteases processed the replicase polyprotein at specific amino acid sequences, and that the patterns of processing at cleavage sites by specific proteases differed among many coronaviruses (Ziebuhr, Snijder, and Gorbalenya, 2000). Moreover, protease and cleavage site interactions are key genetic determinants of protein functions and important in the regulation of the life cycles of coronaviruses. However, little was known about the evolution of protease/cleavage site relationships and determinants of conserved and unique protease functions in the coronavirus life cycle. Further, with the exception of the viral proteases and the C-terminal replicase proteins, little was also known about the functions of nsp1, nsp2, nsp3, and nsp4 (Baker et al., 1989; Baker et al., 1993; Kanjanahaluethai and Baker, 2000; Lee et al., 1991; Lu, Lu, and Denison, 1995). Thus, at the time this research began, several gaps in knowledge existed about the functions and requirements of protease/cleavage site recognition and processing and the roles that the N-terminal replicase proteins play during coronavirus replication.

Coronavirus identification and classification

The members of the family *Coronaviridae* are spherical, enveloped viruses whose surfaces are studded with many trimers of the viral Spike glycoprotein, which can be visualized as a halo or crown surrounding the particle when viewed by negative-stain electron microscopy (Fig 1.1), hence giving the family its "corona" name. Since the identification of avian infectious bronchitis virus (IBV) in chickens in 1937, more than 40 other coronaviruses have been isolated from various birds and mammals, including turkeys, ducks, pigs, dogs, cats, cows, mice, giraffes, bats, deer, whales, and humans.

The coronavirus virion contains a large, single-stranded, positive-sense RNA genome. Through negative-stain electron microscopy and biochemical analysis, the nucleocapsid symmetry of coronaviruses was determined to be helical in nature (Masters, 2006). This was quite surprising given the fact that helical symmetry is commonly observed for negative-sense RNA viruses, while almost all positive-sense RNA animal viruses possess icosahedral nucleocapsids. However, evidence has also supported icosahedral symmetry for the coronavirus transmissible gastroenteritis virus (TGEV) (Risco et al., 1996).

Coronaviruses belong to the order *Nidovirales* and are currently classified as one of two genera, the other being the toroviruses, in the *Coronaviridae* family. It is likely, however, that both the coronaviruses and toroviruses will be separated and classified as distinct families in the future (Gonzalez et al., 2003). The order *Nidovirales* also includes two other families, the *Arteriviridae* and the *Roniviridae*. Together, the nidoviruses exhibit a high level of organization that sets them apart from other nonsegmented positive-sense RNA viruses. Features of the *Nidovirales* include: expression of the

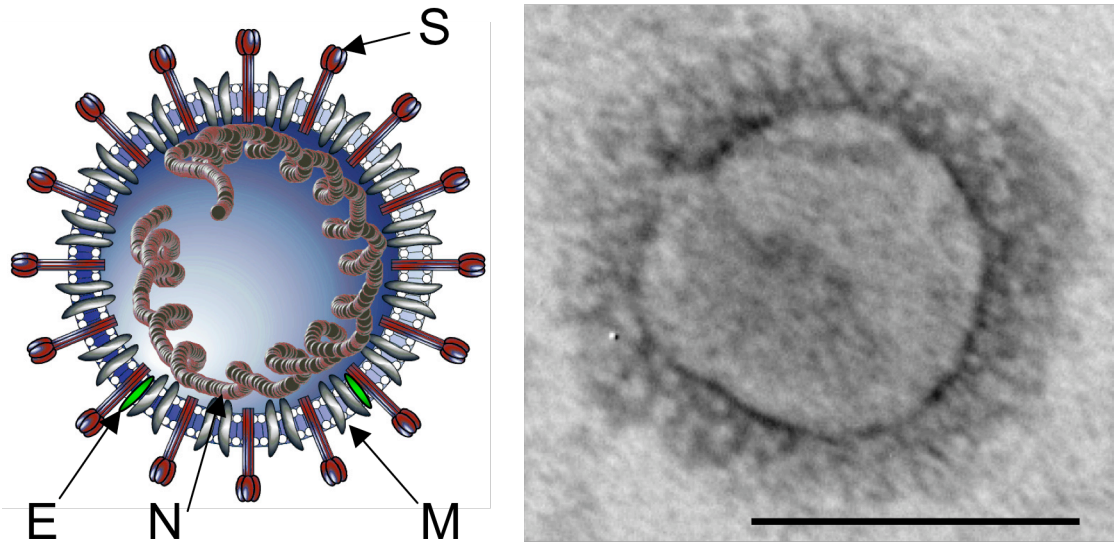

Fig. 1.1. Coronavirus virion structure. Left) Schematic of coronavirus virion. The structural proteins of the virion are indicated by arrows and abbreviations (S, E, M, and N). The spike attachment protein (S) mediates attachment to the receptor on the surface of a permissive cell. M protein (M) is threaded through the lipid bilayer envelope, which is derived from the host cell. M protein mediates curvature of the virion envelope during budding. Nucleocapsid (N) coats the viral RNA and maintains the helical conformation of genome RNA. The envelope protein (E) is present in low copy number in virion membrane, and together with M, is involved in membrane curvature and pinching off of the budding virion. Right) A negative-stain electron micrograph of an MHV virion. The horizontal black bar represents 100 nm. Images from J. Sparks.

entire replicase polyprotein via ribosomal frameshifting; unique enzymatic activities not seen in other positive-strand RNA viruses; and gene expression through the transcription and translation of a set of 3'-coterminal "nested" subgenomic RNAs. This latter feature is the basis for the name of the order, with "nido" being the Latin word for nest.

At the initiation of this research, the coronaviruses were classified into four groups, group 1, 2a, 2b, and 3, originally based on antigenic relationships through utilization of neutralizing antibody assays. However, the discovery of new coronaviruses, extensive genome sequencing, and bioinformatics databases has aided in the current classification of coronaviruses (Gorbalenya, Snijder, and Spaan, 2004). Also, these scientific advances have led to the proposal for a reclassification of coronaviruses. However, a new classification system has yet to be widely accepted and received from the coronavirus field.

For both group 1 and group 2 coronaviruses, the hosts are almost exclusively mammalian, with human coronaviruses present in each of these groups. Group 1 coronaviruses include human coronaviruses, such as HCoV-229E and HCoV-NL63, as well as feline coronaviruses (FCoV and FIPV) and porcine coronaviruses (TGEV and PRCoV). The group 2 viruses have been subdivided into two groups, groups 2a and 2b. Group 2a coronaviruses include the human coronavirus OC43 (HCoV-OC43), HCoV-HKU1, murine hepatitis virus (MHV), and bovine coronavirus (BCoV). Group 2b coronaviruses consist of viruses with a predicted earlier evolutionary offshoot of group 2a, and these viruses include SARS-CoV and newly identified coronaviruses of bats (bat-SARS-CoV) that resemble SARS-CoV. Group 3 coronaviruses are currently known to

only have avian hosts. This group includes viruses that infect chickens (IBV), turkeys (TCoV), pigeons (PCoV), and waterfowl, specifically geese (GCoV) and ducks (DCoV).

Coronavirus disease

Coronaviruses are pathogens of both humans and animals and have both medical and agricultural importance. Diseases caused by coronaviruses include, but are not limited to, gastrointestinal, respiratory, and neurological diseases. Coronavirus infections can be either acute or persistent, and infections can be systemic or restricted to specific organ systems. Though the specific determinants of coronavirus pathogenesis remain undefined, it is thought that both viral replication and host immune responses contribute to the overall severity of disease (Compton, Barthold, and Smith, 1993; Perlman and Netland, 2009).

Coronavirus infections of humans usually result in mild upper respiratory illness with cold-like symptoms (HCoV-229E and HCoV-OC43) that is resolved with little to no treatment necessary (Engel, 1995; Makela et al., 1998). However, patients who were infected with SARS-CoV exhibited lower respiratory tract infection with atypical pneumonia, alveolar damage, pulmonary lesions, and appearance of mononuclear infiltrates, with many individuals succumbing to what was described as acute respiratory distress syndrome (ARDS) (Lai, 2003). The identification of a novel coronavirus associated with severe respiratory disease prompted investigators to explore the possibility that other respiratory tract infections may be caused by coronaviruses. Inspections of archived nasopharyngeal aspirates led to the identification of new human coronaviruses, including HCoV-HKU1, which is associated with pneumonia, and HCoV-

NL63, which causes bronchiolitis (Arden et al., 2005; Ebihara et al., 2005; Woo et al., 2005).

The prototypical model for studies of coronavirus replication and pathogenesis is MHV, which can cause acute and persistent infections in mice. The type of infection and severity of disease is dependent upon the viral strain (e.g. MHV-A59, MHV-2, MHV-JHM, or MHV-S), the age of the animal, and the route of inoculation (Chen and Subbarao, 2007; Compton, Barthold, and Smith, 1993). The two most well documented strains are MHV-A59 and MHV-JHM, which cause severe hepatitis and fatal demyelinating encephalitis, respectively, in naturally infected mice. The Denison laboratory uses MHV-A59 (hereafter referred to as MHV) as a model to investigate mechanisms of coronavirus replication.

Emergence and identification of new coronaviruses

While the host range of the coronavirus family is broad, most coronaviruses naturally infect only one animal species, or at most, a limited number of closely related species. An exception appears to be SARS-CoV, which is suspected to have been transmitted from animal reservoirs to humans. Based on post-pandemic surveillance of coronaviruses from animal populations, it is likely that SARS-CoV transitioned into the human population from endemically infected animals that showed no symptoms of disease. SARS-like coronaviruses have been isolated from animals in China, including Himalayan palm civets, raccoon dogs, and most recently, Chinese horseshoe bats (Lau et al., 2005; Normile, 2005; Vijayanand, Wilkins, and Woodhead, 2004; Wang et al., 2005). Interestingly, the virus that infects these animals is genetically distinct from the variants

isolated in humans. This is somewhat expected due to altered species specificity, but sequence analysis revealed that there is considerable genetic variation between the viruses isolated over the course of the SARS pandemic, especially within the 5' third of the replicase (Chinese, 2004). These findings suggest that there is extraordinary flexibility within the coronavirus genome. Since the emergence of SARS-CoV, new and uncharacterized coronaviruses have also been identified from new hosts (Decaro et al., 2008; Hasoksuz et al., 2007; Mihindukulasuriya et al., 2008), demonstrating that coronaviruses also have the capacity to rapidly adapt to and evolve in new host species.

Coronavirus life cycle

The life cycle of coronaviruses occurs in the cytoplasm of host cells (Fig. 1.2). Attachment of the virion to the host cell surface via a cellular receptor is the first step in the life cycle of coronaviruses. Attachment occurs by interactions between the spike (S) glycoprotein and a cell surface receptor. The cellular receptor for MHV is carcinoembryonic antigen cell adhesion molecule-1a (CEACAM-1a) (Dveksler et al., 1991; Williams, Jiang, and Holmes, 1991), and the cellular receptor for SARS-CoV is human angiotensin converting enzyme-2 (hACE-2) (Li et al., 2003). Following attachment, the viral genome then enters the cell by either direct fusion of the viral lipid envelope with the plasma membrane or by fusion of the viral lipid envelope with an endosomal compartment following receptor-mediated endocytosis (Gallagher and Buchmeier, 2001; Kooi, Cervin, and Anderson, 1991).

After entry into a host cell, the first open reading frame (ORF1) of the RNA genome is translated by cellular ribosomes. ORF1 constitutes approximately two-

thirds of the genome and encodes nonstructural proteins (nsps) 1-16, which are necessary for viral RNA synthesis (Fig. 1.3). The replicase gene encodes ORF1, which is comprised of two open reading frames (ORF1a and ORF1ab) that are connected by a -1 ribosomal frameshift (Bonilla, Gorbalenya, and Weiss, 1994; Breedenbeek et al., 1990; Brierley, 1989; Lee et al., 1991; Pachuk et al., 1989). Translation of ORF1a or ORF1ab results in polyproteins, either pp1a (~495-kDa) or pp1ab (~803-kDa) that are co- and post-translationally processed by either two or three virus-encoded proteases, including either one or two papain-like protease (PLP) domains within nsp3 and the 3C-like cysteine protease, otherwise referred to as 3CLpro or nsp5, to yield intermediate and mature forms of nsps 1-16. All tested nsps to date associate with replication complexes, which are responsible for viral RNA synthesis (Bost et al., 2000; Gosert et al., 2002).

Viral RNA synthesis, discussed later in this chapter, involves both genome replication and subgenomic mRNA transcription. Genome RNA is replicated via a minus-strand intermediate template. Subgenomic mRNAs are generated from genome RNA to allow for translation of structural and other accessory proteins from the ORFs downstream of ORF1 (Sawicki, Sawicki, and Siddell, 2007).

Coronavirus virions contain four structural proteins, S (spike), E (envelope), M (membrane protein), and N (nucleocapsid). S, E, M, and N are translated from subgenomic RNAs 3, 5, 6, and 7, respectively, for MHV. Virion assembly is mediated by E and M proteins interacting with membranes of the ERGIC, resulting in partial curvature of the membrane (Raamsman et al., 2000). E and M proteins are essential for the production of infectious virions, and expression of E and M in the absence of virus

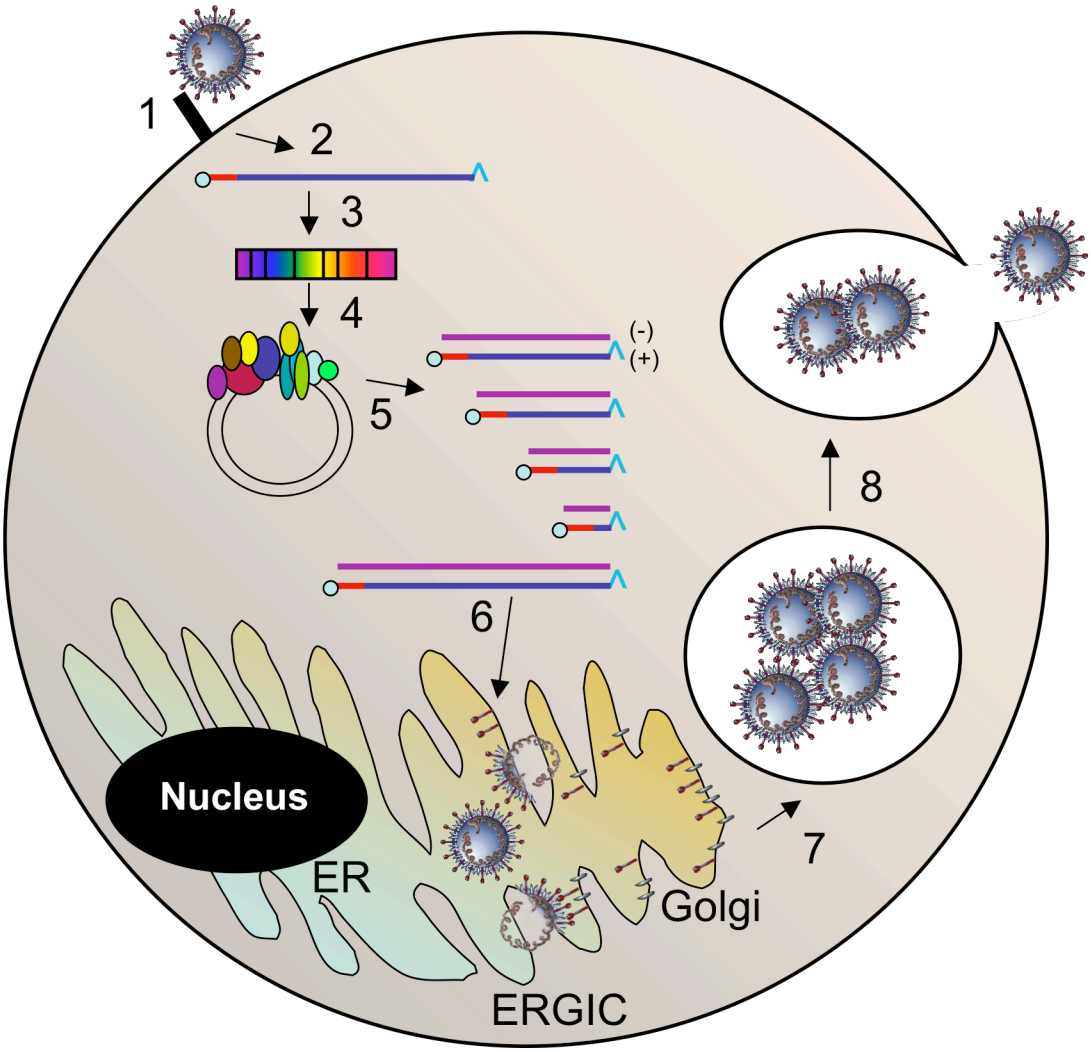

Fig. 1.2. Coronavirus life cycle. Step 1: Coronaviruses attach to receptors on the surface of cells (CEACAM-1a for MHV), which mediates fusion and entry. Step 2: Open reading frame 1 of the positive-sense genome RNA is translated into replicase polyproteins. Step 3: The replicase polyproteins are autoproteolytically processed into intermediate and mature replicase proteins. Step 4: These proteins associate with virus-induced double membrane vesicles in the cell cytoplasm to form replication complexes. Step 5: These replication complexes mediate the synthesis of viral RNA, including genomic and subgenomic (minus-strand (purple) and plus-strand (blue)) species. Step 6: Genome RNA is delivered to sites of assembly in the ER-Golgi Intermediate Compartment (ERGIC), where it is packaged into virions. Step 7: Virions are shuttled to the cell surface in vesicles that (Step 8) fuse with the cell surface, releasing the virus progeny in a process that does not require cell lysis. Schematic provided by R. Graham.

infection has been shown to produce empty virus-like particles (Curtis, Yount, and Baric, 2002; Kuo and Masters, 2002; Ortego et al., 2002; Vennema et al., 1996). Direct molecular interactions between M-S, M-N, N-RNA, and M-RNA result in the packaging of these components into budding virions (Narayanan et al., 2000; Opstelten, Horzinek, and Rottier, 1993; Opstelten et al., 1995; Vennema et al., 1991). The E protein then aids in pinching off of the virion from membranes of the ERGIC ((Fischer et al., 1998). Then, coronavirus virions are shuttled to the plasma membrane in large exocytic vesicles, and virions are released from the cell in a process that does not require cell lysis. The length of time to complete the life cycle varies depending on coronavirus. For MHV, the life cycle lasts approximately 10 to 16 hours.

Translation and processing of the coronavirus replicase

Upon entry into the host cell, the positive-strand RNA genome of coronaviruses functions as an mRNA, from which ORF1 is translated by host cell ribosomes. ORF1 is translated as a polyprotein, either massing approximately 500-kDa (polyprotein 1a [pp1a]) or, due to a -1 ribosomal frameshift, 800-kDa (pp1ab) (Bonilla, Gorbalenya, and Weiss, 1994; Breedenbeek et al., 1990; Brierley, 1989; Lee et al., 1991; Pachuk et al., 1989). Pp1a and pp1ab are co- and post-translationally processed by virus-encoded proteases into intermediate and mature proteins (Fig 1.3). The number of proteases varies depending on the particular coronavirus. All coronaviruses encode 3CLpro within nsp5 (Lu, Lu, and Denison, 1996), which is responsible for mediating processing from the C-terminus of nsp4 through nsp16 (Bost et al., 2000; Denison et al., 1998; Denison et al., 1999; Lu, Sims, and Denison, 1998a).

For processing of nsps 1 through the N-terminus of nsp4, coronaviruses encode either one or two papain-like proteases (PLPs) within nsp3 (Bonilla et al., 1995; Bonilla, Hughes, and Weiss, 1997; Dong and Baker, 1994; Kanjanahaluethai and Baker, 2001; Teng, Pinon, and Weiss, 1999; Ziebuhr, Snijder, and Gorbalenya, 2000). Group 1 and group 2a coronaviruses, such as HCoV-229E and MHV, respectively, each encode two PLPs, PLP1 and PLP2, to process the first three cleavage sites (CSs), or nsp1 through the N-terminus of nsp4. Group 2b and 3 coronaviruses encode only one enzymatically active PLP in the position of PLP2 that is similar to group 1 and 2a coronaviruses. IBV also possesses an inactive PLP remnant in the position of PLP1, while SARS-CoV has little to no sequence homology to a PLP domain located in or near the PLP1 position within nsp3 (Fig. 1.4) (Snijder et al., 2003). The basis for part of this dissertation is the observation that different coronaviruses appear to have evolved related, but distinct, strategies for processing of the N-terminal CSs with PLPs. The importance of the use of one or two PLPs in virus evolution, replication, and pathogenesis is currently unknown.

Prior to research presented in this dissertation, studies have utilized protease inhibitors to abolish polyprotein processing of the replicase, and results revealed that virus-mediated protein processing was essential for ongoing viral RNA synthesis and virus replication (Kim et al., 1995). Studies have also identified the CS amino acid sequences and residues that are critical in the recognition and processing of the polyproteins by coronavirus proteases (see review by (Ziebuhr, Snijder, and Gorbalenya, 2000). These studies have led to the identification of preferred residues in certain positions of the CS amino acid sequences, and it appears that different residues in these

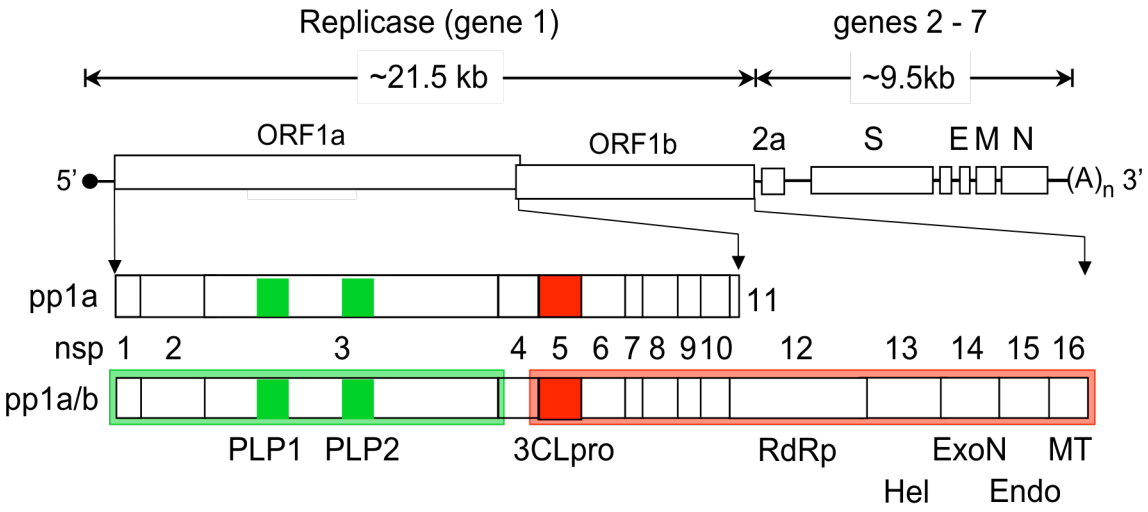

Fig. 1.3. Murine hepatitis virus genome organization and ORF1 translation and processing. Coronavirus genomes are between 27 kb and 32 kb in length. The 31.5 kb genome of MHV contains 7 genes. ORF1 encodes the replicase polyprotein, and downstream ORFs encode structural and accessory proteins. ORF1 has two open reading frames, ORF1a, which encodes an ~495 kDa polyprotein and ORF1ab, which, when translated, encodes an ~800 kDa polyprotein. The polyprotein is then co- and post-translationally processed into intermediate and mature proteins. Mature proteins are distinguished by vertical lines and indicated by nonstructural protein (nsp) number. The vertical lines also indicate cleavage sites. Viral papain-like proteases are indicated by green boxes and by number (PLP1 or PLP2). The viral 3C-like protease (3CLpro) is indicated by a red box (nsp5). Cleavage sites are assigned to a protease group by the linked colored background. Proteases and other key proteins are indicated below the schematic. RdRp, RNA-dependent RNA polymerase; Hel, helicase; ExoN, exoribonuclease; Endo, endoribonuclease; MT, methyltransferase.

positions may control the timing and/or regulation of the production of intermediate and mature proteins during protein processing.

Coronavirus nsps 1 through 4

The 5' third of the coronavirus ORF1, encoding nsps 1, 2, 3, and 4, has considerable variability across coronavirus groups, such as the presence or absence of nsp1, low amino acid sequence similarity and sizes of nsp1 and nsp2, the presence of one or two PLPs within nsp3, and differences in the number of predicted transmembrane domains within nsp4. Most of the variations within nsps 1 through 4 are observed between divergent coronavirus groups, and it has been proposed that the proteins in this region have evolved to adapt to their specific hosts (de Vries et al., 1997). Even though there is considerable diversity within this region of the polyprotein, several proteins or domains have been shown to have similar activities during viral infection.

Nsp1 varies in size between coronavirus groups 1, 2a, and 2b, and group 3 coronaviruses, such as IBV, do not encode nsp1. Upon translation of ORF1 for MHV, nsp1 is co-translationally processed and only detected as a mature protein. For MHV and SARS-CoV, nsp1 has been shown to inhibit host gene expression and is a major pathogenicity factor involved in the suppression of innate immune functions (Kamitani et al., 2006; Narayanan et al., 2008; Zust et al., 2007).

Like nsp1, coronavirus nsp2 varies in size between coronavirus groups, ranging from 65-kDa (MHV) to 87-kDa (HCoV-229E and IBV). It has no known function and aligns poorly to proteins with defined function(s). MHV nsp2 is detected as a mature protein, as well as an nsp2-3 intermediate, and localizes to replication complexes

throughout the course of infection (Bost, Prentice, and Denison, 2001). Nsp2 is not required for virus replication of MHV and SARS-CoV and can be deleted from the replicase polyprotein (Graham et al., 2005).

Nsp3 shares several conserved domains among coronaviruses, including an Ac domain highly enriched in acidic residues and a C-terminal Y domain that possesses putative transmembrane domains (Kanjanahaluethai et al., 2007). Nsp3 also shares an X domain that has sequence homology to the adenosine diphosphate ribose-1" phosphatase. This domain has been shown to be important in producing liver disease and pathology in MHV (Eriksson et al., 2008). Nsp3 also possesses either one or two papain-like protease (PLP) domains, whose activities, substrate specificities, and requirements have been demonstrated *in vitro* (Bonilla et al., 1995; Bonilla, Hughes, and Weiss, 1997; Dong and Baker, 1994; Hughes, Bonilla, and Weiss, 1995; Kanjanahaluethai and Baker, 2000; Teng, Pinon, and Weiss, 1999). These proteases also have a zinc ribbon domain located within each of the protease domains. Because of these unique features of nsp3, it clearly plays a role in both translation and processing of the replicase polyprotein. This protein may also play other roles in the virus life cycle, such as induction and stability of virus-induced membrane rearrangements (Y domain) and transcription (Ac domain and X domain).

Like nsp2, little is known about the function of nsp4. Nsp4 is unique among coronavirus nsps in that it is processed at its N-terminus by a PLP and at its C-terminus by 3CLpro (Gosert et al., 2002; Harcourt et al., 2004; Kanjanahaluethai and Baker, 2000; Kanjanahaluethai and Baker, 2001; Kanjanahaluethai, Jukneliene, and Baker, 2003). For MHV, nsp4 is either detected in its mature form or as an nsp4-10 intermediate protein.

A

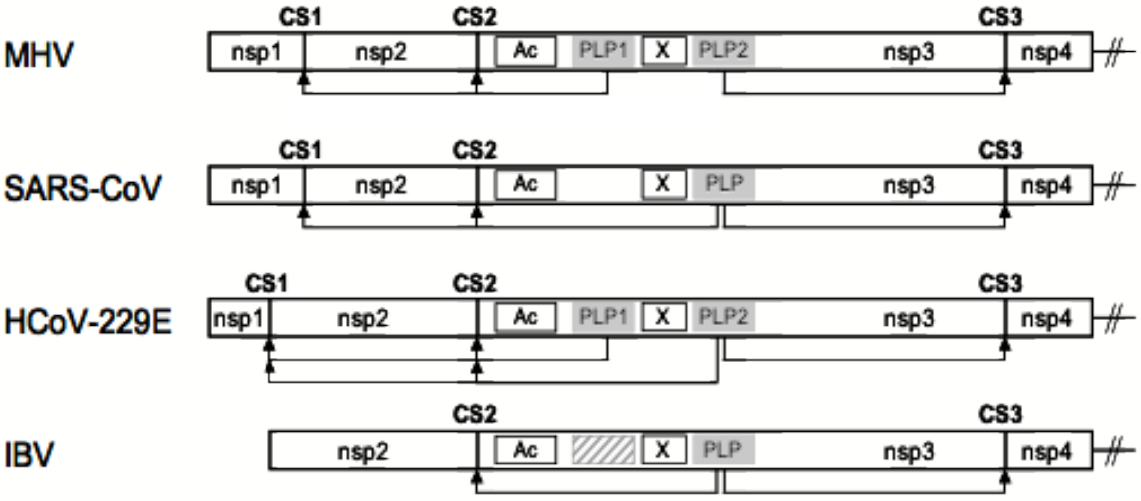

B

Virus	nsp1	nsp2	nsp3	nsp4
MHV	28	65	210	56
SARS-CoV	20	70	213	56
HCoV-229E	9	87	195	54
IBV	n/a	87	195	59

Fig 1.4. Comparison of coronavirus nsp1-nsp4 proteins. A) Nsp1 through nsp4 of representative coronaviruses (MHV: group 2a; SARS-CoV: group 2b; HCoV-229E: group 1; IBV: group 3) are shown, with proteins indicated by nsp number. Papain-like proteases are indicated by gray boxes and number. A hatched gray box represents an inactive remnant of the IBV PLP1 domain. Other domains within nsp3 are indicated by white boxes. Cleavage events mediated by papain-like proteases are illustrated by arrows. **B)** Known or predicted molecular weights of nsp1, 2, 3, and 4 are shown, with mass in kDa. Adapted from R. Graham.

Due to the hydrophobic nature of nsp4, it was predicted to play roles in the formation, organization, and stability of virus-induced membrane rearrangements that are essential for viral RNA synthesis and virus replication.

Papain-like protease structure, specificity, and activities

The three-dimensional structure of the SARS-CoV PLP, PLpro, has been determined by X-ray crystallography (Ratia et al., 2006). The solved structure verified many of the features that were proposed for the HCoV-229E PLP2 catalytic core, confirming the papain and hTFIIS-based homology models (Herold, Siddell, and Gorbalenya, 1999). The structure of SARS-CoV PLpro revealed a fingers-palm-thumb architecture and a catalytic triad consisting of Cys-His-Asp residues (Fig. 1.5). The structure consists of a zinc ribbon domain (fingers), a papain-like fold composed of β-sheets (palm), and an α-helix domain (thumb) which contains the catalytic triad. The structure also resolved an N-terminal addition to the papain-like fold that was structurally similar to the ubiquitin-like (Ubl) domains of both the herpes-associated ubiquitin-specific protease (HAUSP) and ubiquitin-specific protease 14 (USP14) (Ratia et al., 2006; Sulea et al., 2006). Interestingly, the substrate specificity of SARS-CoV PLpro (P4-LXGG-P1), which is shared by many coronavirus PLP2 enzymes, is also common to many deubiquitinating enzymes (Barretto et al., 2005). As predicted, both SARS-CoV PLpro and MHV PLP2 have been shown to possess deubiquitinating activity (Barretto et al., 2005; Lindner et al., 2005; Zheng et al., 2008). Thus, it is possible that coronavirus

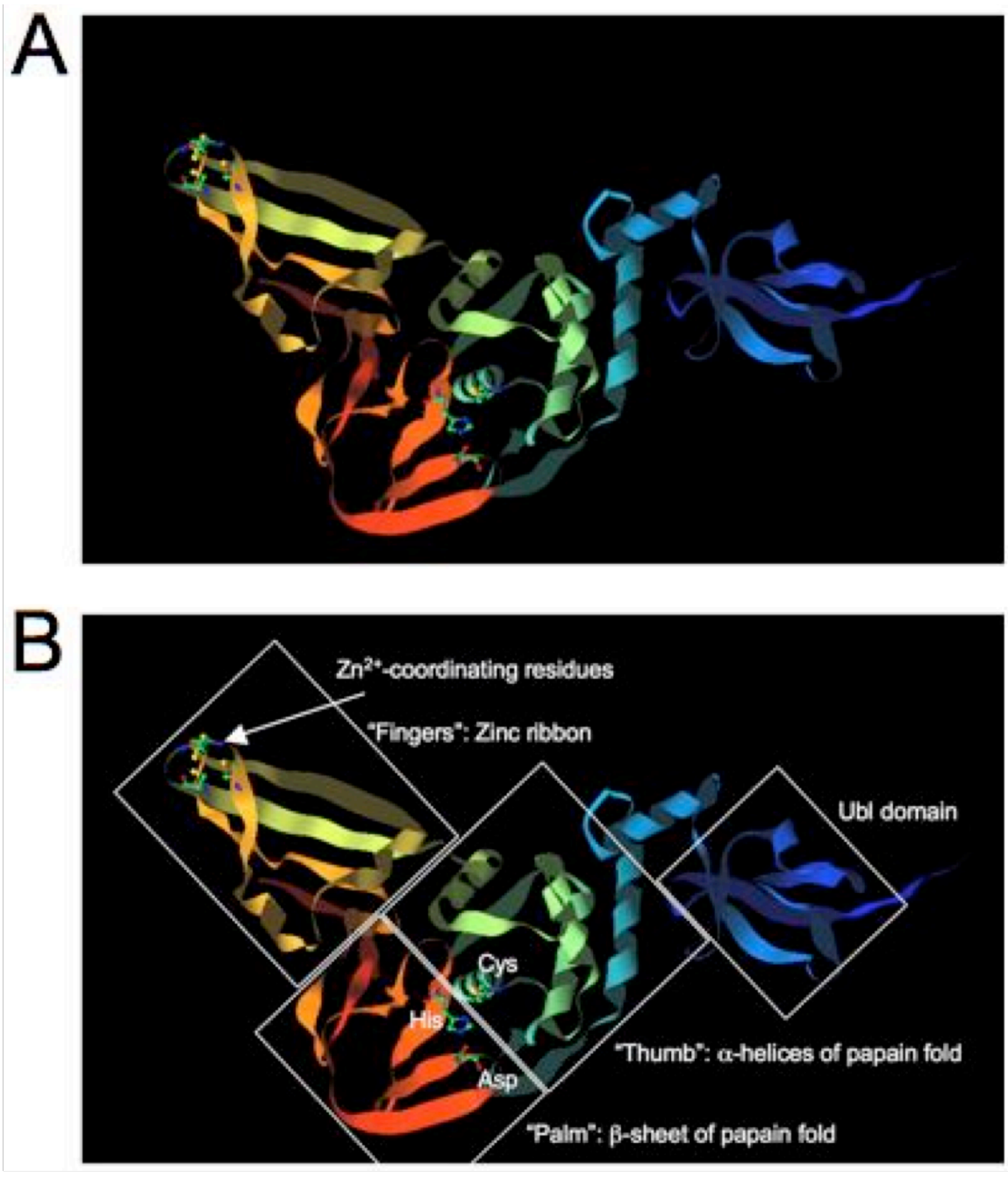
A
B
Zn2+-coordinating residues
"Fingers": Zinc ribbon
Ubl domain
Cys
His
Asp
"Thumb": α-helices of papain fold
"Palm": β-sheet of papain fold

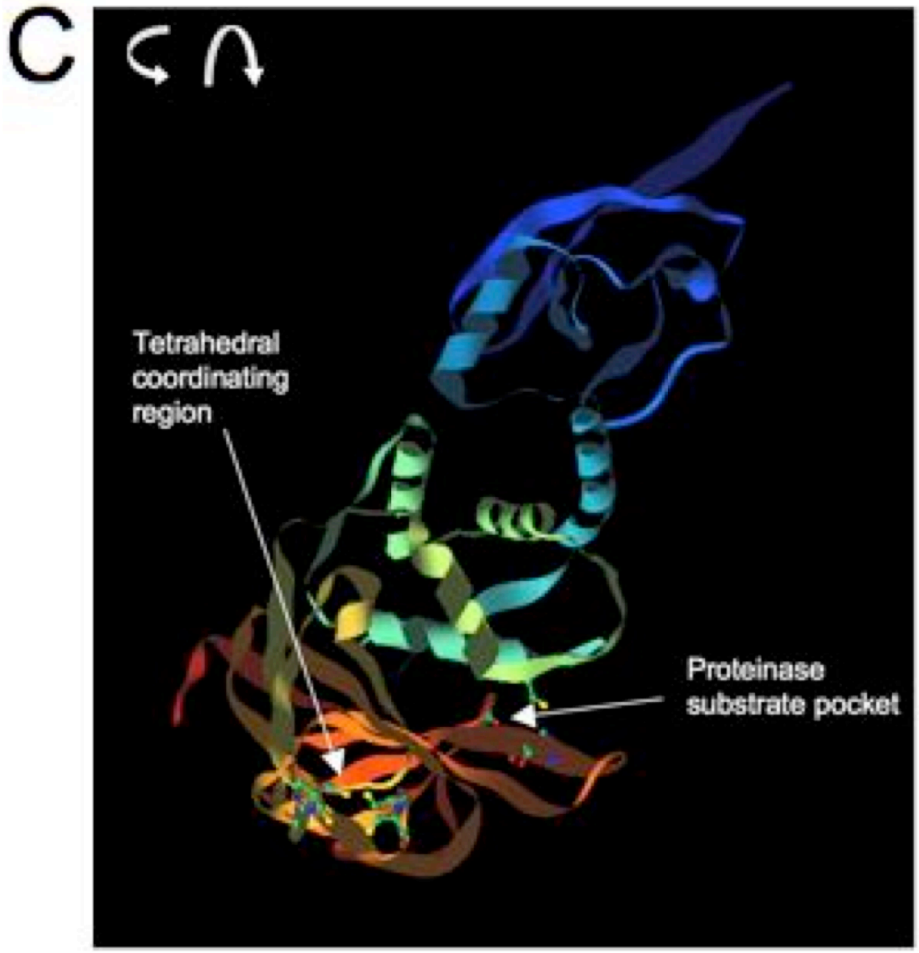

Fig. 1.5. Structure of SARS-CoV PLpro. A) The structure of SARS-CoV PLpro is shown, with secondary structure depicted by ribbons. The four domains are shown by color. **B)** The domains are shown outlined in boxes and labeled: Yellow: zinc ribbon domain (finger), with coordinating residues highlighted as ball-and-stick representations. **C)** Rotation of the molecule displays the protease substrate pocket and the tetrahedral zinc-coordinating loops. Red: b-sheet domain of the papain-like fold (palm), with catalytic residues His and Asp highlighted. Green: a-sheet domain of the papain-like fold (thumb), with catalytic Cys highlighted. Blue: Ubiquitin-like domain (Ubl). Structure was retrieved from the PBD database (PDB ID: 2FE8) and modified using iMol (www.pirx.com/imol). Images provided by R. Graham.

PLP2-like enzymes deubiquitinate either viral or cellular proteins to promote virus replication.

Consistent with the coronavirus PLP2-like enzymes having a restricted substrate specificity, modeling revealed that the active site is only accessible by substrates with small amino acid side chains, preferably glycine residues, in the two positions upstream of the CS. In contrast, modeling of PLP1-like enzymes suggests a more open conformation of the substrate binding pocket than that of PLP2-like enzymes, in which substrates have either a P2 Arg or a Cys followed by a small P1 amino acid directly upstream of the CS (Sulea et al., 2006). While the catalytic inactivation of some PLP1-like enzymes has resulted in the recovery of infectious virus, the catalytic inactivation of PLP2-like enzymes has not been reported or failed to produce infectious virus, suggesting that the catalytic activity of PLP2 is required for virus replication (Graham and Denison, 2006; Ziebuhr et al., 2007).

Coronavirus replication complexes

All viruses utilize strategies that allow for modification of host cells to generate an environment that is suitable for the production of progeny virions. Positive-sense RNA viruses modify intracellular membranes to support viral RNA synthesis. These membrane modifications are made up of viral replicase proteins, cellular proteins, and cellular membranes that assemble into what are termed replication complexes, which are the sites of viral RNA synthesis. For coronaviruses, virus-induced membrane modifications result in the formation of convoluted membranes (CMs) and double membrane vesicles (DMVs), both of which are not present in uninfected cells (Knoops et

al., 2008). While nsps localize to both of these structures, only DMVs have been implicated in viral RNA synthesis (Goldsmith et al., 2004; Gosert et al., 2002). Coronavirus-induced DMVs accumulate over the course of virus infection and range in size from 200 to 350 nm in diameter. *In situ* hybridization with riboprobes that detect viral RNA revealed co-localization of DMVs and viral RNA (Goldsmith et al., 2004; Gosert et al., 2002). Moreover, Immuno-EM analyses have shown that newly synthesized viral RNA associates with DMVs (Goldsmith et al., 2004; Gosert et al., 2002; Knoops et al., 2008; Snijder et al., 2006). Thus, it is presumed that virus-induced DMVs are the sites of coronavirus RNA synthesis.

In addition to products of the coronavirus replicase mediating direct roles in viral RNA synthesis, some nsps are hypothesized to play essential functions in the formation, organization, and stability of virus-induced membrane modifications. A common feature of the replicase from all coronaviruses is the characteristic transmembrane regions encoded in ORF1a. Bioinformatic analyses of the coronavirus replicase reveals that nsps 3, 4, and 6 contain predicted transmembrane domains. These transmembrane domains are thought to be essential for modification of cellular membranes and association of replicase proteins with replication complexes. Because nsps 3, 4, and 6 all contain predicted transmembrane domains, they are the most likely candidates for inducing membrane rearrangements and environments that are suitable for RNA synthesis. These proteins were first predicted to be replicase anchor proteins based on the long stretches of hydrophobic residues in their amino acid sequences (Lee et al., 1991). Membrane topology studies have shown that nsp3, nsp4, and nsp6 all exhibit integral membrane characteristics (Baliji et al., 2009; Kanjanahaluethai et al., 2007; Oostra et al., 2007).

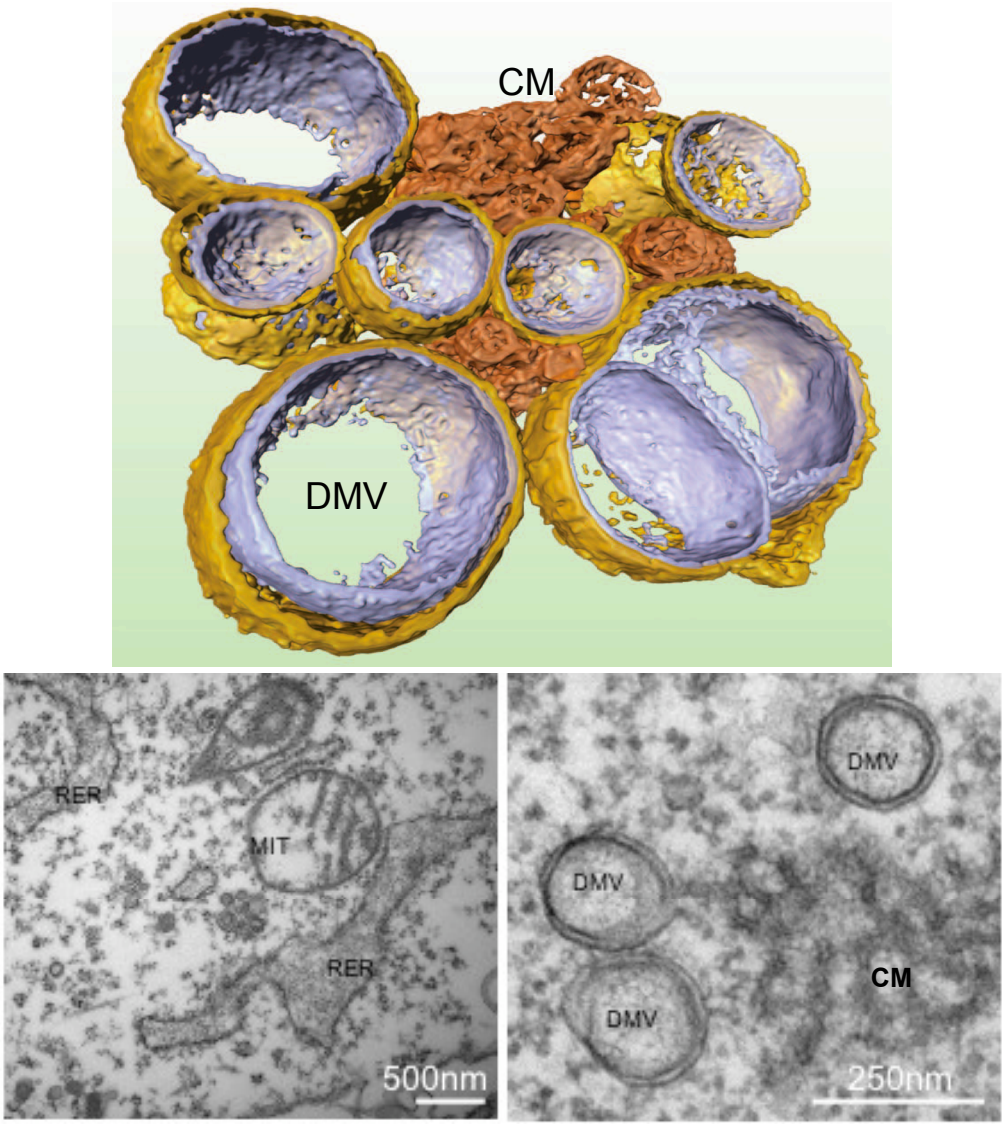

Fig. 1.6. Coronavirus-induced membrane structures. Top: Electron tomographic image showing double membrane vesicles (DMVs) and convoluted membranes (CMs) of SARS-CoV infected cells. Bottom left: EM image of a mock-infected mouse embryonic stem cell. No CMs or DMVs are detected. Bar represents 500 nm. Mit, mitochondria. RER, rough ER. Bottom right: EM image of an MHV-infected mouse embryonic stem cell. Bar represents 250 nm. Images adapted from Knoops et al., 2008 and J. Sparks, unpublished.

However, it is currently unknown if and how these proteins induce the membrane modifications that are observed during coronavirus infection.

Coronavirus RNA synthesis

As members of the *Nidovirales* order, coronaviruses generate not only new genome RNA, but also a 3'-nested set of subgenomic RNAs that each contains the first approximately 70 nucleotides of the 5' leader sequence of the genome. Because these viruses produce two distinct forms of RNA, coronavirus RNA synthesis can be visioned as having two distinct processes. In the first process, the positive-sense genome RNA is transcribed into a negative-sense template RNA complementary to the genome. The negative-sense RNAs are then used as templates for synthesis of new positive-sense RNAs during genome replication of viral RNA synthesis. In the second process, 3'-nested subgenomic RNAs (sgRNAs) are transcribed to serve as templates for translation of the viral structural and accessory proteins. While the transcription process of viral RNA synthesis is poorly understood, evidence is consistent with a discontinuous model of RNA transcription (Pasternak, Spaan, and Snijder, 2006; Sawicki and Sawicki, 1990; Sawicki and Sawicki, 1998; Sawicki and Sawicki, 2005). It is not known whether these two different processes can occur simultaneously or if they compete with each other during RNA synthesis.

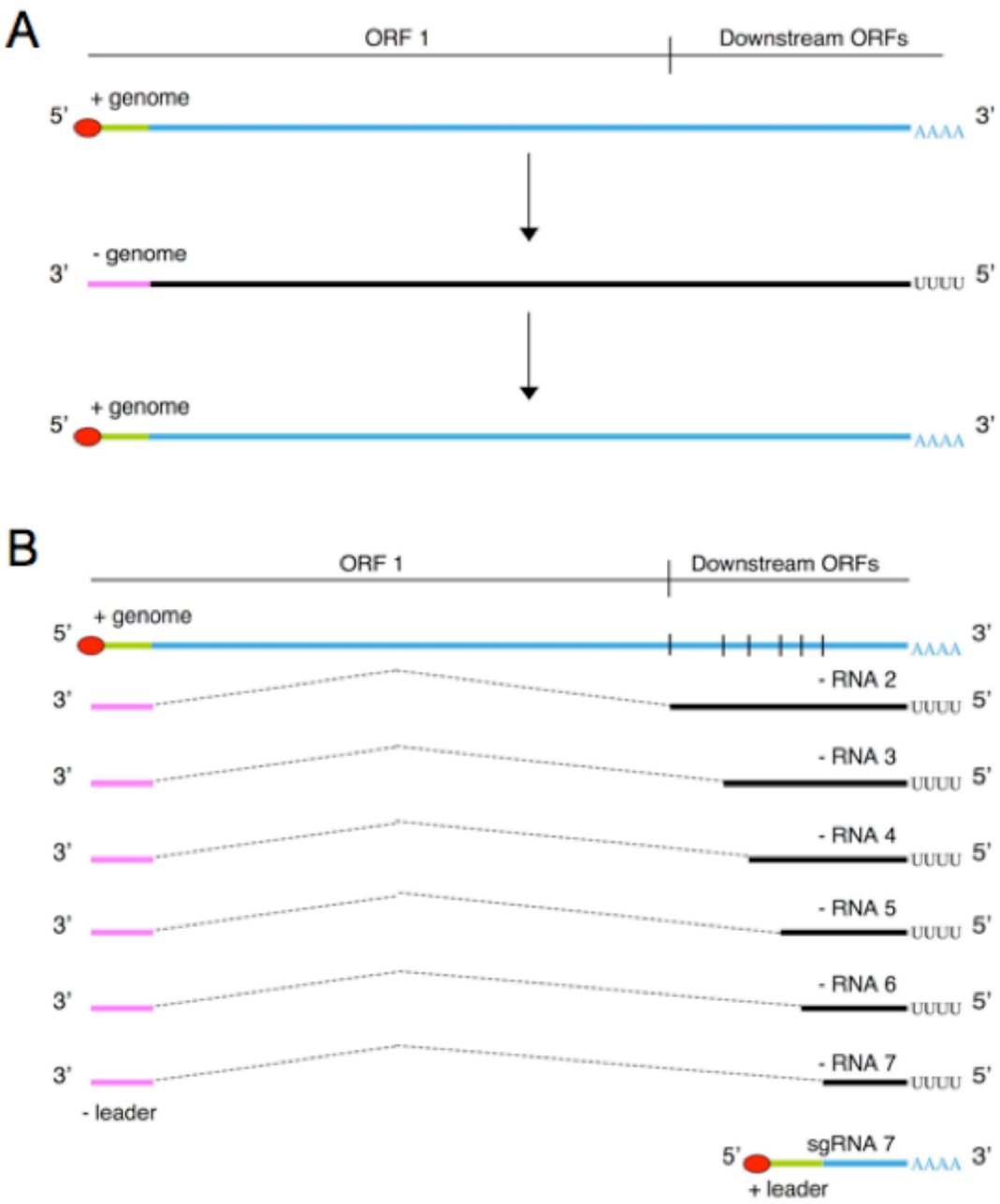

Fig. 1.7. Coronavirus genome replication and subgenomic RNA transcription. Coronavirus RNA synthesis, as outlined above, can be conceptualized as involving two stages. A) In the first stage, the positive-sense genome RNA (+ genome) is transcribed into a negative-sense template RNA (- genome), and then positive-sense genome RNAs are synthesized from negative-sense templates in the genome replication stage. B) In the second stage, 3'-nested subgenomic RNAs are transcribed to serve as templates for translation of the viral structural and accessory proteins. This second stage of viral RNA synthesis is poorly understood, but it is thought to involve a discontinuous RNA transcription model. During negative strand synthesis, the viral RNA-dependent RNA polymerase recognizes virus-specific conserved sequences termed transcriptional regulatory sequences (TRSs), located just upstream of each subgenomic open reading frame. At these locations, the polymerase either reads through to the next TRS or dissociates from the template strand, then reassociates with the leader TRS, located in the 5' UTR, and completes transcription, resulting in the production of subgenomic RNAs that are 3'-coterminal, and that all possess a 5' leader sequence. Figure adapted from Sawicki and Sawicki, 2005.

Before RNA synthesis occurs, ORF1 of the genome RNA must be translated into the replicase polyproteins. The genome RNA also acts as the template for synthesis of negative-sense RNA. In the discontinuous model of RNA transcription, RNA synthesis events produce a series of shorter, sgRNAs of both positive and negative polarity (Baric and Yount, 2000; Sethna, Hofmann, and Brian, 1991; Sethna, Hung, and Brian, 1989). The viral RNA synthesis machinery, including replicase proteins such as the RNA-dependent RNA polymerase, recognizes virus-specific transcriptional regulatory sequences (TRSs), located directly upstream of each subgenomic ORF. Upon encountering a TRS, the RNA-dependent RNA polymerase either transcribes through the TRS or dissociates from the template strand and reassociates with the leader TRS located in the 5' untranslated region (UTR) of another genome template. After the template switching, transcription reinitiates and results in the production of a nested set of negative-sense sgRNAs that are then transcribed into 3'-coterminal positive strand subgenomic mRNAs, all of which contain an identical 5' leader sequence. The specific mechanism of template dissociation and template switching by the polymerase is not well understood, but it is thought to be mediated by complementary binding of the nascent subgenomic TRS with the leader template TRS. Reports have implicated an approximate 8 nucleotide core consensus TRS and nucleotides immediately 5' and 3' of this core sequence in the efficiency of sgRNA transcription (Curtis et al., 2004; Sola et al., 2005).

Coronavirus reverse genetics

Over the past decade, several approaches have proven to be successful for reverse genetic studies of coronaviruses. One method, termed targeted recombination, takes

advantage of the virus's natural ability to homologously recombine for introduction of mutations into the virus via recombination with a non-infectious construct (Masters et al., 1994). This system has been quite useful for study of the viral genome from the Spike gene to the 3' end of the genome, but it has not been useful for studies of ORF1. Within the last few years, several groups have developed alternative strategies that enable reverse genetic manipulation of entire coronavirus genomes. A bacterial artificial chromosome full-length cDNA system has been developed for transmissible gastroenteritis virus (TGEV) studies (Almazan et al., 2000; Gonzalez et al., 2001; Gonzalez et al., 2002), and vaccinia virus-driven full-length cDNA expression systems are available for HCoV-229E, MHV, and IBV (Casais et al., 2001; Coley et al., 2005; Thiel et al., 2001; Thiel and Siddell, 2005). Additionally, cDNA cassette-based constructs have been designed for studies of TGEV, MHV, SARS-CoV, and IBV (Youn, Leibowitz, and Collisson, 2005; Yount, 2000; Yount et al., 2003; Yount et al., 2002).

In the MHV reverse genetic system used in this research, the complete genome is maintained as separately cloned cDNA fragments. Mutations can be engineered into individual fragments at this stage. To assess the effects of a particular mutation, or mutations, in the context of the virus, the cDNA fragments are cut by restriction enzymes, ligated together *in vitro*, transcribed using an incorporated T7 phage promoter, and transfected as infectious, full-length genomic RNA into replication-permissive cells. If the introduced mutations do not render the genome replication-incompetent, virus can then be harvested from the cell supernatant. The Denison laboratory has used this cassette-based reverse genetics system for both MHV and SARS-CoV with great success. This dissertation will describe multiple mutant viruses generated by this system.

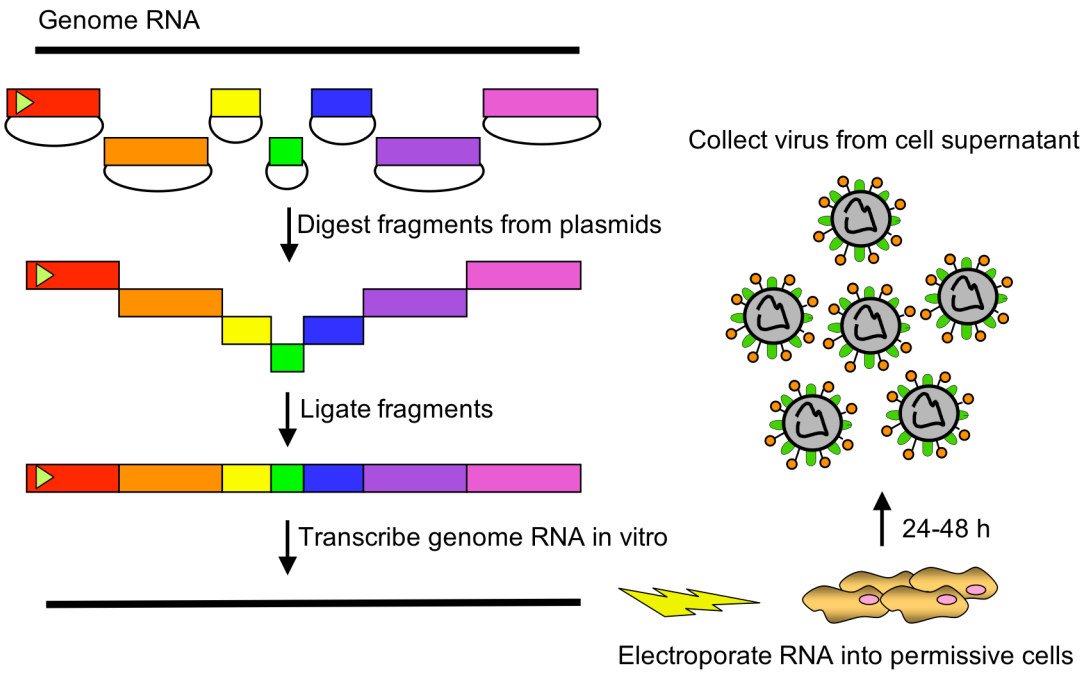

Fig. 1.8. MHV cassette-based cDNA reverse genetics system. A representative schematic of the MHV system is shown. The MHV genomic RNA (black bar) was reverse transcribed and maintained as independent, plasmid-based cDNA cassettes. Mutations are made at this stage. MHV fragments (colored rectangles) are then digested from the parental plasmids using specific restriction enzymes and ligated together by unique restriction overhangs. RNA is *in vitro* transcribed from an incorporated T7 promoter (yellow triangle) at the 5' end of the first MHV cDNA fragment and subsequently electroporated into permissive cells. Virus can be harvested from the cell supernatant 24-48 hours post infection. Adapted from Yount et al., 2002.

Summary

Despite many years of research from multiple investigators, the many details of the mechanisms by which coronaviruses replicate and cause disease remain to be defined. With the invention of coronavirus reverse genetics systems, major advances have been made in defining functions and requirements for those functions of several coronavirus nsps. Previous research in the Denison Laboratory has focused on the cell biology and replication of coronaviruses. My research has focused on both of these areas.

Prior to my dissertation research, MHV nsp2 was shown to be nonessential for virus replication, but deletion of the nsp2 coding sequence from the genome resulted in reduced growth and RNA synthesis. These findings led to several important questions that my research aimed to address. These questions included: Can nsp2 be expressed from alternative locations in the genome? If so, is natively expressed nsp2 required for optimal replication? Does nsp2 expressed from alternate locations affect its function and localization?

The findings from this research and previous work from the Denison lab led to the investigation of interactions between PLPs and CSs. Our lab has shown that PLP-mediated processing of nsps 1-3 is required for optimal replication of MHV, but that catalytic activity of PLP1 is not required for virus replication in culture. Part of my graduate research aimed at extending these studies to address: What are the determinants of PLP-mediated processing of nsps 1-3 in the context of replicase polyprotein expression? What are the requirements for encoding one or two PLPs? Can PLP specificity, the recognition and processing of a CS, be switched by altering the CS amino

acid sequence? Are there additional determinants that are critical for PLP recognition and processing?

Lastly, other work from our laboratory has studied the role nsp4 plays in virus replication and replication complex function. This study demonstrated MHV nsp4 is essential for recovery of infectious virus and identified important residues and domains of nsp4. It is also predicted that nsp4 plays a role in the formation and organization of replication complexes. My research aimed to address the following questions. Is nsp4 glycosylated when expressed from its native genomic location? What effect does nsp4 glycosylation have on virus replication? Does nsp4 regulate virus-induced membrane modifications?

Understanding and studying the functions of coronavirus nsps 1-4 and their processing during virus replication is important for several reasons. These reasons are: (1) PLP-mediated processing regulates the expression and functions of nsps 1-4; (2) although there is considerable sequence diversity, evidence suggests that coronavirus nsps 1-4 have similar functions in their respective life cycles; (3) because nsps 1-4 are the first to be expressed in an infected cell, these nsps are critical in creating a suitable environment that supports early steps in the coronavirus life cycle. Therefore, by elucidating the mechanisms and requirements of coronavirus PLP-mediated processing and functions of the cleavage products in virus replication, the results will contribute to our knowledge of coronavirus evolution and how coronavirus replication occurs inside host cells.

CHAPTER II

MHV MUTANT VIRUSES ENCODING NSP2 AT DIFFERENT GENOMIC LOCI HAVE ALTERED REPLICATION, PROTEIN EXPRESSION, AND LOCALIZATION

Introduction

Positive-sense RNA viruses express polyproteins from their genomic RNA that are proteolytically processed by viral and cellular proteases to yield nonstructural, structural, or both types of proteins. To understand the functions of particular polyproteins and mature proteins of positive-sense RNA viruses, several studies have reported the effects of protein domain deletions in virus replication. Additionally, there had been no published reports showing deletions of entire mature proteins allowed for virus replication of any positive-sense RNA virus until work from the Denison lab reported that the entire coding region of MHV nsp2 and SARS-CoV nsp2 could be deleted from their respective genomes.

The murine hepatitis virus (MHV) nsp2 is a 65-kDa protein that has minimal sequence identity or similarity among different coronavirus groups and has no known or predicted functions. Research from the lab has shown for MHV and SARS-CoV that in-frame deletion of nsp2 (Δnsp2) yields viable mutant viruses (Graham et al., 2005); however, both MHV and SARS-CoV Δnsp2 mutants exhibit a 90% reduction in peak titer and a 50% reduction in viral RNA synthesis.

To determine if expression of nsp2 from non-native sites in the genome could complement the defect in MHV Δnsp2 replication and to gain a better understanding of nsp2 function, the nsp2 coding sequence was engineered at alternative sites in the

genome, both in the absence and presence of the wild-type ORF1a nsp2 sequence. The results indicate that nsp2 can be encoded and expressed alone from ORF4, as a sequence duplication in ORF1a and ORF1b or in ORF1a and ORF4, but not near the end of ORF1a or alone in ORF1b. Duplication of the nsp2 sequence or expression from ORF4 was detrimental to replication compared to wild-type, indicating that the native context of nsp2 expression, and possibly a single copy of the sequence, may be necessary for optimal function in replication. Results also indicate that addition of amino acids at the N- and C- termini of natively expressed nsp2 have no effect on peak viral growth. Mutations at the C-terminus of nsp2 resulted in delays in exponential growth, indicating that the timing of processing of natively expressed nsp2 from the replicase polyprotein is required for optimal replication.

Nsp2 can be encoded at different locations in the coronavirus genome and still allow for virus replication

MHV nonessential ORFs have been shown to tolerate foreign gene insertion (de Haan et al., 2005; Fischer et al., 1997; Oostra et al., 2007). In order to test the effects of nsp2 expression in downstream ORFs, the mutant MHV genome was engineered to have the substitution of the nsp2 coding sequence in place of the nonessential ORF4 coding sequence, while retaining the ORF4 transcriptional regulatory sequence (5'-CUAAAC-3') and start codon (Fig. 2.1 and Table 2.1). To determine if nsp2 could be expressed from alternate locations in the replicase, the nsp2 sequence was engineered at the end of ORF1a following nsp10 (nsp10-11 and nsp10-12 junction) and in ORF1b between nsp13 and nsp14. Since processing between nsp10-12 and nsp13-14 is mediated by nsp5

(3CLpro), minimal 3CLpro-recognition cleavage sites of P2-LeuGln↓Ser-P1' (Lu, Sims, and Denison, 1998b; Pinon, Teng, and Weiss, 1999; Ziebuhr and Siddell, 1999) were introduced at the amino and carboxy termini of nsp2 by the addition of a Ser residue to the N-terminus of nsp2 and LeuGln residues to its C-terminus, leaving the 3CLpro recognition sequences of nsp10, nsp12, nsp13, and nsp14 intact. The wild-type N-terminal nsp2 residue is Val; Ser was selected as a conservative addition that would optimize for cleavage by nsp5. The lab has previously shown that P1' substitutions at the amino-terminus of nsp2 that allow processing (Ala, His) do not affect virus growth or RNA synthesis (7); however, to determine if Ser and LeuGln additions had any effects on nsp2 functions from alternately expressed nsp2 viruses, these mutations were engineered into natively expressed nsp2 in a wild-type virus background.

Infectious viruses were recovered from supernatants of electroporated cells for: ORF4 deletion, with or without ORF1a-nsp2 expression (1a-2/Δ4 and Δ1a-2/Δ4); ORF4-nsp2, with or without ORF1a-nsp2 expression (1a-2/4-2 and Δ1a-2/4-2); ORF1b-nsp2 with ORF1a-nsp2 expression (1a-2/13-2-14); and ORF1a-nsp2 with amino acid additions at the N- and/or C-termini (1a-S2, 1a-2LQ, and 1a-S2LQ). The supernatants from electroporated cells were passaged to expand the populations (passage 1 [P1]), and RNA from cells infected with P1 virus stocks was used to confirm the retention of all engineered changes from recovered mutants. Multiple attempts to recover mutants lacking ORF1a-nsp2 but expressing nsp2 in ORF1b (Δ1a-2/13-2-14) failed to produce infectious virus. Recovery attempts were also unsuccessful for mutants encoding nsp2 in-frame between nsp10-nsp12, with or without ORF1a nsp2 expression (1a-2/10-2-12 and Δ1a-2/10-2-12).

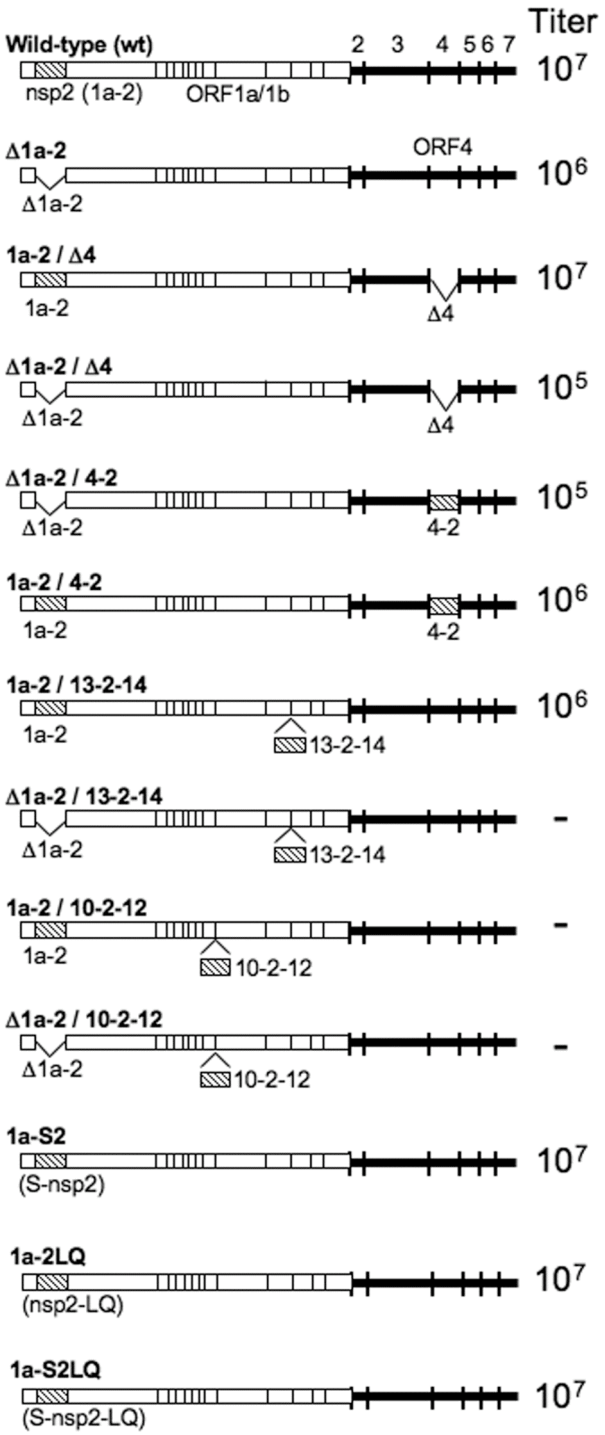

Fig. 2.1. Engineering nsp2 deletions, mutations, rearrangements, and duplications. For each construct, alterations to the genome are shown. Constructs are listed as named in the text. Open reading frames (ORFs) 1-7 are labeled above the wild-type schematic. The nsp2 coding sequence is depicted as a hatched rectangle. Coding region locations and sizes are not drawn to scale. Deletion of the nsp2 and/or ORF4 coding sequences or insertion of nsp2 in ORF1b is indicated by a caret. Protein coding deletions are indicated by a delta (Δ) in the virus name. Nsp2 position is indicated as: ORF1a (1a-2), ORF1b (13-2-14 or 10-2-12), or ORF 4 (4-2). Approximate peak titers of viable viruses are indicated to the right of each construct. Viruses that were not recovered are indicated by a minus sign (-).

Table 2.1. Primers used for mutagenesis.

Primer Name	Sequence	Sense	Purpose
nsp13-nsp2 A	5' GTCAATGACACCACTCGCAAGTATGTGTTTACT	+	PCR partner for nsp13-nsp2 B
nsp13-nsp2 B	5' CGTCTCGCACACTGTAATCGTGGATTGTTAATCTT	-	Insertion mutagenesis partner for A
nsp2 1b Ins C	5' CGTCTCGTGTGTTAAGCCCATCCTGTTTGTGGAC	+	nsp2 ORF1b insertion mutagenesis
nsp2 1b Ins D	5' CGTCTCGCTGTAATCGCGCACAGGGAAACCTCCAGCACTG	-	nsp2 ORF1b insertion mutagenesis
nsp2-nsp14 E	5' CGTCTCGACAGTGTACTACAAATTTGTTTAAGGATTGT	+	Insertion mutagenesis partner for F
nsp2-nsp14 F	5' CATGTGAGCTCAAAGCTGGCAGCCCACGTCAC	-	PCR partner for nsp2-nsp14 E
ORF4 Ins A	5' CAGGCCATAGAAAAGGTCAATGAGTGCGTT	+	PCR partner for ORF4 Ins B primers
ORF4 Ins2 B1	5' CGTCTCGCCATCTATAAATTGTTTAGATTTTCTG	-	Insertion mutagenesis partner for A
ORF4 InsKo B2	5' CGTCTCGTTTATTACTATAAATTGTTTAGATTTTCTG	-	ORF4 deletion partner for A
ORF4 nsp2 C	5' CGTCTCGATGGTTAAGCCCATCCTGTTTGTGGAC	+	nsp2 ORF4 insertion mutagenesis
ORF4 nsp2 D	5' CGTCTCGTTTATTACGCACAGGGAAACCTCCAGCACTG	-	nsp2 ORF4 insertion mutagenesis
ORF4 Ins E	5' CGTCTCGTAAACTCCAAGAGGTTTTGATTATAGTACA	+	Insertion mutagenesis partner for F
ORF4 Ins F	5' CTTAAGGAATTGAACTGCCTCGTCGGCCGT	-	PCR partner for ORF4 Ins E
S-nsp2 F	5' GGGCTATCGCGGTTCTGTTAAGCCCATCCTG	+	Insertion mutagenesis partner for S-nsp2 R
S-nsp2 R	5' CAGGATGGGCTTAACAGAACCGCGATAGCCC	-	Insertion mutagenesis partner for S-nsp2 F
nsp2-LQ F	5' GGTTTCCCTGTGCGCTCCAAGGCAAGAAAGTCGAG	+	Insertion mutagenesis partner for nsp2-LQ R
nsp2-LQ R	5' CTCGACTTTCTTGCCTTGGAGCGCACAGGGAAACC	-	Insertion mutagenesis partner for nsp2-LQ F
158 A F	5' TCCGGCTCGTATGTTGTGTGGAAT	+	PCR partner for S-nsp2 R and nsp2-LQ R
3253 A R	5' CTGCGTCAAGCACAACATCAAGCA	-	PCR partner for S-nsp2 F and nsp2-LQ F

Protein expression and processing from

nsp2 alternate expression and duplication viruses

To determine the expression and processing of nsp2 in mutant virus infections, lysates of radiolabeled, virus-infected DBT cells were immunoprecipitated with antisera against nsp1, nsp2, and nsp3 (Fig. 2.2A). Mature nsp1 (28 kDa) was detected in all mutant virus-infected cells, demonstrating normal processing between nsp1 and nsp2 by the nsp3 papain-like proteinase 1 (PLP1). Mutant viruses that expressed nsp2 from ORF1a (1a-2/Δ4, 1a-2/13-2-14, and 1a-2/4-2) and the Δnsp2 virus (Δ1a-2) all produced similar amounts of nsp1 relative to wild-type, while the Δ1a-2/Δ4 and Δ1a-2/4-2 viruses expressed lower levels of nsp1. Nsp3 was detectable with α–nsp3 in wild-type-infected cells as both mature nsp3 (210 kDa) and intermediate nsp2-3 (275 kDa). Mutant viruses that encoded nsp2 in its native position (1a-2/Δ4, 1a-2/4-2, and 1a-2/13-2-14) also had detectable nsp3 and nsp2-3. Only mature nsp3 was detected in infections with viruses that lacked ORF1a-expressed nsp2 (Δ1a-2, Δ1a-2/Δ4, and Δ1a-2/4-2).

As expected, mutant viruses that did not encode nsp2 at any location (Δ1a-2 and Δ1a-2/Δ4) had no detectable nsp2. Viruses encoding nsp2 from one or two locations in the genome exhibited a range of nsp2 expression levels. The Δ1a-2/4-2 virus expressed low levels of nsp2, while the 1a-2/Δ4 mutant virus expressed nsp2 expression levels similar to wild-type. The 1a-2/4-2 duplication mutant, which encoded nsp2 in both ORF1a and ORF4, expressed higher levels of nsp2 compared to wild-type virus. To test whether the increased expression was due to just two coding locations or if there was also altered levels of ORF4 subgenomic RNA, infected cells were labeled with [^{3}H]-uridine in the presesnce of Actinomycin D, and viral RNAs were measured by densitometry using

ImageJ 1.40 (Rasband, 1997-2008) (Fig. 2.2B). All genomic and subgenomic RNA species were detected, but RNA4 encoding nsp2 in ORF4 in the 1a-2/4-2 virus was expressed with a 2.5 fold increase, as a ratio to RNA7, compared to wild-type virus. This is sufficient to account for the increased nsp2 levels and suggests that insertion of foreign genes in ORF4 may specifically alter mRNA transcription.

The 1a-2/13-2-14 mutant virus, which encoded nsp2 in both ORF1a and ORF1b, expressed overall levels of mature nsp2 that were comparable to wild-type. This could have resulted from either diminished translation from ORF1b or impaired or absent processing. The requirement for in-frame translation of nsp13 and nsp14 for virus viability argues that the in-frame nsp2 must be translated from this location in ORF1b. The efficiency of ribosomal frameshifting and translation of ORF1b relative to ORF1a has not been experimentally tested during virus infection, but is predicted to be less than 25% (Brierley, 1989). This would be consistent with the detection of minimal additional nsp2. The lack of detection would also result if expressed nsp2 was not cleaved from nsp13, nsp14, or both, and thus was not detected as mature nsp2. Also, immunoprecipitation with α–nsp2 or α–nsp13 antisera did not resolve precursors consistent with a predicted size for nsp13-2 (130 kDa), nsp2-14 (130 kDa) or nsp13-2-14 (190 kDa). Taken together, these data indicate that levels of protein expression depend on a combination of the number of coding sequence copies and the context of expression.

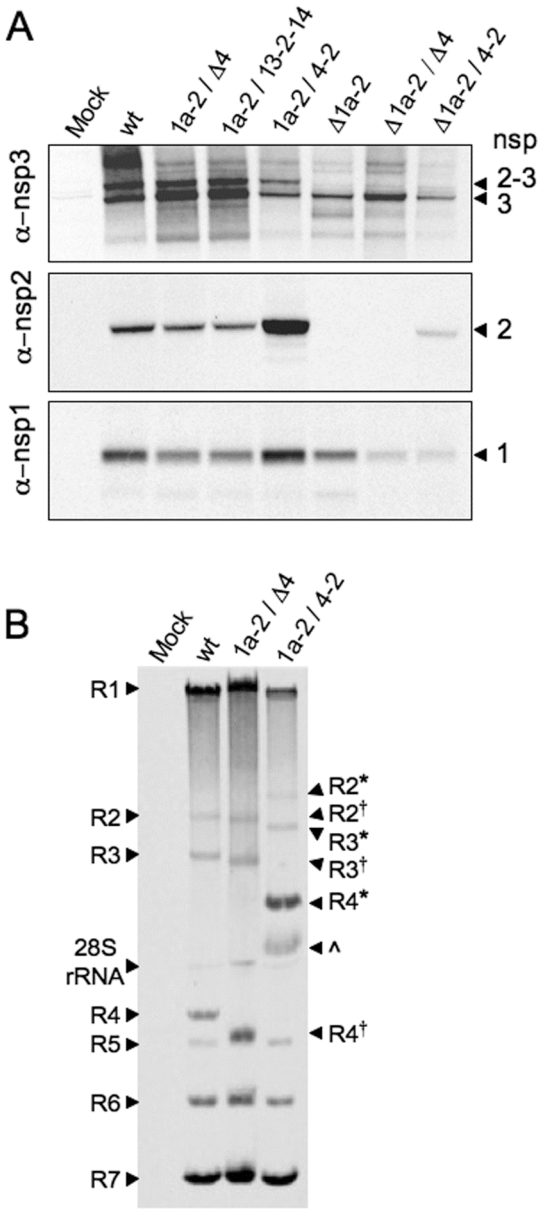

Fig. 2.2. Protein expression, processing, and RNA synthesis of altered nsp2 viruses. DBT cells were infected with viruses as indicated above the gels. **A)** Proteins were radiolabeled, and cell lysates were immunoprecipated with α-nsp1, α-nsp2, and α-nsp3 antibodies. Mock indicates mock-infected cells and wt indicates recombinant wild-type MHV-A59. Nsps are indicated to the right of the gel: nsp2-3 (275 kDa), nsp3 (210 kDa), nsp2 (65 kDa), and nsp1 (28 kDa). **B)** Viral RNA was metabolically labeled with [^{3}H]-uridine in the presence of Actinomycin D from 9 to 11 h p.i. Intracellular RNA was isolated, denatured, and resolved by electrophoresis. Genomic RNA (R1) and subgenomic mRNAs (R2 to R7) are indicated. R2, R3, and R4 from the 1a-2/Δ4 virus are approximately 300 base pairs (bp) shorter than wild-type mRNAs and are indicated by a †. The 1a-2/Δ4 virus was used as a control in which ORF4 is deleted, but its transcriptional regulatory sequence is still present, resulting in R4 co-migrating with R5. R2, R3, and R4 from the 1a-2/4-2 virus, which are approximately 1400 bp longer than wild-type R2, R3, and R4, are indicated with an *. An unknown band, possibly an R4 degradation product, is indicated by a ^. R1 from wild-type and mutant viruses exhibited some variability in migration. This variability is supported by quantification of overall genomic RNA levels (1a-2/Δ4 > wt > 1a-2/4-2). RNA band sizes and quantification were determined by using ImageJ 1.40.

Localization of nsp2 in cells during infection with mutant viruses

To determine if nsp2 localization was affected by genomic location and extent of expression, DBT cells were infected, and at 6 hours post-infection (h p.i.), cells were fixed and stained with antibodies against nsp2 and nsp8, both markers for replication complexes (Bost, Prentice, and Denison, 2001) (Fig. 2.3). Nsp2 and nsp8 signals co-localized in characteristic cytoplasmic perinuclear foci in cells infected with viruses expressing both nsp2 and nsp8 (wt, 1a-2/Δ4, and Δ1a-2/4-2). When expression of nsp2 was absent (Δ1a-2/Δ4), no nsp2 signal was present, while nsp8 signal was still detected in punctate foci. Nsp2 expressed from the 1a-2/4-2 virus showed partial co-localization with nsp8 signal, but nsp2 was also detected as diffuse cytoplasmic fluorescence that was not associated with punctate foci. A possible explanation for this result is that simultaneous expression of nsp2 from ORF1 and ORF4 in the 1a-2/4-2 virus saturates replication complexes. This would be consistent with the observed increase in nsp2 expression (Fig. 2.2A). This conclusion is also supported by the observation that infection with the 1a-2/13-2-14 mutant, which resulted in lower levels of mature nsp2 (Fig. 2.2A), showed co-localization of nsp2 with nsp8, but no additional localization or diffuse fluorescence (Fig. 2.3). While direct proof of differential localization of nsp2 would require unique tags for nsp2 at different loci, it is still clear that alteration of the nsp2 coding location within the genome results in differences in both the extent of protein expression and localization of nsp2 during infection.

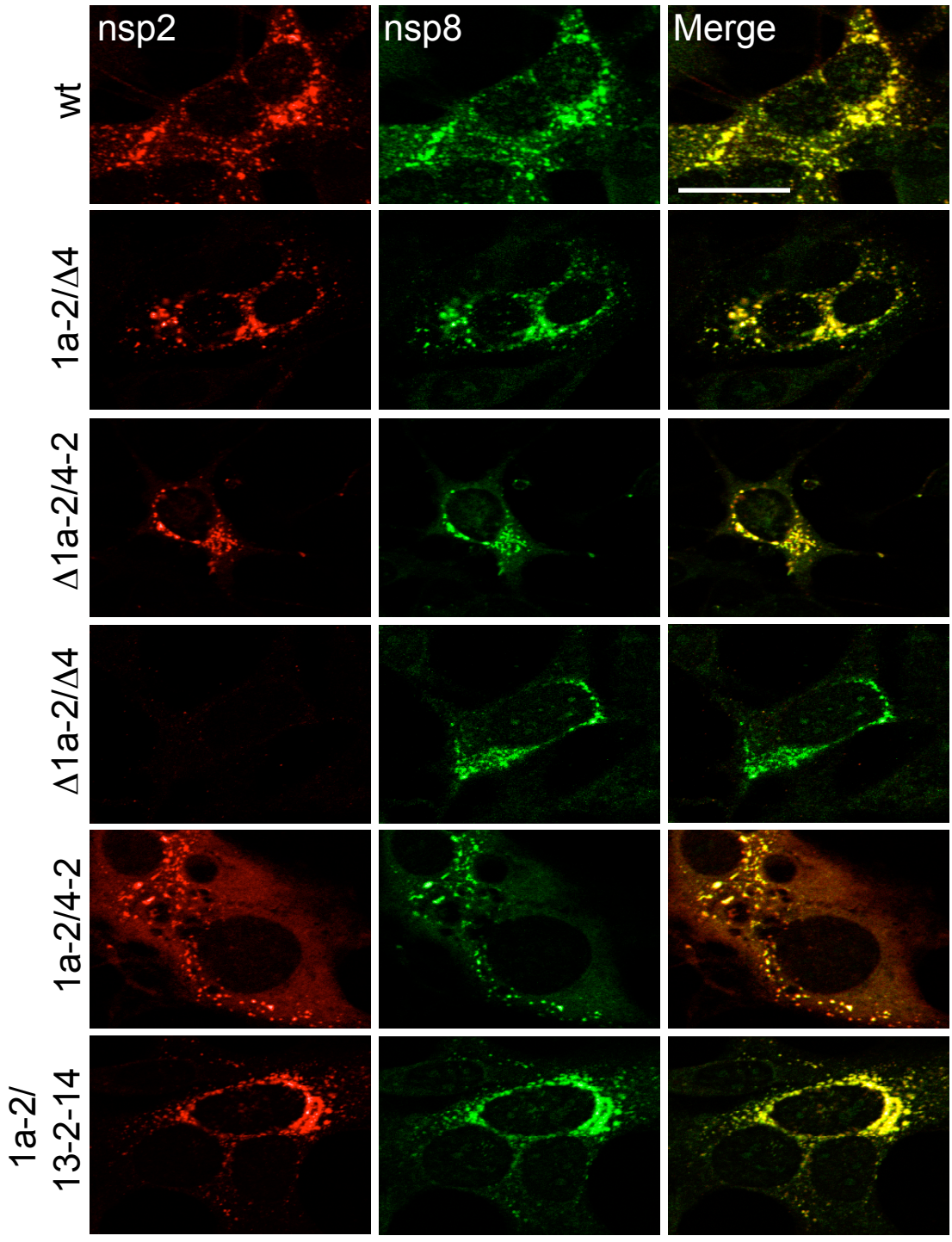

Fig. 2.3. Immunofluorescence of nsp2 mutants. DBT cells on glass coverslips were infected for 6 h, fixed, and stained for nsp2 and nsp8 by Alexa546 conjugated to a secondary IgG antibody and Alexa488 directly conjugated to a primary IgG antibody, respectively. Co-localization is indicated by yellow pixels in the merged images. The bar in the upper right image equals 20 μm and is representative for all images. Images were obtained on a Zeiss LSM510 and were processed in Adobe Photoshop CS2.

Nsp2 encoded at different locations results in varied effects on growth

To assess the effects of alternate nsp2 encoding on virus replication, DBT cells were infected at a multiplicity of infection (MOI)=1 PFU/cell, aliquots of supernatant were saved, and virus was titered by plaque assay (Fig. 2.4). As previously shown (Fischer et al., 1997), deletion of ORF4 resulted in a mutant virus that had growth kinetics and peak titers indistinguishable from wild-type (Fig. 2.4A). Deletion of nsp2 alone (Δ1a-2) resulted in a decrease of ~1 $\log_{10}$ compared to wild-type, also consistent with previous studies (11). Expression of nsp2 from ORF4 in the presence or absence of ORF1a nsp2 was similar to the parental Δ1a-2 mutant in the timing of exponential growth. However, the 1a-2/4-2 mutant virus reached slightly higher titer than the Δ1a-2 virus but did not achieve wild-type growth in 24 h p.i. (Fig. 2.4B), suggesting that increased total levels of nsp2 expression may in fact be detrimental to virus growth fitness. Also, the Δ1a-2/4-2 virus achieved a 0.5-$\log_{10}$ lower peak titer than Δ1a-2, and titer declined more rapidly than that of either Δ1a-2 or 1a-2/4-2 over a 24h period. The results show that ORF4 expression of nsp2 does not complement the deletion of nsp2 from ORF1a and suggest that ORF4 expression of nsp2 in the absence of ORF1a nsp2 expression results in a less fit mutant virus. Similar to the 1a-2/4-2 virus, when nsp2 was expressed in ORF1b (1a-2/13-2-14), growth was delayed in timing and peak titer could not reach that of wild-type virus at 24 h p.i., even though peak titers were still increasing, similar to the 1a-2/4-2 virus (Fig. 2.4B).

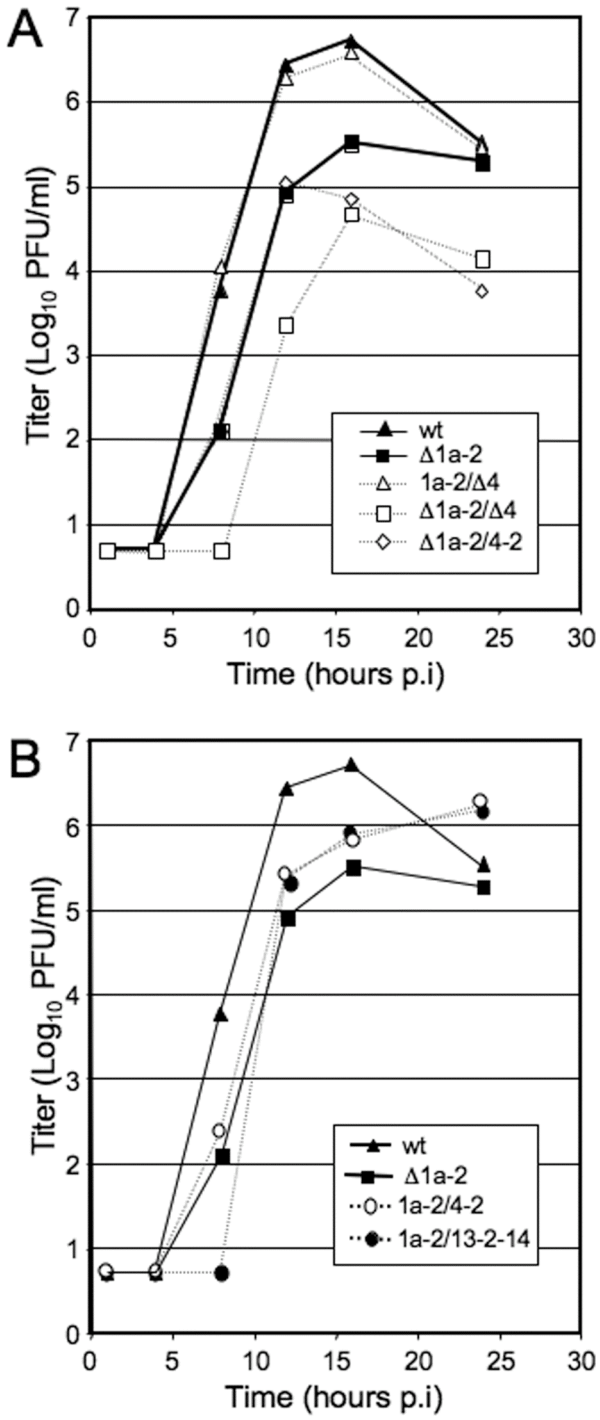

Fig. 2.4. Growth of nsp2 alternate expression viruses. DBT cells were infected with indicated viruses at a multiplicity of infection (MOI) = 1 plaque forming unit (PFU) per cell. Aliquots of supernatant were taken at indicated times p.i. and titered by plaque assay. All infections were performed in the same experiment with replicates. **A)** Nsp2 and ORF4 deletion and ORF4 single expression mutants. **B)** Nsp2 duplication viruses. Wild-type curve and Δ1a-2 curve from A are duplicated in B to allow direct comparison.

It was also surprising to see that deletion of both nsp2 and ORF4 or nsp2 replacement of ORF4 (Δ1a-2/Δ4 and Δ1a-2/4-2) yielded mutants with more delayed and/or decreased growth than deletion of either nsp2 or ORF4 alone (Fig. 2.4A). These results suggest possible interactions and/or cooperative functions of nsp2 and the ORF4 protein(s) in the virus life cycle. Both nsp2 and the ORF4 gene product(s) are group-specific proteins (de Vries et al., 1997; Masters, 2006; Ziebuhr, Thiel, and Gorbalenya, 2001) and may have, as of yet, uncharacterized interactions. Alternatively, it is possible that the known replication defect of the Δnsp2 mutant exacerbates a replication defect in an ORF4 deletion mutant that alone does not manifest as a change in growth kinetics in cell culture. Finally, it is possible that altered RNA folding or protein-RNA interactions resulting from the cumulative deletion of >2kb of genome is responsible for the observed replication defect and decrease in expression of nsps 1-3. This possibility is supported by the result that 1a-2/4-2 virus had a slight growth delay, grew to peak titers >1 $\log_{10}$ higher than Δ1a-2/Δ4, and exhibited higher expression levels of nsps 1-3.

Additions of amino acids at the N- and/or C-termini

of nsp2 affect protein processing but not peak virus growth

Because alternately expressed nsp2 was engineered to contain minimal 3CLpro cleavage sites (P2-LeuGln↓Ser-P1') when introduced between nsp13 and nsp14 to promote cleavage, I next wanted to determine the effects on virus growth by introducing amino acids at the N- and C-termini of nsp2. Therefore, viruses were engineered to have addition of a Ser residue at the N-terminus (1a-S2), LeuGln residues at the C-terminus (1a-2LQ), or both mutations (1a-S2LQ) in the native location of nsp2 (Fig. 2.1 and Table

2.1). Virus growth experiments were performed as previously described at an MOI=0.1 PFU/cell, and the 1a-S2, 1a-2LQ, and 1a-S2LQ viruses reached peak growth similar to wild-type virus (Fig. 2.5A), suggesting that the additional amino acids do not inhibit function(s) of nsp2 in cell culture. However, the 1a-2LQ and 1a-S2LQ viruses were slightly delayed in exponential growth compared to wild-type virus. Protein processing experiments show detection of mature nsp2 in the 1a-2LQ and 1a-S2LQ viruses (Fig. 2.5B), yet pulse-chase analysis reveals decreased expression of mature nsp2 over time in the 1a-2LQ and 1a-S2LQ viruses compared to wild-type virus (Fig. 2.5C). These observations are consistent with the previously described ΔCS2 mutant virus, which has a delay in exponential growth, can reach peak titers similar to wild-type virus, and exhibits no mature nsp2 detection (Fig. 2.5A and 2.5B). Therefore, the additions of amino acids at the N- and C- termini of nsp2 appear to be affecting processing and not the overall functions of nsp2. Additionally, it is not known whether PLP1 or 3CLpro is mediating processing at the C-terminus of nsp2 that has been engineered to contain the minimal 3CLpro cleavage site sequence. Therefore, the delay in timing of exponential growth may be due to PLP1 being unable to process the C-terminus of nsp2, but rather, 3CLpro mediating processing at the engineered site. This would be consistent with later expression of 3CLpro compared to PLP1, which may result in the delay of exponential growth observed in the 1a-2LQ and 1aS2LQ mutant viruses.

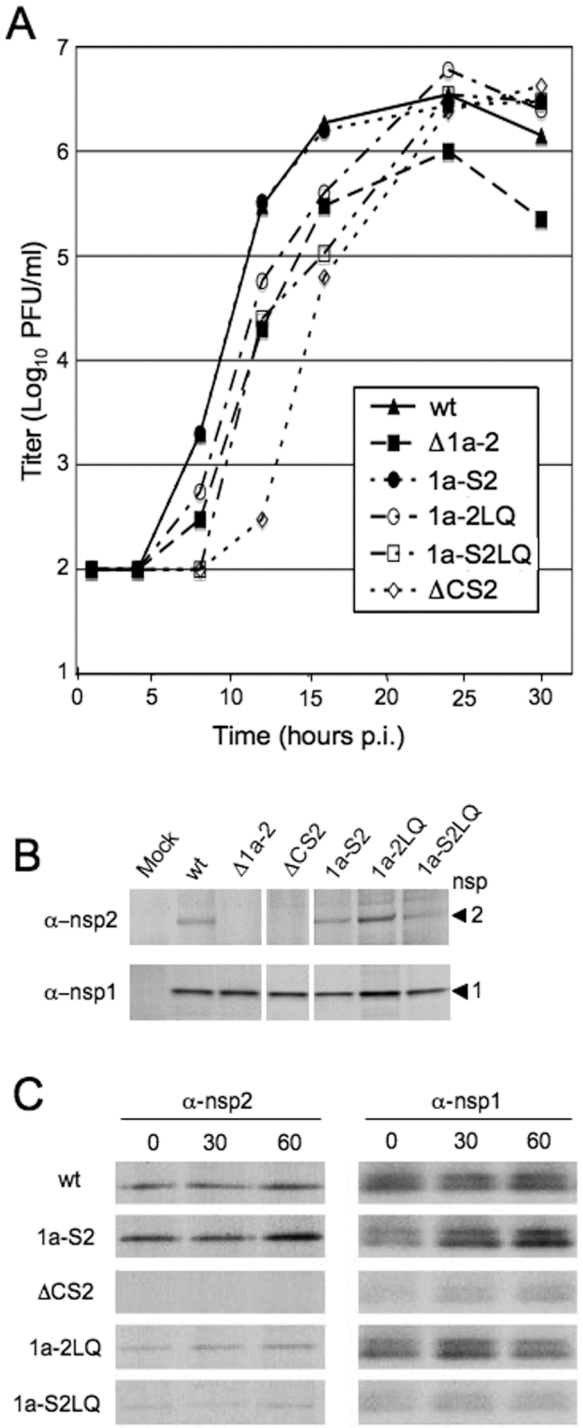

Fig. 2.5. Growth and protein processing of 1a-S2, 1a-2LQ, and 1a-S2LQ viruses. A) DBT cells were infected with indicated viruses at an MOI=0.1 PFU/cell. Viral titers were determined as described above. Infections were performed in the same experiment with replicates. **B)** Protein processing experiments were performed as previously described. Immunoprecipitations were performed with α-nsp1 and α-nsp2 antibodies. All samples were resolved on the same gel, but the image was cropped to remove extraneous lanes. **C)** Pulse-chase analysis was performed by infecting DBT cells at an MOI=10 PFU/cell. Proteins were radiolabeled, and cell lysates were immunoprecipated with α-nsp1 and α-nsp2 antibodies. Viruses are indicated to the left of the gels, and the time of chase (in minutes) is indicated at the top of the gels.

Discussion

The results of this study demonstrate that it is possible for nsp2 to be encoded from alternate locations in the genome, either alone or in combination with ORF1a nsp2, and that alternate location or expression results in a range of effects on growth, expression, RNA synthesis, and localization. Of interest, it was recently reported that an nsp2-EGFP fusion protein could be expressed from the nonessential MHV ORF2b (Verheije et al., 2008). Although the replication phenotype of this virus was not reported, the result is consistent with this study and indicates that additional sites of nsp2 expression/duplication are tolerated. In these experiments, the modest growth defect of an nsp2 deletion is not complemented by expression from ORF1b or ORF4, suggesting that whatever function nsp2 serves, the timing and/or interactions resulting from expression between nsp1 and nsp3 are likely critical for its role. Specifically, it is known that nsp2 is detectable as an nsp2-3 intermediate and that abolition of processing of nsp2 from nsp3 results in a prolonged eclipse phase, while abolition of processing between nsp1 and nsp2 results in diminished growth (Denison et al., 2004; Graham and Denison, 2006). This was consistent with the observation that addition of amino acids to the N-terminus had no effect on processing and had wild-type growth, while addition of residues to the C-terminus of nsp2 altered processing and eclipse phase, but not peak viral growth. Thus, the results suggest nsp2 may serve as an important *cis* regulatory protein for nsp1 and nsp3. The results also indicate that protein processing is also a determinant of nsp2 and/or nsp3 function(s).

This report also demonstrates that the expression of nsp2 from alternate locations in the genome has no effect on its recruitment to replication complexes. However,

encoding nsp2 at both its native location and in place of ORF4 resulted in overexpression of nsp2 and altered its localization. Although nsp2 still localized to replication complexes, overexpression of nsp2 also resulted in nsp2 to be detected as diffuse fluorescence throughout the cytoplasm of infected cells, suggesting that it is possible to saturate replication complexes with nsp2 and potentially other nsps.

Since nsp2 is dispensable for replication, the results presented here cannot directly predict the rearrangement effects of essential replication proteins, such as nsp5 (3CLpro) or nsp12 (RdRp). However, these results have shown that additional protein sequence can be encoded not only in the downstream ORFs but also in the replicase between nsp13 and nsp14, suggesting flexibility in both ORF1a and ORF1b for deletion, introduction, and reordering of protein domains. Demonstration that an ORF1 protein can be expressed from alternate locations and can still target to replication complexes suggests that it will be possible to test the effects of alteration of location and extent of expression of critical replication proteins on virus viability, growth, and pathogenesis. These future studies are further addressed in Chapter V.

CHAPTER III

REWIRING THE MURINE HEPATITIS VIRUS REPLICASE POLYPROTEIN TO FUNCTION WITH A SINGLE PAPAIN-LIKE PROTEASE

Introduction

Before this project began, it was known that virus-encoded proteases of positive-sense RNA viruses are important regulators of their respective life cycles (Ryan and Flint, 1997; Vasiljeva et al., 2003; Ziebuhr, Snijder, and Gorbalenya, 2000). These specific proteases mediate co- and post-translational processing of large polyproteins, resulting in intermediate and mature proteins. The processing events are spatially and temporally regulated, allowing for diverse and distinct functions of intermediate and mature proteins at different stages of the life cycles of these particular viruses. While the cleavage site (CS) amino acid sequences and protease interactions have been identified and studied extensively *in vitro*, less is known about the requirements for processing in the context of complete polyprotein expression during virus replication. These studies are critical for our understanding of how and why these processing events occur and will aid in the establishment of new approaches to interfere with protein processing and attenuate virus replication and pathogenicity.

For coronaviruses, the proteolytic processing of the replicase polyprotein is complex (Fig. 3.1A and 3.1B). Protein processing occurs in a sequential fashion, and prior to the advent of coronavirus reverse genetics systems, it was not possible to study the roles of specific processing events on virus replication. The first study from the Denison lab after the invention of the MHV reverse genetics system addressed the CS

amino acid requirements for processing between nsp1 and nsp2 at CS1. This study showed that processing at CS1 was not required for virus replication; however, blocking cleavage, either by amino acid substitution or by deletion of the critical CS residues, of this processing event resulted in a decrease in virus growth, RNA synthesis, and cytopathic effect (Denison et al., 2004). The lab next addressed whether processing at CS2 was required for infectious virus. Deletion of CS2 resulted in viable virus with no decrease in peak virus titer, but did result in a delay in exponential growth. Due to both CS mutations resulting in viable virus, a mutant genome with deletions of both CS1 and CS2 was generated, and viable virus was recovered. This mutant virus displays no processing at the deleted CSs and manifests a reduction and delay in virus growth, exhibiting growth defects observed in both of the single CS deletion viruses.

Because CS1 and CS2 can be deleted and both are processed by PLP1, the protease activity of PLP1 was abolished, and this resulted in a virus that was severely impaired in growth. Moreover, PLP2 did not process at CS1 or CS2 (Graham and Denison, 2006). In contrast, ablation of PLP1 activity of HCoV-229E revealed that PLP2 was capable of processing at CS1 and CS2 (Ziebuhr et al., 2007). This outcome may be due to the fact that there is more similarity between CSs of HCoV-229E than that of CSs 1-3 of MHV (Fig. 3.1C). Even though both PLP1 and PLP2 of HCoV-229E can process at CS1 and CS2, PLP2 exhibited less efficient processing at CS1 than that of PLP1 but more efficient processing at CS2 than that of PLP1, most likely due to the recognition of proximal CS amino acid sequences by the particular PLP. Unlike MHV and HCoV-229E, SARS-CoV PLpro processes at the first three CSs (Harcourt et al., 2004), all of which have a P4-LXGG-P1 amino acid motif. Similar to SARS-CoV PLpro, MHV PLP2

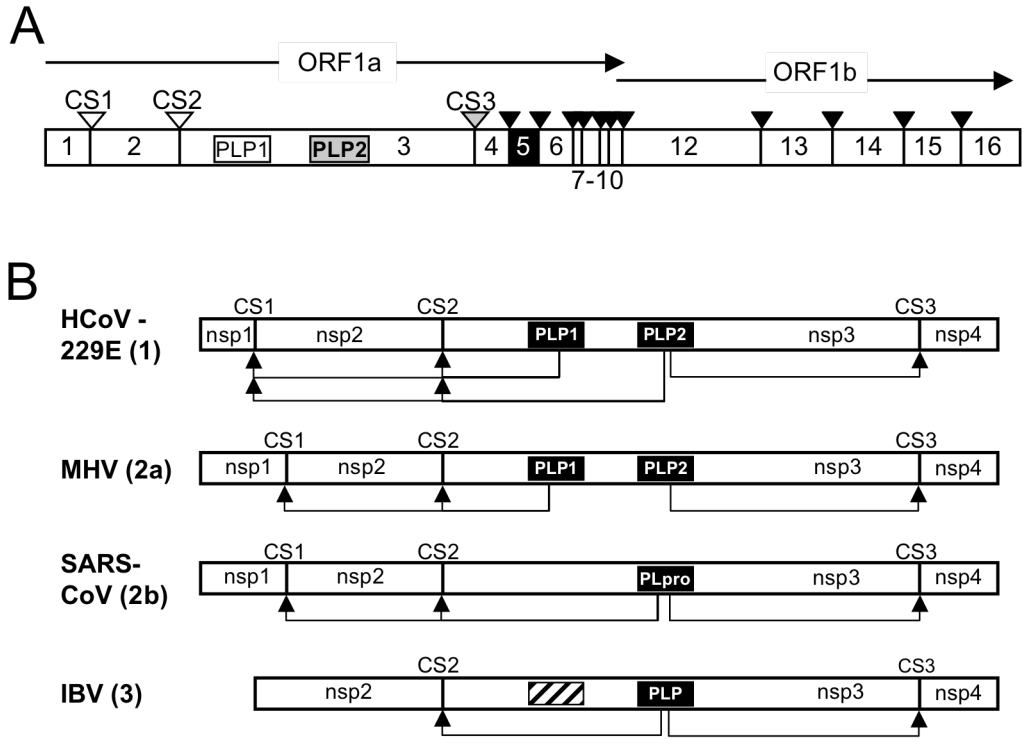

C

Virus		P6	P5	P4	P3	P2	P1	P1'	Protease
HCoV-229E	CS1	G	K	R	G	G	G	N	PLP1/PLP2
(Group 1)	CS2	F	T	K	A	A	G	G	PLP1/PLP2
	CS3	V	A	K	Q	G	A	G	PLP1/PLP2
MHV	CS1	L	K	G	Y	R	G	V	PLP1
(Group 2a)	CS2	W	R	F	P	C	A	G	PLP1
	CS3	F	S	L	K	G	G	A	PLP2
SARS-CoV	CS1	R	E	L	N	G	G	A	PLpro
(Group 2b)	CS2	F	R	L	K	G	G	A	PLpro
	CS3	I	S	L	K	G	G	K	PLpro
IBV	CS2	V	V	C	K	A	G	G	PLP2
(Group 3)	CS3	V	E	K	K	A	G	G	PLP2

Fig. 3.1. MHV replicase organization and comparisons of coronavirus PLP-mediated processing. **(A)** ORF1, or the replicase gene, encodes the replicase polyprotein which is translated into pp1a, or because of a -1 ribosomal frameshift pp1ab. Pp1ab is processed into 16 mature nsps that are indicated by vertical lines and numbers. Viral PLP domains are shown as boxes within nsp3, and 3CLpro (nsp5) is indicated as a black box. Arrowheads and vertical lines represent cleavage sites. PLP1 cleavage sites are linked in white, the PLP2 cleavage site is linked in gray, and the 3CLpro cleavage sites are linked in black. **(B)** Organization of nsp1 to nsp4 is shown for coronaviruses representing the major groups (1, 2a, 2b, and 3). PLPs are indicated by black boxes, and a hatched box indicates a catalytically inactive remnant of PLP1 from IBV. Processing events that have been confirmed *in vitro* or during infection are indicated by arrows. **(C)** The cleavage site amino acid sequences of the coronaviruses listed in panel B are shown from P6 to P1' with the PLP predicted or responsible for processing shown in the right column. The arrow indicates the cleavage site.

cleaves directly downstream of an LXGG amino acid motif. Therefore, the observed variation in the number and activity of PLPs in processing of nsp1-4 is associated with predicted differences in PLP structure and predicted or known CS amino acid sequences. These associations in the number of encoded catalytically active PLPs, PLP structure, and CS amino acid sequences have not been tested mechanistically.

Modeling of different coronavirus PLP enzymes reveals two distinct classes (Sulea et al., 2006). The "restricted" class consists of SARS-CoV PLpro, both HCoV-229E PLP1 and PLP2, IBV PLP, and MHV PLP2. These enzymes are restricted in their substrate specificity and only recognize a small subset of amino acid sequences, with conservation of glycine or alanine in the two positions directly upstream of the peptide cleavage site (CS)(Harcourt et al., 2004; Herold et al., 1998; Lim and Liu, 1998; Lim, Ng, and Liu, 2000; Thiel et al., 2003). The "open" class consists of mainly coronavirus group 2a PLP1 enzymes and recognizes a wider array of substrate amino acid sequences, with a conserved small amino acid residue directly upstream of the CS (Bonilla et al., 1995; Bonilla, Hughes, and Weiss, 1997; Dong and Baker, 1994; Hughes, Bonilla, and Weiss, 1995; Schiller, Kanjanahaluethai, and Baker, 1998). Bioinformatics suggests that PLP specificity, the recognition, binding, and processing of a cleavage site (CS) by a protease, is controlled primarily by amino acids directly upstream of the CS (Sulea et al., 2006). In coronaviruses that possess only one PLP or two restricted-class PLPs, the predicted or confirmed CS amino acid sequences are highly conserved between all CSs recognized by the PLP(s). This is consistent with SARS-CoV PLP-mediated processing and the report from HCoV-229E in that PLP2 was capable of processing CS1 and CS2. In coronaviruses, such as murine hepatitis virus (MHV), that possess both open and

restricted forms of PLPs, CS amino acid sequences are divergent across the CSs, consistent with the report above in which PLP2 was not capable of processing the more divergent CS amino acid sequences of CS1 and CS2. Therefore, it is predicted that only one PLP is necessary to process three CSs that are highly conserved, while two PLPs are necessary for processing at multiple divergent CSs. However, it is unknown if proximal CS amino acid sequences are sufficient for PLP-mediated processing and if protease recognition and processing can be switched by altering CSs.

In the previous work from the Denison lab and Chapter II, amino acid substitutions at CS1 and CS2 were tested to determine the amino acid requirements for PLP1-mediated processing at the specific CSs. Because there is flexibility in processing at the CS amino acid sequences and the number of PLPs varies among coronaviruses, the next area of investigation that was addressed examined the role of CS/PLP interactions. Particularly, this study sought to determine the effect of encoding one or two catalytically active PLPs, investigate the requirements for CS recognition and processing by PLPs, and test whether protease specificity could be switched by substitution of CS amino acid sequences. Replacement of the MHV PLP1 "open" P4-P1 amino acid sequence of CS1 and/or CS2 with the "closed" PLP P4-P1 LKGG sequence from MHV CS3 was introduced in the presence of an active or inactive PLP1. Mutant viruses were recovered with altered protein processing and a range in growth from WT to highly impaired. Substitution of CS3 at CS2 was sufficient for a switch in protease specificity and allowed processing by PLP2, resulting in a virus capable of WT replication in culture. While there was processing at CS2 substituted with CS3, there was no detectable processing at CS1 substituted with CS3. These results demonstrate that P4-P1 CS amino acid

sequences are important determinants of PLP specificity in recognition and processing during virus replication, but also indicate that other determinants are involved in the regulation of PLP-mediated processing and maturation of intermediate and mature nsps 1-3.

Generation and recovery of CS replacement viruses

While the C-terminal half of nsp1 and all of nsp2 are dispensable for replication, alterations of CS/PLP interactions can be highly detrimental for MHV replication or protein processing (Graham and Denison, 2006; Kanjanahaluethai and Baker, 2000). To determine the effect of alteration of the P4-P1 residues of CS1 and CS2, mutations were introduced into the MHV genome that resulted in substitutions of CS1 and/or CS2 with the P4-LKGG-P1 amino acid sequence of CS3, resulting in mutants CS1(3), CS2(3) and the dual cleavage-site mutant CS1/2(3) (Table 3.1). These mutations also were introduced into a catalytically inactive PLP1 (P1ko) background (Graham and Denison, 2006)(Fig. 3.2). Cells were electroporated with genomic RNA for CS1(3), CS2(3), CS1/2(3), and CS1/2(3)+P1ko. The single CS replacement mutant viruses, CS1(3) and CS2(3), exhibited cytopathic effect (CPE) by 24 h post-electroporation, and 90 to 100% of cells were involved in syncytia by 44 h post-electroporation, similar to WT virus. For the double CS replacement viruses, CS1/2(3) and CS1/2(3)+P1ko, CPE was observed by 36 h post-electroporation, and all cells were involved in syncytia by 54 h post-electroporation, exhibiting a delay in CPE compared to WT virus. When passage 1 (P1) virus stocks were sequenced across the cleavage sites and PLP1, all viruses retained the engineered mutations and no other mutations were identified within 300 nucleotides

flanking each side of the cleavage site. The CS1/2(3)+P1ko mutant virus also retained the introduced C1121A/T1122A substitutions that inactivate PLP1 catalytic activity (Graham and Denison, 2006). The results demonstrated that substitutions of the P4-P1 residues at CS1 and CS2 allow recovery of viable viruses and are not required for replication.

All of the above mutants were recovered on initial attempts using the reverse genetics approach for recovery. The engineered substitution of the individual CS1(3) and CS2(3) substitutions in the P1ko background (CS1(3)+P1ko and CS2(3)+P1ko) were also tested for recovery. In dramatic contrast to all other mutants, the CS1(3)+P1ko and CS2(3)+P1ko mutants could not be recovered following multiple attempts by separate investigators in the lab. In addition, no virus could be recovered even after >1 week of blind passage of electroporated cells, a strategy that was successful for the previously reported highly debilitated P1ko mutant (Graham and Denison, 2006). The results indicate that in the setting of P1ko, substitution of both CS1(3) and CS2(3) is necessary for effective virus recovery and productive infection. In combination with the recovered viable mutants, the results suggest that there is cooperative activity between CS1, CS2, and PLP1, or that retention of an intact CS1 or CS2 results in altered interactions with inactivated PLP1 that hinder PLP2 activity or other functions of nsp1, 2, or 3.

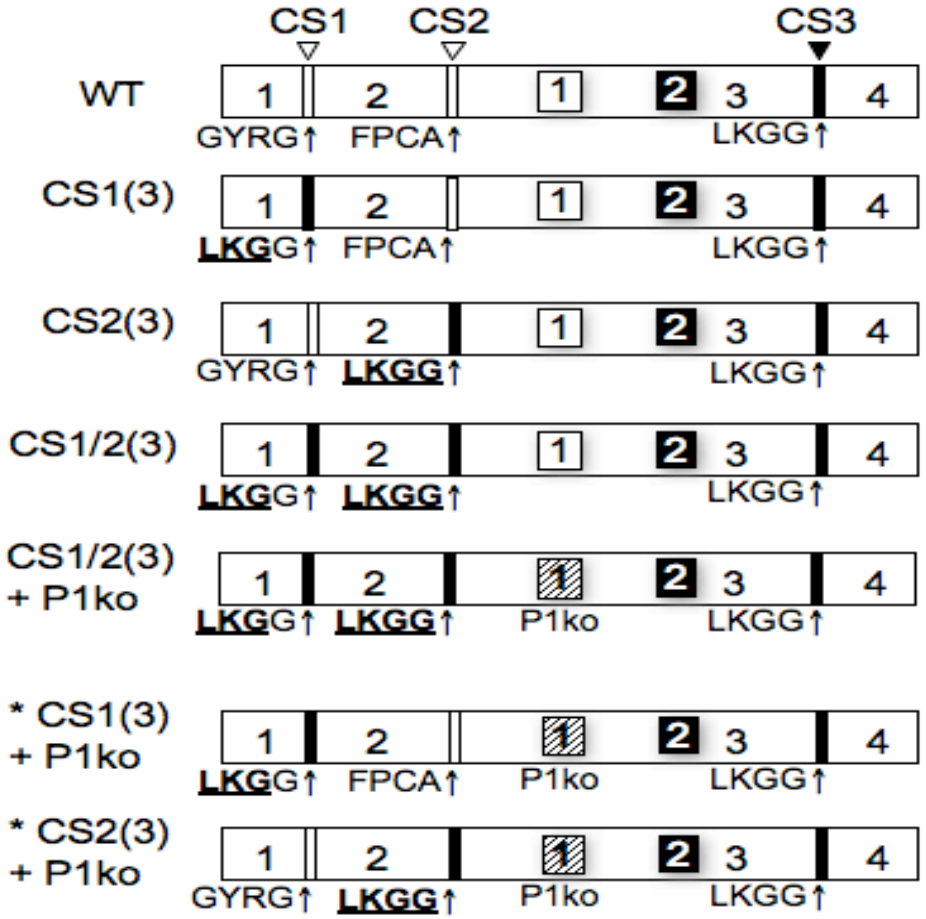

Fig. 3.2. Engineering of cleavage site substitution viruses. The CS substitution viruses were engineered to replace the original CS amino acid sequences at CS1 and/or CS2 with that of the CS3 amino acid sequence P4-LKGG-P1. Both CS substitutions were also engineered into a PLP1ko (P1ko) background. PLPs are shown as numbers in white (PLP1) or black (PLP2) boxes in nsp3. Engineered catalytically inactivated PLP1 is shown as a gray hatched box. Arrowheads indicate cleavage events of WT virus and are linked by white (PLP1) or black (PLP2). P4 through P1 amino acid residues for each CS are shown below each diagram. White and black vertical bars show respective predicted PLP1 and PLP2 cleavage sites. Engineered substitutions are indicated by underlined amino acid sequences. * indicates engineered mutant genomes that could not be recovered as infectious virus (see results). All other mutants were recovered in cell culture.

Table 3.1. Mutagenesis of CS1 and CS2 Substitutions with L-K-G-G Amino Acid Sequences

Primer Name	Sequence	Purpose
CS1(3) Sense	5'-CGT ATG CTC TTC TTA AG**C TTA AAG GG**G GTG TTA AGC CCA TC-3'	Mutagenesis for CS1(3)
CS1(3) Antisense	5'-GAT GGG CTT AAC ACC**CCC TTT AAG** CTT AAG AAG AGC ATA CG-3'	Mutagenesis for CS1(3)
158 Sense	5'-TCC GGC TCG TAT GTT GTG TGG AAT-3'	CS1(3) Splice Overlap Primer
3253 Antisense	5'-CTG CGT CAA GCA CAA CAT CAA GCA-3'	CS1(3) Splice Overlap Primer
CS2(3) Sense	5'P-**GGG GGC** GGC AAG AAA GTC GAG TTT AAC GAC AAG-3'	Mutagenesis for CS2(3)
CS2(3) Antisense	5'-**TTT AAG** CCT CCA GCA CTG ATC TAA CAC GCC AAC-3'	Mutagenesis for CS2(3)

*Bold and Underlined nucleotides are used to show the introduced nucleotides for cleavage site substitutions.
*Only substitution of nine nucleotides were needed for CS1(3) due to a Gly codon in the P1 position of CS1.

Single CS replacement viruses have altered protein processing

To determine the effects of substituting the CS3 LKGG amino acid sequence, the predicted MHV PLP2 recognition sequence, at CS1 or CS2 on protein processing, DBT cells were either mock-infected or infected with WT or the single CS substitution viruses, and cells were then labeled with [^{35}S]Met-Cys. Cytoplasmic lysates of infected cells were immunoprecipitated with antibodies against nsp1 (28 kDa), nsp2 (65 kDa), nsp3 (210 kDa), and the 3CLpro-processed nsp8 (22 kDa). For WT virus, all nsps tested were detected in their mature form, as well as an nsp2-3 precursor that has been previously described (Fig. 3.3A and 3.3B)(Graham and Denison, 2006; Graham et al., 2006). The ΔCS1 virus (Denison et al., 2004), where the two amino acids upstream and one amino acid downstream of CS1 were deleted, was used as a control for comparison of the processing phenotype of the CS1(3) mutant virus. The ΔCS1 and the CS1(3) mutant virus exhibited identical protein processing phenotypes, and each virus produced mature nsp3 and nsp8, confirming that catalytic activity of all three proteases was intact. Unlike WT virus, both the ΔCS1 and CS1(3) mutant viruses exhibited nsp1-2 and nsp1-2-3 fusion proteins and lacked detection of mature nsp1, suggesting that the LKGG amino acid sequence substituted at CS1 is not processed by either PLP1 or PLP2.

Similar to WT virus, all nsps that were tested by immunoprecipitation were detected in their mature form for the CS2(3) mutant virus. Also, an nsp2-3 intermediate protein was detected in the CS2(3) virus, which is seen in WT, and there was no detection of any other precursor or intermediate proteins. Unlike the ΔCS2 mutant virus (Graham and Denison, 2006), where the P2 through P1' residues of the CS amino acid sequence were deleted and which exhibits no detection of mature nsp2 or nsp3, the CS2(3) virus is

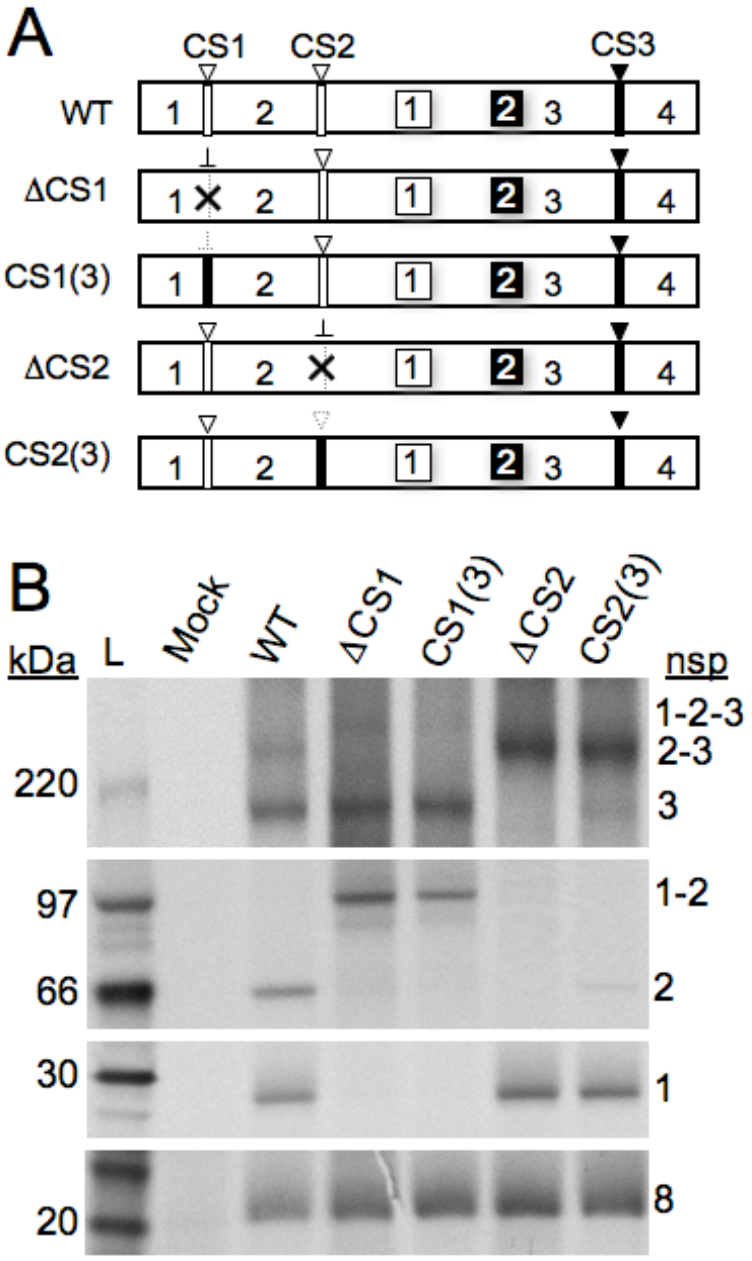

Fig. 3.3. Protein processing of single CS substitution viruses. A) Schematics show patterns of WT and mutant virus protein processing from results in panel **B**. Mutations that were introduced into mutant viruses, cleavage sites, P4-P1 residues and PLPs are as in Fig. 3.2. **X**'s and vertical dashed lines indicate CS deletions where the P2 through P1' amino acids were deleted. A dashed white arrowhead indicates reduced cleavage and protease not determined. ⊥ indicates no cleavage. A dashed ⊥ indicates possible but non-detected cleavage. **B)** Lysates from radiolabeled infected DBT cells were immunoprecipitated with α-nsp1, α-nsp2, α-nsp3, or α-nsp8 as indicated and resolved by 4 to 12% SDS-PAGE and imaged by fluorography. Mature (nsp1, 2, 3, 8), intermediate (nsp2-3), and non-cleaved proteins (nsp1-2-3, and nsp1-2) are indicated at the right of the gels, with molecular mass markers at the left. L, ladder. Mock, mock-infected cells. All images were obtained from a single experiment with separate gels for nsp 1, 2, 3 and 8 immunoprecipitations, and were equivalently treated and exposed to film.

capable of processing nsp2 and nsp3 into their mature forms. However, mature nsp2 and nsp3 in the CS2(3) mutant were present at reduced levels compared to WT virus. Interestingly, the nsp2-3 intermediate protein was detected at higher levels in the CS2(3) mutant virus than that of WT virus. For the CS2(3) virus, the abundance of the nsp2-3 precursor correlated with reduced levels of mature nsp2 and nsp3, while the abundance of mature nsp2 and nsp3 correlated with a reduction in the nsp2-3 precursor seen in WT virus. These data indicate that processing occurs at the LKGG amino acid sequence at CS2, albeit at reduced efficiency compared to WT virus. These data do not indicate, however, which PLP processes at the mutated cleavage site. The results also suggest that there is significant flexibility at CS2 in PLP recognition and processing of the cleavage site, while there is less flexibility in recognition and processing at CS1.

CS1(3) and CS2(3) mutant viruses exhibit varied phenotypes in single-cycle growth experiments

Viral growth experiments were performed to determine if defects in protein processing exhibited by the CS1(3) and CS2(3) mutant viruses were associated with impairments in virus replication (Fig. 3.4). DBT cells were infected at multiplicities of infection (MOIs) of 1 and 0.05 PFU/cell, supernatant was harvested at various times from 1 to 30 h p.i., and virus titers were determined by plaque assay. In single-cycle growth experiments, the CS1(3) mutant virus exhibited exponential growth similar to WT and ΔCS1 mutant viruses (Fig. 3.4A). The CS1(3) mutant virus also displayed a decrease in growth from 4 to 10 h p.i. compared to WT virus. Unlike the ΔCS1 virus which reaches peak titers approximately 10-fold less than WT virus, the CS1(3) virus reaches peak titers

similar to WT virus at 12 h p.i. To determine the extent of the growth defects exhibited between 4 and 10 h p.i. in the CS1(3) mutant virus, I next tested if the CS1(3) virus exhibited more profound growth defects at a lower MOI (Fig. 3.4B). In contrast to the single-cycle growth experiment, the CS1(3) virus did not reach WT titers, exhibiting a 0.5 $\log_{10}$ reduction. The CS1(3) virus also displayed an approximate 0.5 $\log_{10}$ increase in peak titers compared to the ΔCS1 mutant virus. Lastly, WT, ΔCS1, and CS1(3) viruses all displayed similar growth kinetics at a low MOI. These results also indicate that deletion of CS1 has an increased impairment on growth than that of substitution of the native G-Y-R-G amino acid sequence for the CS3 LKGG amino acid sequence.

Similar to the CS1(3) mutant virus, the CS2(3) mutant virus grew similar to WT and reached peak titers at 12 h p.i., but the CS2(3) mutant virus also exhibited a slight decrease in growth at 8 h p.i. compared to WT virus (Fig. 3.4C). The ΔCS2 mutant virus was used as a control and exhibited an approximate 4 h delay in the exponential phase of growth but still reached WT titers. To examine whether the CS2(3) virus displays replication defects that are not observed in single-cycle growth experiments, growth assays were performed at a low MOI (Fig. 3.4D). Unlike the CS1(3) mutant virus which had greater replication defects at a lower MOI, the CS2(3) virus grew indistinguishable from WT virus. These findings indicate that replacement of the CS2 F-P-C-A amino acid sequence by the CS3 LKGG amino acid sequence has no effect on overall virus growth, even though there is reduced processing at the mutated CS (Fig. 3.3B).

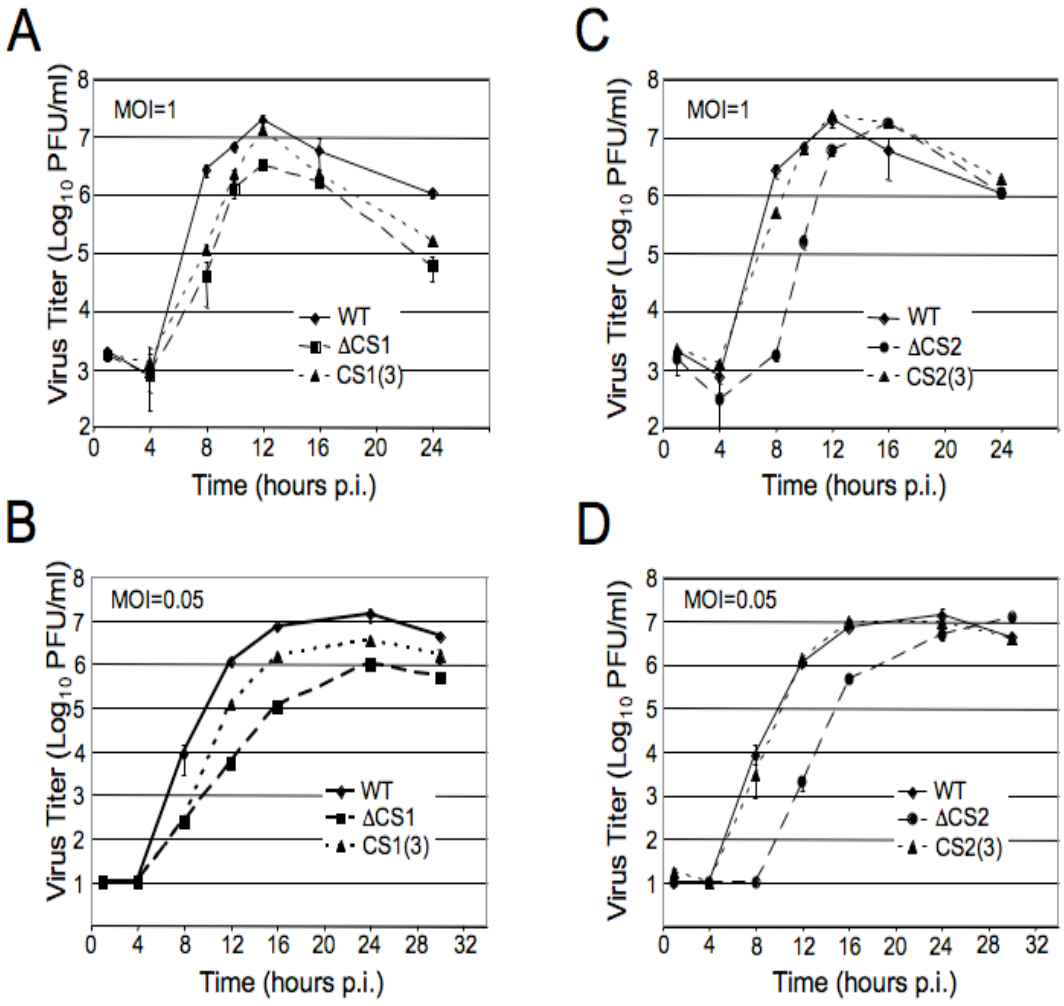

Fig. 3.4. Growth analysis of single CS substitution viruses. DBT cells were infected with the indicated viruses for either single cycle growth (MOI of 1 PFU/cell) or multiple cycle growth (MOI of 0.05 PFU/cell) experiments, and titers were determined by plaque assay. Samples of virus supernatants were collected at predetermined time points between 1 and 30 h p.i. **(A)** Single cycle growth of the CS1(3) mutant virus. **(B)** Multiple cycle growth of the CS1(3) virus. **(C)** Single cycle growth of the CS2(3) mutant virus. **(D)** Multiple cycle growth of the CS2(3) virus. The ΔCS1 and ΔCS2 viruses were used as controls in the growth experiments. Data points indicate the hours when media was harvested for determining titer. Error bars represent standard deviation between samples.

MHV PLP2 processes at CS2 with an LKGG amino acid motif

Because CS1(3) and CS2(3) mutant viruses were viable and to determine if PLP2 can process at altered CS1 and CS2 with LKGG amino acid substitutions, mutant viruses were engineered to contain the LKGG amino acid sequence at both CS1 and CS2 in the presence or absence of a catalytically active PLP1(Fig. 3.5A). To examine the protein processing phenotypes of CS1/2(3) and CS1/2(3)+P1ko viruses, protein immunoprecipitations were performed on radiolabeled, infected cell lysates, and samples were subjected to SDS-PAGE and exposed to film (Fig. 3.5B and 3.5C). Mutant viruses that had deletions of CS1 and CS2 (ΔCS1/2) and both the deletions of CS1 and CS2 in the presence of a catalytically inactivated PLP1 (ΔCS1/2+P1ko) were used as controls(Graham and Denison, 2006). In contrast to WT, nsp1, 2, and 3 proteins and precursors were much less abundantly detected, even after prolonged labeling for all mutant viruses tested. Since nsp8 was detected, the preceding proteins were translated in at least equivalent amounts, thus, their lesser detection could result from aberrant folding, lack of availability of antibody epitopes, or possibly due to degradation. Nevertheless, it was still possible to discern different patterns of processing. Both the ΔCS1/2 and ΔCS1/2+P1ko mutant viruses exhibited identical protein processing phenotypes, displaying an nsp1-2-3 fusion protein and mature nsp8, which was used to show that 3CLpro processing activity remained intact. The CS1/2(3) and CS1/2(3)+P1ko mutant viruses exhibited identical protein processing patterns when compared to one another. Similar to the CS deletion viruses, both the double CS replacement viruses displayed detection of mature nsp8 and an nsp1-2-3 precursor protein. Like WT virus, mature nsp3 was detected in the double CS replacement viruses, confirming that PLP2 catalytic

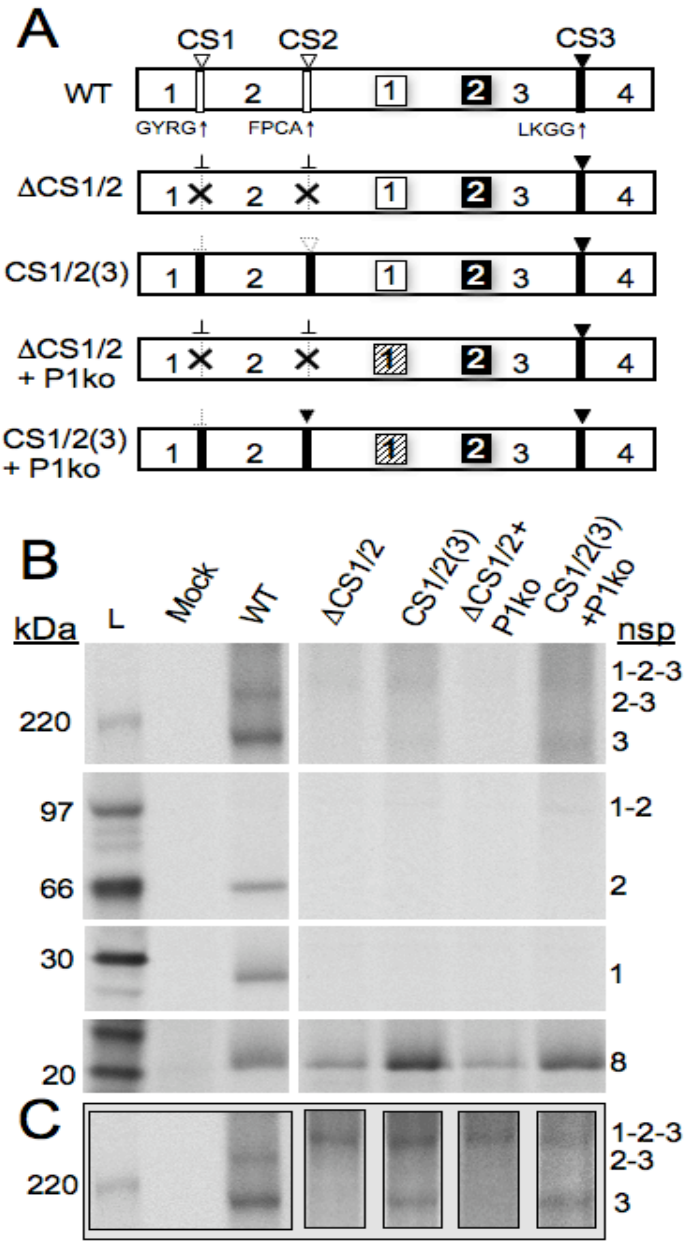

Fig. 3.5. Protein processing of double CS substitution viruses. A) Schematics are shown of WT and mutant viruses that were used in the protein processing experiments shown in the gels below. Notation for schematics is as in Figures 2 and 3. **B) and C)** DBT cells were either mock-infected or infected with the viruses indicated above the gels. Cells were grown in the absence of Met and Cys for 1 h starting at 5 h p.i., and proteins were radiolabeled for WT infection until 80% of cells exhibited CPE or for a total of 8 h. Cell lysates were immunoprecipitated with α-nsp1, α-nsp2, α-nsp3, or α-nsp8. The indicated mature, intermediate, and fusion proteins are indicated at the right of the gels. Molecular weights in kDa are shown at the left. All images in B were obtained from multiple gels from a single experiment with identical exposures. No modifications to the gels were performed. **C)** Lanes from top panel in B were individually adjusted for brightness and contrast for exposure of nsp3 to show relationships of nsp1-2-3, nsp2-3, and nsp3.

activity was intact. Unlike that of WT virus, no mature nsp1, nsp2, or nsp2-3 intermediate proteins were detected in the CS replacement viruses. Unlike that of WT and double CS deletion viruses, the double CS replacement viruses also displayed detection of an nsp1-2 fusion protein. Because the CS1/2(3)+P1ko mutant virus exhibited an nsp1-2 fusion protein and mature nsp3, protein processing occurs at the substituted CS3 amino acid sequence LKGG at the second CS position. Due to inactivation of the PLP1 catalytic activity in the CS1/2(3)+P1ko virus, PLP2 is capable of processing the substituted CS3 amino acid sequence at the CS2 position. However, there was no detection of mature nsp1 in the CS1/2(3)+P1ko virus, suggesting that PLP2 does not cleave at CS1 substituted with an LKGG amino acid motif.

Double CS replacement viruses exhibit both delays and decreases in virus growth

Since the double CS replacement viruses were viable and exhibited altered processing phenotypes compared to WT and the double CS deletion viruses, I analyzed the effects of altered processing on the growth of the double CS replacement viruses at an MOI of 1 PFU/cell (Fig. 3.6A). The CS1/2(3) and CS1/2(3)+P1ko mutant viruses displayed identical growth, exhibiting a 4 h lag in exponential growth and a slight decrease in peak titers compared to WT virus. Growth analysis was not performed at a high MOI with the control ΔCS1/2 and ΔCS1/2+P1ko viruses due to the low titers of both stocks; therefore, an MOI of 0.05 was used to analyze and compare growth between the double CS replacement viruses and the double CS deletion viruses in multiple rounds of infection (Fig. 3.6B). Similar to an MOI of 1 PFU/cell, the double CS replacement viruses grew indistinguishable from each other and exhibited a 4 h lag and a 0.5 $\log_{10}$

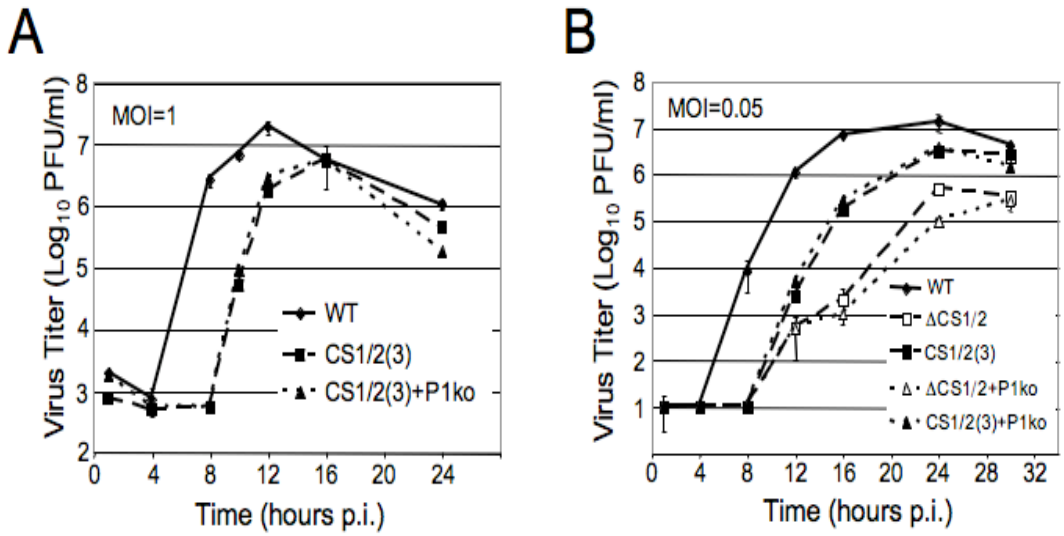

Fig. 3.6. Growth analysis of double CS substitution viruses. DBT cells were either infected with WT or double CS substitution viruses for growth analysis. Samples of virus supernatants were collected at predetermined time points between 1 and 30 h p.i. **(A)** Single cycle growth (MOI of 1 PFU/cell). **(B)** Multiple cycle growth (MOI of 0.05 PFU/cell). The double CS deletion viruses were used as controls in the growth expereiment shown in panel B. Data points represent the titer from media harvested at the indicated time points. The double CS substitution viruses and their CS deletion counterparts are linked in boxes and triangles with identical dashed lines for clarity. Error bars represent standard deviation of the mean between samples.

reduction in peak titer compared to WT virus. The double CS replacement viruses exhibited the same delay in exponential growth as the double CS deletion viruses; however, peak titers were approximately 1 $\log_{10}$ higher in the CS replacement viruses. Also, introduction of catalytically inactive PLP1 had no affect on growth of the double CS replacement virus. This growth analysis demonstrates that replacing both CS1 and CS2 with an LKGG amino acid motif results in more robust growth than that of the double CS deletion viruses, but the double CS replacement viruses have reduced growth fitness compared to either replacing CS1 or CS2 amino acid sequences alone (Fig. 3.4).

Discussion

To determine if requirements other than CSs and PLPs are necessary for protein processing of nsps 1-3 of MHV, we tested whether replacement of proximal CS amino acid residues was sufficient to switch PLP specificity and if the CS substitutions affected virus growth and the regulation and processing of intermediate and mature proteins of MHV. In this report, we have demonstrated that MHV PLP2 is capable of processing directly downstream of its recognition sequence, P4-LKGG-P1, at a different location in the replicase polyprotein. Specifically, substitution of the LKGG amino acid sequence for FPCA at CS2 allows processing by PLP2, albeit at reduced efficiency compared to processing at the natural location in WT virus. Although processing occurred at the LKGG amino acid sequence at CS2, there was no detection of processing at CS1 that was substituted with the LKGG motif. Therefore, it is possible to switch protease specificity with the proximal CS recognition sequence; however, other determinants, besides the

proximal CS amino acid sequence, are required for PLP recognition and/or efficient processing.

The altered processing phenotypes of the CS substitutions resulted in differential effects on virus growth. The CS1(3) virus, where CS3 was substituted at the CS1 position in the genome, exhibited no detectable signs of processing at the mutated cleavage site, yet virus growth is more robust than that of the ΔCS1 mutant virus. This suggests two possibilities for the increased growth fitness. First, the substituted LKGG sequence at CS1 alters the nsp1-2 fusion protein and allows for more intact functions of the fused nsp1-2 protein than deletion of CS1. Alternatively, protein processing at the substituted LKGG amino acid motif at CS1 may be occurring at levels below the limit of detection but sufficient to enhance replication fitness. Also, the CS1(3) virus and the double CS replacement viruses have similar processing patterns, reach similar peak titers, yet the double CS replacements exhibit a delay in exponential growth, suggesting CS1 and CS2 may function cooperatively or as a unit and defects in processing at both CS1 and CS2 result in the additive detrimental effects on processing and virus replication.

A previously published report from our lab has shown that the catalytic inactivation of PLP1 alone results in recovery of a virus that exhibits severely debilitated growth, reaching peak titers 5 to 6 $\log_{10}$ PFU/ml less than WT virus (Graham and Denison, 2006). In the present study, the introduction of a catalytically inactive PLP1 into the background of either the double CS replacement or the double CS deletion viruses has no effect on processing or growth when compared to the double CS replacement or double CS deletion viruses with intact PLP1 activity. This data suggests that either deletion or CS substitution of CS1 and CS2 blocks the recognition and binding of PLP1

with the altered CS. This data also suggests that the ablation of the catalytic activity of PLP1 does not influence recognition and binding of the PLP with its respective CSs. Therefore, we speculate that the inactivated PLP could still bind the native CSs but not cleave the recognized amino acid sequences, resulting in prolonged or irreversible binding of the inactive PLP1 with the native CSs, thus impairing nsps 1-3 functions. This possibility is supported by the comparison of the severely debilitated growth seen in the P1ko and increased growth observed in the ΔCS1/2+P1ko and CS1/2(3)+P1ko viruses (Graham and Denison, 2006). This model also could explain our inability to recover the CS1(3) + PL1ko and CS2(3) + PL1ko mutant viruses, where one intact PLP1 CS may interact with inactive PLP1 to alter nsp1-2-3 folding, processing, and function. Future studies will test this model by deletion of the PLP1 domain of nsp3 or the PLP1 substrate binding and catalytic residues in the setting of combinations of intact, deleted, and substituted, CS1, CS2, and CS3.

PLP-mediated processing at substituted cleavage sites. The observed defects in protein processing exhibited by the CS substitution viruses may be due to several potential factors. One potential model is that MHV PLP2 requires more than the proximal LXGG amino acid motif for efficient recognition and/or processing at CSs. *In vitro* analysis of SARS-CoV PLpro demonstrated that an LXGG amino acid sequence was both necessary and sufficient for PLpro processing (Barretto et al., 2005). MHV PLP2 and SARS-CoV PLpro share 32% identity and 44% amino acid sequence similarity, and structural modeling of MHV PLP2 based on SARS-CoV PLpro crystal structure predicted similar structures and substrate binding pockets (Sulea et al., 2006). However, *in vitro* analysis of MHV CS3 demonstrated that a P6 Phe-to-Ala substitution

inhibited PLP2 processing at CS3 (Kanjanahaluethai, Jukneliene, and Baker, 2003). Since only Ala substitution was tested at the P6 position, it remains unknown if P6 Phe is absolutely required for WT-like processing by PLP2 at CS3. Our engineered CS1(3) has a P6-Trp, while CS2(3) has a P6-Leu. We can conclude that P6-Leu allows processing by PLP2 following LKGG. Our system will allow us to determine whether differences in P6 or other residues affect PLP2 recognition and cleavage at CS1 and CS2, for example by substituting Trp, Leu or Phe at each location. Additionally, it may be possible to use adaptive passage of the debilitated CS1/2(3) mutants with and without P1ko to recapitulate the evolution of an optimal protease/cleavage site interaction.

Coronaviruses: one or two PLPs? While at least one PLP domain is absolutely conserved among coronaviruses, two PLP domains are only conserved in the group 1 and group 2a coronaviruses. In these coronavirus groups, CS amino acid sequences are more divergent and potentially need two PLPs to efficiently process nsps 1-3. This led to the hypothesis that proximal CS amino acid sequences were the major determinant for PLP recognition and processing. Our results, however, show that CS amino acid sequences are not the only determinants for PLP recognition and processing and encoding one or two active PLPs within nsp3. The requirement of one or two active PLPs may be due to other functions of the PLP enzymes. In addition to processing nsps 1-3, coronavirus PLPs have been shown to be multifunctional enzymes. Both SARS-CoV PLpro and MHV PLP2 are potent inhibitors of type I interferon production (Lindner et al., 2005; Zheng et al., 2008), suggesting that these enzymes may also promote viral growth in infected hosts. Also, both of these enzymes, as well as PLP2 from HCoV-NL63, have shown to be deubiquitinating enzymes (Barretto et al., 2005; Chen et al., 2007; Lindner et

al., 2005; Zheng et al., 2008). This function of SARS-CoV PLpro, HCoV-NL63 PLP2, and MHV PLP2 suggests that coronaviruses employ a strategy to hijack or modulate the host cell ubiquitination machinery to help support virus replication. While functions of SARS-CoV PLpro, HCoV-NL63 PLP2, and MHV PLP2 domains have been studied, little is known about possible functions of PLP1 domains, besides their roles in polyprotein processing. Therefore, group 1 and 2a coronaviruses may encode PLP1 enzymes that have multiple functions, which are beneficial to virus replication in their particular host. The use of one or two PLPs is consistent within phylogenetic coronavirus groups, even within more closely related, recently defined subgroups such as 2a (MHV) and 2b (SARS-CoV). It is reasonable to speculate that paralogous duplication or loss of a second PLP and correlated alteration of cleavage site specificity could represent an important evolutionary event in the divergence and adaptation of coronaviruses (Ziebuhr, Thiel, and Gorbalenya, 2001).

To date, this is the first report to test the effects of switching RNA virus polyprotein CS recognition sequences, which resulted in processing by a different viral protease, on replication and protein processing. While the engineered MHV viruses resemble the relationship of CSs and protease activities of SARS-CoV nsps 1-3, the engineered mutations were detrimental for MHV replication. Both the findings that protease specificity can be altered and that the alteration of cleavage site/protease interactions are detrimental to virus replication suggest that the MHV mutants may be powerful tools to study the implications of rewiring coronavirus nsps 1-3 and altering protease specificity on virus replication, pathogenesis, and attenuation. These potential future directions will be discussed in detail in Chapter V.

CHAPTER IV

MURINE HEPATITIS VIRUS NSP4 REGULATES VIRUS-INDUCED MEMBRANE MODIFICATIONS AND REPLICATION COMPLEX FUNCTION

Introduction

Coronavirus nsps 1-4 are intricately linked by PLP-mediated processing, and these processing events are important for regulating the functions of intermediate and mature proteins during the virus life cycle, including the timing and formation of replication complexes.

All positive-strand RNA viruses rely on host intracellular membranes to form replication complexes, which are defined as the sites of viral RNA synthesis (Denison, 2008; Novoa et al., 2005; Restrepo-Hartwig and Ahlquist, 1996; Salonen, Ahola, and Kaariainen, 2005; Schaad, Jensen, and Carrington, 1997). These virus-induced membrane modifications are critical for creating an environment that supports viral RNA synthesis, as well as protecting newly-synthesized viral RNA. For many positive-strand RNA viruses, specific replicase proteins, often containing multiple hydrophobic domains, have been implicated in targeting to and modifying host membranes, ultimately leading to the formation of replication complexes. Analysis of amino acid sequences and *in vitro* biochemical studies of coronavirus nsps 3, 4, and 6 have shown that these three nsps all have transmembrane domains that are likely important for virus-induced membrane modifications (Baliji et al., 2009; Kanjanahaluethai et al., 2007; Lee et al., 1991). In this chapter, the role of MHV nsp4 was determined for several processes in the coronavirus life cycle through the utilization of multiple experimental approaches.

MHV nsp4 is processed by papain-like protease 2 (PLP2) at its amino terminus, resulting in an nsp4-10 precursor, and after this initial processing event, nsp5 (3Clpro) mediates processing at the carboxy terminus of nsp4 (Fig. 4.1A) (Gosert et al., 2002; Harcourt et al., 2004; Kanjanahaluethai and Baker, 2000; Kanjanahaluethai and Baker, 2001; Kanjanahaluethai, Jukneliene, and Baker, 2003). The predicted molecular mass of nsp4 is 56-kDa, but it is detected as a 44-kDa protein by SDS-PAGE (Kanjanahaluethai and Baker, 2001; Lu, Lu, and Denison, 1996).

All tested coronavirus nsps localize to replication complexes that are located on virus-induced double membrane vesicles (DMVs), and nsp4 has been proposed to play roles in the formation, organization, and function of these virus replication complexes (Gosert et al., 2002; Perlman and Netland, 2009). Nsp4 has been shown to associate with membrane fractions of infected cells and is resistant to membrane extraction following Triton X-114 treatment, indicating that nsp4 is an integral membrane protein (Gosert et al., 2002). Bioinformatics of MHV nsp4 amino acid sequence predicted that nsp4 has four transmembrane domains (TM1-4). MHV nsp4 has also been shown to be required for rescue of infectious virus (Sparks, Lu, and Denison, 2007), as well as TM1-3, but TM4 is dispensable for recovery of infectious virus in cell culture. Charge-to-alanine substitutions between TM1 and TM2 of nsp4 result in viruses with phenotypes ranging from non-recoverable to viruses that exhibit reduced virus growth, RNA synthesis, and protein processing (Sparks, Lu, and Denison, 2007).

Analysis of nsp4 from multiple coronaviruses across all coronavirus groups predicts N-linked glycosylation sites for all tested nsp4 sequences. The glycosylation sites, or sequons, Asn-X-Ser, Asn-X-Thr, and rarely Asn-X-Cys are amino acid

sequences that are recognized for glycosylation of the Asn (N) residue. Even though coronaviruses contain putative glycosylation sites within nsp4, there is little conservation of these sites between groups. Group 2a coronaviruses, such as MHV and human coronavirus HCoV-OC43, have two conserved putative N-linked glycosylation sites, N176 and N237 (Fig. 4.1B), while the group 2b SARS-CoV and group 3 Avian Infectious Bronchitis Virus (IBV), have different putative glycosylation sites, N131 or N48, respectively (Lim, Ng, and Liu, 2000; Oostra et al., 2007). Although the glycosylation of nsp4 from group 1 coronaviruses has not been investigated, residues N176 and N237 of MHV nsp4, N131 of SARS-CoV, and N48 of IBV nsp4 have been shown to be glycosylated when nsp4 is plasmid-expressed in cells or when nsp4 is expressed from non-native locations in the coronavirus genome (Clementz et al., 2008; Lim, Ng, and Liu, 2000; Oostra et al., 2007). Clementz et al. reported that N176 of MHV nsp4 is not required for virus replication, and that an N176A mutant virus grows identically to wild-type (wt) virus (Clementz et al., 2008). In that study, the N176A mutant virus-expressed nsp4 migrated faster than wt nsp4 by SDS-PAGE, consistent with altered protein modification such as loss of glycosylation. However, this was not further investigated in the study. In contrast, N237A and N176A/N237A mutant viruses could not be recovered.

Although these studies have led to an increased understanding of various aspects of nsp4, it remains unknown if N176 and/or N237 are glycosylated during infection and if the putative nsp4 glycosylation sites of MHV or other coronaviruses serve roles in membrane modifications or replication complex formation and function. In this study, I tested the glycosylation status of MHV nsp4, expressed from its native genomic location,

and the role of nsp4 glycosylation sites on virus growth, viral RNA synthesis, nsp4 localization, and replication complex morphology by engineering and recovering nsp4 mutants with alanine substitutions at N176 (N176A), N237 (N237A), or both (N176A/N237A). Results show that virus-expressed nsp4 is glycosylated at both N176 and N237 during infection, that glycosylation at either or both sites is dispensable for virus growth in cell culture, and that alanine substitution of N176, N237, or both results in defects in virus growth and RNA synthesis. Further, results demonstrate that loss of nsp4 glycosylation is associated with the presence of aberrant or disrupted double membrane vesicles (hereafter referred to as irregular DMVs) and increased prevalence of virus-induced convoluted membranes (CMs). The degree of irregular DMVs and increased CMs from the nsp4 mutant viruses directly correlated with an impairment in viral RNA synthesis and growth. These results demonstrate that nsp4 plays a critical role in the formation, stability, and structure of virus-induced membrane modifications. Finally, the results also support the conclusion that the physical structure and stability of DMVs is essential for efficient RNA synthesis and/or protection of viral RNAs and optimal replication of coronaviruses.

Generation and recovery of nsp4 glycosylation mutant viruses

Group 2a coronaviruses contain conservation of putative glycosylation sites in nsp4 at N176 and N237 (Fig. 4.1B). To determine if nsp4 is glycosylated at residues N176 and N237 in the context of MHV infection and what roles nsp4 glycosylation may play in the virus life cycle, viruses were engineered to contain asparagine-to-alanine substitutions at either N176, N237, or both residues N176 and N237 of nsp4 (Fig. 4.1C

and Table 4.1). Cells were electroporated with genomic RNA for N176A, N237A, or N176A/N237A mutant viruses. All three mutant viruses induced cytopathic effect (CPE) by 36 h post-electroporation, and 90 to 100% of cells were involved in syncytia by 46 to 50 h post- electroporation, similar to wt virus. Viruses were passaged and sequenced across the nsp4 coding sequence, confirming both the presence of engineered mutations and lack of any other mutations in nsp4. In contrast to previous reports, these results demonstrate that mutants with alanine substitution at N176, N237, or both are viable, demonstrating that the N176 and N237 residues are not required for replication in cell culture. To determine if compensating mutations occurred outside of the nsp4 sequence during recovery of N237A and N176A/N237A mutant viruses, the complete genome of the N176A/N237A mutant virus was sequenced, and there were no additional mutations present in the genome. These results demonstrate that the recovery of N237A and N176A/N237A mutant viruses was not due to second site compensating mutations and that the Asn residues are not required for virus viability.

Nsp4 is glycosylated at both N176 and N237 during MHV infection

Previous studies have demonstrated that treatment of lysates with endoglycosidase H (Endo H) results in a mobility shift of nsp4 expressed from plasmid in HeLa cells (Clementz et al., 2008; Oostra et al., 2007) or from nsp4-EGFP expressed in recombinant virus from an alternate location (in place of ORF2) (Clementz et al., 2008; Oostra et al., 2007), consistent with glysosylation of nsp4 with mannose-rich oligosaccharides in the ER and lack of nsp4 trafficking through Golgi. However, there has been no demonstration of N-linked glycosylation of native nsp4 in wt virus or

Table 4.1. Asparagine-to-alanine mutagenesis of MHV nsp4

Primer Name	Sequence	Purpose
N176A Sense	5'-GCC GCC TCT CTG TAT AGT TCT TTG GCT-3'	Mutagenesis for N176A
N176A Antisense	5'P-GTG CAT AAC ACC CCC TGT ATA ACA ATA AGG-3'	Mutagenesis for N176A
N237A Sense	5'-GCC CGT TCA TGG GTA TTG AAC AAC CCG TAT-3'	Mutagenesis for N237A
N237A Antisense	5'P-AAA ATT AAA GCA GAT ACC CTC CTC GGC-3'	Mutagenesis for N237A

*Underlined letters denote nucleotides used to introduce alanine substitutions

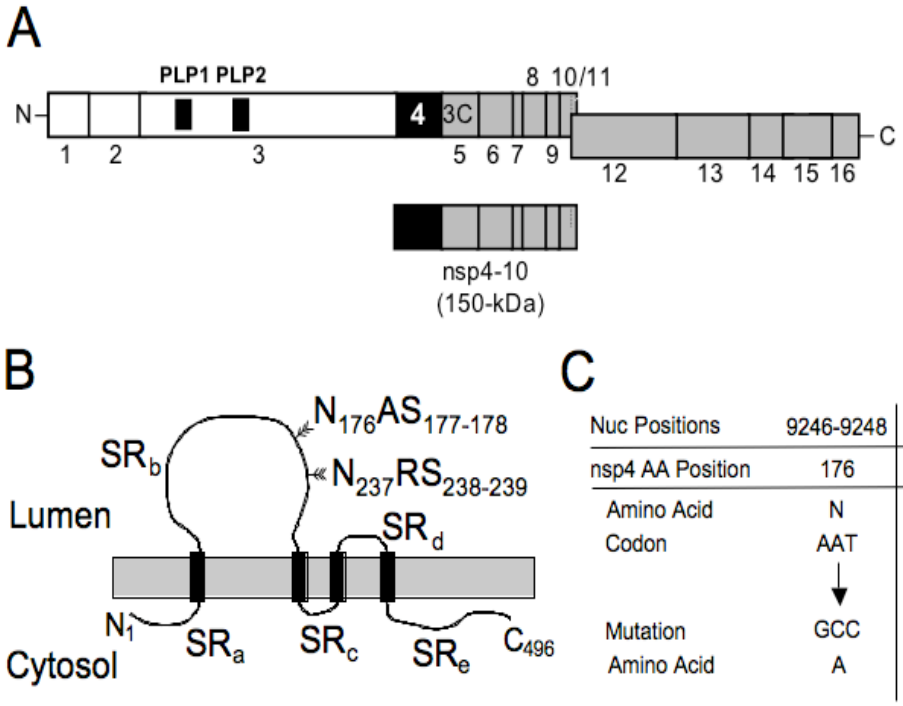

Fig. 4.1. Processing, glycosylation, and mutagenesis of nsp4. A) Schematic of MHV nsp4 processing. Three virus-encoded proteases process polyprotein 1ab (pp1ab) into intermediate precursors and 16 mature nsps. Papain-like proteases 1 and 2 (PLP1 and PLP2) are shown as black boxes within nsp3, while the nsp5 protease (3CLpro) is shown in gray. PLP-mediated processing of nsps is linked by white boxes, and 3CLpro processing is linked by gray boxes. Nsp4 is shown in black. Nsps are indicated by number. The nsp4-10 precursor is also shown. **B) Proposed topology and N-linked glycosylation sites of nsp4.** MHV nsp4 is a 496-aa protein that has four predicted transmembrane domains (TM 1-4, black rectangles) and five soluble regions (SR a-e). Location of N-linked glycosylation residues Asn176 and Asn237 (N176 and N237) are indicated in SR_b and predicted luminal and cytoplasmic domains are indicated (Oostra et al., 2007). **C) Engineered nsp4 glycosylation mutants**. Nsp4 glycosylation mutants were engineered by replacing the AAT asparagine codons at both N176 and N237 with a GCC alanine codon. Nucleotide numbers correspond to genomic position, and amino acid numbers correspond to nsp4 position.

identification of specific Asn residues subject to N-linked glycosylation. To test whether natively expressed MHV nsp4 is glycosylated during infection, immunoprecipitated nsp4 from wt MHV infection was mock-treated or treated with Endo H (Fig. 4.2A). Mock-treated nsp4 was detected as a 44 kDa protein by SDS-PAGE, while Endo H treatment resulted in a faster migrating, 39 kDa protein. The nsp4-10 precursor was detected in both cases by α–nsp4. The replicase protein nsp8 is not modified by N-linked glycosylation and was not affected by Endo H treatment (Fig. 4.2A). The nsp4-10 precursor that was treated with Endo H and detected using anti-nsp8 exhibited a sharper band than that of the untreated nsp4-10 precursor. A possible explanation for this is that removal of N-linked glycans may alter what nsp4-10 precursors can be detected by anti-nsp8, e.g. nsp4-10 with certain posttranslational modifications.

To test whether N176 and/or N237 were targeted for glycosylation, nsp4 immunoprecipitated following infection of DBT cells with N176A, N237A, and N176A/N237A mutant viruses was treated with Endo H (Fig. 4.2B). Untreated nsp4 from N176A and N237A mutants migrated identically and more rapidly than untreated wt nsp4 (42 kDa), but more slowly than wt nsp4 treated with Endo H (39 kDa). When nsp4 from N176A and N237A mutant viruses was treated with Endo H, both proteins were detected at 39 kDa, identical to Endo H-treated wt nsp4. Nsp4 from the N176A/N237A mutant virus migrated to 39 kDa, whether untreated or treated with Endo H. The results indicate that nsp4 expressed from its native genomic location is specifically glycosylated at residues N176 and N237 and also demonstrate that no other N-linked glycosylation occurs in nsp4.

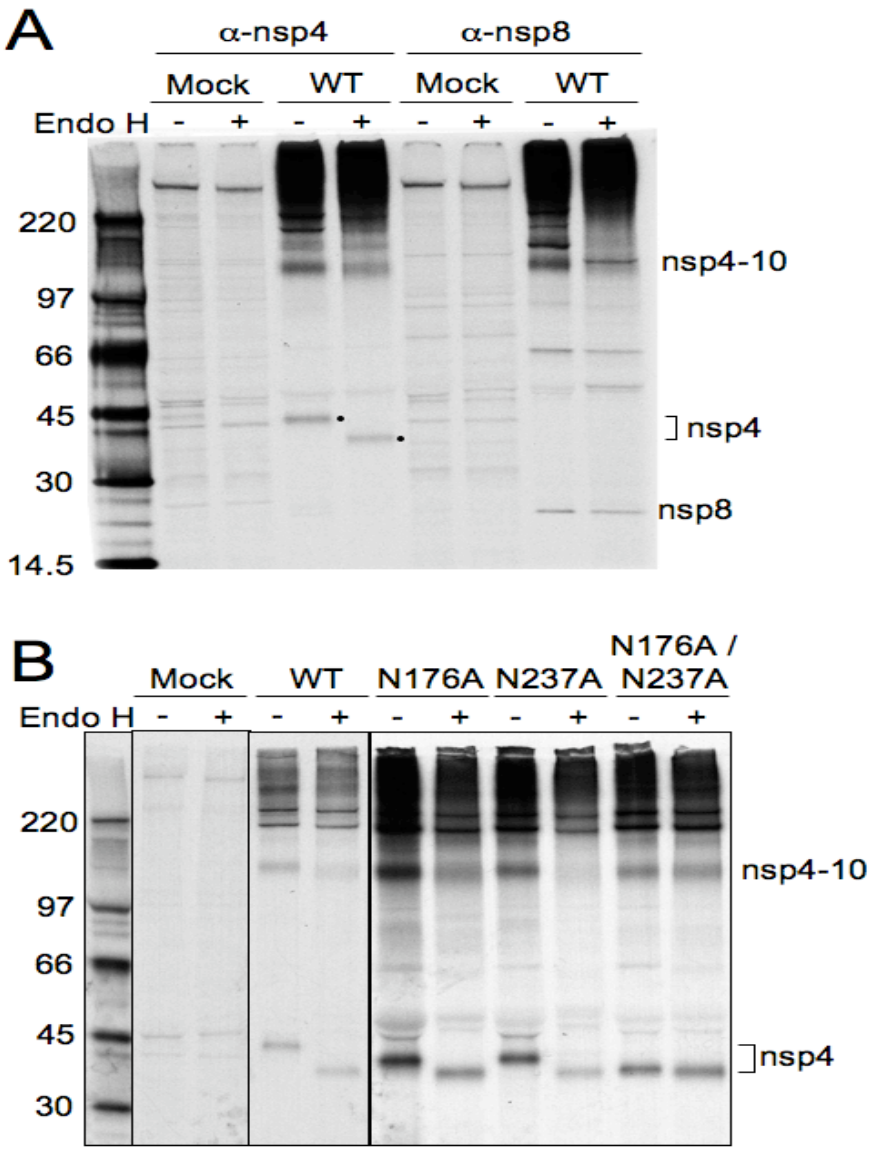

Fig. 4.2. Protein expression and glycosylation of nsp4. Cytoplasmic lysates were generated from radiolabeled DBT cells that were either mock-infected or infected with wt, N176A, N237A, or N176A/N237A viruses. Labeled proteins were immunoprecipitated using antiserum against nsp4 or nsp8**. A) Endo H treatment of wt nsp4 and nsp8**. Immunoprecipitated nsp4 and nsp8 were either mock-treated or treated with Endo H to analyze N-linked glycosylation. After Endo H treatment for 3 h, proteins were resolved on SDS-PAGE and visualized by fluorography. Black dots indicate either glycosylated or unglycosylated forms of nsp4. **B) Endo H treatment of nsp4 glycosylation mutants**. Immunoprecipitated nsp4 from wt or nsp4 glycosylation mutants was mock-treated or treated with Endo H. All samples in each individual panel were resolved on the same gel and had the same exposure time, but in panel B, the images were cropped to remove non-relevant lanes. Molecular weight markers are shown to the left of each gel.

Nsp4 glycosylation mutant viruses exhibit defects in virus replication

To determine whether nsp4 glycosylation mutant viruses display replication defects, DBT cells were infected with wt, N176A, N237A, and N176A/N237A viruses at an MOI of 1 PFU/cell (Fig. 4.3A). Samples of infected cell culture medium were taken at predetermined time points from 1 to 24 hours post-infection (h p.i.), and virus titers of each sample were determined by plaque assay. The N176A mutant virus exhibited growth kinetics and peak titers indistinguishable from wt virus, consistent with the study by Clementz et al (Clementz et al., 2008). The N237A and N176A/N237A mutant viruses grew indistinguishably from each other and reached peak titers similar to wt virus; however, compared to wt and N176A, the N237A and N176A/N237A viruses exhibited a delay and decrease in growth between 4 and 12 h p.i. The N176A/N237A mutant did not appear more impaired in growth than the N237A mutant alone. Since the N237A and N176A/N237A mutant viruses exhibited growth defects, experiments were performed that next tested whether N176A had subtle growth defects by repeating the growth assays at an MOI of 0.01 PFU/cell (Fig. 4.3B). Under these conditions the N237A and N176A/N237A mutants demonstrated the same delay as with a higher MOI. In contrast, for the N176A mutant virus, the lower MOI infection revealed a subtle defect in growth, displaying a delay in peak titer similar to that of N237A and N176A/N237A mutants. The experiments demonstrate that N176 and N237 both are important for exponential growth, but loss of either or both glycosylation sites still allows for wt peak titers. The contributions of N176 and N237 are independent and non-redundant, as indicated by growth defects of either N176A or N237A, but are not additive or synergistic. Finally, the

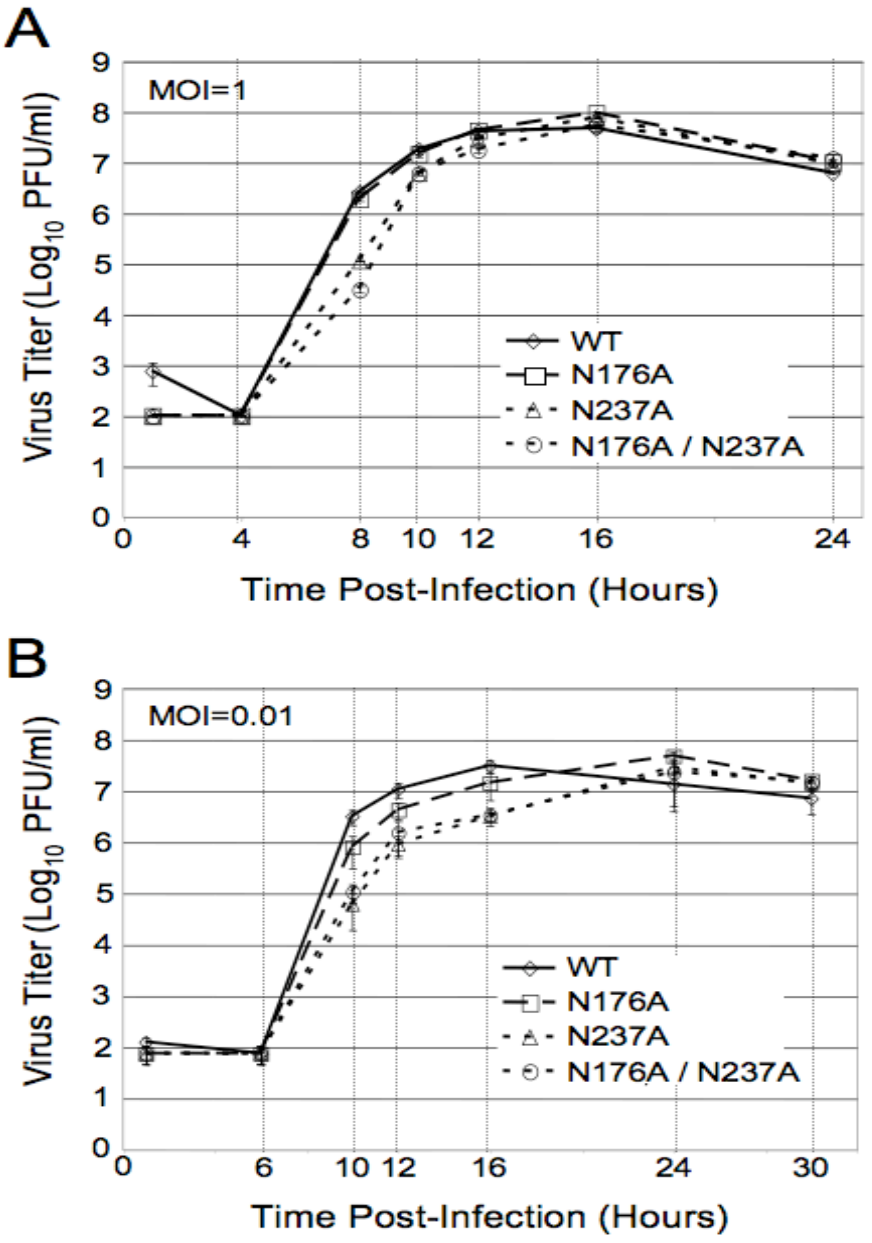

Fig. 4.3. Growth analysis of nsp4 glycosylation mutant viruses. DBT cells were infected with the indicated viruses for: **A)** single cycle growth at an MOI of 1 PFU/cell for 24 h; or **B)** for multiple cycle growth at an MOI of 0.01 PFU/cell for 30 h. Samples of virus supernatants were collected at times indicated beneath the graphs. Virus titers were determined by plaque assay with DBT cells. Error bars represent standard deviations from the mean based on samples from multiple replicates.

results suggest that glycosylation of nsp4 is important for nsp4 function during virus replication.

Nsp4 glycosylation mutants have reduced viral RNA synthesis

Since previous studies have shown that mutations in nsp4 affect viral RNA synthesis (Sparks, Lu, and Denison, 2007), experiments were conducted to determine if the growth defects of nsp4 glycosylation mutants were associated with changes in viral RNA synthesis (Fig. 4.4). DBT cells were mock-infected or infected with wt, N176A, N237A, or N176A/N237A mutant viruses at an MOI of 5 PFU/cell to maximize single round infection, and infected cells were metabolically labeled with [^{3}H]uridine in the presence of actinomycin D for 2 h intervals from 3 to 15 h p.i. Total RNA was extracted from harvested cells and measured for incorporation of [^{3}H]uridine. Peak incorporation of [^{3}H]uridine for wt MHV occurred from 9 to 11 h p.i., similar to a previously published report (Graham and Denison, 2006). For all three nsp4 mutant viruses, peak incorporation was delayed compared to wt, occurring between 11 and 13 h p.i.

Delays in the timing of peak viral RNA synthesis displayed by the nsp4 glycosylation mutant viruses were also associated with decreases in the amount of RNA synthesized over the course of the infection. The N176A mutant virus synthesized approximately 80% of the maximum amount of incorporation seen for wt over a 2 h labeling period. Both the N237A and the N176A/N237A mutant viruses exhibited a 50% reduction in peak viral RNA synthesis. These data demonstrate that there is an overall decrease in viral RNA synthesis in the nsp4 mutant viruses compared to wt virus. In addition, the delay and decrease in RNA synthesis correlated with the kinetics and peak

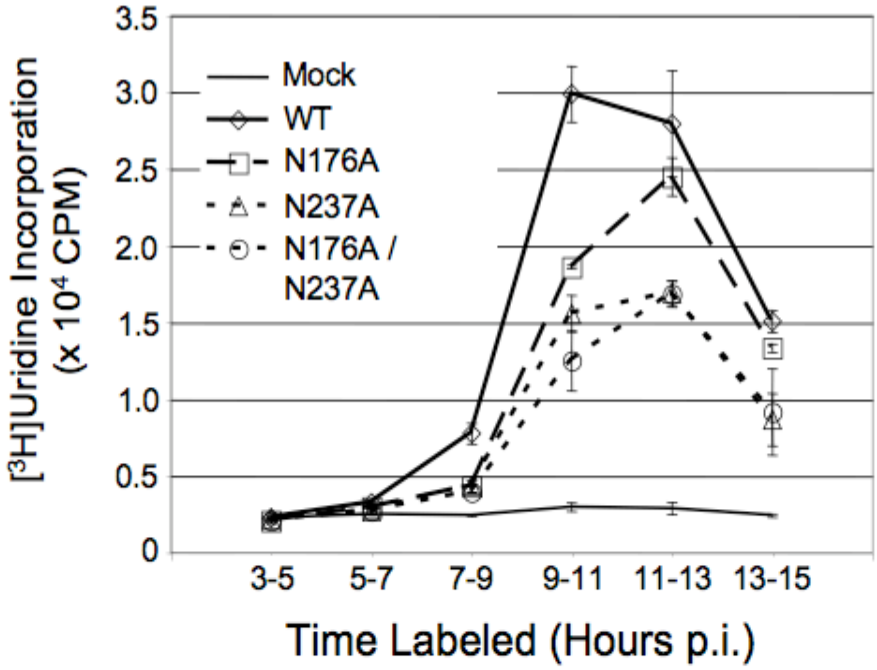

Fig. 4.4. RNA synthesis of nsp4 glycosylation mutant viruses. DBT cells in 6-well plates were mock-infected or infected with wt, N176A, N237A, or N176A/N237A viruses at an MOI of 5 PFU/cell. Cells were treated with Actinomycin D for 30 min prior to addition of radiolabel. Cells were metabolically labeled with [^{3}H]uridine for the intervals indicated, cells were lysed, and [^{3}H]uridine incorporation was quantified by liquid scintillation counting of TCA-precipitable RNA. Data points represent the mean counts/minute (cpm) of two individual experiments, and error bars represent the standard deviations between two experiments.

titer of infectious viruses, suggesting that alteration of viral RNA synthesis was responsible for the growth defects from the N176A and N237A substitutions.

Removal of nsp4 glycosylation sites does not alter nsp4 localization

Nsp4 colocalizes with other replicase nsps in cytoplasmic replication complexes that are sites of viral RNA synthesis, and nsp4 has been predicted to be critical for formation of these complexes. To test if altered RNA synthesis resulting from the N176A and N237A substitutions was associated with altered nsp4 interactions with other replicase proteins, the localization of nsp4 was compared by immunofluorescence with nsp8, a well described marker for replication complexes, and with the viral membrane protein (M), a marker for sites of virus assembly in the ERGIC and Golgi and distinct from replication complexes. DBT cells on glass coverslips were infected with wt, N176A, N237A or N176A/N237A viruses for 6 hours, fixed, and probed for nsp4, nsp8, and M. For wt and all nsp4 mutant viruses, nsp4 colocalized extensively with nsp8 in punctate perinuclear and cytoplasmic foci (Fig. 4.5A). However, there was a visual trend for fewer and less intense fluorescent foci in the cells infected with the nsp4 mutants compared to wt virus, suggesting that there may be fewer forming or altered replication complexes in the nsp4 mutant virus infections (Fig. 4.5A and data not shown). When nsp4 was compared with M (Fig. 4.5B), wt and mutant viruses had identical patterns of non-colocalization of nsp4 with M, consistent with previous studies of MHV replicase proteins and indicating that nsp4 is not altered in its relationship to sites of assembly and not localized to the ERGIC or Golgi. The results demonstrate that nsp4 mutant viruses

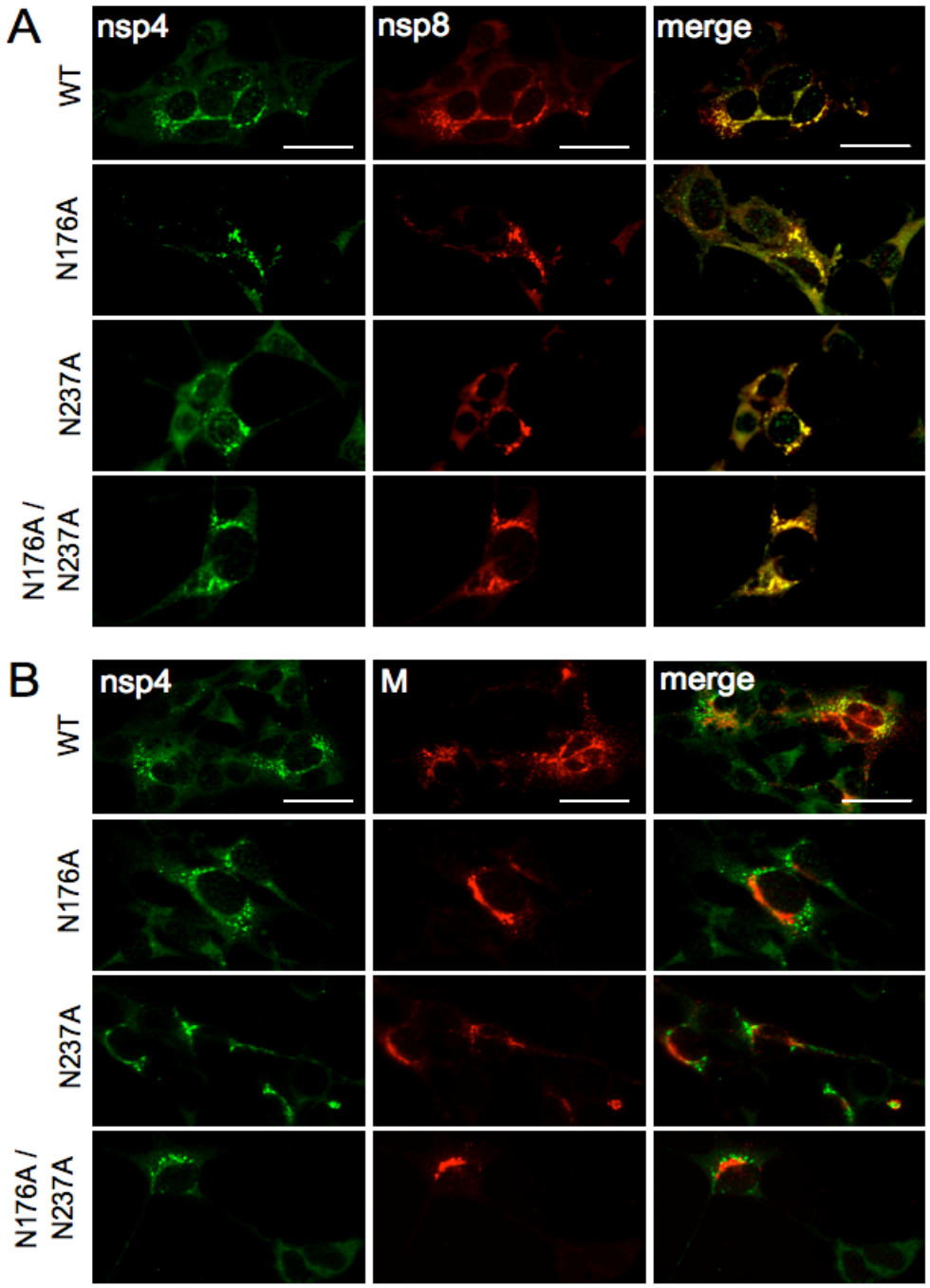

Fig. 4.5. Immunofluorescence of nsp4 localization. DBT cells on glass coverslips were infected with the indicated viruses at an MOI of 10 PFU/cell. At 6 h p.i., cells were fixed and probed with antibodies to nsp4, nsp8, and membrane (M) protein and analyzed by immunofluorescence using a Zeiss Axiovert 200 microscope at 40× magnification. **A) Nsp4 colocalizes with nsp8.** Infected cells were analyzed by indirect immunofluorescence using α-nsp4 (Alexa 488-green) and direct immunofluorescence by Alexa 546 conjugated to α-nsp8 (red). Yellow pixels represent colocalization of overlapping green and red pixels. **B) Nsp4 does not colocalize with M protein**. Infected cells were probed by indirect immunofluorescence using rabbit α-nsp4 (green) and mouse α-M (red). The scale bar in the upper images in panels A and B equals 20 μM and is representative of all other images.

are able to form cytoplasmic replication complexes and retain interactions with other replicase nsps and that glycosylation of nsp4 is not required for this process.

Nsp4 glycosylation mutant viruses induce altered membrane rearrangements and irregular DMVs

Based on the replication defects and subtle visual variability observed during immunofluorescence analysis of nsp4 mutants, experiments were performed that next investigated whether the nsp4 glycosylation mutants have altered membrane rearrangements. Transmission electron microscopy (TEM) was used to visualize the ultrastructure of membrane modifications in infected cells. DBT cells were mock-infected or infected with wt or the nsp4 glycosylation mutant viruses at an MOI of 5 PFU/cell. At 6 h p.i., cells were fixed in 2% glutaraldehyde and processed for TEM analysis. For mock-infected cells, the cellular architecture and organelle morphology was intact (Fig. 4.6A). Cells infected with wt virus exhibited clearing of cytoplasmic contents and swollen ER and Golgi (Fig. 4.6B). Cells infected with the three nsp4 glycosylation mutant viruses also demonstrated swelling of ER and Golgi and cytoplasmic clearing, albeit less so than during wt infection (Fig. 4.6C-E).

In contrast, there was a striking difference between cells infected with wt and nsp4 mutants in the relationship and ultrastructure of virus-induced DMVs and convoluted membranes (CMs). WT- and nsp4 mutant-infected cells exhibited virus-induced CMs and DMVs, structures that have been identified in replication complexes and associated with viral RNA synthesis (Gosert et al., 2002; Knoops et al., 2008), while no DMVs or CMs were observed in mock-infected cells. CMs were detected in wt and

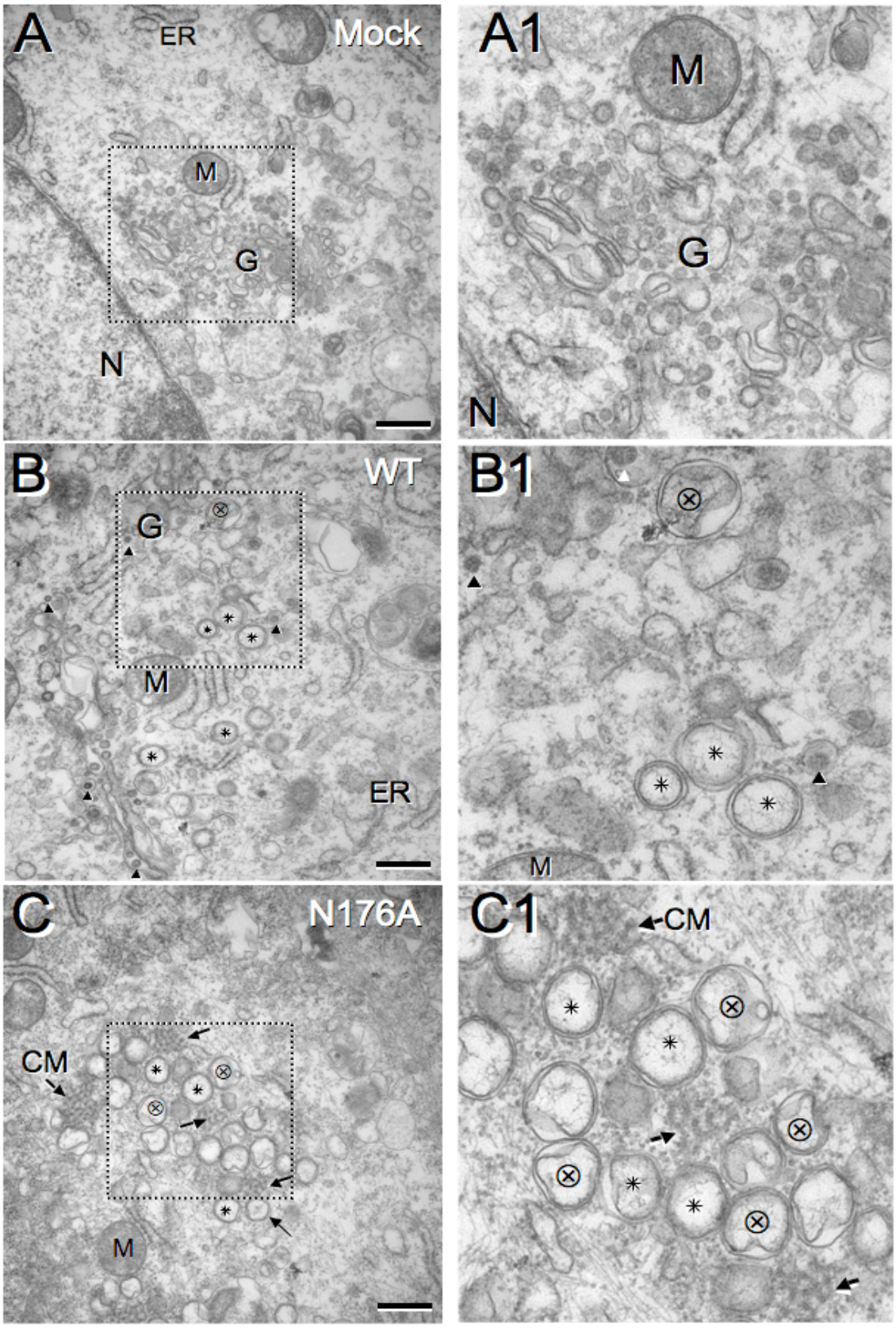
A
ER
Mock
M
G
N
A1
M
G
N
B
WT
G
M
ER
B1
M
C
N176A
CM
M
C1
CM

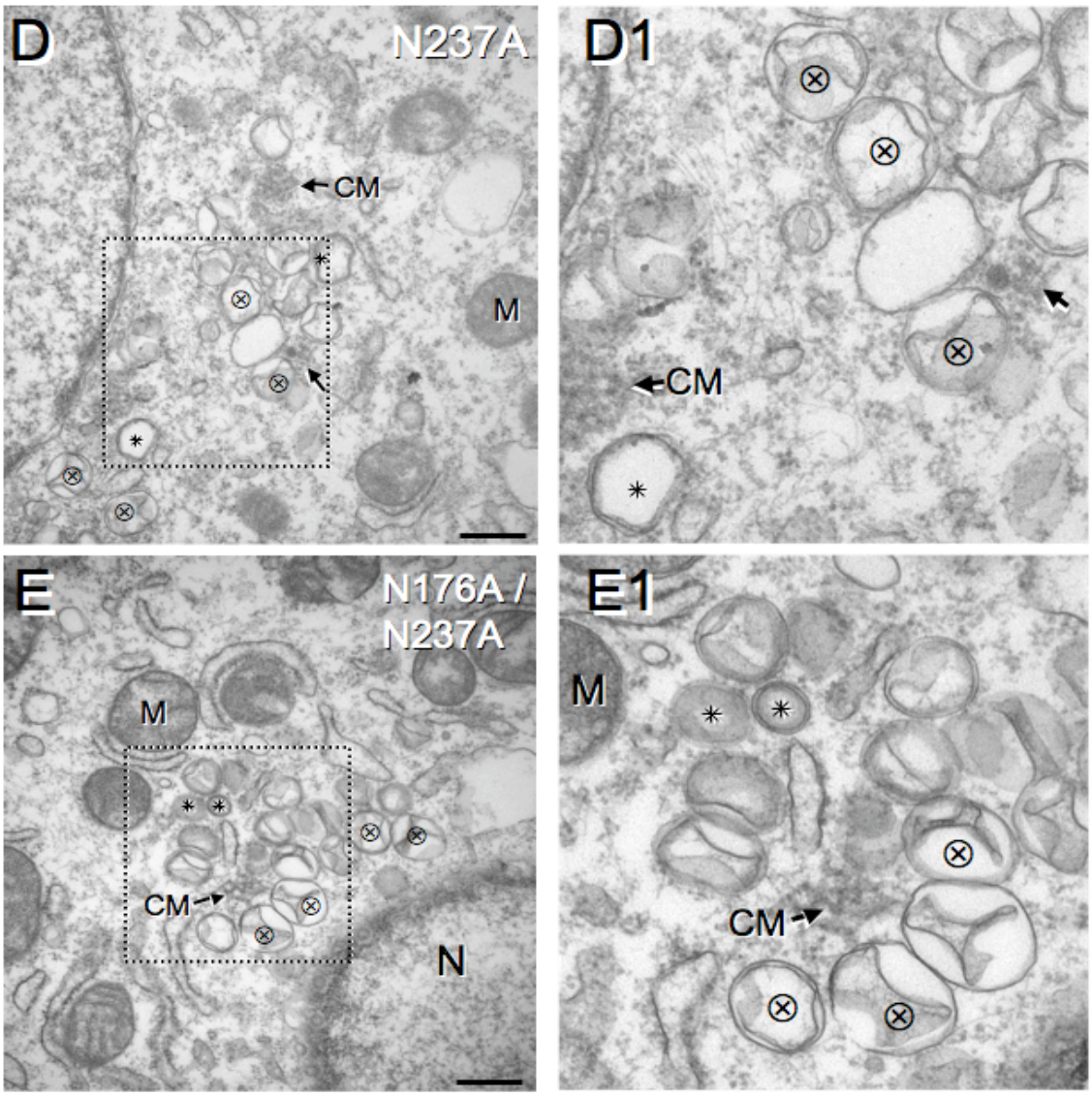

Fig. 4.6. EM analysis of replication complexes and DMVs from wt and nsp4 mutants. DBT cells were mock-infected or infected with wt, N176A, N237A, or N176A/N237A viruses. Cells were harvested in 2% glutaraldehyde and processed for TEM analysis. **A and A1)** Mock-infected cells. **B and B1)** wt MHV infection. **C and C1)** N176A mutant virus infection. **D and D1)** N237A and **E and E1)** N176A/N237A mutant virus infections. Dotted boxes in the left image indicate area of magnification in right image. The scale bar in the left images represents 500 nm. Arrowheads indicate dark-stained, individual virions, which are located above the arrowheads. Black arrows point to CMs. * indicates examples of regular DMV structure. ⊗ shows examples of irregular DMV structure. N, nucleus; ER, endoplasmic reticulum; G, Golgi apparatus; M, mitochondria; CM, convoluted membranes.

mutant virus-infected cells and always in close proximity of DMVs. However, DMVs were observed in the presence or absence of CMs for all viruses. The CMs were observed more frequently in EM sections of cells infected with N176A, N237A, and N176A/N237A mutant viruses compared to wt (Fig. 4.6C, 4.6D, 4.6E). The vast majority of DMVs in wt-infected cells exhibited characteristic DMV morphology of a circular shape, regular diameter, and ultrastructure of closely approximated inner and outer membranes. A small subset of DMVs manifested a partial separation of the inner and outer membranes and exhibited a slightly larger diameter, but these were rare. In contrast, cells infected with the nsp4 glycosylation mutants demonstrated DMVs with altered shape and diameter and with increasingly aberrant (irregular) ultrastructure, consisting of severely detached and collapsed inner membranes that was not observed in any wt-infected cells. The number of irregular DMVs and extent of DMV derangement was most profound in N237A and N176A/N237A mutant-infected cells and visibly greater than that detected in cells infected with N176A alone.

Because the EM images were originally selected based on the detection of DMVs, EM images were selected and used to quantitatively compare: 1) prevalence of CMs; 2) ratio of regular (wt-like) and irregular DMVs; and 3) the diameter of regular and irregular DMVs (Table 4.2 and Fig. 4.7). Since the images were selected only for presence of DMVs, the quantitative analysis that was performed was unbiased for these specified parameters. The prevalence of CMs was determined by comparing images where CMs were observed or not observed in EM sections selected based on the presence of DMVs, since CMs were only found in the presence of DMVs. While there was no statistical difference between wt and N176A in the ratio of sections with both CMs and DMVs

Table 4.2. Analysis of Virus-Induced Membrane Structures

Virus	Total Cell Sections with Evidence of Infection	Sections with CMs and DMVs	Sections with DMVs Only	Total DMVs Counted	Regular DMVs	Irregular DMVs	Average Regular DMV Diameter (nm)	Average Irregular DMV Diameter (nm)
WT	24	8	16	102	86	16	255.2 ± 31.4	323.2 ± 35.6
N176A	21	11	10	127	96	31	257.0 ± 52.3	324.2 ± 31.8
N237A	11	9	2	72	36	36	264.6 ± 53.6	372.5 ± 41.6
N176A/N237A	21	18	3	117	60	57	270.4 ± 56.1	371.3 ± 41.6

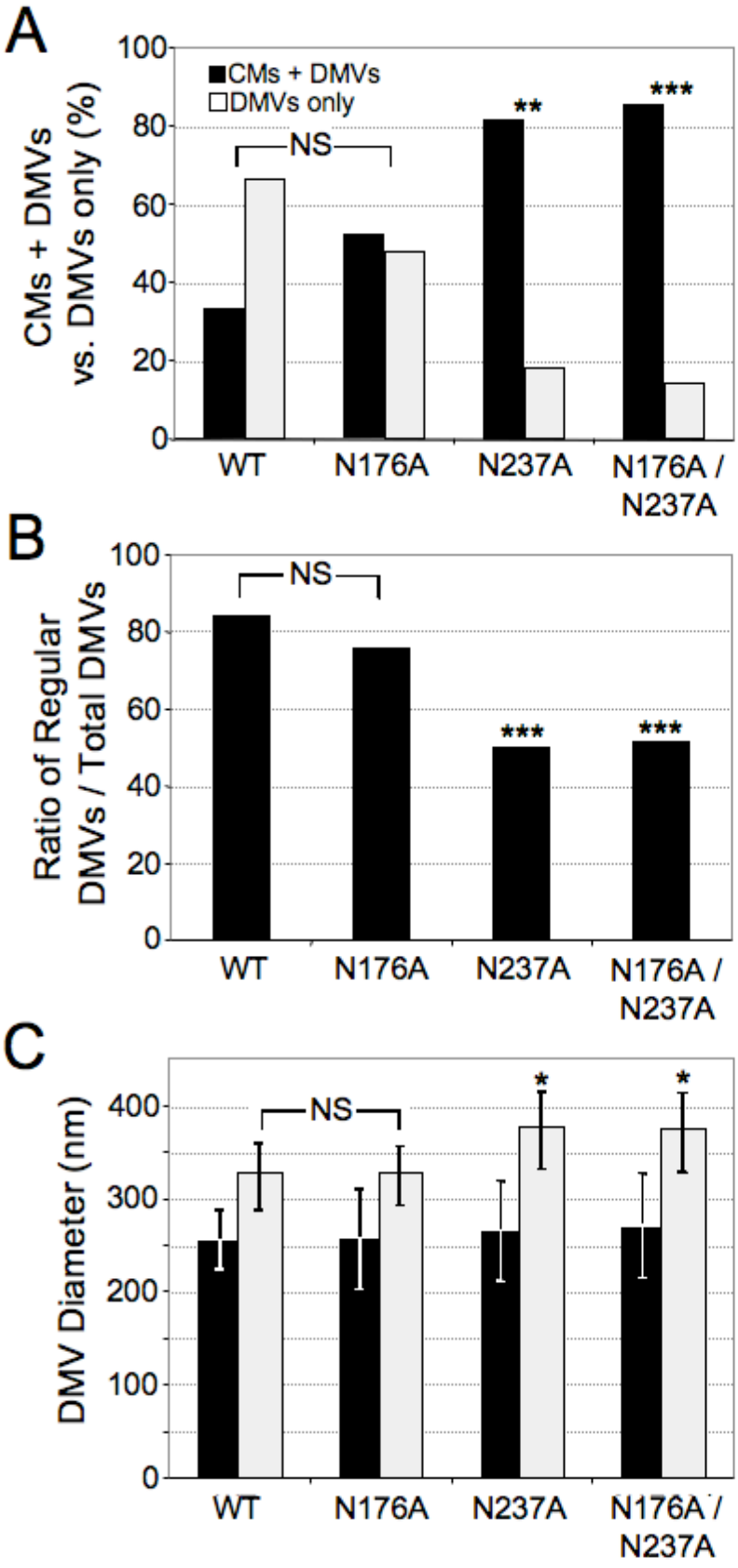
A
CMs + DMVs vs. DMVs only (%)
CMs + DMVs
DMVs only
NS
**
***
0
20
40
60
80
100
WT
N176A
N237A
N176A / N237A
B
Ratio of Regular DMVs / Total DMVs
NS
***
***
0
20
40
60
80
100
WT
N176A
N237A
N176A / N237A
C
DMV Diameter (nm)
NS
*
*
0
100
200
300
400
WT
N176A
N237A
N176A / N237A

Fig. 4.7. Quantitative analysis of CMs and DMVs. A) CMs and DMVs. All EM images were analyzed for the presence of CMs and DMVs based on characteristic EM morphology. Because CMs were only found in the presence of DMVs in all TEM sections observed, the ratio of total cell sections with CMs + DMVs could be compared to the presence of cell sections with DMVs alone. Black bars indicate presence of both CMs and DMVs, while white bars represent the presence of DMVs alone. Chi square analysis was used to compare the presence of CMs + DMVs to DMVs alone. **B) Ratios of DMVs with regular morphology compared to total DMVs (regular + irregular).** Total DMVs and DMVs with regular morphology were counted for all viruses in TEM images and the ratio of regular DMVs to total DMVs was determined. **C) Diameter of regular and irregular DMVs of wt and nsp4 mutants**. DMVs were measured in Image J by the widest diameter in nm of outer membranes. Black bars indicate regular DMVs, while white bars indicate irregular DMVs. Error bars indicate standard deviation. There was no significant difference (not labeled in the figure) in diameter of regular DMVs between wt and nsp4 mutant viruses. ANOVA followed by Tukey tests indicated a significant difference in the diameter of irregular DMVs of the N237A and N176A/N237A viruses compared to both wt and N176A viruses. * ($p < 0.05$), ** ($p<0.01$), and *** (p,0.001) indicates levels of statistical significance compared to wt virus. NS, no significance.

versus DMVs alone, the N237A and N176A/N237A mutants had significantly increased ratios of detection of both CMs and DMVs compared to DMVs alone ($p<0.01$ for N237A and $p<0.001$ for N176A/N237A) (Fig. 4.7A). Analysis of the ratio of regular DMVs to total DMVs (regular + irregular) demonstrated a significant increase in irregular DMVs in cells infected with N237A and N176A/N237A mutant viruses ($p < 0.001$) when compared to cells infected with wt or N176A viruses (Fig. 4.7B). The observations also revealed more irregular DMVs in N176A than wt, but the regular DMV/total DMV ratios were not significantly different. Finally, the measurement of regular DMVs of both wt and all nsp4 glycosylation mutant viruses revealed no difference in their diameters (widest diameter of outer membrane) (Fig. 4.7C). In contrast, the mean diameter of irregular DMVs in the N237A and N176A/N237A mutant viruses was significantly greater than that of either wt virus or the N176A mutant virus (Fig. 4.7C). This analysis indicates that nsp4 is likely critical for the organization and stability of DMVs and for the relationship and evolution of membrane modifications (CMs and DMVs) over the course of infection.

Discussion

Although multiple studies have investigated the roles of nonstructural proteins in inducing membrane rearrangements, understanding the role of glycosylation of nonstructural proteins from positive-strand RNA viruses remains limited. A study of the flavivirus yellow fever virus demonstrated that NS1 glycosylation was important for several functions in the virus life cycle (Lindenbach and Rice, 1999; Muylaert et al., 1996). NS1 interacts with membranes and is involved in replicase function (Lindenbach

and Rice, 1999), and removal of NS1 glycosylation by asparagine-to-alanine substitution results in impaired virus growth, RNA synthesis, and pathogenesis (Muylaert et al., 1996).

Coronaviruses, like other positive-strand RNA viruses, induce the formation of DMVs that serve as scaffolds for replication/transcription complexes. Exogenous expression of the poliovirus transmembrane proteins 2BC and 3A results in DMVs that are indistinguishable from those formed during wt infection (Schlegel et al., 1996; Suhy, Giddings, and Kirkegaard, 2000). Equine arteritis virus (EAV), which is classified with coronaviruses in the order *Nidovirales*, induces DMVs similar to coronaviruses (Pedersen et al., 1999). Exogenous plasmid expression of EAV nsp2 and nsp3 is sufficient to induce membrane modifications resulting in membrane structures similar to those seen during EAV infection, and mutations within EAV nsp3 also result in altered virus-induced membrane rearrangements (Posthuma et al., 2008; Snijder et al., 2001). EAV nsp3 is a tetra-spanning integral membrane protein implicated in DMV formation and organization. Of interest, an introduced Asn substitution (T873N) in an EAV nsp3 luminal domain resulted in nsp3 glycosylation *in vitro*, but was highly detrimental when introduced into the genome and only recovered as a pseudoreversion (N873H) that abolished the glycosylation site. Thus for another nidovirus, the glycosylation status of a membrane modifying replicase protein is also important for DMV formation and RNA synthesis during virus replication.

This report confirms multiple roles of MHV nsp4 in the virus life cycle, including optimal virus replication, RNA synthesis, and its importance in the modification and morphology of virus-induced membrane structures. In this study, it was shown that MHV

nsp4 is glycosylated and functions as a membrane modification protein that regulates virus-induced membrane rearrangements. Nsp4 glycosylation mutant viruses display highly irregular DMVs and an increased prevalence of CMs relative to DMVs alone. The extent of disrupted DMVs in the nsp4 glycosylation mutant viruses correlated directly with decreases in RNA synthesis and virus replication. These data suggest that altered membranous structures from the nsp4 glycosylation mutants result in a reduced capacity to synthesize viral RNA or protect viral RNA from degradation, ultimately leading to impaired virus fitness.

Previous studies have concluded that nsp4 is required for MHV replication and have identified determinants of membrane topology, subcellular localization, and function (Clementz et al., 2008; Oostra et al., 2007; Sparks, Lu, and Denison, 2007). This study is the first to recover and characterize the importance of multiple nsp4 glycosylation events on virus replication, viral RNA synthesis, and virus-induced membrane modifications during coronavirus infection. Clementz et al. recovered an nsp4 N176A mutant, but were unable to recover an N237A or N176A/N237A mutant (Clementz et al., 2008). Their N176A mutant grew with similar kinetics to wt at an MOI of 0.1 PFU/cell at 33^{o}C and 39^{o}C, but was not further characterized in that report. In contrast to the previously published report, the N237A and N176A/N237A mutant viruses were able to be recovered and characterized. The reasons for the differences in recovery can only be speculated. The background of cloned MHV genome fragments should be identical since the MHV genome fragments were jointly developed with the Denison lab and the Baric lab. In addition, I performed RT-PCR sequencing of the complete genome from the recovered N176A/N237A mutant virus, which verified the

engineered mutations and also confirmed that the rest of the genome was identical, with no additional mutations of any kind, to the published recombinant MHV-A59 sequence. Thus, there were no other compensating mutations to account for or consider for the recovery of the mutant virus. The lab has also experienced occasional mutations in the genome fragments during preparation for genome assembly that have prevented recovery of even known viable mutants and would therefore speculate that this could account for the non-recovery of N237A and N176A/N237A mutant viruses by Clementz et al. These results clearly demonstrate that the N176 and N137 residues and the associated glycosylation events are not required for MHV replication in cell culture. Since no other mutations were identified in the genome RNA from the recovered N176A/N237A mutant virus, it can be concluded that the profound and distinct phenotypes in virus replication, RNA synthesis, and virus-induced cellular membrane modifications are due to the introduced mutations alone.

Potential functions of nsp4 glycosylation. Modification of proteins by addition of N-linked glycans may result in numerous effects on protein functions (Fiedler and Simons, 1995; Helenius and Aebi, 2001). Therefore, glycosylation of nsp4 may be important for a variety of reasons. One potential mechanism of nsp4 glycosylation is proper protein folding (Helenius, 1994; Paulson, 1989). By removing N-linked glycans, the overall structure of nsp4 may be altered during protein folding. This mechanism is supported by the findings in this report in that the nsp4 glycosylation mutant viruses displayed impairments in virus replication, viral RNA synthesis, and virus-induced membrane modifications. Other explanations are possible for the role of nsp4 glycosylation on replication complex formation and membrane modifications. For

instance, glycosylation of nsp4 may be important for protein stability and prevention of nsp4 degradation (Klausner and Sitia, 1990). Lastly, it is possible that the N-linked glycans, either directly or through modification of nsp4 structure, recruit cellular factors that are involved in membrane rearrangements. Future studies are needed to distinguish between these possibilities.

Models of nsp4 function on replication complex formation, morphology, and organization. Evidence from this study has led to potential models addressing the effect nsp4 has on replication complex formation, morphology, and organization. One possible model is that nsp4 may regulate the transition or formation of different membrane modifications (i.e. CMs and DMVs). The evidence from this report in that there was an increased prevalence of CMs in relation to DMVs in the N237A and N176A/N237A mutant viruses suggests that MHV nsp4 may be a major player in the transition of these virus-induced membrane rearrangements from one membrane structure to another. Other findings in that there was an increased presence of aberrant or deranged DMVs in the N237A and N176A/N237A mutant viruses from this report suggests another possibility in that the formation of intact, functional DMVs is regulated by nsp4.

A second potential model of nsp4 function is that the curvature and size of DMVs are regulated by nsp4 (Perlman and Netland, 2009). In N237A and N176A/N237A mutant virus-infected cells, irregular DMVs were much larger and had highly disrupted inner membranes. The N237A and N176A/N237A mutant viruses also exhibited decreases in RNA synthesis, indicating that these irregular DMVs may not be functioning properly and that curvature and size may be important for proper function. This model is supported by the fact that all virus-infected cells produced regular DMVs, although at

different proportions, and that all regular DMVs were similar in size. Cells infected with wt or N176A viruses, those that had higher levels of RNA synthesis compared to the N237A and N176A/N237A mutant viruses, also had a higher percentage of regular DMVs. These data suggest that curvature and size are important for DMV function**.**

A third model is that nsp4 functions in tethering or "pushing" the inner membrane to the outer membrane of the DMVs. The proximity of the inner membrane to the outer membrane may be important for creating an environment optimal for RNA synthesis and/or protection of newly synthesized viral RNAs. This model is supported by the fact that the prevalence of aberrant DMVs in the nsp4 glycosylation mutants was directly related to the extent of impairment of RNA synthesis and virus growth. These results suggest that irregular DMVs have a reduced capacity to synthesize and/or protect viral RNAs and are also the first to provide direct evidence suggesting that the physical size, morphology, and stability of virus-induced DMVs is important for efficient viral RNA synthesis and optimal virus production. On the other hand, the results also show clearly that glycosylation of nsp4 is not absolutely required for formation of "regular" DMVs, and that replication complex function can still ultimately allow virus replication to wt titers, albeit with delayed kinetics.

To date, all coronavirus nsp4s that were subjected to Endo H treatment have been shown to be glycosylated in the lumen of the ER between the first and second predicted transmembrane domains of nsp4 in exogenous expression experiments, including group 2a MHV nsp4, group 2b SARS-CoV nsp4, and group 3 IBV nsp4 (Clementz et al., 2008; Lim, Ng, and Liu, 2000; Oostra et al., 2007). It will be interesting to see whether glycosylation of nsp4 is conserved among other coronaviruses, specifically group 1

coronaviruses, and what effect the loss of glycosylation sites has on virus replication, RNA synthesis, and replication complex morphology. Finally, it will also be intriguing to determine if other nonstructural proteins from coronaviruses and other RNA viruses are glycosylated and what effects glycosylation has on the individual protein's function(s).

CHAPTER V

SUMMARY AND FUTURE DIRECTIONS

Introduction

At the start of this dissertation, research in coronavirus biology was expanding rapidly, and research efforts were increasing dramatically due to two key events. The establishment of reverse genetics systems for coronaviruses and the outbreak of a new human coronavirus that caused severe disease served as the dominant forces for an extraordinary push in understanding coronavirus replication and biology. Within recent years, multiple investigators have contributed to our increased knowledge of many aspects of coronavirus biology.

It was within this resurgence of research that I began my graduate studies. Prior to the invention of reverse genetics systems for coronaviruses, studies of the coronavirus replicase were largely limited to the use of biochemical and cell imaging experiments for the identification and analysis of intermediate and mature replicase proteins. While these studies were critical in the identification of CSs, protein detection and analysis, and localization studies, it was not possible to address the effects of cleavage events and functions of replicase proteins on virus replication. Through the utilization of a powerful reverse genetics system for MHV, my research addressed multiple questions to ultimately lead to a better understanding of how coronaviruses replicate in host cells. Specifically, my research has increased our understanding of the mechanisms and requirements of polyprotein processing, the evolution of PLP-mediated processing of nsps 1-4 of

coronaviruses, the importance of coronavirus genome organization, and the discovery of specific functions of replicase proteins during virus replication. The findings from my research have opened new areas to explore in the coronavirus field, as well as in the discipline of RNA viruses. This chapter will summarize the main findings of this dissertation, highlight recent advances, and engage in the new and interesting ideas, questions, and potential future work generated from this graduate research.

Effects of encoding nsp2 at different genomic loci

Prior to my work on alternate expression studies of MHV nsp2, a published report from the lab had shown that the nsp2 coding sequence and protein is dispensible for virus replication of both MHV and SARS-CoV (Graham et al., 2006). The deletion of the nsp2 domain of the MHV and SARS-CoV replicase polyproteins resulted in a 90% reduction in growth and a 50% reduction in RNA synthesis. Although nsp2 is the most variable replicase protein across coronaviruses, the deletion of nsp2 from both MHV and SARS-CoV resulted in similar effects on virus growth, RNA synthesis, and protein processing phenotypes, suggesting that the nsp2 sequences evolved or adapted to have similar functions in virus replication. These results also demonstrated that there is considerable flexibility for mutations and reorganization of the coronavirus genome.

The goal of my project was to determine whether expression of nsp2 from non-native sites in the coronavirus genome could complement the replication defect of a virus lacking nsp2 in its native context, in order to test the hypothesis that the context and levels of expression of nsp2 are essential for optimal replication, its localization, and its function . Therefore, the nsp2 coding sequence was engineered into alternative locations

of the MHV genome, both in the presence and absence of the native-expressed nsp2 coding sequence. Multiple sites were chosen to introduce the nsp2 coding region, and the introduction of the nsp2 sequence resulted in both viable and nonrecoverable mutant viruses. Moreover, none of the alternate-encoding nsp2 viruses complemented the growth defect observed with the mutant MHV Δnsp2 virus. Interestingly, overexpression of nsp2 by encoding it at two locations in the genome, one copy at its native location and the other in place of ORF4, was detrimental to virus replication and altered nsp2 localization, where nsp2 was still localized to punctate perinuclear foci but was also diffusely distributed throughout the cytoplasm.

The results generated from this study demonstrate that nsp2 expressed from its native location in the genome is required for optimal MHV replication. Native expression of nsp2 may be important for a variety of reasons. It is possible that the nsp2 RNA coding sequence provides stability to the genome, preventing its degradation. Secondly, the nsp2 coding sequence may recruit other factors that are important in regulation of transcription or translation during the virus life cycle. A more likely model is that the known nsp2-3 precursor that is detected during virus infection plays a role in the timing and/or regulation of virus replication. Abolition or impaired cleavage between nsps 2-3 results in a virus with significant delays in exponential growth. My results support the conclusion that proper nsp2 function may depend on being expressed as an nsp2-3 intermediate protein prior to processing and that the sequential order of processing likely has specific functions that have not yet been characterized.

Finally, this study resulted in additional questions that my graduate research aimed to address. While addition of residues at the N-terminus did not affect growth and

protein processing, addition of LeuGln residues at the C-terminus of nsp2 resulted in delays in virus growth and protein processing. Because LeuGln amino acids, key residues in nsp5 recognition and cleavage, were added downstream of the native CysAla amino acids, key residues recognized by PLP1, it is not known which protease was mediating processing at the engineered site. This gave rise to several interesting questions, including: (1) which protease is responsible for cleaving altered CS2?; (2) how much flexibility is there in the amino acid sequences upstream and downstream of CSs that will still allow processing?; (3) are proximal CS amino acid residues all that are necessary for protease recognition and processing?; and (4) can viral protease recognition and processing be switched by altering CS amino acid sequences? My next project aimed at understanding the requirements for protease recognition and processing at CSs.

Rewiring the MHV replicase polyprotein to function with one PLP

The research described above and previous studies of coronaviruses have analyzed the effects of CS mutations and deletions in the replicase polyprotein on virus replication, protein processing, and RNA synthesis. Recently, our lab and others have shown that catalytic activity of MHV PLP1 and HCoV-229E is not absolutely required for virus viability and replication (Graham and Denison, 2006; Ziebuhr et al., 2007). While PLP1 catalytic activity is not required for virus replication, the overall effects of PLP1 catalytic inactivation were remarkably different when comparing the two viruses. For MHV, the catalytic inactivation of PLP1 resulted in a severely debilitated mutant virus that only reached peak titers of ~10^3 PFU/ml and exhibited no processing at CS1 and CS2. On the other hand, the inactivation of PLP1 from HCoV-229E resulted in a

virus that grew only 2 $\log_{10}$ PFU/ml less than wild-type HCoV-229E. Also, HCoV-229E PLP2 was capable of processing at CS1, CS2, and CS3, unlike that of MHV PLP2, which only processes at CS3. Because the first three CS amino acid sequences are divergent for MHV and are similar for HCoV-229E and other coronaviruses that encode only one PLP, it was predicted that the CS amino acid sequence controls the requirement of encoding one or two catalytically active PLPs.

The second goal of my research was to test the hypothesis that the proximal CS amino acid sequences are sufficient for protease recognition and processing and whether protease specificity could be switched from PLP1 to PLP2 by substituting the proximal CS amino acid sequences. The MHV PLP2 CS recognition sequence P4-LXGG-P1 was introduced in place of CS1 and/or CS2 in the presence or absence of catalytically active PLP1. Viable viruses were recovered and protein expression studies demonstrated that PLP2 can process downstream of LXGG amino acid sequences at CS2; however, there was no detectable processing at the first CS that was substituted with LXGG. These findings indicate that the LXGG amino acid motif is necessary for processing by PLP2, but other factors are also required for efficient PLP-mediated processing of nsps 1-3.

The potential factors that may be required for efficient processing are highlighted in Fig. 5.1. One potential factor is that the recognition sequence of MHV PLP2 requires more than the LXGG motif. Amino acids upstream and/or downstream of this motif may be necessary for optimal recognition, binding, and processing by PLP2. A previous study that identified the third CS of MHV also showed that the P6 residue upstream of the CS may be important for PLP2 recognition and processing *in vitro* (Kanjanahaluethai, Jukneliene, and Baker, 2003). Secondly, proteolytic processing at CS1 and/or CS2 may

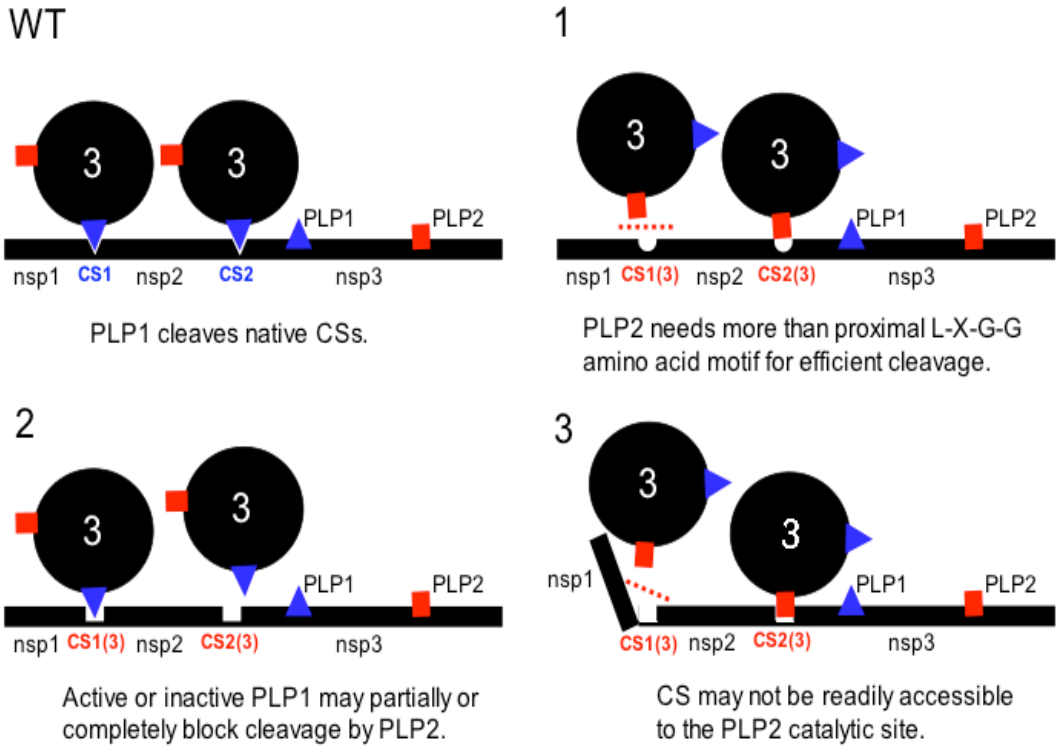

Fig. 5.1. Proposed models of inefficient proteolytic processing at substituted CSs. During wild-type MHV processing of nsps 1-3, PLP1 mediates efficient processing at both CS1 and CS2. When CS1 or CS2 was replaced with the PLP2 L-X-G-G recognition motif, there was either no or reduced processing observed at the mutated CSs. The three proposed models of inefficient processing are shown. (1) Amino acids directly upstream and/or downstream of the PLP2 recognition sequence are required for efficient protein processing. (2) After translation or by interactions of amino acids upstream and/or downstream of the mutated CS, PLP1 blocks the CS, inhibiting PLP2 from accessing the CS. (3) Due to other constraints within nsps 1-3, PLP2 is blocked from accessing the mutated CSs. PLP1 is shown as a blue triangle, and its CSs are shown in blue. PLP2 is shown as a red rectangle, and its CSs are linked in red. Models are shown as trans-cleavage models for simplification.

occur fully or partially by cis-cleavage. After translation of the N-terminal replicase polyprotein, MHV PLP1 may be in close association with CS1 and/or CS2. This could potentially block or inhibit the recognition and cleavage by PLP2 at substituted LKGG amino acid motifs at these locations. Lastly, instead of PLP1 blocking proteolytic cleavage, inefficient processing may be due to structural constraints within nsps 1-3 that do not allow access of the CS recognition sequence into the PLP2 catalytic site. These structural constraints may be due to protein folding of a hypothetical nsp1-2 intermediate or possibly to the location of PLP2 within nsp3. The likelihood that multiple factors play a role in processing of nsps 1-3 is highly likely, and potentially all three of these proposed factors, and possibly factors not mentioned, play a role in optimal protein processing.

To better understand the evolutionary relationships and protein processing of coronavirus PLPs, mutations were engineered into MHV so that the organization of MHV nsps 1-3 would be similar to that of SARS-CoV. Although the engineered virus had similar CS amino acid sequences and only one catalytically active PLP, the engineered MHV mutant was debilitated in growth, indicating that engineered CS and PLP organization of MHV similar to SARS-CoV is detrimental for virus replication. These data also suggest that coronavirus nsps 1-3 have evolved to function cooperatively. The observed significant variability in nsps 1-3 across divergent coronaviruses and evidence for rapid evolution in SARS-CoV nsps 1-3 during the epidemic both support this possibility. This concept will be discussed further under future studies later in this chapter.

Role of nsp4 in the coronavirus life cycle

Prior to my work studying MHV nsp4, it was known that nsp4 demonstrated characteristics of an integral membrane protein (Gosert et al., 2002). It was also predicted that nsp4 likely plays a key role in virus-induced membrane modifications (Perlman and Netland, 2009). A recent study from our lab demonstrated that nsp4 is required for production of infectious virus, and mutations within nsp4 result in decreased RNA synthesis (Sparks, Lu, and Denison, 2007). Additionally, it was shown that plasmid-expressed nsp4 is glycosylated in transfected cells (Clementz et al., 2008; Oostra et al., 2007); however, it was not known if nsp4 was glycosylated during infection and what effects glycosylation may have on nsp4 function.

The main focus of my research was to test the hypothesis that nsp4 serves critical functions in the formation and function of replication complexes that are located on double membrane vesicles (DMVs). In addition, I sought to determine whether nsp4 is glycosylated and if nsp4 glycosylation is required for nsp4 function(s). Mutant viruses were generated with mutations at nsp4 residues N176, N237, or both to test the effects of these mutations on growth, RNA synthesis, nsp4 glycosylation, and nsp4 localization. MHV nsp4 was shown to be glycosylated at residues N176 and N237. The three nsp4 glycosylation mutant viruses, N176A, N237A, and N176A/N237A, all exhibited defects in virus growth and RNA synthesis. The N237A and N176A/N237A displayed growth and RNA synthesis defects that were greater than that of the N176A mutant virus. Transmission electron microscopic analysis of ultrastructure from infected cells demonstrated that the nsp4 mutants had aberrant morphology of virus-induced DMVs when compared to those infected with wt virus, with the N237A and N176A/N237A

having severely disrupted DMVs. Interestingly, the degree of altered DMV morphology directly correlated with the reductions in viral RNA synthesis and virus growth observed for the nsp4 mutant viruses. The results demonstrate that nsp4 plays a critical role in the organization and stability of DMVs and suggest that N176 and N237 play specific roles in nsp4 membrane modifications and stability. The results also support the concept that the formation and physical structure of DMVs is essential for efficient RNA synthesis and optimal replication of coronaviruses.

While the exact function(s) of nsp4 remain to be elucidated, results from this study provide evidence supporting potential mechanisms of the function(s) of nsp4 on replication complex formation, organization, and morphology (Fig. 5.2). One proposed model is that nsp4 functions in the regulation or timing of the transition and formation of virus-induced membrane modifications. For example, nsp4 may play a role in the transition of convoluted membranes (CMs) to DMVs or from DMVs to CMs. This mechanism of nsp4 is supported by the fact that there was an increased presence of CMs in the nsp4 mutant infections compared to wt virus infections. A second possible model is that nsp4 regulates the size and curvature of DMVs. Because infections with mutant nsp4 exhibited DMVs that were larger, wider, and had disrupted inner membranes compared to wt infections, nsp4 may function in controlling the shape of virus-induced DMVs. Finally, nsp4 may function in bringing the inner membrane in close approximation to the outer membrane, either through "pushing" the inner membrane out towards the outer membrane or by a tethering mechanism. This potential mechanism is supported by the fact that DMVs observed in the nsp4 mutant virus infections had disrupted and collapsed inner membranes compared to DMVs from wt infection.

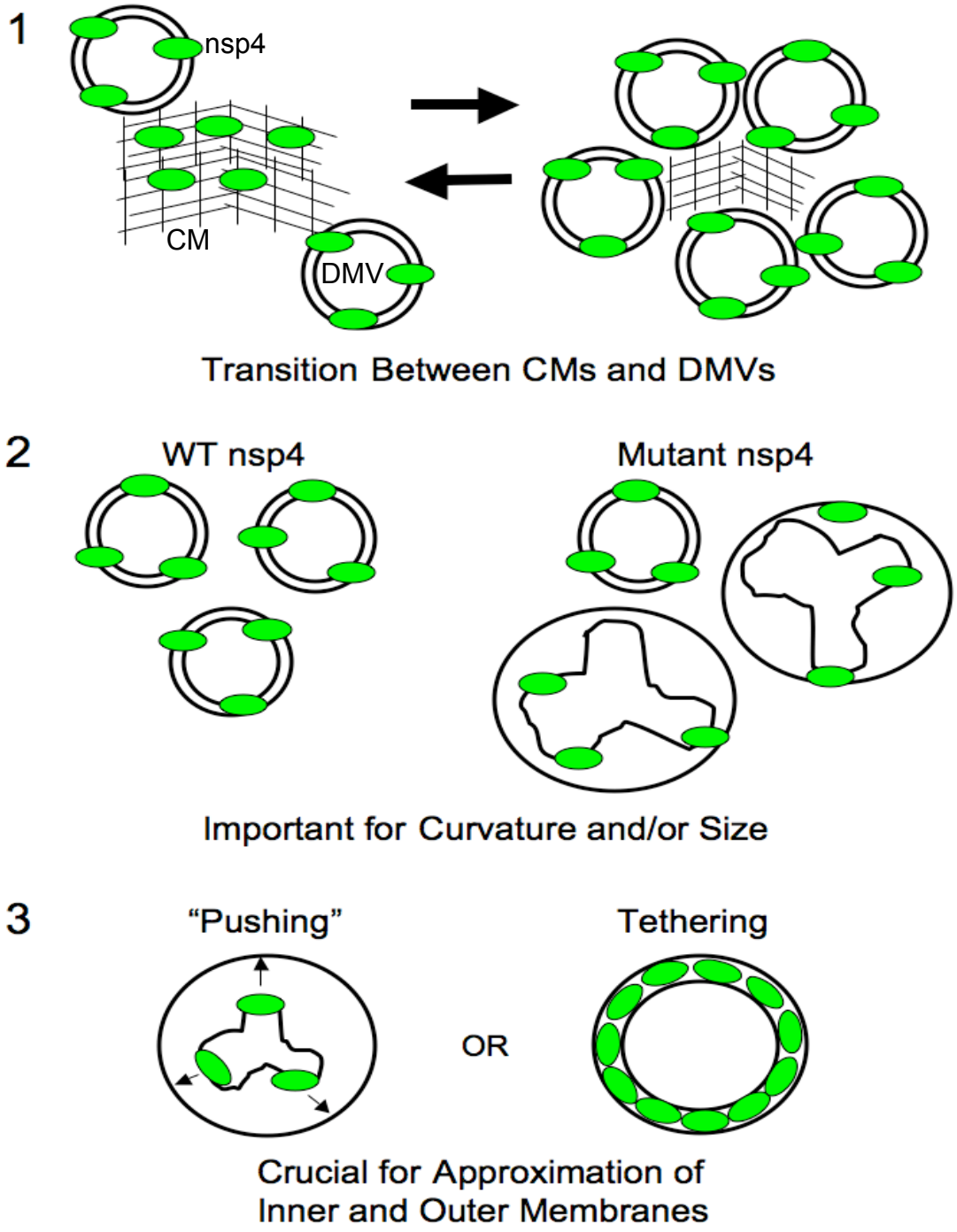

Fig. 5.2. Potential mechanisms of nsp4 function(s). Nsp4 has been proposed to function in the formation, organization, and morphology of virus-induced membrane modifications. The findings from this study led to several potential models of nsp4 function. Nsp4 is shown as a green oval. Membranes are shown as black lines. (1) Nsp4 may function as a key regulatory protein in the transition of virus-induced membrane structures observed during infection. (2) Nsp4 may be crucial for the shape, size, and stability of virus-induced membrane structures. (3) Nsp4 may function in shaping or expanding the inner membrane to the outer membrane. Alternatively, nsp4 may function in tethering the inner membrane to the outer membrane.

While the exact function(s) of nsp4 have yet to be determined, this report confirms that nsp4 is critical in multiple steps of the virus life cycle, likely through modification of cellular membranes. The nsp4 mutant viruses and the experimental approaches generated in this study provide powerful tools to further dissect mechanisms of the cell biology and replication of coronaviruses.

Implications and potential applications of this research

Although the 2002 – 2003 SARS outbreak was short-lived, the recent identification of bats as reservoirs for coronaviruses and the discovery of coronaviruses causing disease in new host species strongly argue that coronaviruses will remain a threat to agriculture and public health (Lau et al., 2005). Currently, there are no FDA approved vaccines for the prevention of human coronavirus infections, and there remain no clinically proven treatments for coronavirus infections. Research presented in this dissertation that aims at understanding the cell biology and replication of coronaviruses is critical and necessary for the development of antiviral therapies and vaccines to treat and prevent diseases, such as SARS.

The work presented in this dissertation focused on understanding the mechanisms of PLP-mediated processing and analysis of the cleavage products. PLP-mediated processing is common to all coronaviruses and is thought to be required for virus replication. Inhibition of PLP-mediated processing by either catalytic inactivation of the specific protease or by altering the CSs recognized by PLPs results in virus replication defects. This makes these proteases ideal targets for small molecule or peptide inhibitors that disrupt the proteases' functions. Also, either inhibiting or altering cleavage events

through reverse genetics approaches provides attractive means for vaccine design. The viral protein nsp4 of coronaviruses is also another attractive candidate for antivirals and potential vaccine development. Because nsp4 exhibits integral membrane characteristics and functions as a regulator of virus-induced membrane modifications that is necessary for replication, small molecule or peptide inhibitors that disrupt membrane interactions, replication complex association, and potential protein/protein interactions could reduce virus replication and either block or inhibit the progression and symptoms of disease.

Positive-strand RNA viruses have evolved similar strategies to usurp cellular components to aid in translation, formation of virus replication complexes, and other processes necessary for virus replication. Therefore, investigating the mechanisms of coronavirus replication will also aid in our understanding of the replication strategies utilized by other positive-strand RNA viruses.

Future studies: nsp2 function and replicase organization

In order to understand the mechanisms of coronavirus replication, it will be necessary to determine the functions of viral replicase proteins in the virus life cycle. Research presented in Chapter II has yielded new potential avenues of study. Determining the function(s) of nsp2 will be challenging since it is a dispensible protein, there is no sequence homology to any known proteins, and there are no predicted functions. However, it is known that nsp2 localizes to replication complexes and deletion of nsp2 results in reduced viral RNA synthesis and growth. In an nsp2 deletion mutant, replication complexes appear identical to those observed in wild-type infection. This suggests that nsp2 may be a modulatory or an adapter protein that interacts with other

nsps and influences viral RNA synthesis, or nsp2 may function in recruitment of cellular proteins that optimize RNA synthesis or replication complex formation. Recent evidence suggests both of these possibilities. A recent study analyzing the intraviral protein-protein interactions of SARS-CoV showed that nsp2 co-immunoprecipitates with other nsps, including nsp3, nsp4, nsp6, nsp8, nsp11, and nsp16 (von Brunn et al., 2007). The multitude of interactions suggests that nsp2 functions as a link to and between other nsps. Evidence from our laboratory also shows that exogenously expressed nsp2 is diffuse throughout the cytoplasm of transfected cells (Graham et al., 2005); however, upon infection of MHV lacking nsp2, exogenous nsp2 relocalizes to replication complexes, also suggesting a function in intraviral protein interactions. Another report has shown that SARS-CoV nsp2 also interacts with prohibitin 1 and prohibitin 2 through overexpression studies using tagged versions of nsp2 (Cornillez-Ty et al., 2009). Prohibitin 1 and prohibitin 2 are evolutionarily conserved proteins and have been implicated in multiple cellular processes, including cell cycle progression, cell migration, cellular differentiation, apoptosis, and mitochondrial biogenesis. It will be interesting to see if nsp2 interacts with prohibitin and possibly other cellular proteins during coronavirus infection. Also, siRNA knockdown of prohibitin may reveal the potential role of nsp2 and prohibitin in virus replication. Because nsp2 has shown to interact with multiple proteins and there are no known or predicted functions of nsp2, a solved crystal structure of nsp2 may be essential to provide key insights into the possible interactions and function(s) of this protein.

Because nsp2 is not required for replication, the results presented in Chapter II cannot predict the effects of rearrangement of essential replication proteins. However, the

report also demonstrated that gene deletions, insertions, and duplications of replicase proteins were tolerated in the coronavirus genome, suggesting flexibility in coronavirus ORF organization and function. This study has demonstrated that ORF1b and ORF4 tolerate insertion of the nsp2 coding sequence, and other studies have shown that other nonessential ORFs also tolerate expression of coronavirus and foreign proteins (de Haan et al., 2005; Oostra et al., 2007). Thus, this study provides a platform for the investigation into the significance of replicase organization and into the functions and placement of essential replicase intermediate and mature proteins in the replicase gene. For example, nsp5 (3CLpro) is an essential protein that is first expressed as an nsp4-10 intermediate protein and is eventually processed into its mature form. However, it is not known whether the placement of nsp5 in the replicase and/or if the nsp4-10 intermediate serves key roles in the coronavirus life cycle. These proposed studies will utilize the genomic areas that tolerated sequence deletions and insertions identified from the research presented in Chapter II to discover the functions of intermediate and mature proteins and the importance of replicase organization of coronaviruses.

Future studies: plasticity of nsps 1-3 and rewiring replicase CSs

The 5' third of the coronavirus ORF1, encoding nsps 1-3, accounts for the region of highest sequence diversity in the replicase across coronavirus groups. Although there is high sequence variability in this region, several reports have shown that nsps 1-3 and domains of nsps 1-3 from various coronaviruses in different groups have similar functions within the particular host of the specific virus (Barretto et al., 2005; Chen et al., 2007; Graham et al., 2005; Kamitani et al., 2006; Lindner et al., 2005; Zheng et al., 2008;

Zust et al., 2007). This suggests that nsps 1-3 have acquired sequence diversity, but retained similar functions, through evolution and adaptation in their respective hosts. Because nsps 1-3 are processed by either one or two PLPs within nsp3, it has been proposed that the proteins encoded in this region have coevolved with nsp3 to mediate specific functions, such as regulation of cleavage events, within the particular host of the coronavirus (de Vries et al., 1997; Ziebuhr, Snijder, and Gorbalenya, 2000; Ziebuhr, Thiel, and Gorbalenya, 2001). Results from Chapter III are consistent with this hypothesis in that organization of PLPs and CSs within nsps 1-3 of group 2a MHV which mimic those of group 2b SARS-CoV altered protein processing and virus replication. These data suggest that coronavirus nsps 1-3 have evolved to function as a cooperative unit during virus replication. In order to determine if nsps 1-3 function cooperatively during coronavirus replication, the coding sequence of nsps 1-3 of MHV could be replaced with SARS-CoV nsps 1-3 or vice versa (Fig. 5.3). Because the Denison lab possesses reverse genetics systems for both of these viruses, it is possible to test the cooperative activity and effects of swapping nsps 1-3 of MHV and SARS-CoV on virus replication. Because studies have shown that nsps 1-3 have similar known and/or predicted functions, it is possible that swapping of MHV nsps 1-3 with that of SARS-CoV nsps 1-3 may have no detrimental effects on virus replication. On the other hand, the swapping of nsps 1-3 may alter virus replication or other known activities, such as host mRNA degradation by nsp1, due to adaptation of coronaviruses to their specific hosts.

Future studies are also needed to address the requirements of PLP-mediated processing of coronavirus nsps 1-3. Results from Chapter III have shown that

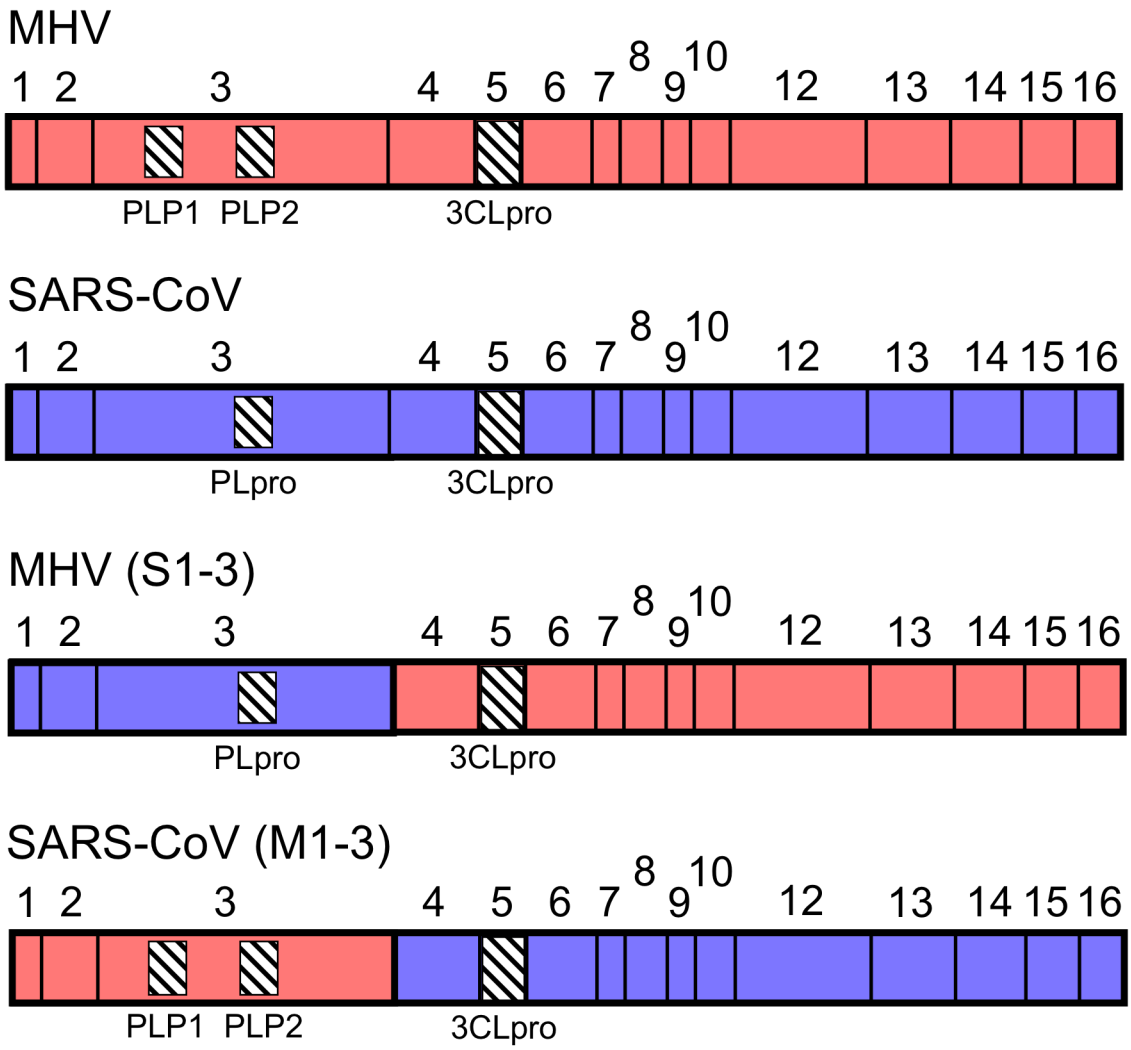

Fig. 5.3. Exchange of MHV and SARS-CoV nsps 1-3. Schematic depicting replicase organization of MHV and SARS-CoV. The replicase organization of MHV and SARS-CoV are shown in red and blue, respectively. In order to determine the cooperative activity of coronavirus nsps 1-3, the coding sequence of MHV nsps 1-3 will be switched with SARS-CoV nsps 1-3 and vice versa. S1-3 represents SARS-CoV nsps 1-3, and M1-3 represents MHV nsps 1-3. The hatched box indicates protease domains in both coronaviruses. The numbers above boxes indicate nsp number, and vertical lines indicate cleavage events.

requirements or determinants other than proximal CS amino acid sequences are necessary for protein processing of nsps 1-3. A potential approach to better understand the mechanisms of coronavirus PLP-mediated processing is to utilize the recovery of key mutant viruses, specifically the CS1/2(3) and CS1/2(3)+P1ko viruses, in passage experiments. By passing these CS mutant viruses, mutations may arise in nsps 1, 2, and/or 3 that will give insights into the modes of PLP-mediated processing. The passage experiments will also provide information into the adaptation and evolution of PLPs and nsps 1-3 of coronaviruses.

Experiments from this dissertation and other reports have shown that CS amino acid sequences are important regulators of the processing of intermediate and mature proteins of positive-strand RNA viruses (Bedard and Semler, 2004; Lawson and Semler, 1990; Palmenburg, 1990; Ryan and Flint, 1997; Snijder et al., 1995; Vasiljeva et al., 2003; Weiss et al., 1994; Ziebuhr, Snijder, and Gorbalenya, 2000). One potential way in which protease recognition and processing can be regulated is by subtle differences in the CS amino acid sequences (Table 5.1). Therefore, the binding of a CS and the rate at which it is cleaved depends on amino acid residues upstream and downstream of the CS. In addition, CS amino acid sequences may be responsible for the production of intermediate proteins that are required or beneficial for virus replication. For instance, MHV PLP1 prefers an Arg residue at the P2 position and a small amino acid at the P1 position. CS2 is also processed by PLP1, but a Cys is observed in the P2 position (Bonilla et al., 1995; Bonilla, Hughes, and Weiss, 1997; Dong and Baker, 1994; Hughes, Bonilla, and Weiss, 1995; Teng, Pinon, and Weiss, 1999; Teng and Weiss, 2002). This may be the reason why nsp1 is co-translationally processed and not observed as an nsp1-

MHV

nsp	P4	P3	P2	P1		P1'	Protease
1 - 2	G	Y	R	G	↓	V	PLP1
2 - 3	F	P	C	A	↓	G	PLP1
3 - 4	L	K	G	G	↓	A	PLP2
4 - 5	S	F	L	Q	↓	S	nsp5
5 - 6	V	K	L	Q	↓	S	nsp5
6 - 7	S	Q	I	Q	↓	S	nsp5
7 - 8	Q	A	L	Q	↓	S	nsp5
8 - 9	V	V	L	Q	↓	N	nsp5
9 - 10	V	R	L	Q	↓	A	nsp5
10 - 12	S	Q	F	Q	↓	S	nsp5
12 - 13	A	V	L	Q	↓	S	nsp5
13 - 14	P	R	L	Q	↓	C	nsp5
14 - 15	T	R	L	Q	↓	S	nsp5
15 - 16	P	R	L	Q	↓	A	nsp5

SARS-CoV

nsp	P4	P3	P2	P1		P1'	Protease
1 - 2	L	N	G	G	↓	A	PLpro
2 - 3	L	K	G	G	↓	A	PLpro
3 - 4	L	K	G	G	↓	K	PLpro
4 - 5	A	V	L	Q	↓	S	nsp5
5 - 6	V	T	F	Q	↓	G	nsp5
6 - 7	A	T	L	Q	↓	A	nsp5
7 - 8	L	S	M	Q	↓	G	nsp5
8 - 9	V	K	L	Q	↓	N	nsp5
9 - 10	V	R	L	Q	↓	A	nsp5
10 - 12	P	L	M	Q	↓	S	nsp5
12 - 13	T	V	L	Q	↓	A	nsp5
13 - 14	A	T	L	Q	↓	A	nsp5
14 - 15	T	R	L	Q	↓	S	nsp5
15 - 16	P	K	L	Q	↓	A	nsp5

Table 5.1. Cleavage sites, proteases, and protein processing of coronavirus nsps 1-16. The P4 through P1' amino acids are shown for all cleavage sites in the MHV and SARS-CoV replicase polyprotein. The protease that processes each site is shown to the right. The arrow indicates cleavage.

2 or an nsp1-2-3 intermediate. Also, the lab has discovered another intermediate in virus replication, an nsp7-10 intermediate protein. Instead of a Leu at the P2 position between nsp6 and nsp7, an Ile is present at the P2 position. Interestingly, a Leu is observed at almost every other P2 position that is processed by nsp5. To test whether CS amino acid sequences are responsible for the production of intermediate and mature proteins, amino acid substitutions can be made at critical residues of the CSs to determine if certain residues are necessary for the production of intermediate and mature proteins. These experiments will determine which intermediates are necessary or important in virus replication and potentially allow the identification of other intermediate proteins that occur during coronavirus replication. The proposed experiments may also allow for the order of replicase protein processing to be determined for coronaviruses. These experiments will provide a better understanding into the regulation of polyprotein processing of coronaviruses, as well as establish new methods into the attenuation of coronavirus replication. Finally, these studies will also aid in our understanding of polyprotein processing and regulation of mature nsps of other positive-strand RNA viruses.

Future studies: the function(s) of nsp4 in virus-induced membrane modifications

While the exact function(s) of nsp4 have yet to be determined, findings from this dissertation indicate that nsp4 functions as a regulator of virus-induced membrane modifications. In order to address and determine the specific function(s) of nsp4, a time course analyzing ultrastructure of infected cells by EM was performed to uncover the function of nsp4 in membrane modifications over the course of an infection. Because

results have shown that the N176A/N237A nsp4 mutant virus exhibited alterations in virus-induced membrane modifications compared to wild-type virus at 6 h p.i., the two viruses were compared from 2 to 10 h p.i. at 2 h intervals to analyze similarities and differences in membrane alterations over the duration of the infection (Fig. 5.4). At 2 h p.i., there was no evidence of infection for both wild-type and the N176A/N237A mutant viruses. While both wild-type and N176A/N237A exhibiting swelling of ER membranes at 4 h p.i., only wild-type infected cells exhibited virus-induced CMs and DMVs, suggesting that the N176A/N237A mutant exhibits delays in the formation of CMs and DMVs. After 6 h, vesicle packets were observed in wild-type infection, as well as CMs and DMVs. There was also extensive cytoplasmic clearing and disrupted cisternae in the mitochondria. Unlike that of wild-type infection, there were no vesicle packets observed and very little cytoplasmic clearing and disrupted mitochondria, also suggesting a delay in the timing and production of virus-induced membrane structures. Also, DMVs exhibited separation of inner and outer membranes in the N176A/N237A mutant virus infections; however, this appeared to be less pronounced than the previous study from Chapter IV. Also consistent with the findings presented in Chapter IV, the N176A/N237A mutant exhibited a qualitative increase in the presence of CMs. At the latest times analyzed by EM, DMVs appear to become unstable and less structured. Specifically, DMVs from the N176A/N237A virus infection have lost either their inner or outer membrane and appear as single-membraned vesicles at 10 h p.i.

These data suggest that nsp4 functions in the stability and formation of virus-induced membrane structures. Throughout the time course, the N176A/N237A mutant virus appeared to be delayed in virus-induced membrane modifications and cellular

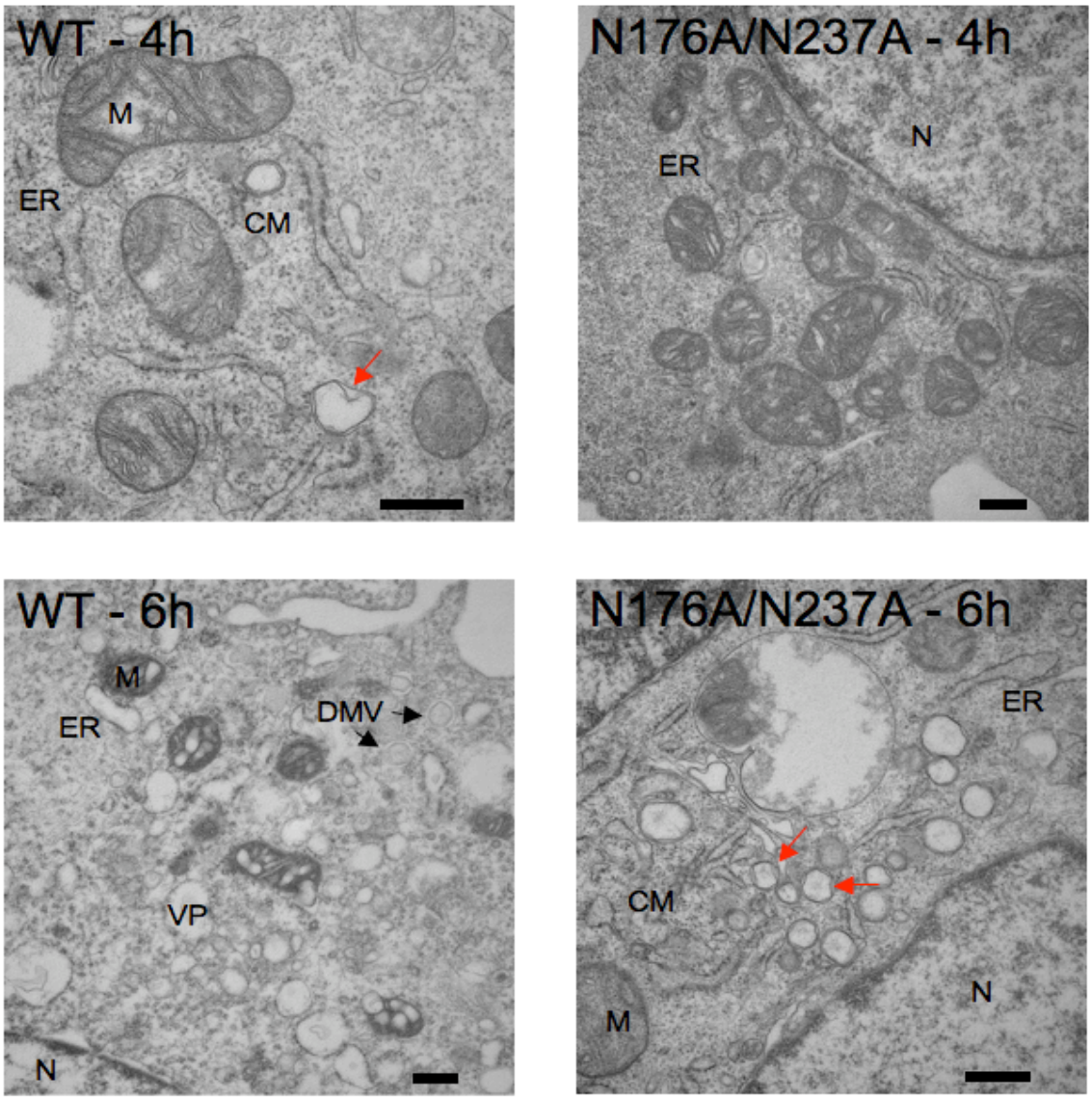
WT - 4h
M
ER
CM
N176A/N237A - 4h
ER
N
WT - 6h
M
ER
DMV
VP
N
N176A/N237A - 6h
ER
CM
N
M

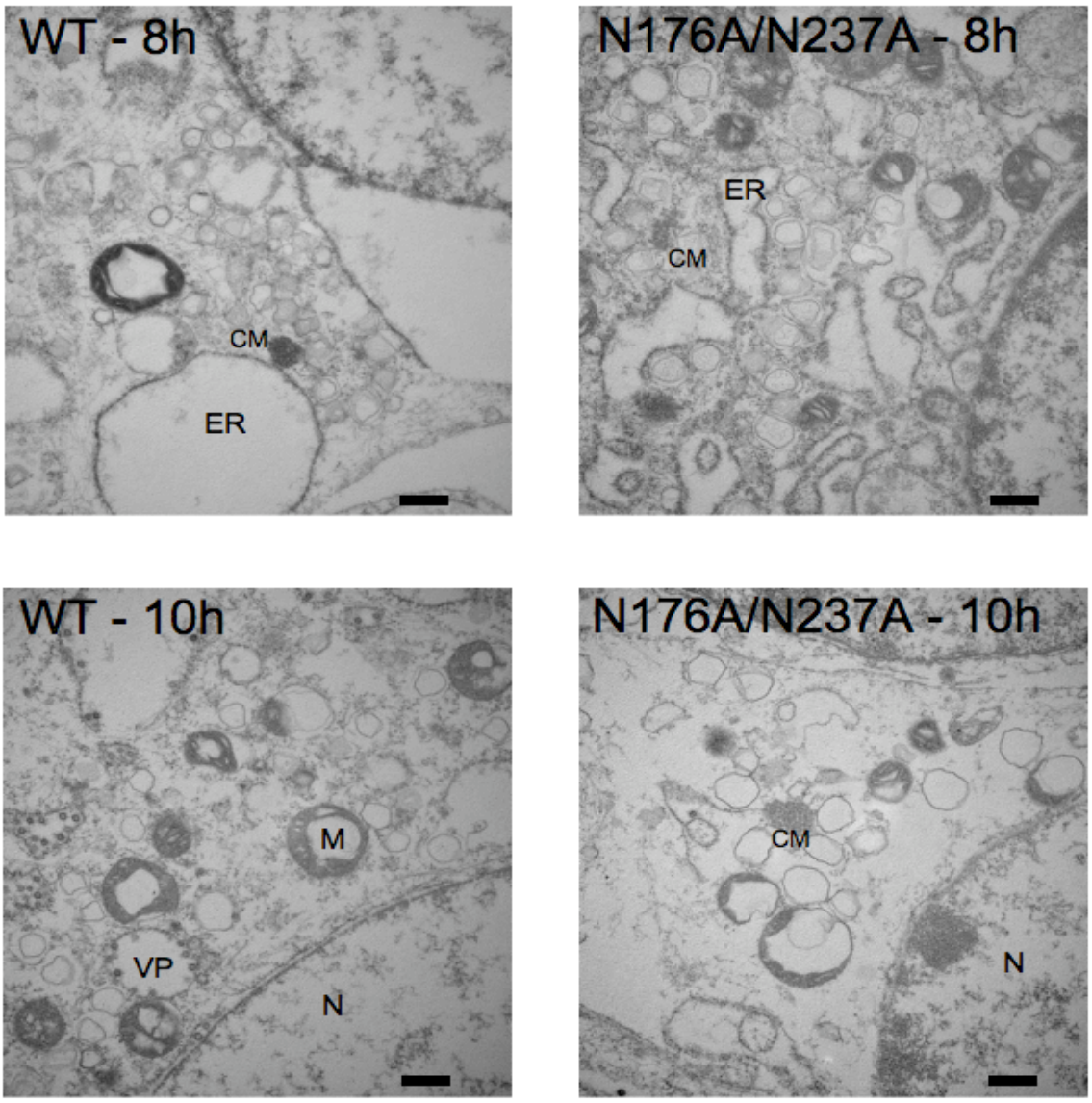

Fig. 5.4. EM time course of virus-induced membrane structures. DBT cells were infected with wt or N176A/N237A viruses. At 2 h intervals, cells were harvested in 2% glutaraldehyde and processed for TEM analysis. The scale bar in the images represents 500 nm. Black arrows point to regular DMVs. Red arrows show examples of irregular DMV structure. N, nucleus; ER, endoplasmic reticulum; M, mitochondria; CM, convoluted membranes; DMV, double membrane vesicle; VP, vesicle packet.

pathology compared to wild-type virus. While the findings presented here are consistent with those of Chapter IV, it appears that the rate of infection may be occurring faster in the EM time course experiment compared to the EM analysis in Chapter IV. This is supported by comparing wild-type infection at 6 h p.i. from both EM experiments. This may also account for the differences in DMV alterations observed in the N176A/N237A mutant infections from both experiments. Also, the quality of the membrane staining is better in the analysis from Chapter IV than at later times of infection in the EM time course. Therefore, a more comprehensive time course, e.g. 1 h intervals from 2 to 10 h p.i., is necessary to confirm nsp4's function(s) in the formation and organization of virus-induced membrane modifications. Lastly, time course experiments using immunofluorescence assays will also aid in determining nsp4's function(s) in the formation and stability of replication complexes over the duration of an infection.

Future studies: glycosylation of nsps

Analysis of the nsp3, nsp4, and nsp6 amino acid sequences and biochemical studies have shown all of these proteins have transmembrane domains that are likely critical for virus-induced membrane modifications (Baliji et al., 2009; Kanjanahaluethai et al., 2007; Oostra et al., 2007). Moreover, these reports have also analyzed the topology of these three proteins and have shown that the N- and C-termini of nsp3, nsp4, and nsp6 are all located within the cytoplasm. Research presented in this dissertation has shown that nsp4 is N-glycosylated during infection, and another study has demonstrated that nsp3 is N-glycosylated through plasmid expression of nsp3 (Table 5.2), which is consistent with glycosylation of these proteins in the ER lumen and lack of trafficking

nsp	No. of Putative N-linked Glycosylation Sites
1	2
2	2
3	7 (1 confirmed *in vitro)*
4	2 (2 confirmed during replication)
5	1
6	0
7	0
8	1
9	1
10	0
12	2
13	4
14	1
15	2
16	4

Table 5.2. Number of putative and confirmed N-linked glycosylation sites of MHV replicase proteins. The numbers of N-X-S and N-X-T glycosylation sequences in each replicase protein are indicated in the right column. The rarely N-linked glycosylated sequence N-X-C was not added to the number of N-linked glycosylation sites in the table. X stands for any amino acid except proline.

through Golgi (Kanjanahaluethai et al., 2007). Upon amino acid sequence analysis of all the replicase proteins, all have predicted N-linked glycosylation sites, except for nsp6 and nsp7 (Table 5.2). This dissertation has shown that glycosylation of nsp4 is critical for viral RNA synthesis and virus-induced membrane modifications; therefore, glycosylation of other nsps may be important for their overall functions. Specifically, it will be interesting to see if nsp3 is N-glycosylated during infection and what effects nsp3 glycosylation has on replication complex function and virus-induced membrane structures.

If any of the nsps that exhibit putative N-linked glycosylation sites, besides nsp3 and nsp4, are actually glycosylated, the specific proteins most likely would have to be shuttled into the ER lumen, since all the N- and C-termini of the transmembrane proteins nsp3, nsp4, and nsp6 are presumably located in the cytoplasm. Another possibility is that the predicted topology of nsp3, nsp4, and/or nsp6 is inaccurate, leading to the N-linked glycosylation of specific nsps. It is likely, though, that the C-terminus of nsp6 is cytoplasmic because data presented in Chapter IV has shown that nsp8 is not glycosylated in the ER, even though it has a putative N-linked glycosylation site. This would also suggest that any nsps downstream of nsp6 would not exhibit N-linked glycosylation unless the specific nsp was shuttled or translocated into the ER.

Currently, coronavirus RNA synthesis and the formation of virus-induced membrane structures are not well understood. While the exact sites of viral RNA synthesis are unknown, viral RNA has been shown to localize on DMVs and CMs, as well as on the inside of DMVs. Coronavirus nsps have also been shown to localize to

these same structures, which are a reticulovesicular network of membrane rearrangements. Because N-linked glycosylation occurs in the ER and DMVs and CMs are formed from or utilize hijacked ER membranes, analysis of the glycosylation events and status of certain nsps, specifically those that have been implicated in membrane rearrangements, RNA binding, and RNA synthesis, will provide a better understanding of where and how viral RNA synthesis occurs, how viral RNA is protected from detection and degradation by the cell, and how viral RNA is shuttled from sites of synthesis to sites of virion assembly.

Concluding remarks

Positive-strand RNA viruses are similar in many ways. These include: (1) their genomes function as mRNAs; (2) they replicate within the cytoplasm of host cells; (3) they utilize polyprotein processing as a mechanism to regulate protein expression and function; and (4) they induce membrane modifications and rearrangements of host cell membranes to form structures that support their viral RNA synthesis. These areas of overlap exhibited by all positive-strand RNA viruses are key avenues of research to better understand their life cycles and other important events that take place during infection, which will lead to potential vaccines and therapeutics that aid in the prevention and alleviation of diseases caused by these viruses. This dissertation has presented new research in several of these areas of interest, including polyprotein processing, the importance of genome organization, and replication complex structure and organization.

Basic scientific research is the foundation for discoveries that increase our understanding and knowledge of the world around us, and graduate school education is a

major contributor to these discoveries. The underlying purpose of any graduate education is learning and developing how to analyze and answer simple to complex problems by critically thinking about, evaluating, and answering the questions that address the problem at hand. This ability is fundamental in any discipline of basic scientific research.

The research presented in this dissertation is my modest contribution to the basic sciences and the field of microbiology. It is with hope that the data and reagents described in this dissertation will provide a basis for the future investigation of the cell biology and replication of positive-strand RNA viruses and aid in the development of vaccines and therapeutics to prevent and combat virus infections.

CHAPTER VI

MATERIAL AND METHODS

Wild-type virus, cells, and antibodies

Recombinant wild-type MHV strain A59 (wt; GenBank accession number AY910861) was used as the wild-type control for all experiments. Delayed brain tumor (DBT) cells expressing the MHV receptor carcinoembryonic antigen cell adhesion molecule-1 (Chen et al., 1997; Hirano, Fujiwara, and Matumoto, 1976; Yount et al., 2002) and baby hamster kidney cells expressing the MHV receptor (BHK-MHVR) (Chen and Baric, 1996; Chen et al., 1997; Yount et al., 2002) were grown in Dulbecco's modified Eagle medium (DMEM) (Gibco) supplemented with 10% fetal calf serum (FCS) for all experiments. Medium for BHK-MHVR cells was supplemented with G418 (Mediatech) at 0.8 mg/ml to maintain selection for cells expressing the MHVR.

Rabbit polyclonal antibodies were used in biochemical experiments and have been previously described. Antibodies include include α-nsp1 (VU221)(Brockway et al., 2004), α-nsp2 (VU154)(Sims, Ostermann, and Denison, 2000), α-nsp3 (VU164)(Graham et al., 2005), α-nsp4 (VU158)(Sparks, Lu, and Denison, 2007), α-nsp8 (VU123) (Bost, Prentice, and Denison, 2001), and α-M (J.1.3) (Brockway et al., 2003).

Construction and generation of mutant MHV cDNA plasmids

Mutant cDNA plasmids that contained the desired mutations were generated through multiple PCR techniques. All PCR reactions were performed with the following

parameters: initial denaturation at 95°C once for 2 min, denaturation at 95°C for 75 s, annealing at various temperatures, depending on the melting temperature of the primers, for 75 s, extension at 72°C for 1 min per kilobase, and repeating the denaturing, annealing, and extension steps for a total of 35 to 45 cycles.

For MHV nsp2 duplication, insertion, and mutagenesis, several PCR mutagenesis strategies were performed. Primers listed in Table 2.1 were used for introduction of desired mutations into the fragment of interest. Insertion of nsp2 in ORF1b was achieved by generating compatible restriction overhangs by PCR. The PCR products to introduce nsp2 in ORF1b were ligated, and ligations were then cloned into Fragment F using native *Drd I* and *BstB I* restriction sites. Deletion of ORF4 and insertion of nsp2 in place of ORF4 were also generated using this method. For deletion of ORF4, PCR was performed using primers that would delete ORF4, and ligations were then cloned into fragment G using *Mlu I* and *EcoR V* sites. Insertion of nsp2 in place of ORF4 was achieved by ligating the PCR products, and the ligations that contained the nsp2 coding sequence in place of ORF4 was introduced into fragment G using using *Mlu I* and *EcoR V* restriction sites. Additions to the N- and C-terminus of nsp2 were added using the splicing by overlap extension method, and PCR products with the N- and C-terminal nsp2 mutations were digested, along with fragment A, and the digested PCR product was ligated into the fragment. The constructs generated for all mutations were confirmed by sequencing.

For substitution of the position 4 through position 1 (P4 – P1) CS amino acids at CS1 and CS2 (ORF1a nucleotides 939 to 950 and 2694 to 2705, respectively), PCR mutagenesis was performed using the MHV-A59 infectious clone fragment A (pCR-XL-TopoA), which consists of nucleotides 1 to 4882, as template DNA(Yount et al., 2002).

The splicing by overlap extension method with the ExSite/QuikChange mutagenesis kit (Stratagene) was used to replace CS1 with CS3(Horton et al., 1989). Changes to the manufacturer's protocol include the use of Pfu Turbo DNA polymerase instead of the ExSite DNA polymerase mix. For substitution of CS2 with CS3, PCR mutagenesis with primers that amplified all of fragment A was performed with the Fail-Safe PCR kit (Epicentre). For CS3 replacement of CS1, PCR products were gel purified, digested with restriction endonucleases SacII and AleI and ligated into fragment A that had also been digested with SacII and AleI.

For introduction of both CS substitutions into the same fragment, restriction endonucleases SacII and AleI were used to digest both fragments containing the mutated CSs. The fragment that contained CS1 replaced by CS3 was then ligated into fragment A containing substitution of CS2 by the CS3 sequence. Lastly, a catalytically inactive PLP1 (PLP1ko)(Graham and Denison, 2006), where the catalytic Cys and adjacent Trp residues are mutated to Ala, and both CS substitutions were engineered into the same fragment by restriction endonuclease digestion with XhoI of a fragment containing the CS1 to CS3 substitution and of a fragment containing both the CS2 to CS3 substitution and the PLP1ko mutation. The fragments were then ligated overnight at 16°C. All generated cDNA fragments were sequenced to confirm the introduced mutations and absence of spontaneous mutations.

For introduction of asparagine-to-alanine substitutions in the nsp4 coding sequence (ORF1a nucleotides 8721 to 10208), PCR was performed using the MHV-A59 infectious clone fragment B (pCR-XL-pSMART B) as a template. Fragment B of the MHV-A59 clone contains MHV ORF1a nsp4 nucleotides 8721 to 9555 (Yount et al.,

2002). Asparagine-to-alanine codon changes were introduced using the ExSite/QuikChange mutagenesis kit (Stratagene) with primers in Table 4.1. Changes to the manufacturer's protocol included the use of Pfu Turbo and Pfu Ultra instead of the ExSite DNA polymerase blend. Products were ligated and sequenced across the MHV genome-containing region of fragment B to ensure that PCR amplification did not introduce any unintended mutations. For introduction of both N176A and N237A, restriction endonuclease EcoN I was used to digest both single nsp4 glycosylation mutant plasmids, and ligation was used to introduce both mutations into the same plasmid. The plasmid was then sequenced to confirm the engineered mutations and absence of unintended muations.

Generation of MHV mutant viruses

Viruses containing the engineered mutations within the MHV genome were produced using the infectious cDNA assembly strategy for MHV-A59 that has been previously described by Yount et al. (Yount et al., 2002) and modified by Denison et al. (Denison et al., 2004) and Sparks et al (Sparks, Lu, and Denison, 2007). Briefly, plasmids containing the seven cDNA cassettes that make up the MHV genome were digested using the appropriate restriction enzymes. The correct restriction fragments were gel-purified and ligated together overnight at 16°C. The ligated DNA was purified, *in vitro* transcribed, and electroporated with N gene transcripts into BHK-MHVR cells. The electroporated cells were then laid over a layer of 2.5×10^6 uninfected DBT cells in a 75 cm^2 flask and incubated at 37°C. Virus viability was determined by cytopathic effect (CPE), in this case syncytia formation, in the electroporated cell culture. Progeny virus

in the cell culture medium of electroporated cells (passage 0 [P0]) was passaged onto uninfected DBT cells (P1), and the virus released from cells in the culture medium was designated as the P1 stock, which was titered and used for all experiments.

RT-PCR and sequencing of recovered viruses

Total intracellular RNA was harvested from P1-infected cells using TRIzol (Invitrogen) according to the manufacturer's protocol. Extracted RNA was used as a template for RT-PCR. Reverse transcription was performed using Superscript III reverse transcriptase (Invitrogen) and random hexamers (Roche). Primers complementary to genome nucleotides of sense and antisense polarity were then used to amplify the coding region of interest by PCR. These PCR products were sequenced to confirm the retention of the engineered mutations and the absence of additional mutations in the coding sequence of interest. For full genome sequencing, primers complementary to specific genome sequences were amplified by PCR using the reverse transcription products to produce amplicons that covered the entire genome. The amplicons were gel purified and directly analyzed by automated DNA sequencing.

Protein immunoprecipitations

For steady-state radiolabeling of proteins and immunoprecipitations, cells were grown on 60-mm dishes and infected at an MOI of 1, 5, or 10 PFU/cell with wt or MHV mutant viruses and incubated at 37°C. At 4 to 5.5 h p.i., medium was aspirated and replaced with medium lacking methionine and cysteine and supplemented with Act D (Sigma) at a final concentration of 20 μg/ml. After addition of Act D for 30 min to 1 h,

cells were radiolabeled with [^{35}S] methionine-cysteine ([^{35}S]Met-Cys) at a concentration of 0.08 mCi/ml. When cells reached ~90% involvement in syncytia, radiolabeled cells were washed once in PBS and then lysed in 1 ml of lysis buffer lacking sodium dodecyl sulfate (SDS) (1% NP-40, 0.5% sodium deoxycholate, 150 mM NaCl, and 50 mM Tris, pH 8.0). Lysates were then centrifuged at 6,000 × g for 3 minutes to remove cellular debris and nuclei, and the supernatant was collected. Immunoprecipitations were performed in a final volume of 1 ml, using protein A-sepharose beads (Sigma), 50 to 100 μl of radiolabeled lysate, 1:200 or 1:500 dilutions of polyclonal antisera, and proteinase inhibitor (Roche) in lysis buffer. Immunoprecipitations were then performed as previously described (Sparks, Lu, and Denison, 2007).

For pulse-chase analysis, DBT cells were infected with an MOI of 10 PFU/cell. At 6 h p.i., cells were trypsinized and resuspended in 10 ml total volume of media. Cells were centrifuged for 5 min at 1000 RPM, and the cells were resuspended and rotated in a 1.5 ml eppendorf tube with medium lacking methionine and cysteine and supplemented with Act D (Sigma) at a final concentration of 20 μg/ml. At 7 h p.i., cells were radiolabeled with [^{35}S]Met-Cys at a concentration of 0.08 mCi/ml for 1 hour. Cells were centrifuged, washed once with prewarmed PBS, and resuspended in 1 ml of complete media with 100 μg/ml cycloheximide. The predetermined time points were harvested, washed once in PBS, and harvested with lysis buffer. Immunoprecipitations were then performed as noted above.

For endoglycosidase H (Endo H) treatment, supernatant was transferred to a new tube after heating at 70°C for 10 min. Endo H (Sigma) was added to the supernatant according to the manufacturer's protocol, and the mixture was incubated at 37°C for 3 h.

Proteins were resolved by SDS-PAGE in 4 to 12% polyacrylamide gradient Bis-Tris gels (NuPage; Invitrogen) and analyzed by fluorography. ^{14}C-labeled high molecular weight markers (NEB) and a full-range rainbow marker were used as molecular weight standards.

Viral growth assays

For viral growth determination (Denison et al., 2004), DBT cells were infected with wt or nsp4 glycosylation mutant viruses at the MOIs indicated. Following a 45 min absorption period at 37°C with periodic swirling, medium was aspirated, and the cells were washed three times in PBS. Prewarmed 37°C medium was then added back to the cells, and the cells were incubated at 37°C. Aliquots of medium were taken from 1 to 30 h p.i., and virus titers were determined by plaque assay as previously described(Kim et al., 1995).

Genomic and subgenomic viral RNA analysis

For genomic and subgenomic analysis of viral RNA, cells in 60-mm dishes were mock-infected or infected at an MOI of 5 PFU/cell. Following a 45 min absorption at 37°C, medium containing virus was removed, and cells were washed twice in PBS. Cells were pretreated with ActD from 8.5 to 9 h p.i., after which [^{3}H]uridine was added to a final concentration of 50 μCi/ml, and cells were incubated for 2 h. At 11 h p.i., total intracellular RNA was isolated using TRIzol reagent (Invitrogen) according to the manufacturer's protocol. From the total volume of each RNA sample, 2.5% was denatured using glyoxal loading dye (Ambion) at 50°C for 30 min and resolved by electrophoresis

in 1% agarose gels. After electrophoresis, gels were incubated in 100% methanol for 1 h, in 1% 2,5-diphenyloxazole in methanol for 1 h, and in water for 2 h. Gels were then dried by vacuum filtration at 50°C and exposed to X-ray film.

Metabolic labeling of viral RNA

DBT cells were either mock-infected or infected at an MOI of 5 PFU/cell with wt or nsp4 glycosylation mutant viruses in 6-well plates. Following a 45 min absorption at 37°C, medium containing virus was removed, and cells were washed twice in PBS. Cells were then incubated in growth medium at 37°C until 30 min prior to labeling, when medium was replaced with fresh medium containing 20 μg/ml Act D. After this 30 min treatment, [^{3}H]uridine was added to a final concentration of 40 μCi/ml, and cells were incubated at 37°C for 2 h intervals from 3 to 15 h p.i. At the end of each labeling period, cells were lysed in lysis buffer (described above), and nuclei were removed by centrifugation at 14,000 × g for 3 min. RNA in 10% of each lysate was precipitated with chilled 5% trichloroacetic acid (TCA) onto glass microfiber filters (Whatman), washed twice in fresh 5% TCA and twice in 95% ethanol, and dried using vacuum filtration. Radiolabel incorporation was quantitated by liquid scintillation counting.

Immunofluorescence assays

DBT cells grown on glass coverslips were infected with wt or nsp4 glycosylation mutant viruses at an MOI of 10 PFU/cell. At 6 h p.i., medium was aspirated from cells, and cells were fixed in 100% methanol at -20°C. Cells were rehydrated in PBS for 10 min, blocked in PBS containing 5% bovine serum albumin (BSA), and then aspirated.

For indirect immunofluorescence, cells were incubated with primary antibody (α-nsp2, 1:200; α-nsp4, 1:200; α-M, 1:1000) in wash solution (PBS containing 1% BSA and 0.05% NP-40) for 1 h at room temperature. Cells were washed in wash solution three times for 5 min/wash. Cells were then incubated with secondary antibody (goat α-rabbit-Alexa 488, 1:1000; goat anti-mouse Alexa 546, 1:1000; Molecular Probes) for 30 min at room temperature. Cells were washed again three times for 5 min/wash, followed by a final wash in PBS, and rinsed with distilled water. For direct immunofluorescence, α-nsp8 was purified using HiTrap rProtein A FF columns (GE Life Sciences) for fast protein liquid chromatography. α-nsp8 was directly conjugated using the Alexa Fluor 488 or 546 protein labeling kit (Invitrogen) according to the manufacturer's protocol. Cells were incubated with α-nsp8 at a concentration of 1:500, following the same procedure as above. Coverslips were mounted with Aquapolymount (Polysciences) and visualized using a Zeiss LSM510 or a Zeiss Axiovert 200 microscope with a 40× oil immersion lens. Images were processed and merged using Adobe Photoshop CS2 or CS3.

Transmission electron microscopy (TEM) analysis

DBT cells were mock-infected or infected with wt or nsp4 glycosylation mutant viruses at an MOI of 5 PFU/cell in a 60-mm dish and incubated at 37°C. At 6 h p.i., medium was aspirated, and cells were washed once with PBS. The cells were then fixed in 2% glutaraldehyde for 10 minutes, scraped off the dishes, and centrifuged at 0.5 × g for 3 min. The initial 2% glutaraldehyde was aspirated, fresh 2% glutaraldehyde was added to the fixed cells for 1 h, aspirated, and fresh glutaraldehyde was added to the fixed

cells for overnight incubation at 4°C. Cells were washed three times in PBS, transferred to 1% osmium tetroxide in diH_2O for 1 h, and washed three times in diH_2O. Cells were stained *en bloc* in 1% aqueous uranyl acetate for 1 h, and washed three times in diH_2O. Dehydration of cells was carried out gradually using graded series of ethanol and increasing the times each remained in solution, starting with 30%, followed by 50%, 70%, 95%, and finally absolute ethanol. Propylene oxide was used as a transitional solvent to replace the dehydration solution. Cells were transferred to a 1:1 araldite:propylene oxide mixture for 1 hour and then placed in pure araldite in a vacuum oven for another hour to help pull resin through the tissue. Pure resin specimens were then transferred into capsules containing fresh resin and finally placed into an oven overnight to polymerize. Ultra-thin serial sections (50-60 nm) from polymerized blocks were obtained using a Leica UCT Ultracut microtome (Leica Microsystems, Vienna, Austria), transferred to formvar-coated slot grids, and examined using a Phillips CM10 TEM (FEI Company, Hillsboro, OR) equipped with an Advantage Plus 2 megapixel Digital CCD System for CM10 TEM (Advanced Microscopy Techniques, Danvers, MA).

Statistical analyses

For statistical analyses, DMVs were characterized into two groups, either regular (defined by inner membranes in close approximation with the outer membrane) or irregular DMVs (defined by moderate to severe disruption or separation of the inner membrane with the outer membrane). Chi square analysis using contingency tables was performed comparing the number of regular-formed DMVs to irregular-formed DMVs of

wt and nsp4 glycosylation mutant viruses. Chi square analysis was also performed to compare the presence of both CMs and DMVs to the presence of DMVs only. Because CMs were only found in the presence of DMVs, the presence of CMs and DMVs was compared to the presence of DMVs alone in a given TEM section. Diameters of DMVs were measured using ImageJ 1.40g (http://rsb.info.nih.gov/ij). Diameters were defined by measuring the widest diameter from the outside membrane of one side to the outside membrane of the opposite side of a single DMV. To determine whether there was a statistical difference between the diameters of DMVs, analysis of variance (ANOVA) was used to compare wt and nsp4 glycosylation mutant viruses. Because a statistical difference was indicated through ANOVA, Tukey tests were used to perform pair-wise comparisons of all viruses. P values were determined to indicate significance.

APPENDIX A

MURINE CORONAVIRUSES ENCODING NSP2 AT DIFFERENT GENOMIC LOCI HAVE ALTERED REPLICATION, PROTEIN EXPRESSION, AND LOCALIZATION

JOURNAL OF VIROLOGY, Dec. 2008, p. 11964–11969 Vol. 82, No. 23
0022-538X/08/$08.00+0 doi:10.1128/JVI.01126-07

Murine Coronaviruses Encoding nsp2 at Different Genomic Loci Have Altered Replication, Protein Expression, and Localization[▽]

Mark J. Gadlage,[2,3] Rachel L. Graham,[1,3]† and Mark R. Denison[1,2,3]*

Departments of Pediatrics[1] and Microbiology and Immunology[2] and The Elizabeth B. Lamb Center for Pediatric Research,[3] Vanderbilt University Medical Center, Nashville, Tennessee

Received 23 May 2007/Accepted 17 September 2008

Partial or complete deletion of several coronavirus nonstructural proteins (nsps), including open reading frame 1a (ORF1a)-encoded nsp2, results in viable mutant proteins with specific replication defects. It is not known whether expression of nsps from alternate locations in the genome can complement replication defects. In this report, we show that the murine hepatitis virus nsp2 sequence was tolerated in ORF1b with an in-frame insertion between nsp13 and nsp14 and in place of ORF4. Alternate encoding or duplication of the nsp2 gene sequence resulted in differences in nsp2 expression, processing, and localization, was neutral or detrimental to replication, and did not complement an ORF1a Δnsp2 replication defect. The results suggest that wild-type genomic organization and expression of nsps are required for optimal replication.

Coronaviruses are positive-sense RNA viruses that translate the first open reading frames (ORFs; ORF1a and ORF1b) of their 30-kb genome RNA into polyproteins that are co- and posttranslationally processed into intermediate and mature nonstructural proteins (nsps; nsps 1 to 16). The nsps interact on cytoplasmic membranes at sites of viral RNA synthesis, referred to as replication complexes (4, 5, 10, 17, 22, 25). Translation of ORF1b, which encodes several proteins confirmed or predicted to be essential for viral RNA synthesis, requires a ribosomal frameshift event at the end of ORF1a that occurs at 10 to 40% efficiency in vitro (2, 9, 13–15, 18, 21, 23).

The murine hepatitis virus (MHV) nsp2 is a 65-kDa protein that has minimal sequence identity or similarity among different coronavirus groups and has no known or predicted functions. We have shown for MHV and severe acute respiratory syndrome coronavirus (SARS-CoV) that in-frame deletion of nsp2 (Δnsp2) yields viable mutant viruses (12). However, both MHV and SARS-CoV Δnsp2 mutants exhibit a 90% reduction in peak titer and a 50% reduction in viral RNA synthesis. To determine if expression of nsp2 from nonnative sites could complement the defect in MHV Δnsp2 replication, we engineered the nsp2 coding sequence at alternate sites in the genome both in the absence and in the presence of the wild-type ORF1a nsp2 sequence. The results indicate that nsp2 can be encoded and expressed alone from ORF4, as a sequence duplication in ORF1a and ORF1b or in ORF1a and ORF4, but not near the end of ORF1a or alone in ORF1b. Duplication or expression of the nsp2 sequence from ORF4 was detrimental to replication compared to that of the wild type, indicating that the native context of nsp2 expression, and possibly a single copy of the sequence, may be necessary for optimal function in replication. Results also indicate that the addition of amino acids at the N and C termini of natively expressed nsp2 has no effect on peak viral growth.

nsp2 can be encoded in replication-competent mutant viruses in ORF4 and between nsp13 and nsp14 in ORF1b. MHV nonessential ORFs have been shown to tolerate foreign gene insertion (3, 8, 19). In order to test the effects of nsp2 expression in downstream ORFs, we engineered a mutant MHV genome by substitution of the nsp2 coding sequence in place of the nonessential ORF4 coding sequence, while retaining the ORF4 transcriptional regulatory sequence (5′-CUAAAC-3′) and start codon (Fig. 1 and Table 1). To determine if nsp2 could be expressed from alternate locations in the replicase, we engineered the nsp2 sequence at the end of ORF1a following nsp10 (nsp10-11 and nsp10-12 junction) and in ORF1b between nsp13 and nsp14. Since processing between nsp10-12 and nsp13-14 is mediated by nsp5 (3CLpro), we designed minimal 3CLpro recognition cleavage sites of P2-LeuGln ↓ Ser-P1′ (16, 20, 27) at the amino and carboxyl termini of nsp2 by the addition of a Ser residue to the N terminus of nsp2 and LeuGln residues to its C terminus, leaving the 3CLpro recognition sequences of nsp10, nsp12, nsp13, and nsp14 intact. The wild-type N-terminal nsp2 residue is Val; we selected Ser as a conservative addition that would optimize for cleavage by nsp5. We have previously shown that P1′ substitutions at the amino terminus of nsp2 that allow processing (Ala, His) do not affect virus growth or RNA synthesis (6); however, to determine if Ser and LeuGln additions had any effects on nsp2 functions of alternately expressed nsp2 viruses, these mutations were engineered into natively expressed nsp2 in a wild-type virus background.

Infectious viruses with the following mutations were recovered from supernatants of electroporated cells: ORF4 deletion, with or without ORF1a nsp2 expression (1a-2/Δ4 and Δ1a-2/Δ4); ORF4 nsp2 with or without ORF1a nsp2 expression (1a-2/4-2 and Δ1a-2/4-2); ORF1b nsp2 with ORF1a nsp2 expression (1a-2/13-2-14); and ORF1a nsp2 with amino acid additions at the N and/or C terminus (1a-S2, 1a-2LQ, and 1a-S2LQ). The supernatants from electroporated cells were passed to expand the populations (pas-

* Corresponding author. Mailing address: Department of Pediatrics, Vanderbilt University Medical Center, D6217 MCN, 1161 21st Ave. S, Nashville, TN 37232. Phone: (615) 343-9881. Fax: (615) 343-9723. E-mail: mark.denison@vanderbilt.edu.

† Present address: University of North Carolina at Chapel Hill, Chapel Hill, NC 27599-7435.

▽ Published ahead of print on 24 September 2008.

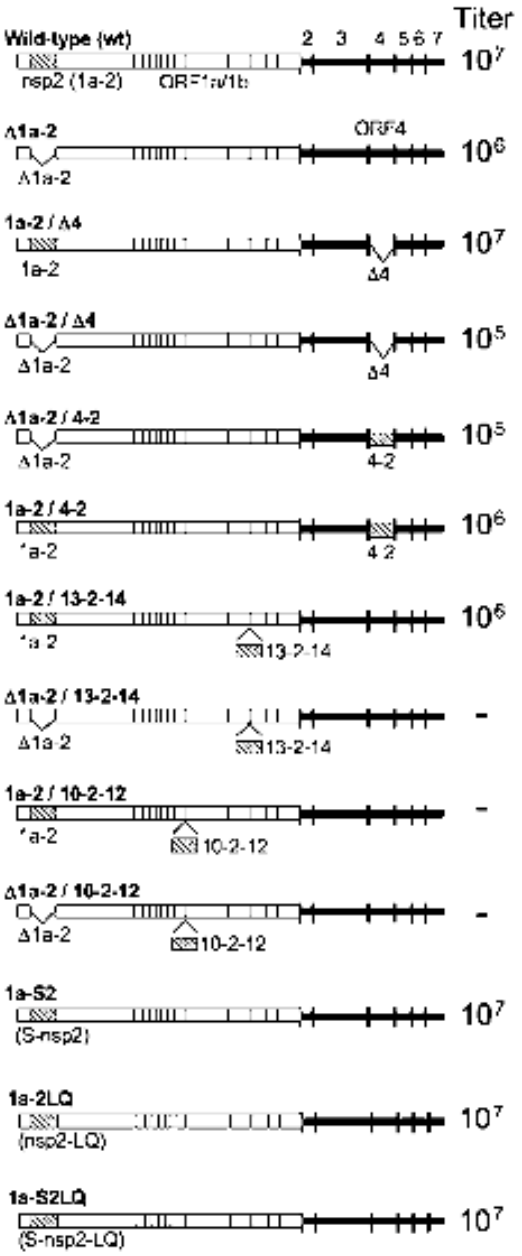

FIG. 1. Engineering nsp2 deletions, mutations, rearrangements, and duplications. For each construct, alterations to the genome are shown. Constructs are listed as named in the text. ORFs 1 to 7 are labeled above the wild-type schematic. The nsp2 coding sequence is depicted as a hatched rectangle. Coding region locations and sizes are not drawn to scale. Deletion of the nsp2 and/or ORF4 coding sequence or insertion of nsp2 in ORF1b is indicated by a caret. Protein coding deletions are indicated by a delta (Δ) in the virus name. The nsp2 position is indicated as ORF1a (1a-2), ORF1b (13-2-14 or 10-2-12), or ORF4 (4-2). Approximate peak titers of viable viruses are indicated to the right of each construct. Viruses that were not recovered are indicated by a minus sign (−).

sage 1 [P1]), and RNA from cells infected with P1 virus stocks was used to confirm the retention of all engineered changes from recovered mutants. Multiple attempts to recover mutants lacking ORF1a nsp2 but expressing nsp2 in ORF1b (Δ1a-2/13-2-14) failed to produce infectious virus. We also were not able to recover mutants encoding nsp2 in-frame between nsp10 and nsp12, with or without ORF1a nsp2 expression (1a-2/10-2-12 and Δ1a-2/10-2-12).

Protein expression and processing from nsp2 alternate expression and duplication viruses. To determine the expression and processing of nsp2 in mutant virus infections, lysates of radiolabeled, virus-infected DBT cells were immunoprecipitated with antisera against nsp1, nsp2, and nsp3 (Fig. 2A). Mature nsp1 (28 kDa) was detected in all mutant virus-infected cells, demonstrating normal processing between nsp1 and nsp2 by the nsp3 papain-like proteinase 1 (PLP1). Mutant viruses that expressed nsp2 from ORF1a (1a-2/Δ4, 1a-2/13-2-14, and 1a-2/4-2) and the Δnsp2 virus (Δ1a-2) all produced similar amounts of nsp1 relative to that of the wild type, while the Δ1a-2/Δ4 and Δ1a-2/4-2 viruses expressed lower levels of nsp1. nsp3 was detectable with anti-nsp3 in wild-type-infected cells as both mature nsp3 (210 kDa) and intermediate nsp2-3 (275 kDa). Mutant viruses that encoded nsp2 in its native position (1a-2/Δ4, 1a-2/4-2, and 1a-2/13-2-14) also had detectable nsp3 and nsp2-3. Only mature nsp3 was detected in infections with viruses that lacked ORF1a-expressed nsp2 (Δ1a-2, Δ1a-2/Δ4, and Δ1a-2/4-2).

As expected, mutant viruses that did not encode nsp2 at any location (Δ1a-2 and Δ1a-2/Δ4) had no detectable nsp2. Viruses encoding nsp2 from one or two locations in the genome exhibited a range of nsp2 expression levels. The Δ1a-2/4-2 virus expressed low levels of nsp2, while the 1a-2/Δ4 mutant virus expressed nsp2 at levels similar to those expressed by the wild type. The 1a-2/4-2 duplication mutant, which encoded nsp2 in both ORF1a and ORF4, expressed higher levels of nsp2 than the wild-type virus. To test whether the increased expression was due to just two coding locations or if there were also altered levels of ORF4 subgenomic RNA, infected cells were labeled with [^{3}H]uridine in the presence of actinomycin D, and viral RNAs were measured by densitometry by using ImageJ 1.40 (http://rsb.info.nih.gov/ij/) (Fig. 2B). All genomic and subgenomic RNA species were detected, but RNA4 encoding nsp2 in ORF4 in the 1a-2/4-2 virus was expressed with a 2.5-fold increase, as a ratio to RNA7, compared to wild-type virus. This is sufficient to account for the increased nsp2 levels and suggests that insertion of foreign genes in ORF4 may specifically alter mRNA transcription.

The 1a-2/13-2-14 mutant virus, which encoded nsp2 in both ORF1a and ORF1b, expressed overall levels of mature nsp2 that were comparable to those expressed by the wild type. This could have resulted from either diminished translation from ORF1b or impaired or absent processing. The requirement for in-frame translation of nsp13 and nsp14 for virus viability argues that the in-frame nsp2 must be translated from this loca-

TABLE 1. Description of primers

Primer	Sequence	Sense	Purpose
nsp13-nsp2 A	5′GTCAATGACACCACTCGCAAGTATGTGTTTACT	+	PCR partner for nsp13-nsp2 B
nsp13-nsp2 B	5′CGTCTCGCACACTGTAATCGTGGATTGTTAATCTT	−	Insertion mutagenesis partner for A
nsp2 1b Ins C	5′CGTCTCGTGTGTTAAGCCCATCCTGTTTGTGGAC	+	nsp2 ORF1b insertion mutagenesis
nsp2 1b Ins D	5′CGTCTCGCTGTAATCGCGCACAGGGAAACCTCCAGCACTG	−	nsp2 ORF1b insertion mutagenesis
nsp2-nsp14 E	5′CGTCTCGACAGTGTACTACAAATTTGTTTAAGGATTGT	+	Insertion mutagenesis partner for F
nsp2-nsp14 F	5′CATGTGAGCTCAAAGCTGGCAGCCCACGTCAC	−	PCR partner for nsp2-nsp14 E
ORF4 Ins A	5′CAGGCCATAGAAAAGGTCAATGAGTGCGTT	+	PCR partner for ORF4 Ins B primers
ORF4 Ins2 B1	5′CGTCTCGCCATCTATAAATTGTTTAGATTTTCTG	−	Insertion mutagenesis partner for A
ORF4 InsKo B2	5′CGTCTCGTTTATTACTATAAATTGTTTAGATTTTCTG	−	ORF4 deletion partner for A
ORF4 nsp2 C	5′CGTCTCGATGGTTAAGCCCATCCTGTTTGTGGAC	+	nsp2 ORF4 insertion mutagenesis
ORF4 nsp2 D	5′CGTCTCGTTTATTACGCACAGGGAAACCTCCAGCACTG	−	nsp2 ORF4 insertion mutagenesis
ORF4 Ins E	5′CGTCTCGTAAACTCCAAGAGGTTTTGATTATAGTACA	+	Insertion mutagenesis partner for F
ORF4 Ins F	5′CTTAAGGAATTGAACTGCCTCGTCGGCCGT	−	PCR partner for ORF4 Ins E
S-nsp2 F	5′GGGCTATCGCGGTTCTGTTAAGCCCATCCTG	+	Insertion mutagenesis partner for S-nsp2 R
S-nsp2 R	5′CAGGATGGGCTTAACAGAACCGCGATAGCCC	−	Insertion mutagenesis partner for S-nsp2 F
nsp2-LQ F	5′GGTTTCCCTGTGCGCTCCAAGGCAAGAAAGTCGAG	+	Insertion mutagenesis partner for nsp2-LQ R
nsp2-LQ R	5′CTCGACTTTCTTGCCTTGGAGCGCACAGGGAAACC	−	Insertion mutagenesis partner for nsp2-LQ F
158 A F	5′TCCGGCTCGTATGTTGTGTGGAAT	+	PCR partner for S-nsp2 R and nsp2-LQ R
3253 A R	5′CTGCGTCAAGCACAACATCAAGCA	−	PCR partner for S-nsp2 F and nsp2-LQ F

tion in ORF1b. The efficiency of ribosomal frameshifting and translation of ORF1b relative to ORF1a has not been experimentally tested during virus infection but is predicted to be less than 25% (2). This would be consistent with the detection of minimal additional nsp2. The lack of detection would also result if expressed nsp2 was not cleaved from nsp13 or nsp14, or both and thus was not detected as mature nsp2. Immunoprecipitation with anti-nsp2 or anti-nsp13 antisera did not resolve precursors consistent with a predicted size for nsp13-2 (130 kDa), nsp2-14 (130 kDa), or nsp13-2-14 (190 kDa) (data not shown). Taken together, these data indicate that the level of protein expression depends on a combination of the number of coding sequence copies and the context of expression.

Localization of nsp2 in cells during infection with mutant viruses. To determine if nsp2 localization was affected by genomic location and extent of expression, DBT cells were infected, and at 6 h postinfection (p.i.), cells were fixed and stained with antibodies against nsp2 and nsp8, both markers for replication complexes (1) (Fig. 3). nsp2 and nsp8 signals colocalized in characteristic cytoplasmic perinuclear foci in cells infected with viruses expressing both nsp2 and nsp8 (wild type, 1a-2/Δ4, and Δ1a-2/4-2). When expression of nsp2 was absent (Δ1a-2/Δ4), no nsp2 signal was present, while nsp8 signal was still detected in punctate foci. nsp2 expressed from the 1a-2/4-2 virus showed partial colocalization with nsp8 signal, but nsp2 was also detected as diffuse cytoplasmic fluorescence that was not associated with punctate foci. A possible explanation for this result is that simultaneous expression of nsp2 from ORF1 and ORF4 in the 1a-2/4-2 virus saturates replication complexes. This would be consistent with the observed increase in nsp2 expression (Fig. 2A). This conclusion is also supported by the observation that infection with the 1a-2/13-2-14 mutant, which resulted in lower levels of mature nsp2 (Fig. 2A), showed colocalization of nsp2 with nsp8, but no additional localization or diffuse fluorescence (Fig. 3). While direct proof of differential localization of nsp2 would require unique tags for nsp2 at different loci, it is still clear that alteration of nsp2 coding location within the genome results in differences in both extent of protein expression and localization of nsp2 during infection.

nsp2 encoded at different loci results in varied effects on viral growth but does not complement nsp2 deletion from ORF1a. To assess the effects of alternate nsp2 encoding on viral replication, DBT cells were infected at a multiplicity of infection (MOI) of 1 PFU/cell, aliquots of supernatant were saved, and titers of virus were determined by a plaque assay (Fig. 4). As has been shown previously (8), the deletion of ORF4 resulted in a mutant virus that had growth kinetics and peak titers indistinguishable from those of the wild type (Fig. 4A). Deletion of nsp2 alone (Δ1a-2) resulted in a decrease of ~1 $\log_{10}$ compared to the wild type, also consistent with previous studies (11). Expression of nsp2 from ORF4 in the presence or absence of ORF1a nsp2 was similar to that of the parental Δ1a-2 mutant in the timing of exponential growth. However, the 1a-2/4-2 virus reached a slightly higher titer than the Δ1a-2 virus but did not achieve wild-type growth at 24 h p.i. (Fig. 4B), suggesting that expression of nsp2 at increased total levels may in fact be detrimental to virus growth fitness. Also, the Δ1a-2/4-2 virus achieved a 0.5-$\log_{10}$ lower peak titer than the Δ1a-2 virus, and the titer declined more rapidly than that of either the Δ1a-2 or the 1a-2/4-2 virus over a 24-h period. The results show that ORF4 expression of nsp2 does not complement the deletion of nsp2 from ORF1a and suggest that ORF4 expression of nsp2 in the absence of ORF1a nsp2 expression results in a less-fit mutant virus. When nsp2 was expressed in ORF1b (1a-2/13-2-14), growth was delayed in timing, and peak titer could not reach that of the wild-type virus at 24 h p.i., even though peak titers were still increasing, similarly to the 1a-2/4-2 virus (Fig. 4B).

We were surprised that the deletion of both nsp2 and ORF4 or nsp2 replacement of ORF4 (Δ1a-2/Δ4 and Δ1a-2/4-2) yielded mutants with more delayed and/or decreased growth than deletion of either nsp2 or ORF4 alone (Fig. 4A). These results suggest possible interactions and/or cooperative functions of nsp2 and the ORF4 protein(s) in the viral life cycle. Both nsp2 and the ORF4 gene product(s) are group-specific proteins (7, 17, 28) and may have as-yet-uncharacterized interactions. Alternatively, it is possible that the known replication defect of the Δnsp2 mutant exacerbates a replication defect in an ORF4 deletion mutant that alone does not manifest as a

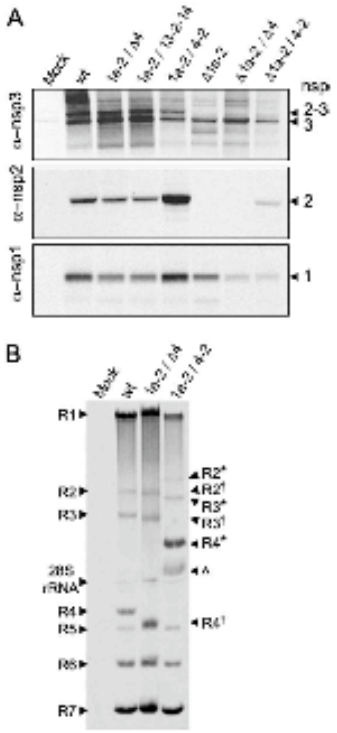

FIG. 2. Protein expression, processing, and RNA synthesis of altered nsp2 viruses. DBT cells were infected with viruses as indicated above the gels. (A) Proteins were radiolabeled, and cell lysates were immunoprecipitated with anti-nsp1, anti-nsp2, and anti-nsp3 antibodies. "Mock" indicates mock-infected cells and "wt" indicates recombinant wild-type MHV-A59. nsps are indicated to the right of the gel: nsp2-3 (275 kDa), nsp3 (210 kDa), nsp2 (65 kDa), and nsp1 (28 kDa). (B) Viral RNA was metabolically labeled with [^{3}H]uridine in the presence of actinomycin D from 9 to 11 h p.i. Intracellular RNA was isolated, denatured, and resolved by electrophoresis. Genomic RNA (R1) and subgenomic mRNAs (R2 to R7) are indicated. R2, R3, and R4 from the 1a-2/Δ4 virus are approximately 300 bp shorter than wild-type mRNAs and are indicated by a superscript †. The 1a-2/Δ4 virus was used as a control in which ORF4 is deleted, but its transcriptional regulatory sequence is still present, resulting in R4 comigrating with R5. R2, R3, and R4 from the 1a-2/4-2 virus, which are approximately 1,400 bp longer than wild-type R2, R3, and R4, are indicated with *. An unknown band, possibly an R4 degradation product, is indicated by a caret. R1 from wild-type and mutant viruses exhibited some variability in migration. This variability is supported by quantification of overall genomic RNA levels (1a-2/Δ4 > wt > 1a-2/4-2). RNA band sizes and quantification were determined by using ImageJ 1.40. α, anti.

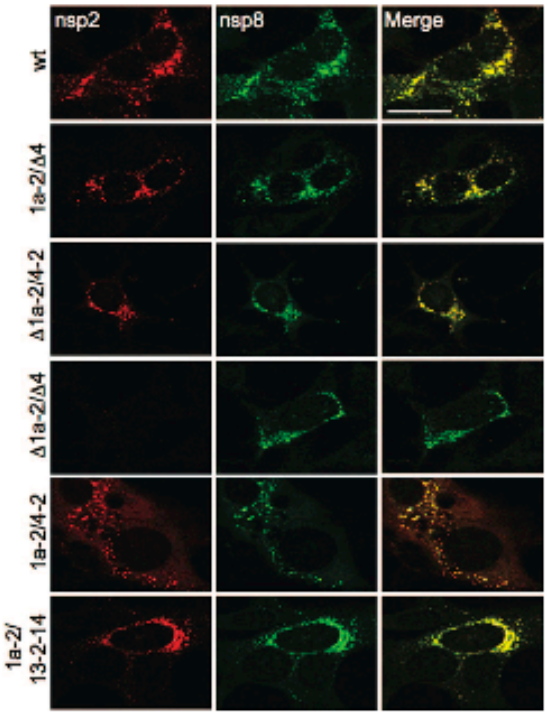

FIG. 3. Immunofluorescence of nsp2 mutants. DBT cells on glass coverslips were infected for 6 h, fixed, and stained for nsp2 and nsp8 by Alexa546 conjugated to a secondary immunoglobulin G (IgG) antibody and by Alexa488 directly conjugated to a primary IgG antibody, respectively. Colocalization is indicated by yellow pixels in the merged images. The bar in the upper right image equals 20 μm and is representative for all images. Images were obtained on a Zeiss LSM510 and were processed in Adobe Photoshop CS2.

change in growth kinetics in culture. Finally, it is possible that altered RNA folding or protein-RNA interactions resulting from the cumulative deletion of >2 kb of genome is responsible for the observed replication defect and decrease in expression of nsps 1 to 3. This possibility is supported by the result that 1a-2/4-2 virus had a slight growth delay, grew to peak titers of >1 $\log_{10}$ higher than those of Δ1a-2/Δ4, and exhibited higher expression levels of nsps 1 to 3.

Additions of amino acids at the N and/or C terminus of nsp2 do not affect peak viral growth. Because alternately expressed nsp2 was engineered to contain minimal 3CLpro cleavage sites (P2-LeuGln ↓ Ser-P1′) when introduced between nsp13 and nsp14 to promote cleavage, we next wanted to determine the effects of introducing amino acids at the N and C termini of nsp2 on viral growth. Therefore, viruses were engineered to have an addition of a Ser residue at the N terminus (1a-S2), LeuGln residues at the C terminus (1a-2LQ), or both mutations (1a-S2LQ) in the native location of nsp2 (Fig. 1 and Table 1). Viral growth experiments were performed as previously described at an MOI of 0.1 PFU/cell, and the 1a-S2, 1a-2LQ, and 1a-S2LQ viruses reached peak growth similar to that of wild-type virus (Fig. 5A), suggesting that the additional amino acids do not inhibit functions of nsp2 in cell culture. However, the 1a-2LQ and 1a-S2LQ viruses were slightly delayed in exponential growth compared to wild-type virus. Protein processing experiments show detection of mature nsp2 in the 1a-2LQ and 1a-S2LQ viruses (Fig. 5B), yet pulse-chase analysis reveals decreased expression of mature nsp2 in the 1a-2LQ and 1a-S2LQ viruses compared to wild-type virus (Fig. 5C). These observations are consistent with the previously described ΔCS2 mutant virus, which has a delay in exponential growth, can reach peak titers similar to those of wild-type virus, and exhibits no mature nsp2 detection (Fig. 5A and B). There-

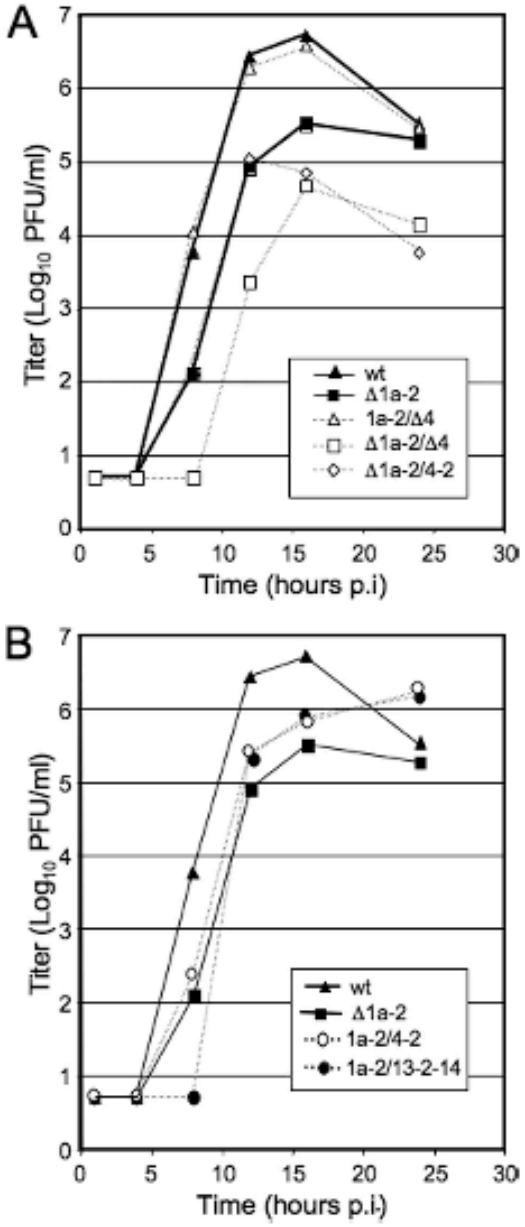

FIG. 4. Growth of nsp2 alternate expression viruses. DBT cells were infected with indicated viruses at an MOI of 1 PFU per cell. Aliquots of supernatant were taken at indicated times p.i., and titers were determined by a plaque assay. All infections were performed in the same experiment with replicates. (A) nsp2 and ORF4 deletion and ORF4 single expression mutants. (B) nsp2 duplication viruses. Wild-type curve and Δ1a-2 curve from panel A are duplicated in panel B to allow direct comparison.

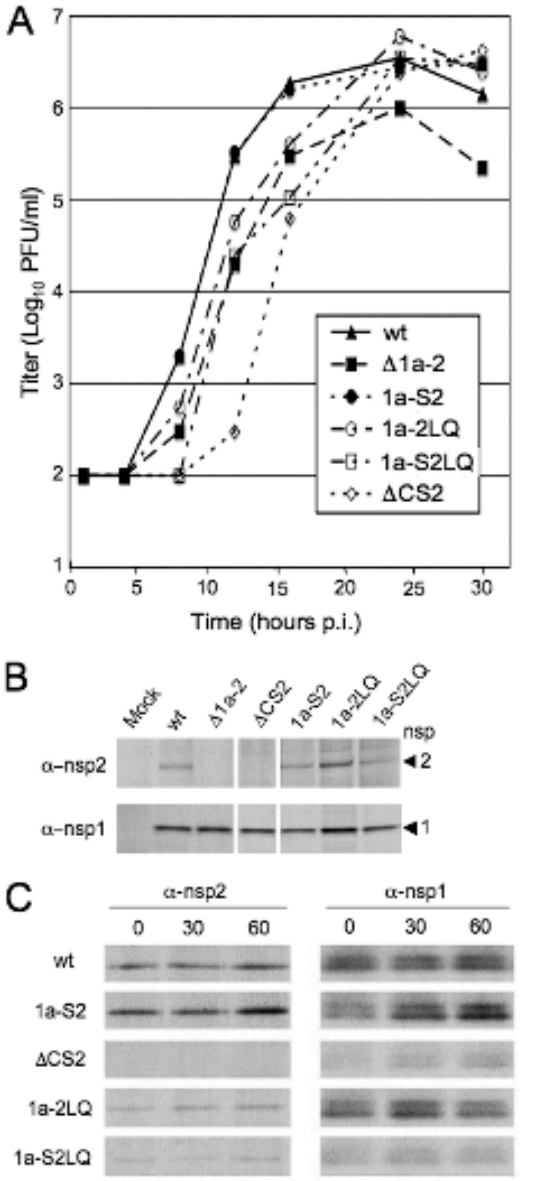

FIG. 5. Growth and protein processing of 1a-S2, 1a-2LQ, and 1a-S2LQ viruses. (A) DBT cells were infected with indicated viruses at an MOI of 0.1 PFU/cell. Viral titers were determined as described in the text. Infections were performed in the same experiment with replicates. (B) Protein processing experiments were performed as previously described. Immunoprecipitations were performed with anti-nsp1 and anti-nsp2 antibodies. All samples were resolved on the same gel, but the image was cropped to remove extraneous lanes. (C) Pulse-chase analysis was performed by infecting DBT cells at an MOI of 10 PFU/cell. Proteins were radiolabeled, and cell lysates were immunoprecipitated with anti-nsp1 and anti-nsp2 antibodies. The presence of an nsp1 doublet has been previously described and may be due to alternative cleavage or posttranslational modifications of nsp1 (24). Viruses are indicated to the left of the gels, and the time of chase (in minutes) is indicated at the top of the gels. α, anti.

fore, the additions of amino acids at the N and C termini of nsp2 appear to affect processing and not the overall functions of nsp2.

The results of this study demonstrate that it is possible for nsp2 to be encoded from alternate locations in the genome, either alone or in combination with ORF1a nsp2, and that alternate location or expression results in a range of effects on growth, expression, RNA synthesis, and localization. Of interest, it was recently reported that an nsp2-EGFP fusion protein could be expressed from the nonessential MHV ORF2b (26). Although the replication phenotype of this virus was not reported, the result is consistent with our study and indicates that additional sites of nsp2 expression/duplication are tolerated. In our experiments, the modest growth defect of an nsp2 deletion is not complemented by expression from ORF1b or ORF4, suggesting that whatever function nsp2 serves, the timing and/or interactions resulting from expression between nsp1 and nsp3 are likely critical for its role. Specifically, it is known that nsp2 is detectable as an nsp2-3 intermediate and that abolition of processing of nsp2 from nsp3 results in a prolonged eclipse phase, while abolition of processing between nsp1 and nsp2 results in diminished growth (6, 11). This was consistent with our observation that the addition of amino acids to the N terminus had no effect on processing and had wild-type growth, while the addition of residues to the C terminus of nsp2 altered processing and eclipse phase, but not peak viral growth. Thus, the results suggest that nsp2 may serve as an important *cis* regulatory protein for nsp1 and nsp3.

Since nsp2 is dispensable for replication, the results here cannot directly predict the rearrangement effects of essential replication proteins, such as nsp5 (3CLpro) and nsp12 (RNA-dependent RNA polymerase). However, our results have shown that additional protein sequence can be encoded not only in the downstream ORFs but also in the replicase between nsp13 and nsp14, suggesting flexibility in both ORF1a and ORF1b for deletion, introduction, and reordering of protein domains. Demonstration that an ORF1 protein can be expressed from alternate locations and can still target to replication complexes suggests that it will be possible to test the effects of alteration of location and extent of expression of critical replication proteins on virus viability, growth, and pathogenesis.

This work was supported by the National Institutes of Health grant AI26603. M.J.G. was supported by the Training Grant in Mechanisms of Vascular Disease through the Vanderbilt University School of Medicine (5T32HL007751). R.L.G. was also supported by the Training Grant for Cellular, Biochemical, and Molecular Sciences through the Vanderbilt University School of Medicine (5T32GM008554). Additional support was provided by the Vanderbilt Cell Imaging Shared Resource (Public Health Service award CA68485).

REFERENCES

1. **Bost, A. G., E. Prentice, and M. R. Denison.** 2001. Mouse hepatitis virus replicase protein complexes are translocated to sites of M protein accumulation in the ERGIC at late times of infection. Virology **285:**21–29.
2. **Brierley, I., P. Digard, and S. C. Inglis.** 1989. Characterization of an efficient coronavirus ribosomal frameshift signal: requirement for an RNA pseudoknot. Cell **57:**537–547.
3. **de Haan, C. A., B. J. Haijema, D. Boss, F. W. Heuts, and P. J. Rottier.** 2005. Coronaviruses as vectors: stability of foreign gene expression. J. Virol. **79:** 12742–12751.
4. **Denison, M. R., A. C. Sims, C. A. Gibson, and X. T. Lu.** 1998. Processing of the MHV-A59 gene 1 polyprotein by the 3C-like proteinase. Adv. Exp. Med. Biol. **440:**121–127.
5. **Denison, M. R., W. J. Spaan, Y. van der Meer, C. A. Gibson, A. C. Sims, E. Prentice, and X. T. Lu.** 1999. The putative helicase of the coronavirus mouse hepatitis virus is processed from the replicase gene polyprotein and localizes in complexes that are active in viral RNA synthesis. J. Virol. **73:**6862–6871.
6. **Denison, M. R., B. Yount, S. M. Brockway, R. L. Graham, A. C. Sims, X. Lu, and R. S. Baric.** 2004. Cleavage between replicase proteins p28 and p65 of mouse hepatitis virus is not required for virus replication. J. Virol. **78:**5957–5965.
7. **de Vries, A. A. F., M. C. Horzinek, P. J. M. Rottier, and R. J. deGroot.** 1997. The genome organization of the nidovirales: similarities and differences between arteri-, toro, and coronaviruses. Semin. Virol. **8:**33–47.
8. **Fischer, F., C. F. Stegen, C. A. Koetzner, and P. S. Masters.** 1997. Analysis of a recombinant mouse hepatitis virus expressing a foreign gene reveals a novel aspect of coronavirus transcription. J. Virol. **71:**5148–5160.
9. **Gorbalenya, A. E., E. V. Koonin, A. P. Donchenko, and V. M. Blinov.** 1989. Coronavirus genome: prediction of putative functional domains in the nonstructural polyprotein by comparative amino acid sequence analysis. Nucleic Acids Res. **17:**4847–4861.
10. **Gosert, R., A. Kanjanahaluethai, D. Egger, K. Bienz, and S. C. Baker.** 2002. RNA replication of mouse hepatitis virus takes place at double-membrane vesicles. J. Virol. **76:**3697–3708.
11. **Graham, R. L., and M. R. Denison.** 2006. Replication of murine hepatitis virus is regulated by papain-like proteinase 1 processing of nonstructural proteins 1, 2, and 3. J. Virol. **80:**11610–11620.
12. **Graham, R. L., A. C. Sims, S. M. Brockway, R. S. Baric, and M. R. Denison.** 2005. The nsp2 replicase proteins of murine hepatitis virus and severe acute respiratory syndrome coronavirus are dispensable for viral replication. J. Virol. **79:**13399–13411.
13. **Ivanov, K. A., T. Hertzig, M. Rozanov, S. Bayer, V. Thiel, A. E. Gorbalenya, and J. Ziebuhr.** 2004. Major genetic marker of nidoviruses encodes a replicative endoribonuclease. Proc. Natl. Acad. Sci. USA **101:**12694–12699.
14. **Ivanov, K. A., V. Thiel, J. C. Dobbe, Y. van der Meer, E. J. Snijder, and J. Ziebuhr.** 2004. Multiple enzymatic activities associated with severe acute respiratory syndrome coronavirus helicase. J. Virol. **78:**5619–5632.
15. **Koonin, E. V.** 1991. The phylogeny of RNA-dependent RNA polymerases of positive-strand RNA viruses. J. Gen. Virol. **72:**2197–2206.
16. **Lu, X. T., A. C. Sims, and M. R. Denison.** 1998. Mouse hepatitis virus 3C-like protease cleaves a 22-kilodalton protein from the open reading frame 1a polyprotein in virus-infected cells and in vitro. J. Virol. **72:**2265–2271.
17. **Masters, P. S.** 2006. The molecular biology of coronaviruses. Adv. Virus Res. **66:**193–292.
18. **Minskaia, E., T. Hertzig, A. E. Gorbalenya, V. Campanacci, C. Cambillau, B. Canard, and J. Ziebuhr.** 2006. Discovery of an RNA virus 3′->5′ exoribonuclease that is critically involved in coronavirus RNA synthesis. Proc. Natl. Acad. Sci. USA **103:**5108–5113.
19. **Oostra, M., E. G. te Lintelo, M. Deijs, M. H. Verheije, P. J. Rottier, and C. A. de Haan.** 2007. Localization and membrane topology of coronavirus nonstructural protein 4: involvement of the early secretory pathway in replication. J. Virol. **81:**12323–12336.
20. **Piñón, J. D., H. Teng, and S. R. Weiss.** 1999. Further requirements for cleavage by the murine coronavirus 3C-like proteinase: identification of a cleavage site within ORF1b. Virology **263:**471–484.
21. **Ricagno, S., M. P. Egloff, R. Ulferts, B. Coutard, D. Nurizzo, V. Campanacci, C. Cambillau, J. Ziebuhr, and B. Canard.** 2006. Crystal structure and mechanistic determinants of SARS coronavirus nonstructural protein 15 define an endoribonuclease family. Proc. Natl. Acad. Sci. USA **103:**11892–11897.
22. **Schiller, J. J., A. Kanjanahaluethai, and S. C. Baker.** 1998. Processing of the coronavirus mhv-jhm polymerase polyprotein: identification of precursors and proteolytic products spanning 400 kilodaltons of ORF1a. Virology **242:** 288–302.
23. **Snijder, E. J., P. J. Bredenbeek, J. C. Dobbe, V. Thiel, J. Ziebuhr, L. L. Poon, Y. Guan, M. Rozanov, W. J. Spaan, and A. E. Gorbalenya.** 2003. Unique and conserved features of genome and proteome of SARS-coronavirus, an early split-off from the coronavirus group 2 lineage. J. Mol. Biol. **331:**991–1004.
24. **Sparks, J. S., E. F. Donaldson, X. Lu, R. S. Baric, and M. R. Denison.** 2008. A novel mutation in murine hepatitis virus nsp5, the viral 3C-like proteinase, causes temperature-sensitive defects in viral growth and protein processing. J. Virol. **82:**5999–6008.
25. **van der Meer, Y., E. J. Snijder, J. C. Dobbe, S. Schleich, M. R. Denison, W. J. Spaan, and J. K. Locker.** 1999. Localization of mouse hepatitis virus nonstructural proteins and RNA synthesis indicates a role for late endosomes in viral replication. J. Virol. **73:**7641–7657.
26. **Verheije, M. H., M. Raaben, M. Mari, E. G. Te Lintelo, F. Reggiori, F. J. van Kuppeveld, P. J. Rottier, and C. A. de Haan.** 2008. Mouse hepatitis coronavirus RNA replication depends on GBF1-mediated ARF1 activation. PLoS Pathog. **4:**e1000088.
27. **Ziebuhr, J., and S. G. Siddell.** 1999. Processing of the human coronavirus 229E replicase polyproteins by the virus-encoded 3C-like proteinase: identification of proteolytic products and cleavage sites common to pp1a and pp1ab. J. Virol. **73:**177–185.
28. **Ziebuhr, J., V. Thiel, and A. E. Gorbalenya.** 2001. The autocatalytic release of a putative RNA virus transcription factor from its polyprotein precursor involves two paralogous papain-like proteases that cleave the same peptide bond. J. Biol. Chem. **276:**33220–33232.

APPENDIX B

MURINE HEPATITIS VIRUS NONSTRUCTURAL PROTEIN 4 REGULATES VIRUS-INDUCED MEMBRANE MODIFICATIONS AND REPLICATION COMPLEX FUNCTION

JOURNAL OF VIROLOGY, Jan. 2010, p. 280–290 Vol. 84, No. 1
0022-538X/10/$12.00 doi:10.1128/JVI.01772-09

Murine Hepatitis Virus Nonstructural Protein 4 Regulates Virus-Induced Membrane Modifications and Replication Complex Function[▽]

Mark J. Gadlage,[2,3] Jennifer S. Sparks,[2,3] Dia C. Beachboard,[2] Reagan G. Cox,[2] Joshua D. Doyle,[2,3] Christopher C. Stobart,[2,3] and Mark R. Denison[1,2,3,4]*

Departments of Pediatrics,[1] Microbiology and Immunology,[2] The Elizabeth Lamb Center for Pediatric Research,[3] and the Monroe Carroll, Jr., Children's Hospital,[4] Vanderbilt University Medical Center, Nashville, Tennessee

Received 21 August 2009/Accepted 13 October 2009

Positive-strand RNA viruses induce modifications of cytoplasmic membranes to form replication complexes. For coronaviruses, replicase nonstructural protein 4 (nsp4) has been proposed to function in the formation and organization of replication complexes. Murine hepatitis virus (MHV) nsp4 is glycosylated at residues Asn176 (N176) and N237 during plasmid expression of nsp4 in cells. To test if MHV nsp4 residues N176 and N237 are glycosylated during virus replication and to determine the effects of N176 and N237 on nsp4 function and MHV replication, alanine substitutions of nsp4 N176, N237, or both were engineered into the MHV-A59 genome. The N176A, N237A, and N176A/N237A mutant viruses were viable, and N176 and N237 were glycosylated during infection of wild-type (wt) and mutant viruses. The nsp4 glycosylation mutants exhibited impaired virus growth and RNA synthesis, with the N237A and N176A/N237A mutant viruses demonstrating more profound defects in virus growth and RNA synthesis. Electron microscopic analysis of ultrastructure from infected cells demonstrated that the nsp4 mutants had aberrant morphology of virus-induced double-membrane vesicles (DMVs) compared to those infected with wt virus. The degree of altered DMV morphology directly correlated with the extent of impairment in viral RNA synthesis and virus growth of the nsp4 mutant viruses. The results indicate that nsp4 plays a critical role in the organization and stability of DMVs. The results also support the conclusion that the structure of DMVs is essential for efficient RNA synthesis and optimal replication of coronaviruses.

Positive-strand RNA viruses rely on host intracellular membranes to form replication complexes, defined as sites of viral RNA synthesis (11, 34, 40–42). These virus-induced membrane modifications are crucial for creating an environment that supports viral RNA synthesis, as well as protecting newly synthesized viral RNA. For many positive-strand RNA viruses, specific replicase proteins, often containing multiple hydrophobic domains, have been implicated in targeting to and modifying host membranes, ultimately leading to the formation of replication complexes.

The coronavirus murine hepatitis virus (MHV) is an enveloped, positive-strand RNA virus that contains a 31.4-kb genome, consisting of seven open reading frames (ORFs). ORF1 encodes the replicase/transcriptase polyprotein, while ORFs 2 to 7 encode structural and accessory proteins. ORF1 comprises approximately two-thirds of the genome and is translated as either polyprotein 1a (pp1a) or, due to a −1 ribosomal frameshift, pp1ab (3, 5, 6, 28, 34). pp1a and pp1ab are processed by three virus-encoded proteases to yield 16 nonstructural proteins (nsp1 to 16) (Fig. 1A) (1, 3, 13, 21, 32, 48). Analysis of nsp3, nsp4, and nsp6 amino acid sequences and *in vitro* biochemical studies have shown that these three nsp's all have transmembrane domains that are likely important for virus-induced membrane modifications (2, 23, 28). MHV nsp4 is processed by papain-like protease 2 (PLP2) at its amino terminus, resulting in an nsp4-to-10 precursor, and after this initial processing event, nsp5 (3Clpro) mediates processing at the carboxy terminus of nsp4 (15, 17, 21, 22, 24). The predicted molecular mass of nsp4 is 56 kDa, but it is detected as a 44-kDa protein by sodium dodecyl sulfate-polyacrylamide gel electrophoresis (SDS-PAGE) (22, 31).

All tested coronavirus nsp's localize to replication complexes that are located on virus-induced double-membrane vesicles (DMVs), and nsp4 has been proposed to play roles in the formation, organization, and function of these virus replication complexes (15, 38). nsp4 has been shown to associate with membrane fractions of infected cells and is resistant to membrane extraction following Triton X-114 treatment, indicating that nsp4 is an integral membrane protein (15). Bioinformatics of the MHV nsp4 amino acid sequence predicted that nsp4 has four transmembrane domains (TM1 to 4). MHV nsp4 has also been shown to be required for rescue of infectious virus (45), as have TM1 to 3, but TM4 is dispensable for recovery of infectious virus in culture. Charge-to-alanine substitutions between TM1 and TM2 of nsp4 result in viruses with phenotypes ranging from nonrecoverable to viruses that exhibit reduced virus growth, RNA synthesis, and protein processing (45).

Analysis of nsp4 from multiple coronaviruses across all coronavirus groups predicts N-linked glycosylation sites for all tested nsp4 sequences. The glycosylation sites, or sequons, Asn-X-Ser, Asn-X-Thr, and rarely Asn-X-Cys, are amino acid sequences

* Corresponding author. Mailing address: Department of Pediatrics, Vanderbilt University Medical Center, D6217 MCN, 1161 21st Ave. S., Nashville, TN 37232-2581. Phone: (615) 343-9881. Fax: (615) 343-9723. E-mail: mark.denison@vanderbilt.edu.

▽ Published ahead of print on 21 October 2009.

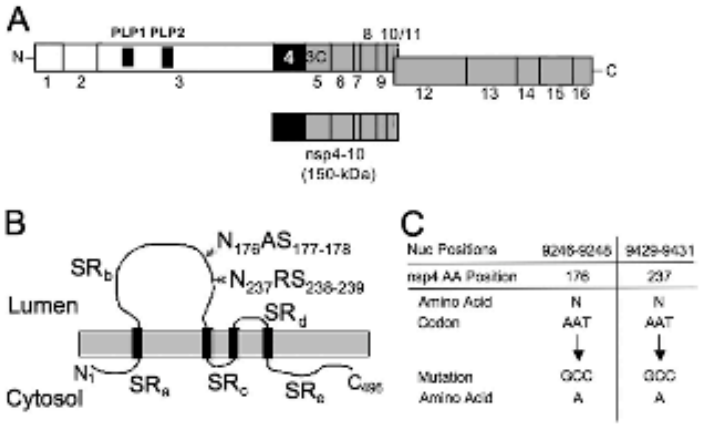

FIG. 1. Processing, glycosylation, and mutagenesis of nsp4. (A) Schematic of MHV nsp4 processing. Three virus-encoded proteases process pp1ab into intermediate precursors and 16 mature nsp's. PLP1 and PLP2 are shown as black boxes within nsp3, while the nsp5 protease (3CLpro) is shown in gray. PLP-mediated processing of nsp's is linked by white boxes, and 3CLpro processing is linked by gray boxes. Nsp4 is shown in black. Nsp's are indicated by number. The nsp4-to-10 precursor is also shown. (B) Proposed topology and N-linked glycosylation sites of nsp4. MHV nsp4 is a 496-amino acid protein that has four predicted transmembrane domains (TM1 to 4, black rectangles) and five soluble regions ($SR_{a\ to\ e}$). Locations of N-linked glycosylation residues Asn176 and Asn237 (N176 and N237) are indicated in SR_b, and predicted luminal and cytoplasmic domains are indicated (35). (C) Engineered nsp4 glycosylation mutants. Nsp4 glycosylation mutants were engineered by replacing the AAT asparagine codons at both N176 and N237 with a GCC alanine codon. Nucleotide numbers correspond to genomic position, and amino acid numbers correspond to nsp4 position.

that are recognized for glycosylation of the Asn (N) residue. Even though coronaviruses contain putative glycosylation sites within nsp4, there is little conservation of these sites between groups. Group 2a coronaviruses, such as MHV and human coronavirus HCoV-OC43, have two conserved putative N-linked glycosylation sites, N176 and N237 (Fig. 1B), while the group 2b severe acute respiratory syndrome coronavirus (SARS-CoV) and group 3 avian infectious bronchitis virus (IBV), have different putative glycosylation sites, N131 and N48, respectively (29, 35). Although the glycosylation of nsp4 from group 1 coronaviruses has not been investigated, residues N176 and N237 of MHV nsp4, N131 of SARS-CoV, and N48 of IBV nsp4 have been shown to be glycosylated when nsp4 is plasmid expressed in cells or when nsp4 is expressed from nonnative locations in the coronavirus genome (10, 29, 35). Clementz et al. reported that N176 of MHV nsp4 is not required for virus replication and that an N176A mutant virus grows identically to wild-type (wt) virus (10). In that study, the N176A mutant virus-expressed nsp4 migrated faster than wt nsp4 as determined by SDS-PAGE, consistent with altered protein modification, such as loss of glycosylation. However, this was not further investigated in the study. In contrast, N237A and N176A/N237A mutant viruses could not be recovered.

Although these studies have led to an increased understanding of various aspects of nsp4, it remains unknown if N176 and/or N237 is glycosylated during infection and if the putative nsp4 glycosylation sites of MHV or other coronaviruses serve roles in membrane modifications or replication complex formation and function. In this study, we tested the glycosylation status of MHV nsp4, expressed from its native genomic location, and the role of nsp4 glycosylation sites on virus growth, viral RNA synthesis, nsp4 localization, and replication complex morphology by engineering and recovering nsp4 mutants with alanine substitutions at N176 (N176A), N237 (N237A), or both (N176A/N237A). We show that virus-expressed nsp4 is glycosylated at both N176 and N237 during infection, that glycosylation at either or both sites is dispensable for virus growth in cell culture, and that alanine substitution of N176, N237, or both results in defects in virus growth and RNA synthesis. Further, we show that loss of nsp4 glycosylation is associated with the presence of aberrant or disrupted DMVs (hereafter referred to as irregular DMVs) and increased prevalence of virus-induced convoluted membranes (CMs). The degree of irregular DMVs and increased CMs from the nsp4 mutant viruses directly correlated with an impairment in viral RNA synthesis and growth. These results demonstrate that nsp4 plays a critical role in the formation, stability, and structure of virus-induced membrane modifications. Finally, the results also support the conclusion that the physical structure and stability of DMVs are essential for efficient RNA synthesis and/or protection of viral RNAs and optimal replication of coronaviruses.

MATERIALS AND METHODS

wt virus, cells, and antibodies. Recombinant wt MHV strain A59 (GenBank accession number AY910861) was used as the wt control for all experiments. Delayed brain tumor (DBT) cells expressing the MHV receptor carcinoembryonic antigen cell adhesion molecule-1 (9, 20, 47) and baby hamster kidney cells expressing the MHV receptor (BHK-MHVR) (8, 9, 47) were grown in Dulbecco's modified Eagle medium (Gibco) supplemented with 10% fetal calf serum for all experiments. Medium for BHK-MHVR cells was supplemented with G418 (Mediatech) at 0.8 mg/ml to maintain selection for cells expressing the MHVR. Rabbit polyclonal antibodies were used in biochemical experiments and have been described previously. Antibodies include anti-nsp4 (VU158) (45), anti-nsp8 (VU123) (4), and anti-M (J.1.3) (7).

Asparagine-to-alanine mutagenesis of nsp4. For introduction of asparagine-to-alanine substitutions in the nsp4 coding sequence (ORF1a nucleotides 8721 to 10208), PCR was performed using the MHV-A59 infectious clone fragment B

TABLE 1. Asparagine-to-alanine mutagenesis of MHV nsp4

Primer name	Sequence[a]	Purpose
N176A Sense	5′-GCC GCC TCT CTG TAT AGT TCT TTG GCT-3′	Mutagenesis for N176A
N176A Antisense	5′P-GTG CAT AAC ACC CCC TGT ATA ACA ATA AGG-3′	Mutagenesis for N176A
N237A Sense	5′-GCC CGT TCA TGG GTA TTG AAC AAC CCG TAT-3′	Mutagenesis for N237A
N237A Antisense	5′P-AAA ATT AAA GCA GAT ACC CTC CTC GGC-3′	Mutagenesis for N237A

[a] Underlined letters denote nucleotides used to introduce alanine substitutions.

(pCR-XL-pSMART B) as a template. Fragment B of the MHV-A59 clone contains MHV ORF1a nsp4 nucleotides 8721 to 9555 (47). Asparagine-to-alanine codon changes were introduced using the ExSite/QuikChange mutagenesis kit (Stratagene) with the primers listed in Table 1. Changes to the manufacturer's protocol included the use of *Pfu* Turbo and *Pfu* Ultra instead of the ExSite DNA polymerase blend. PCR was performed using the following parameters: initial denaturation at 95°C once for 2 min, denaturation at 95°C for 1 min, annealing at various temperatures depending on the primers for 1 min, extension at 72°C for 7 min, and repeating of the denaturing, annealing, and extension steps for a total of 40 cycles. Products were ligated and sequenced across the MHV genome-containing region of fragment B to ensure that PCR amplification did not introduce any unintended mutations. For introduction of both N176A and N237A, restriction endonuclease EcoN I was used to digest both single nsp4 glycosylation mutant plasmids, and ligation was used to introduce both mutations into the same plasmid.

Generation of MHV nsp4 glycosylation mutant viruses. Viruses containing the engineered mutations within nsp4 were produced using the infectious cDNA assembly strategy for MHV-A59 that has previously been described by Yount et al. (47) and modified by Denison et al. (12) and Sparks et al. (45). Briefly, plasmids containing the seven cDNA cassettes that make up the MHV genome were digested using the appropriate restriction enzymes. The correct restriction fragments were gel purified and ligated together overnight at 16°C. The ligated DNA was purified, in vitro transcribed, and electroporated with N gene transcripts into BHK-MHVR cells. The electroporated cells were then laid over a layer of 2.5×10^6 uninfected DBT cells in a 75-cm^2 flask and incubated at 37°C. Virus viability was determined by cytopathic effect, in this case syncytium formation, in the electroporated cell culture. Progeny virus in the cell culture medium of electroporated cells (passage 0 [P0]) was passaged onto uninfected DBT cells (P1), and the virus released from cells in the culture medium was designated P1 stock, the titer was determined, and it was used for all experiments.

RT-PCR and sequencing of recovered viruses. Total intracellular RNA was harvested from P1-infected cells using TRIzol (Invitrogen) according to the manufacturer's protocol. Extracted RNA was used as a template for reverse transcription (RT)-PCR. RT was performed using Superscript III reverse transcriptase (Invitrogen) and random hexamers (Roche). Primers complementary to genome nucleotides 8486 to 8502 (sense) and 10361 to 10345 (antisense) were then used to amplify the nsp4 coding region by PCR. These PCR products were sequenced to confirm the retention of the engineered mutations and the absence of additional mutations in the nsp4 coding sequence.

Protein immunoprecipitations. For radiolabeling of proteins and immunoprecipitations, cells were grown on 60-mm dishes and infected at a multiplicity of infection (MOI) of 10 PFU/cell with wt or nsp4 glycosylation mutant viruses and incubated at 37°C. At 4 h postinfection (p.i.), medium was aspirated and replaced with medium lacking methionine and cysteine and supplemented with actinomycin D (Act D; Sigma) at a final concentration of 20 μg/ml. At 5 h p.i., cells were radiolabeled with [^{35}S]methionine-cysteine ([^{35}S]Met-Cys) at a concentration of 0.08 mCi/ml. When cells reached ~90% involvement in syncytia, radiolabeled cells were washed once in phosphate-buffered saline (PBS), and then lysed in 1 ml of lysis buffer lacking SDS (1% NP-40, 0.5% sodium deoxycholate, 150 mM NaCl, and 50 mM Tris, pH 8.0). Lysates were then centrifuged at $6,000 \times g$ for 3 min to remove cellular debris and nuclei, and the supernatant was collected. Immunoprecipitations were performed in a final volume of 1 ml, using protein A-Sepharose beads (Sigma), 50 μl of radiolabeled lysate, 1:200 (anti-nsp4) or 1:500 (anti-nsp8) dilutions of polyclonal antisera, and proteinase inhibitor (Roche) in lysis buffer. Immunoprecipitations were then performed as previously described (45). For endoglycosidase H (Endo H) treatment, supernatant was transferred to a new tube after heating at 70°C for 10 min. Endo H (Sigma) was added to the supernatant according to the manufacturer's protocol, and the mixture was incubated at 37°C for 3 h. Proteins were resolved by SDS-PAGE in 4 to 12% polyacrylamide gradient Bis-Tris gels (NuPage; Invitrogen) and analyzed by fluorography. ^{14}C-labeled high-molecular-weight markers (NEB) and a full-range rainbow marker were used as molecular weight standards.

Viral growth assays. For viral growth determination (12), DBT cells were infected with wt or nsp4 glycosylation mutant viruses at the MOIs indicated. Following a 45-min absorption period at 37°C with periodic swirling, medium was aspirated, and the cells were washed three times in PBS. Prewarmed 37°C medium was then added back to the cells, and the cells were incubated at 37°C. Aliquots of medium were taken from 1 to 30 h p.i., and virus titers were determined by plaque assay as previously described (25).

Metabolic labeling of viral RNA. DBT cells were either mock infected or infected at an MOI of 5 PFU/cell with wt or nsp4 glycosylation mutant viruses in six-well plates. Following a 45-min absorption at 37°C, medium containing virus was removed, and cells were washed twice in PBS. Cells were then incubated in growth medium at 37°C until 30 min prior to labeling, when medium was replaced with fresh medium containing 20 μg/ml Act D. After this 30-min treatment, [^{3}H]uridine was added to a final concentration of 40 μCi/ml, and cells were incubated at 37°C for 2-h intervals from 3 to 15 h p.i. At the end of each labeling period, cells were lysed in lysis buffer (described above), and nuclei were removed by centrifugation at $14,000 \times g$ for 3 min. RNA in 10% of each lysate was precipitated with chilled 5% trichloroacetic acid (TCA) onto glass microfiber filters (Whatman), washed twice in fresh 5% TCA and twice in 95% ethanol, and dried using vacuum filtration. Radiolabel incorporation was quantitated by liquid scintillation counting.

Immunofluorescence assays. DBT cells grown on glass coverslips were infected with wt or nsp4 glycosylation mutant viruses at an MOI of 10 PFU/cell. At 6 h p.i., medium was aspirated from cells, and cells were fixed in 100% methanol at −20°C. Cells were rehydrated in PBS for 10 min, blocked in PBS containing 5% bovine serum albumin, and then aspirated. For indirect immunofluorescence, cells were incubated with primary antibody (anti-nsp4, 1:200; anti-M, 1:1,000) in wash solution (PBS containing 1% bovine serum albumin and 0.05% NP-40) for 1 h at room temperature. Cells were washed in wash solution three times for 5 min/wash. Cells were then incubated with secondary antibody (goat anti-rabbit Alexa 488, 1:1,000; goat anti-mouse Alexa 546, 1:1,000; Molecular Probes) for 30 min at room temperature. Cells were washed again three times for 5 min/wash, subjected to a final wash in PBS, and rinsed with distilled water. For direct immunofluorescence, anti-nsp8 was purified using HiTrap rProtein A FF columns (GE Life Sciences) for fast protein liquid chromatography. Anti-nsp8 was directly conjugated using the Alexa Fluor 546 protein labeling kit (Invitrogen) according to the manufacturer's protocol. Cells were incubated with anti-nsp8 at a concentration of 1:500, following the same procedure as above. Coverslips were mounted with Aquapolymount (Polysciences) and visualized using a Zeiss Axiovert 200 microscope with a 40× oil immersion lens. Images were processed and merged using Adobe Photoshop CS3.

TEM analysis. DBT cells were mock infected or infected with wt or nsp4 glycosylation mutant viruses at an MOI of 5 PFU/cell in a 60-mm dish and incubated at 37°C. At 6 h p.i., medium was aspirated, and cells were washed once with PBS. The cells were then fixed in 2% glutaraldehyde for 10 min, scraped off the dishes, and centrifuged at $0.5 \times g$ for 3 min. The initial 2% glutaraldehyde was aspirated, fresh 2% glutaraldehyde was added to the fixed cells for 1 h and aspirated, and fresh glutaraldehyde was added to the fixed cells for overnight incubation at 4°C. Cells were washed three times in PBS, transferred to 1% osmium tetroxide in distilled water (diH_2O) for 1 h, and washed three times in diH_2O. Cells were stained en bloc in 1% aqueous uranyl acetate for 1 h and washed three times in diH_2O. Dehydration of cells was carried out gradually using a graded series of ethanol and increasing the times each remained in solution, starting with 30%, followed by 50%, 70%, 95%, and finally absolute ethanol. Propylene oxide was used as a transitional solvent to replace the dehydration solution. Cells were transferred to a 1:1 araldite-propylene oxide mixture for 1 h and then placed in pure araldite in a vacuum oven for another hour to help pull resin through the tissue. Pure resin specimens were then transferred into capsules containing fresh resin and finally placed into an oven overnight to polymerize. Ultra-thin serial sections (50 to 60 nm) from polymerized blocks were obtained using a Leica UCT Ultracut microtome (Leica Microsystems,

Vienna, Austria), transferred to formvar-coated slot grids, and examined using a Phillips CM10 TEM (FEI Company, Hillsboro, OR) equipped with an Advantage Plus 2-megapixel digital charge-coupled-device system for CM10 transmission electron microscopy (TEM) (Advanced Microscopy Techniques, Danvers, MA).

Statistical analyses. For statistical analyses, DMVs were characterized into two groups, either regular (defined by inner membranes in close approximation with the outer membrane) or irregular DMVs (defined by moderate to severe disruption or separation of the inner membrane with the outer membrane). Chi-square analysis using contingency tables was performed by comparing the number of regularly formed DMVs to irregularly formed DMVs of wt and nsp4 glycosylation mutant viruses. Chi-square analysis was also performed to compare the presence of both CMs and DMVs to the presence of DMVs only. Because CMs were found only in the presence of DMVs, the presence of CMs and DMVs was compared to the presence of DMVs alone in a given TEM section. Diameters of DMVs were measured using ImageJ 1.40g (http://rsb.info.nih.gov/ij). Diameters were defined by measuring the widest diameter from the outside membrane of one side to the outside membrane of the opposite side of a single DMV. To determine whether there was a statistical difference between the diameters of DMVs, analysis of variance (ANOVA) was used to compare wt and nsp4 glycosylation mutant viruses. Because a statistical difference was indicated through ANOVA, Tukey tests were used to perform pair-wise comparisons of all viruses. *P* values were determined to indicate significance.

RESULTS

Recovery of nsp4 glycosylation mutant viruses. Group 2a coronaviruses contain conservation of putative glycosylation sites in nsp4 at N176 and N237 (Fig. 1B). To determine if nsp4 is glycosylated at residues N176 and N237 in the context of MHV infection and what roles nsp4 glycosylation may play in the virus life cycle, viruses were engineered to contain asparagine-to-alanine substitutions at either N176, N237, or both residues N176 and N237 of nsp4 (Fig. 1C). Cells were electroporated with genomic RNA for N176A, N237A, or N176A/N237A mutant viruses. All three mutant viruses induced cytopathic effect by 36 h postelectroporation, and 90 to 100% of cells were involved in syncytia by 46 to 50 h postelectroporation, similar to wt virus. Viruses were passaged and sequenced across the nsp4 coding sequence, confirming both the presence of engineered mutations and lack of any other mutations in nsp4. In contrast to previous reports, our results demonstrate that mutants with alanine substitution at N176, N237, or both are viable, demonstrating that the N176 and N237 residues are not required for replication in cell culture. To determine if compensating mutations occurred outside of the nsp4 sequence during recovery of the N237A and N176A/N237A mutant viruses, the complete genome of the N176A/N237A mutant virus was sequenced, and there were no additional mutations present in the genome. These results demonstrate that the recovery of the N237A and N176A/N237A mutant viruses was not due to second-site compensating mutations and that the Asn residues are not required for virus viability.

nsp4 is glycosylated at both N176 and N237 during MHV infection. Previous studies have demonstrated that treatment of lysates with Endo H results in a mobility shift of nsp4 expressed from plasmid in HeLa cells (10, 35) or from nsp4-enhanced green fluorescent protein expressed in recombinant virus from an alternate location (in place of ORF2) (10, 35), consistent with glycosylation of nsp4 with mannose-rich oligosaccharides in the endoplasmic reticulum (ER) and the lack of nsp4 trafficking through Golgi. However, there has been no demonstration of N-linked glycosylation of native nsp4 in wt virus or identification of specific Asn residues subject to N-linked glycosylation. To test whether natively expressed MHV

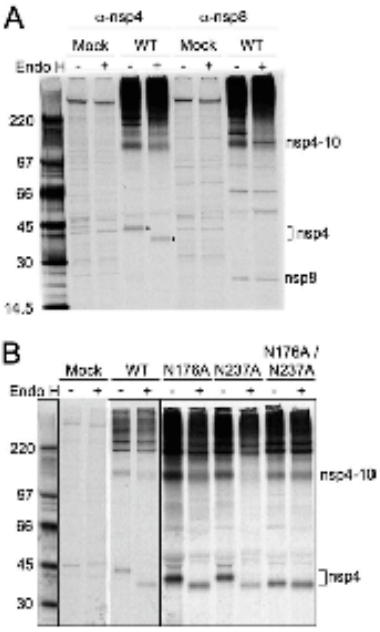

FIG. 2. Protein expression and glycosylation of nsp4. Cytoplasmic lysates were generated from radiolabeled DBT cells that were either mock infected or infected with wt, N176A, N237A, or N176A/N237A viruses. Labeled proteins were immunoprecipitated using antiserum against nsp4 or nsp8. (A) Endo H treatment of wt nsp4 and nsp8. Immunoprecipitated nsp4 and nsp8 were either mock treated or treated with Endo H to analyze N-linked glycosylation. After Endo H treatment for 3 h, proteins were resolved on SDS-PAGE and visualized by fluorography. Black dots indicate either glycosylated or unglycosylated forms of nsp4. α-nsp4, anti-nsp4; α-nsp8, anti-nsp8. (B) Endo H treatment of nsp4 glycosylation mutants. Immunoprecipitated nsp4 from the wt or nsp4 glycosylation mutants was mock treated or treated with Endo H. All samples in each panel were resolved on the same gel and had the same exposure time, but the images shown in panel B were cropped to remove nonrelevant lanes. Molecular weight markers (in thousands) are shown to the left of each gel.

nsp4 is glycosylated during infection, immunoprecipitated nsp4 from wt MHV infection was mock treated or treated with Endo H (Fig. 2A). Mock-treated nsp4 was detected as a 44-kDa protein by SDS-PAGE, while Endo H treatment resulted in a faster-migrating, 39-kDa protein. The nsp4-to-10 precursor was detected in both cases by anti-nsp4. The replicase protein nsp8 is not modified by N-linked glycosylation and was not affected by Endo H treatment (Fig. 2A). The nsp4-to-10 precursor that was treated with Endo H and detected using anti-nsp8 exhibited a sharper band than that of the untreated nsp4-to-10 precursor. A possible explanation for this is that removal of N-linked glycans may alter which nsp4-to-10 precursors can be detected by anti-nsp8, e.g., nsp4-to-10 with certain post-translational modifications.

To test whether N176 and/or N237 was targeted for glycosylation, nsp4 immunoprecipitated following infection of DBT cells with N176A, N237A, and N176A/N237A mutant viruses was treated with Endo H (Fig. 2B). Untreated nsp4 from N176A

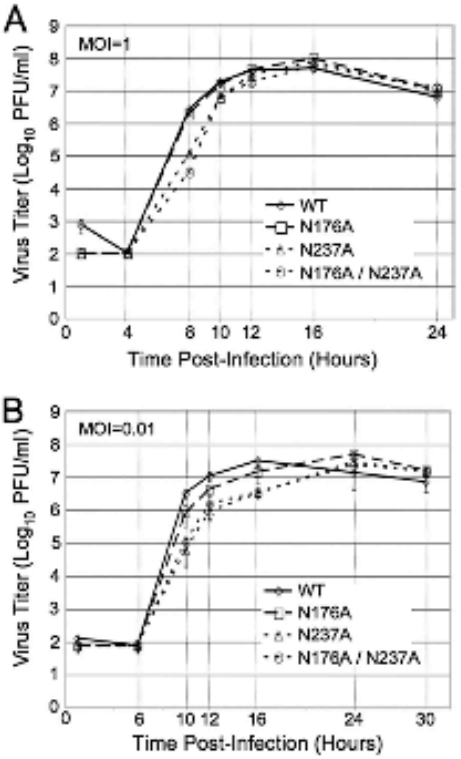

FIG. 3. Growth analysis of nsp4 glycosylation mutant viruses. DBT cells were infected with the indicated viruses for single cycle growth at an MOI of 1 PFU/cell for 24 h (A) or for multiple cycle growth at an MOI of 0.01 PFU/cell for 30 h (B). Samples of virus supernatants were collected at the times indicated beneath the graphs. Virus titers were determined by plaque assay with DBT cells. Error bars represent standard deviations from the mean based on samples from multiple replicates.

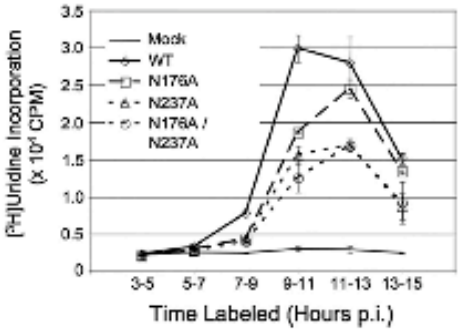

FIG. 4. RNA synthesis of nsp4 glycosylation mutant viruses. DBT cells in six-well plates were mock infected or infected with wt, N176A, N237A, or N176A/N237A viruses at an MOI of 5 PFU/cell. Cells were treated with Act D for 30 min prior to addition of radiolabel. Cells were metabolically labeled with [^{3}H]uridine for the intervals indicated, cells were lysed, and [^{3}H]uridine incorporation was quantified by liquid scintillation counting of TCA-precipitable RNA. Data points represent the mean counts/minute (CPM) of two individual experiments, and error bars represent the standard deviations between two experiments.

and N237A mutants migrated identically and more rapidly than untreated wt nsp4 (42 kDa) but more slowly than wt nsp4 treated with Endo H (39 kDa). When nsp4 from N176A and N237A mutant viruses was treated with Endo H, both proteins were detected at 39 kDa, identical to Endo H-treated wt nsp4. nsp4 from the N176A/N237A mutant virus migrated to 39 kDa, whether untreated or treated with Endo H. The results indicate that nsp4 expressed from its native genomic location is specifically glycosylated at residues N176 and N237 and also demonstrate that no other N-linked glycosylation occurs in nsp4.

nsp4 glycosylation mutant viruses exhibit defects in virus replication. To determine whether nsp4 glycosylation mutant viruses display replication defects, DBT cells were infected with wt, N176A, N237A, and N176A/N237A viruses at an MOI of 1 PFU/cell (Fig. 3A). Samples of infected cell culture medium were taken at predetermined time points from 1 to 24 h p.i., and virus titers of each sample were determined by plaque assay. The N176A mutant virus exhibited growth kinetics and peak titers indistinguishable from those of wt virus, consistent with the study by Clementz et al. (10). The N237A and N176A/N237A mutant viruses grew indistinguishably from each other and reached peak titers similar to those of wt virus; however, compared to wt and N176A, the N237A and N176A/N237A viruses exhibited a delay and decrease in growth between 4 and 12 h p.i. The N176A/N237A mutant did not appear more impaired in growth than the N237A mutant alone. Since the N237A and N176A/N237A mutant viruses exhibited growth defects, we next tested whether N176A had subtle growth defects by repeating the growth assays at an MOI of 0.01 PFU/cell (Fig. 3B). Under these conditions, the N237A and N176A/N237A mutants demonstrated the same delay compared to mutants infected at a higher MOI. In contrast, for the N176A mutant virus, the lower MOI infection revealed a subtle defect in growth, displaying a delay in peak titer similar to that of N237A and N176A/N237A mutants. The experiments demonstrate that N176 and N237 both are important for exponential growth, but loss of either or both glycosylation sites still allows for wt peak titers. The contributions of N176 and N237 are independent and nonredundant, as indicated by growth defects of either N176A or N237A but are not additive or synergistic. Finally, the results suggest that glycosylation of nsp4 is important for nsp4 function during virus replication.

nsp4 glycosylation mutants have reduced viral RNA synthesis. Since previous studies have shown that mutations in nsp4 affect viral RNA synthesis (45), we conducted experiments to determine if the growth defects of nsp4 glycosylation mutants were associated with changes in viral RNA synthesis (Fig. 4). DBT cells were mock infected or infected with wt, N176A, N237A, or N176A/N237A mutant viruses at an MOI of 5 PFU/cell to maximize single-round infection, and infected cells were metabolically labeled with [^{3}H]uridine in the presence of Act D for 2-h intervals from 3 to 15 h p.i. Total RNA was extracted from harvested cells and measured for incorporation of [^{3}H]uridine. Peak incorporation of [^{3}H]uridine for wt MHV occurred from 9 to 11 h p.i., similar to the results from a

previously published report (16). For all three nsp4 mutant viruses, peak incorporation was delayed compared to wt, occurring between 11 and 13 h p.i. Delays in the timing of peak viral RNA synthesis displayed by the nsp4 glycosylation mutant viruses were also associated with decreases in the amount of RNA synthesized over the course of the infection. The N176A mutant virus synthesized approximately 80% of the maximum amount of incorporation seen for wt over a 2-h labeling period. Both the N237A and the N176A/N237A mutant viruses exhibited a 50% reduction in peak viral RNA synthesis. These data demonstrate that there is an overall decrease in viral RNA synthesis in the nsp4 mutant viruses compared to wt virus. In addition, the delay and decrease in RNA synthesis correlated with the kinetics and peak titer of infectious viruses, suggesting that alteration of viral RNA synthesis was responsible for the growth defects from the N176A and N237A substitutions.

Removal of nsp4 glycosylation sites does not alter nsp4 localization. nsp4 colocalizes with other replicase nsp's in cytoplasmic replication complexes that are sites of viral RNA synthesis, and nsp4 has been predicted to be critical for formation of these complexes. To test if altered RNA synthesis resulting from the N176A and N237A substitutions was associated with altered nsp4 interactions with other replicase proteins, the localization of nsp4 was compared by immunofluorescence with nsp8, a well-described marker for replication complexes, and with the viral membrane protein (M), a marker for sites of virus assembly in the ER-Golgi intermediate compartment and Golgi and distinct from replication complexes. DBT cells on glass coverslips were infected with wt, N176A, N237A, or N176A/N237A viruses for 6 h, fixed, and probed for nsp4, nsp8, and M. For wt and all nsp4 mutant viruses, nsp4 colocalized extensively with nsp8 in punctate perinuclear and cytoplasmic foci (Fig. 5A). However, there was a visual trend for fewer and less-intense fluorescent foci in the cells infected with the nsp4 mutants compared to wt virus, suggesting that there may be fewer-forming or altered replication complexes in the nsp4 mutant virus infections (Fig. 5A and data not shown). When nsp4 was compared with M (Fig. 5B), wt and mutant viruses had identical patterns of noncolocalization of nsp4 with M, consistent with previous studies of MHV replicase proteins and indicating that nsp4 is not altered in its relationship to sites of assembly and not localized to the ER-Golgi intermediate compartment or Golgi. The results demonstrate that nsp4 mutant viruses are able to form cytoplasmic replication complexes and retain interactions with other replicase nsp's and that glycosylation of nsp4 is not required for this process.

nsp4 glycosylation mutant viruses induce altered membrane rearrangements and irregular DMVs. Based on the replication defects and subtle visual variability observed during immunofluorescence analysis of nsp4 mutants, we next investigated whether nsp4 glycosylation mutants have altered membrane rearrangements. TEM was used to visualize the ultrastructure of membrane modifications in infected cells. DBT cells were mock infected or infected with wt or the nsp4 glycosylation mutant viruses at an MOI of 5 PFU/cell. At 6 h p.i., cells were fixed in 2% glutaraldehyde and processed for TEM analysis. For mock-infected cells, the cellular architecture and organelle morphology were intact (Fig. 6A). Cells infected with wt virus exhibited clearing of cytoplasmic contents and swollen ER and Golgi (Fig. 6B). Cells infected with the three nsp4 glycosylation

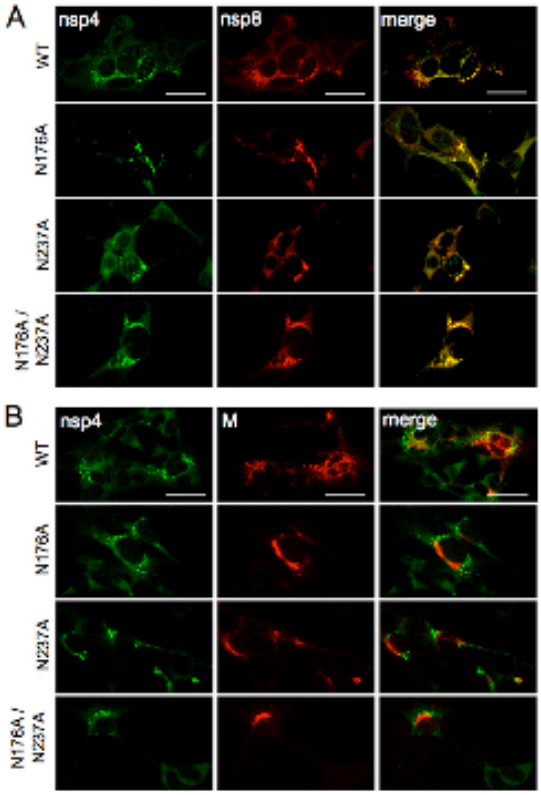

FIG. 5. Immunofluorescence of nsp4 localization. DBT cells on glass coverslips were infected with the indicated viruses at an MOI of 10 PFU/cell. At 6 h p.i., cells were fixed, probed with antibodies to nsp4, nsp8, and membrane (M) protein, and analyzed by immunofluorescence using a Zeiss Axiovert 200 microscope at ×40 magnification. (A) nsp4 colocalizes with nsp8. Infected cells were analyzed by indirect immunofluorescence using anti-nsp4 (Alexa 488, green) and direct immunofluorescence by Alexa 546 conjugated to anti-nsp8 (red). Yellow pixels represent colocalization of overlapping green and red pixels. (B) nsp4 does not colocalize with M protein. Infected cells were probed by indirect immunofluorescence using rabbit anti-nsp4 (green) and mouse anti-M (red). The scale bar in the upper images in panels A and B equals 20 μM and is representative of all other images.

mutant viruses also demonstrated swelling of ER and Golgi and cytoplasmic clearing, albeit less so than during wt infection (Fig. 6C to E).

In contrast, there was a striking difference between cells infected with wt and nsp4 mutants in the relationship and ultrastructure of virus-induced DMVs and CMs. wt- and nsp4 mutant-infected cells exhibited virus-induced CMs and DMVs, structures that have been identified with replication complexes and associated with viral RNA synthesis (15, 27), while no DMVs or CMs were observed with mock-infected cells. CMs were detected with wt and mutant virus-infected cells and always in close proximity to DMVs. However, DMVs were observed in the presence or absence of CMs for all viruses. The CMs were observed more frequently with electron microscopy (EM)

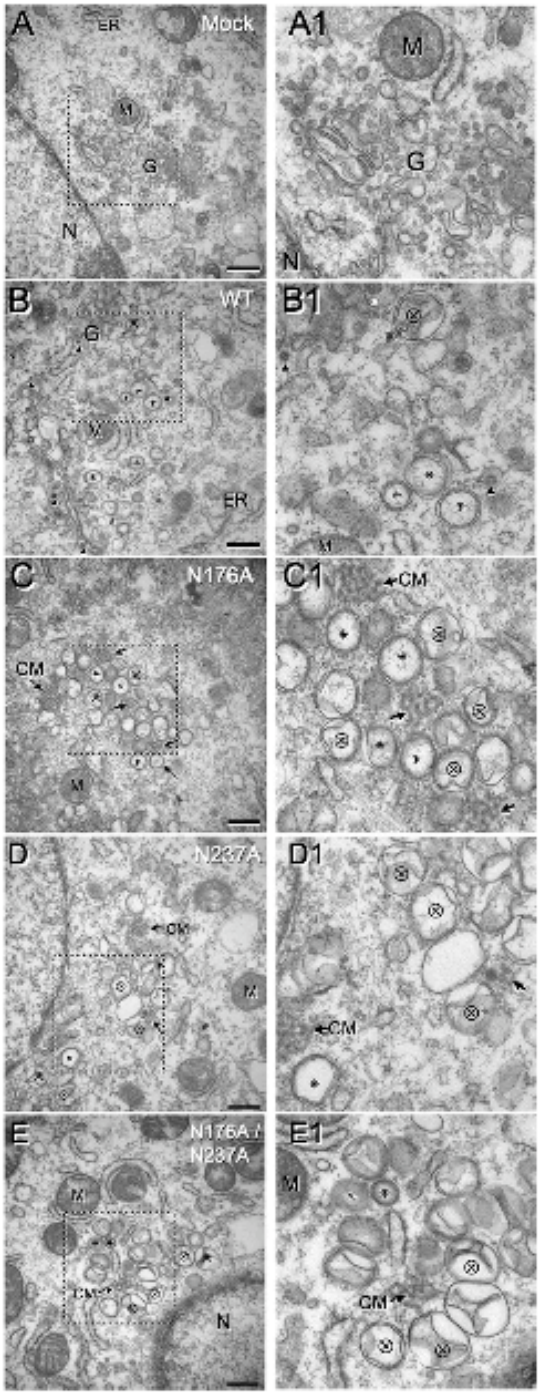

FIG. 6. TEM analysis of replication complexes and DMVs from the wt and nsp4 mutants. DBT cells were mock infected or infected with wt, N176A, N237A, or N176A/N237A viruses. Cells were harvested in 2% glutaraldehyde and processed for TEM analysis. (A and A1) Mock-infected cells. (B and B1) wt MHV infection. (C and C1) N176A mutant virus infection. (D and D1) N237A mutant virus infection. (E and E1) N176A/N237A mutant virus infection. Dotted boxes in the left images indicate area of magnification in right image. The scale bar in the left images represents 500 nm. Arrowheads indicate dark-stained, individual virions, which are located above the arrowheads. Black arrows point to CMs. ⋆ indicates examples of regular DMV structure. ⊗ shows examples of irregular DMV structure. N, nucleus; G, Golgi apparatus; M, mitochondria.

sections of cells infected with N176A, N237A, and N176A/N237A mutant viruses compared to wt (Fig. 6C to E). The vast majority of DMVs in wt-infected cells exhibited the characteristic DMV morphology of a circular shape, regular diameter, and ultrastructure of closely approximated inner and outer membranes. A small subset of DMVs manifested a partial separation of the inner and outer membranes and exhibited a slightly larger diameter, but these were rare. In contrast, cells infected with the nsp4 glycosylation mutants demonstrated DMVs with altered shape and diameter and with increasingly aberrant (irregular) ultrastructure, consisting of severely detached and collapsed inner membranes that were not observed with any wt-infected cells. The number of irregular DMVs and the extent of DMV derangement were most profound in N237A and N176A/N237A mutant-infected cells and visibly greater than those detected with cells infected with N176A alone.

Because the EM images were originally selected based on the detection of DMVs, we used EM images to quantitatively compare (i) the prevalences of CMs, (ii) the ratios of regular (wt-like) and irregular DMVs, and (iii) the diameters of regular and irregular DMVs (Table 2 and Fig. 7). Since the images were selected only for the presence of DMVs, we proposed that quantitative analysis was unbiased for these parameters. The prevalence of CMs was determined by comparing images in which CMs were observed or not observed in EM sections selected based on the presence of DMVs, since CMs were found only in the presence of DMVs. While there was no statistical difference between wt and N176A in the ratios of sections with both CMs and DMVs versus DMVs alone, the N237A and N176A/N237A mutants had significantly increased ratios of detection of both CMs and DMVs compared to DMVs alone ($P < 0.01$ for N237A and $P < 0.001$ for N176A/N237A) (Fig. 7A). Analysis of the ratio of regular DMVs to total DMVs (regular plus irregular) demonstrated a significant increase in irregular DMVs in cells infected with N237A and N176A/N237A mutant viruses ($P < 0.001$) compared to cells infected with wt or N176A viruses (Fig. 7B). We did observe more irregular DMVs with N176A than with wt, but the regular DMV/total DMV ratios were not significantly different. Finally, the measurements of the regular DMVs of both wt and all nsp4 glycosylation mutant viruses reveal no difference in their diameters (widest diameter of outer membrane) (Fig. 7C). In contrast, the mean diameter of irregular DMVs in the N237A and N176A/N237A mutant viruses was significantly larger than that of either wt virus or the N176A mutant virus (Fig. 7C). This analysis indicates that nsp4 is likely critical for the organization and stability of DMVs and for the relation-

TABLE 2. Analysis of virus-induced membrane structures

Virus	Total no. of:						Avg regular DMV diam (nm)	Avg irregular DMV diam (nm)
	Cell sections with evidence of infection	Sections with CMs and DMVs	Sections with DMVs only	DMVs counted	Regular DMVs	Irregular DMVs		
WT	24	8	16	102	86	16	255.2 ± 31.4	323.2 ± 35.6
N176A	21	11	10	127	96	31	257.0 ± 52.3	324.2 ± 31.8
N237A	11	9	2	72	36	36	264.6 ± 53.6	372.5 ± 41.6
N176A/N237A	21	18	3	117	60	57	270.4 ± 56.1	371.3 ± 41.6

ship and evolution of membrane modifications (CMs and DMVs) over the course of infection.

DISCUSSION

Although multiple studies have investigated the roles of nsp's in inducing membrane rearrangements, understanding the role of glycosylation of nsp's from positive-strand RNA viruses remains limited. A study of the flavivirus yellow fever virus demonstrated that NS1 glycosylation was important for several functions in the virus life cycle (30, 33). NS1 interacts with membranes and is involved in replicase function (30), and removal of NS1 glycosylation by asparagine-to-alanine substitution results in impaired virus growth, RNA synthesis, and pathogenesis (33).

Coronaviruses, like other positive-strand RNA viruses, induce the formation of DMVs that serve as scaffolds for replication/transcription complexes. Exogenous expression of the poliovirus transmembrane proteins 2BC and 3A results in DMVs that are indistinguishable from those formed during wt infection (43, 46). Equine arteritis virus (EAV), which is classified with coronaviruses in the order *Nidovirales*, induces DMVs similar to coronaviruses (37). Exogenous plasmid expression of EAV nsp2 and nsp3 is sufficient to induce membrane modifications resulting in membrane structures similar to those seen during EAV infection, and mutations within EAV nsp3 also result in altered virus-induced membrane rearrangements (39, 44). EAV nsp3 is a tetra-spanning integral membrane protein implicated in DMV formation and organization. Of interest, an introduced Asn substitution (T873N) in an EAV nsp3 luminal domain resulted in nsp3 glycosylation *in vitro* but was highly detrimental when introduced into the genome and recovered only as a pseudoreversion (N873H) that abolished the glycosylation site. Thus, for another nidovirus, the glycosylation status of a membrane-modifying replicase protein is also important for DMV formation and RNA synthesis during virus replication.

Our report confirms multiple roles of MHV nsp4 in the virus life cycle, including optimal virus replication and RNA synthesis, as well as its importance in the modification and morphology of virus-induced membrane structures. In this study, we show that MHV nsp4 is glycosylated and functions as a membrane modification protein that regulates virus-induced membrane rearrangements. nsp4 glycosylation mutant viruses display highly irregular DMVs and an increased prevalence of CMs relative to DMVs alone. The extent of disrupted DMVs in the nsp4 glycosylation mutant viruses correlated directly with decreases in RNA synthesis and virus replication. These data suggest that altered membranous structures from the nsp4 glycosylation mutants result in a reduced capacity to synthesize viral RNA and/or protect viral RNA from degradation, ultimately leading to impaired virus fitness.

Previous studies have concluded that nsp4 is required for MHV replication and have identified determinants of membrane topology, subcellular localization, and function (10, 35, 45). This study is the first to recover and characterize the importance of multiple nsp4 glycosylation events to virus replication, viral RNA synthesis, and virus-induced membrane modifications during coronavirus infection. Clementz et al. recovered an nsp4 N176A mutant but were unable to recover an N237A or N176A/N237A mutant (10). Their N176A mutant grew with kinetics similar to those of wt at an MOI of 0.1 PFU/cell at 33°C and 39°C but was not further characterized in that report. In contrast to the results in the previously published report, we were able to recover and characterize the N237A and N176A/N237A mutant viruses. The reasons for the differences in recovery can only be speculated. The backgrounds of cloned MHV genome fragments should be identical since the MHV genome fragments were jointly developed by our lab and the lab of Baric and coworkers (47). In addition, we performed RT-PCR sequencing of the complete genome from the recovered N176A/N237A mutant virus, which verified the engineered mutations and also confirmed that the rest of the genome was identical, with no additional mutations of any kind, to the published recombinant MHV-A59 sequence. Thus, there were no other compensating mutations to account for or consider for the recovery of the mutant virus. We have experienced occasional mutations in the genome fragments during preparation for genome assembly that have prevented recovery of even known viable mutants and would therefore speculate that this could account for the nonrecovery of N237A and N176A/N237A mutant viruses by Clementz et al. Our results clearly demonstrate that the N176 and N137 residues and the associated glycosylation events are not required for MHV replication in cell culture. Since no other mutations in the genome RNA from the recovered N176A/N237A mutant virus were identified, we can conclude that the profound and distinct phenotypes in virus replication, RNA synthesis, and virus-induced cellular membrane modifications are due to the introduced mutations alone.

Potential functions of nsp4 glycosylation. Modification of proteins by addition of N-linked glycans may result in numerous effects on protein functions (14, 19). Therefore, glycosylation of nsp4 may be important for a variety of reasons. One potential mechanism of nsp4 glycosylation is proper protein folding (18, 36). By removing N-linked glycans, the overall

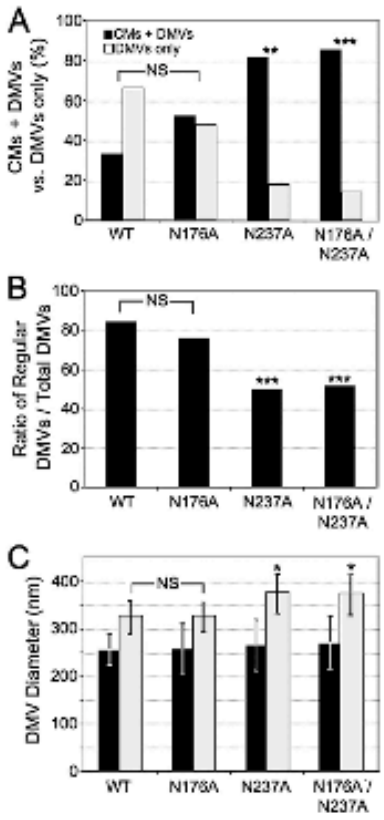

FIG. 7. Quantitative analysis of CMs and DMVs. (A) CMs and DMVs. All EM images were analyzed for the presence of CMs and DMVs based on characteristic EM morphology. Because CMs were found only in the presence of DMVs in all TEM sections observed, the ratio of total cell sections with CMs plus DMVs to the total of cell sections with DMVs alone could be examined. Black bars indicate presence of both CMs and DMVs, while white bars represent the presence of DMVs alone. Chi-square analysis was used to compare the presence of CMs plus DMVs to DMVs alone. (B) Ratios of DMVs with regular morphology to total DMVs (regular plus irregular). Total DMVs and DMVs with regular morphology were counted with TEM images for all viruses, and the ratio of regular DMVs to total DMVs was determined. (C) Diameter of regular and irregular DMVs of the wt and nsp4 mutants. DMVs were measured in Image J by the widest diameter in nm of outer membranes. Black bars indicate regular DMVs, while white bars indicate irregular DMVs. Error bars indicate standard deviation. There was no significant difference (not labeled in the figure) in the diameters of regular DMVs between wt and nsp4 mutant viruses. ANOVA followed by Tukey tests indicated a significant difference in the diameters of irregular DMVs of the N237A and N176A/N237A viruses compared to those of both wt and N176A viruses. * ($P < 0.05$), ** ($P < 0.01$), and *** ($p < 0.001$) indicate levels of statistical significance compared to wt virus. NS, no significance.

structure of nsp4 may be altered during protein folding. This mechanism is supported by the findings in this report, in that the nsp4 glycosylation mutant viruses displayed impairments in virus replication, viral RNA synthesis, and virus-induced membrane modifications. Other explanations are possible for the role of nsp4 glycosylation in replication complex formation and membrane modifications. For instance, glycosylation of nsp4 may be important for protein stability and prevention of nsp4 degradation (26). Lastly, it is possible that the N-linked glycans, either directly or through modification of nsp4 structure, recruit cellular factors that are involved in membrane rearrangements. Future studies are needed to distinguish between these possibilities.

Models of nsp4 function in replication complex formation, morphology, and organization. Evidence from this study has led to potential models addressing the effect nsp4 has on replication complex formation, morphology, and organization. One possible model is that nsp4 may regulate the transition or formation of different membrane modifications (i.e., CMs and DMVs). The evidence from this report that there was an increased prevalence of CMs in relation to DMVs in the N237A and N176A/N237A mutant viruses suggests that MHV nsp4 may be a major player in the transition of these virus-induced membrane rearrangements from one membrane structure to another. Other findings from this report that there was an increased presence of aberrant or deranged DMVs in the N237A and N176A/N237A mutant viruses suggest another possibility that the formation of intact, functional DMVs is regulated by nsp4.

A second potential model of nsp4 function is that the curvature and size of DMVs are regulated by nsp4 (38). In N237A and N176A/N237A mutant virus-infected cells, irregular DMVs were much larger and had highly disrupted inner membranes. The N237A and N176A/N237A mutant viruses also exhibited decreases in RNA synthesis, indicating that these irregular DMVs may not be functioning properly and that curvature and size may be important for proper function. This model is supported by the fact that all virus-infected cells produced regular DMVs, although at different proportions, and that all regular DMVs were similar in size. Cells infected with wt or N176A viruses, those that had levels of RNA synthesis higher than those of the N237A and N176A/N237A mutant viruses, also had a higher percentage of regular DMVs. These data suggest that curvature and size are important for DMV function.

A third model is that nsp4 functions in tethering or "pushing" the inner membrane to the outer membrane of the DMVs. The proximity of the inner membrane to the outer membrane may be important for creating an environment optimal for RNA synthesis and/or protection of newly synthesized viral RNAs. This model is supported by the fact that the prevalence of aberrant DMVs in the nsp4 glycosylation mutants was directly related to the extent of impairment of RNA synthesis and virus growth. These results suggest that irregular DMVs have a reduced capacity to synthesize and/or protect viral RNAs and are also the first to provide direct evidence suggesting that the physical size, morphology, and stability of virus-induced DMVs are important for efficient viral RNA synthesis and optimal virus production. On the other hand, the results also show clearly that glycosylation of nsp4 is not absolutely required for formation of "regular" DMVs and that replication complex function can still ultimately allow virus replication to wt titers, albeit with delayed kinetics.

To date, all coronavirus nsp4's that were subjected to Endo H treatment have been shown to be glycosylated in the lumen

of the ER between the first and second predicted transmembrane domains of nsp4 in exogenous expression experiments, including group 2a MHV nsp4, group 2b SARS-CoV nsp4, and group 3 IBV nsp4 (10, 29, 35). It will be interesting to see whether glycosylation of nsp4 is conserved among other coronaviruses, specifically group 1 coronaviruses, and what effect the loss of glycosylation sites has on virus replication, RNA synthesis, and replication complex morphology.

This study has demonstrated the importance of MHV nsp4 glycosylation sites in virus replication, replication complex morphology and organization, and viral RNA synthesis. Because nsp4 has been shown to have integral membrane characteristics and no predicted enzymatic activities, it is rational to propose that nsp4 involvement in viral RNA synthesis is due to replication complex formation, other possible membrane modifications, and/or protein interactions. The nsp4 glycosylation mutant viruses generated in this study will provide powerful tools to further dissect the definitive mechanisms of nsp4 function on replication complex formation and its roles in the virus life cycle.

ACKNOWLEDGMENTS

We thank Elvin Woodruff for TEM assistance and image analysis. We also thank Megan Culler and Xiaotao Lu for technical assistance. We thank Michelle Becker and Lance Eckerle for advice and critical reviews of the manuscript.

Support for this work was provided by National Institutes of Health grant R01 AI50083 (M.R.D.) from the National Institute of Allergy and Infectious Diseases. M.J.G. was supported by the Training Grant in Mechanisms of Vascular Disease through the Vanderbilt University School of Medicine (T32 HL007751). J.S.S. was supported by Public Health Service award T32 CA009385. This work was also supported by the Elizabeth B. Lamb Center for Pediatric Research.

REFERENCES

1. **Baker, S. C., K. Yokomori, S. Dong, R. Carlisle, A. E. Gorbalenya, E. V. Koonin, and M. M. Lai.** 1993. Identification of the catalytic sites of a papain-like cysteine proteinase of murine coronavirus. J. Virol. **67:**6056–6063.
2. **Baliji, S., S. A. Cammer, B. Sobral, and S. C. Baker.** 2009. Detection of nonstructural protein 6 (nsp6) in murine coronavirus-infected cells and analysis of the transmembrane topology using bioinformatics and molecular approaches. J. Virol. **83:**6957–6962.
3. **Bonilla, P. J., A. E. Gorbalenya, and S. R. Weiss.** 1994. Mouse hepatitis virus strain A59 RNA polymerase gene ORF 1a: heterogeneity among MHV strains. Virology **198:**736–740.
4. **Bost, A. G., E. Prentice, and M. R. Denison.** 2001. Mouse hepatitis virus replicase protein complexes are translocated to sites of M protein accumulation in the ERGIC at late times of infection. Virology **285:**21–29.
5. **Bredenbeek, P. J., C. J. Pachuk, A. F. H. Noten, J. Charite, W. Luytjes, S. R. Weiss, and W. J. M. Spaan.** 1990. The primary structure and expression of the second open reading frame of the polymerase gene of the coronavirus MHV-A59; a highly conserved polymerase is expressed by an efficient ribosomal frameshifting mechanism. Nucleic Acids Res. **18:**1825–1832.
6. **Brierley, I., P. Digard, and S. C. Inglis.** 1989. Characterization of an efficient coronavirus ribosomal frameshift signal: requirement for an RNA pseudoknot. Cell **57:**537–547.
7. **Brockway, S. M., C. T. Clay, X. T. Lu, and M. R. Denison.** 2003. Characterization of the expression, intracellular localization, and replication complex association of the putative mouse hepatitis virus RNA-dependent RNA polymerase. J. Virol. **77:**10515–10527.
8. **Chen, W., and R. S. Baric.** 1996. Molecular anatomy of mouse hepatitis virus persistence: coevolution of increased host cell resistance and virus virulence. J. Virol. **70:**3947–3960.
9. **Chen, W., V. J. Madden, C. J. Bagnell, and R. S. Baric.** 1997. Host-derived intracellular immunization against mouse hepatitis virus infection. Virology **228:**318–332.
10. **Clementz, M. A., A. Kanjanahaluethai, T. E. O'Brien, and S. C. Baker.** 2008. Mutation in murine coronavirus replication protein nsp4 alters assembly of double membrane vesicles. Virology **375:**118–129.
11. **Denison, M. R.** 2008. Seeking membranes: positive-strand RNA virus replication complexes. PLoS Biol. **6:**e270.
12. **Denison, M. R., B. Yount, S. M. Brockway, R. L. Graham, A. C. Sims, X. Lu, and R. S. Baric.** 2004. Cleavage between replicase proteins p28 and p65 of mouse hepatitis virus is not required for virus replication. J. Virol. **78:**5957–5965.
13. **Denison, M. R., P. W. Zoltick, S. A. Hughes, B. Giangreco, A. L. Olson, S. Perlman, J. L. Leibowitz, and S. R. Weiss.** 1992. Intracellular processing of the N-terminal ORF 1a proteins of the coronavirus MHV-A59 requires multiple proteolytic events. Virology **189:**274–284.
14. **Fiedler, K., and K. Simons.** 1995. The role of N-glycans in the secretory pathway. Cell **81:**309–312.
15. **Gosert, R., A. Kanjanahaluethai, D. Egger, K. Bienz, and S. C. Baker.** 2002. RNA replication of mouse hepatitis virus takes place at double-membrane vesicles. J. Virol. **76:**3697–3708.
16. **Graham, R. L., and M. R. Denison.** 2006. Replication of murine hepatitis virus is regulated by papain-like proteinase 1 processing of nonstructural proteins 1, 2, and 3. J. Virol. **80:**11610–11620.
17. **Harcourt, B. H., D. Jukneliene, A. Kanjanahaluethai, J. Bechill, K. M. Severson, C. M. Smith, P. A. Rota, and S. C. Baker.** 2004. Identification of severe acute respiratory syndrome coronavirus replicase products and characterization of papain-like protease activity. J. Virol. **78:**13600–13612.
18. **Helenius, A.** 1994. How N-linked oligosaccharides affect glycoprotein folding in the endoplasmic reticulum. Mol. Biol. Cell **5:**253–265.
19. **Helenius, A., and M. Aebi.** 2001. Intracellular functions of N-linked glycans. Science **291:**2364–2369.
20. **Hirano, N., K. Fujiwara, and M. Matumoto.** 1976. Mouse hepatitis virus (MHV-2). Plaque assay and propagation in mouse cell line DBT cells. Jpn. J. Microbiol. **20:**219–225.
21. **Kanjanahaluethai, A., and S. C. Baker.** 2000. Identification of mouse hepatitis virus papain-like proteinase 2 activity. J. Virol. **74:**7911–7921.
22. **Kanjanahaluethai, A., and S. C. Baker.** 2001. Processing of the replicase of murine coronavirus: papain-like proteinase 2 (PLP2) acts to generate p150 and p44. Adv. Exp. Med. Biol. **494:**267–273.
23. **Kanjanahaluethai, A., Z. Chen, D. Jukneliene, and S. C. Baker.** 2007. Membrane topology of murine coronavirus replicase nonstructural protein 3. Virology **361:**391–401.
24. **Kanjanahaluethai, A., D. Jukneliene, and S. C. Baker.** 2003. Identification of the murine coronavirus MP1 cleavage site recognized by papain-like proteinase 2. J. Virol. **77:**7376–7382.
25. **Kim, J. C., R. A. Spence, P. F. Currier, X. T. Lu, and M. R. Denison.** 1995. Coronavirus protein processing and RNA synthesis is inhibited by the cysteine proteinase inhibitor e64d. Virology **208:**1–8.
26. **Klausner, R. D., and R. Sitia.** 1990. Protein degradation in the endoplasmic reticulum. Cell **62:**611–614.
27. **Knoops, K., M. Kikkert, S. H. Worm, J. C. Zevenhoven-Dobbe, Y. van der Meer, A. J. Koster, A. M. Mommaas, and E. J. Snijder.** 2008. SARS-coronavirus replication is supported by a reticulovesicular network of modified endoplasmic reticulum. PLoS Biol. **6:**e226.
28. **Lee, H.-J., C.-K. Shieh, A. E. Gorbalenya, E. V. Koonin, N. LaMonica, J. Tuler, A. Bagdzhadzhyan, and M. M. C. Lai.** 1991. The complete sequence (22 kilobases) of murine coronavirus gene 1 encoding the putative proteases and RNA polymerase. Virology **180:**567–582.
29. **Lim, K. P., L. F. Ng, and D. X. Liu.** 2000. Identification of a novel cleavage activity of the first papain-like proteinase domain encoded by open reading frame 1a of the coronavirus Avian infectious bronchitis virus and characterization of the cleavage products. J. Virol. **74:**1674–1685.
30. **Lindenbach, B. D., and C. M. Rice.** 1999. Genetic interaction of flavivirus nonstructural proteins NS1 and NS4A as a determinant of replicase function. J. Virol. **73:**4611–4621.
31. **Lu, X. T., Y. Q. Lu, and M. R. Denison.** 1996. Intracellular and in vitro translated 27-kDa proteins contain the 3C-like proteinase activity of the coronavirus MHV-A59. Virology **222:**375–382.
32. **Lu, Y., X. Lu, and M. R. Denison.** 1995. Identification and characterization of a serine-like proteinase of the murine coronavirus MHV-A59. J. Virol. **69:**3554–3559.
33. **Muylaert, I. R., T. J. Chambers, R. Galler, and C. M. Rice.** 1996. Mutagenesis of the N-linked glycosylation sites of the yellow fever virus NS1 protein: effects on virus replication and mouse neurovirulence. Virology **222:**159–168.
34. **Novoa, R. R., G. Calderita, R. Arranz, J. Fontana, H. Granzow, and C. Risco.** 2005. Virus factories: associations of cell organelles for viral replication and morphogenesis. Biol. Cell **97:**147–172.
35. **Oostra, M., E. G. te Lintelo, M. Deijs, M. H. Verheije, P. J. M. Rottier, and C. A. M. de Haan.** 2007. Localization and membrane topology of coronavirus nonstructural protein 4: involvement of the early secretory pathway in replication. J. Virol. **81:**12323–12336.
36. **Paulson, J. C.** 1989. Glycoproteins: what are the sugar chains for? Trends Biochem. Sci. **14:**272–276.
37. **Pedersen, K. W., Y. van der Meer, N. Roos, and E. J. Snijder.** 1999. Open reading frame 1a-encoded subunits of the arterivirus replicase induce endoplasmic reticulum-derived double-membrane vesicles which carry the viral replication complex. J. Virol. **73:**2016–2026.
38. **Perlman, S., and J. Netland.** 2009. Coronaviruses post-SARS: update on replication and pathogenesis. Nat. Rev. Microbiol. **7:**439–450.

39. **Posthuma, C. C., K. W. Pedersen, Z. Lu, R. G. Joosten, N. Roos, J. C. Zevenhoven-Dobbe, and E. J. Snijder.** 2008. Formation of the arterivirus replication/transcription complex: a key role for nonstructural protein 3 in the remodeling of intracellular membranes. J. Virol. **82:**4480–4491.
40. **Restrepo-Hartwig, M. A., and P. Ahlquist.** 1996. Brome mosaic virus helicase- and polymerase-like proteins colocalize on the endoplasmic reticulum at sites of viral RNA synthesis. J. Virol. **70:**8908–8916.
41. **Salonen, A., T. Ahola, and L. Kaariainen.** 2005. Viral RNA replication in association with cellular membranes. Curr. Top. Microbiol. Immunol. **285:**139–173.
42. **Schaad, M. C., P. E. Jensen, and J. C. Carrington.** 1997. Formation of plant RNA virus replication complexes on membranes: role of an endoplasmic reticulum-targeted viral protein. EMBO J. **16:**4049–4059.
43. **Schlegel, A., T. J. Giddings, M. S. Ladinsky, and K. Kirkegaard.** 1996. Cellular origin and ultrastructure of membranes induced during poliovirus infection. J. Virol. **70:**6576–6588.
44. **Snijder, E. J., H. van Tol, N. Roos, and K. W. Pedersen.** 2001. Non-structural proteins 2 and 3 interact to modify host cell membranes during the formation of the arterivirus replication complex. J. Gen. Virol. **82:**985–994.
45. **Sparks, J. S., X. Lu, and M. R. Denison.** 2007. Genetic analysis of murine hepatitis virus nsp4 in virus replication. J. Virol. **81:**12554–12563.
46. **Suhy, D. A., T. H. Giddings, and K. Kirkegaard.** 2000. Remodeling the ER by poliovirus infection and by individual viral proteins: an autophagy-like origin for virus-induced vesicles. J. Virol. **74:**8953–8965.
47. **Yount, B., M. R. Denison, S. R. Weiss, and R. S. Baric.** 2002. Systematic assembly of a full-length infectious cDNA of mouse hepatitis virus strain A59. J. Virol. **76:**11065–11078.
48. **Ziebuhr, J., E. J. Snijder, and A. E. Gorbalenya.** 2000. Virus-encoded proteinases and proteolytic processing in the Nidovirales. J. Gen. Virol. **81(4):** 853–879.

REFERENCES

Almazan, F., Gonzalez, J. M., Penzes, Z., Izeta, A., Calvo, E., Plana-Duran, J., and Enjuanes, L. (2000). Engineering the largest RNA virus genome as an infectious bacterial artificial chromosome. *Proc Natl Acad Sci U S A* **97**(10)**,** 5516-21.

Anand, K., Ziebuhr, J., Wadhwani, P., Mesters, J. R., and Hilgenfeld, R. (2003). Coronavirus main proteinase (3CLpro) structure: basis for design of anti-SARS drugs. *Science* **300**(5626)**,** 1763-7.

Arden, K. E., Nissen, M. D., Sloots, T. P., and Mackay, I. M. (2005). New human coronavirus, HCoV-NL63, associated with severe lower respiratory tract disease in Australia. *J Med Virol* **75**(3)**,** 455-62.

Baker, S. C., Shieh, C.-K., Soe, L. H., Chang, M.-F., Vannier, D. M., and Lai, M. M. C. (1989). Identification of a domain required for autoproteolytic cleavage of murine coronavirus gene A polyprotein. *J. Virol.* **63**(9)**,** 3693-3699.

Baker, S. C., Yokomori, K., Dong, S., Carlisle, R., Gorbalenya, A. E., Koonin, E. V., and Lai, M. M. (1993). Identification of the catalytic sites of a papain-like cysteine proteinase of murine coronavirus. *J Virol* **67**(10)**,** 6056-63.

Baliji, S., Cammer, S. A., Sobral, B., and Baker, S. C. (2009). Detection of nonstructural protein 6 (nsp6) in murine coronavirus-infected cells and analysis of the transmembrane topology using bioinformatics and molecular approaches. *J Virol* **83**(13), 6957-62.

Baric, R. S., and Yount, B. (2000). Subgenomic negative-strand RNA function during mouse hepatitis virus infection. *J Virol* **74**(9)**,** 4039-46.

Barretto, N., Jukneliene, D., Ratia, K., Chen, Z., Mesecar, A. D., and Baker, S. C. (2005). The papain-like protease of severe acute respiratory syndrome coronavirus has deubiquitinating activity. *J Virol* **79**(24)**,** 15189-98.

Bedard, K. M., and Semler, B. L. (2004). Regulation of picornavirus gene expression. *Microbes Infect* **6**(7)**,** 702-13.

Bonilla, P. J., Gorbalenya, A. E., and Weiss, S. R. (1994). Mouse hepatitis virus strain A59 RNA polymerase gene ORF 1a: heterogeneity among MHV strains. *Virology* **198**(2)**,** 736-40.

Bonilla, P. J., Hughes, S. A., Pinon, J. D., and Weiss, S. R. (1995). Characterization of the leader papain-like proteinase of MHV-A59: identification of a new in vitro cleavage site. *Virology* **209**(2)**,** 489-97.

Bonilla, P. J., Hughes, S. A., and Weiss, S. R. (1997). Characterization of a second cleavage site and demonstration of activity in trans by the papain-like proteinase of the murine coronavirus mouse hepatitis virus strain A59. *J Virol* **71**(2)**,** 900-9.

Bost, A. G., Carnahan, R. H., Lu, X. T., and Denison, M. R. (2000). Four proteins processed from the replicase gene polyprotein of mouse hepatitis virus colocalize in the cell periphery and adjacent to sites of virion assembly. *J Virol* **74**(7)**,** 3379-87.

Bost, A. G., Prentice, E., and Denison, M. R. (2001). Mouse hepatitis virus replicase protein complexes are translocated to sites of M protein accumulation in the ERGIC at late times of infection. *Virology* **285,** 21-29.

Breedenbeek, P. J., Pachuk, C. J., Noten, A. F. H., Charite, J., Luytjes, W., Weiss, S. R., and Spaan, W. J. M. (1990). The primary structure and expression of the second open reading frame of the polymerase gene of the coronavirus MHV-A59; a highly conserved polymerase is expressed by an efficient ribosomal frameshifting mechanism. *Nucleic Acids Res.* **18**(7)**,** 1825-1832.

Brierley, I., Digard, P., and Inglis, S. C. (1989). Characterization of an efficient coronavirus ribosomal frameshift signal: requirement for an RNA pseudoknot. *Cell* **57,** 537-547.

Brockway, S. M., Clay, C. T., Lu, X. T., and Denison, M. R. (2003). Characterization of the expression, intracellular localization, and replication complex association of the putative mouse hepatitis virus RNA-dependent RNA polymerase. *J Virol* **77**(19)**,** 10515-27.

Brockway, S. M., Lu, X. T., Peters, T. R., Dermody, T. S., and Denison, M. R. (2004). Intracellular localization and protein interactions of the gene 1 protein p28 during mouse hepatitis virus replication. *J Virol* **78**(21)**,** 11551-62.

Casais, R., Thiel, V., Siddell, S. G., Cavanagh, D., and Britton, P. (2001). Reverse genetics system for the avian coronavirus infectious bronchitis virus. *J Virol* **75**(24)**,** 12359-69.

Chen, J., and Subbarao, K. (2007). The Immunobiology of SARS*. *Annu Rev Immunol* **25,** 443-72.

Chen, W., and Baric, R. S. (1996). Molecular anatomy of mouse hepatitis virus persistence: coevolution of increased host cell resistance and virus virulence. *J Virol* **70**(6)**,** 3947-60.

Chen, W., Madden, V. J., Bagnell, C. J., and Baric, R. S. (1997). Host-derived intracellular immunization against mouse hepatitis virus infection. *Virology* **228**(2)**,** 318-32.

Chen, Z., Wang, Y., Ratia, K., Mesecar, A. D., Wilkinson, K. D., and Baker, S. C. (2007). Proteolytic processing and deubiquitinating activity of papain-like proteases of human coronavirus NL63. *J Virol* **81**(11)**,** 6007-18.

Chinese, S. M. E. C. (2004). Molecular evolution of the SARS coronavirus during the course of the SARS epidemic in China. *Science* **303**(5664)**,** 1666-9.

Clementz, M. A., Kanjanahaluethai, A., O'Brien, T. E., and Baker, S. C. (2008). Mutation in murine coronavirus replication protein nsp4 alters assembly of double membrane vesicles. *Virology* **375**(1)**,** 118-29.

Coley, S. E., Lavi, E., Sawicki, S. G., Fu, L., Schelle, B., Karl, N., Siddell, S. G., and Thiel, V. (2005). Recombinant mouse hepatitis virus strain A59 from cloned, full-length cDNA replicates to high titers in vitro and is fully pathogenic in vivo. *J Virol* **79**(5)**,** 3097-106.

Compton, S. R., Barthold, S. W., and Smith, A. L. (1993). The cellular and molecular pathogenesis of coronaviruses. *Lab Anim Sci* **43**(1)**,** 15-28.

Cornillez-Ty, C. T., Liao, L., Yates, J. R., 3rd, Kuhn, P., and Buchmeier, M. J. (2009). Severe acute respiratory syndrome coronavirus nonstructural protein 2 interacts with a host protein complex involved in mitochondrial biogenesis and intracellular signaling. *J Virol* **83**(19)**,** 10314-8.

Curtis, K. M., Yount, B., and Baric, R. S. (2002). Heterologous gene expression from transmissible gastroenteritis virus replicon particles. *J Virol* **76**(3)**,** 1422-34.

Curtis, K. M., Yount, B., Sims, A. C., and Baric, R. S. (2004). Reverse genetic analysis of the transcription regulatory sequence of the coronavirus transmissible gastroenteritis virus. *J Virol* **78**(11)**,** 6061-6.

de Haan, C. A., Haijema, B. J., Boss, D., Heuts, F. W., and Rottier, P. J. (2005). Coronaviruses as vectors: stability of foreign gene expression. *J Virol* **79**(20)**,** 12742-51.

de Vries, A. A. F., Horzinek, M. C., Rottier, P. J. M., and deGroot, R. J. (1997). The genome organization of the nidovirales: similarities and differenced between arteri-, toro, and coronaviruses. *Sem. Virology* **8,** 33-47.

Decaro, N., Martella, V., Elia, G., Campolo, M., Mari, V., Desario, C., Lucente, M. S., Lorusso, A., Greco, G., Corrente, M., Tempesta, M., and Buonavoglia, C. (2008). Biological and genetic analysis of a bovine-like coronavirus isolated from water buffalo (Bubalus bubalis) calves. *Virology* **370**(1)**,** 213-22.

Denison, M. R. (2008). Seeking membranes: positive-strand RNA virus replication complexes. *PLoS Biol* **6**(10)**,** e270.

Denison, M. R., Sims, A. C., Gibson, C. A., and Lu, X. T. (1998). Processing of the MHV-A59 gene 1 polyprotein by the 3C-like proteinase. *Adv Exp Med Biol* **440,** 121-7.

Denison, M. R., Spaan, W. J., van der Meer, Y., Gibson, C. A., Sims, A. C., Prentice, E., and Lu, X. T. (1999). The putative helicase of the coronavirus mouse hepatitis virus is processed from the replicase gene polyprotein and localizes in complexes that are active in viral RNA synthesis. *J Virol* **73**(8)**,** 6862-71.

Denison, M. R., Yount, B., Brockway, S. M., Graham, R. L., Sims, A. C., Lu, X., and Baric, R. S. (2004). Cleavage between replicase proteins p28 and p65 of mouse hepatitis virus is not required for virus replication. *J Virol* **78**(11)**,** 5957-65.

Denison, M. R., Zoltick, P. W., Hughes, S. A., Giangreco, B., Olson, A. L., Perlman, S., Leibowitz, J. L., and Weiss, S. R. (1992). Intracellular processing of the N-terminal ORF 1a proteins of the coronavirus MHV-A59 requires multiple proteolytic events. *Virology* **189**(1)**,** 274-84.

Dong, S., and Baker, S. C. (1994). Determinants of the p28 cleavage site recognized by the first papain-like cysteine proteinase of murine coronavirus. *Virology* **204**(2)**,** 541-9.

Dveksler, G. S., Pensiero, M. N., Cardellichio, C. B., Williams, R. K., Jiang, G. S., Holmes, K. V., and Dieffenbach, C. W. (1991). Cloning of the mouse hepatitis virus (MHV) receptor: expression in human and hamster cell lines confers susceptibility to MHV. *J Virol* **65**(12)**,** 6881-91.

Ebihara, T., Endo, R., Ma, X., Ishiguro, N., and Kikuta, H. (2005). Detection of human coronavirus NL63 in young children with bronchiolitis. *J Med Virol* **75**(3)**,** 463-5.

Engel, J. P. (1995). Viral upper respiratory infections. *Semin Respir Infect* **10**(1)**,** 3-13.

Eriksson, K. K., Cervantes-Barragan, L., Ludewig, B., and Thiel, V. (2008). Mouse hepatitis virus liver pathology is dependent on ADP-ribose-1"-phosphatase, a viral function conserved in the alpha-like supergroup. *J Virol* **82**(24)**,** 12325-34.

Fiedler, K., and Simons, K. (1995). The role of N-glycans in the secretory pathway. *Cell* **81**(3)**,** 309-12.

Fischer, F., Stegen, C., Masters, P., and Samsonoff, W. (1998). Analysis of constructed E gene mutants of mouse hepatitis virus confirms a pivotal role for E protein in coronavirus assembly. *J Virol* **72(10)**(Oct)**,** 7885-94.

Fischer, F., Stegen, C. F., Koetzner, C. A., and Masters, P. S. (1997). Analysis of a recombinant mouse hepatitis virus expressing a foreign gene reveals a novel aspect of coronavirus transcription. *J Virol* **71**(7)**,** 5148-60.

Gallagher, T. M., and Buchmeier, M. J. (2001). Coronavirus spike proteins in viral entry and pathogenesis. *Virology* **279**(2)**,** 371-4.

Goldsmith, C. S., Tatti, K. M., Ksiazek, T. G., Rollin, P. E., Comer, J. A., Lee, W. W., Rota, P. A., Bankamp, B., Bellini, W. J., and Zaki, S. R. (2004). Ultrastructural characterization of SARS coronavirus. *Emerg Infect Dis* **10**(2)**,** 320-6.

Gonzalez, J. M., Almazan, F., Penzes, Z., Calvo, E., and Enjuanes, L. (2001). Cloning of a transmissible gastroenteritis coronavirus full-length cDNA. *Adv Exp Med Biol* **494,** 533-6.

Gonzalez, J. M., Gomez-Puertas, P., Cavanagh, D., Gorbalenya, A. E., and Enjuanes, L. (2003). A comparative sequence analysis to revise the current taxonomy of the family Coronaviridae. *Arch Virol* **148**(11)**,** 2207-35.

Gonzalez, J. M., Penzes, Z., Almazan, F., Calvo, E., and Enjuanes, L. (2002). Stabilization of a full-length infectious cDNA clone of transmissible gastroenteritis coronavirus by insertion of an intron. *J Virol* **76**(9)**,** 4655-61.

Gorbalenya, A. E., Snijder, E. J., and Spaan, W. J. (2004). Severe acute respiratory syndrome coronavirus phylogeny: toward consensus. *J Virol* **78**(15)**,** 7863-6.

Gosert, R., Kanjanahaluethai, A., Egger, D., Bienz, K., and Baker, S. C. (2002). RNA replication of mouse hepatitis virus takes place at double-membrane vesicles. *J Virol* **76**(8)**,** 3697-708.

Graham, R. L., and Denison, M. R. (2006). Replication of murine hepatitis virus is regulated by papain-like proteinase 1 processing of nonstructural proteins 1, 2, and 3. *J Virol* **80**(23)**,** 11610-20.

Graham, R. L., Sims, A. C., Baric, R. S., and Denison, M. R. (2006). The nsp2 proteins of mouse hepatitis virus and SARS coronavirus are dispensable for viral replication. *Adv Exp Med Biol* **581,** 67-72.

Graham, R. L., Sims, A. C., Brockway, S. M., Baric, R. S., and Denison, M. R. (2005). The nsp2 replicase proteins of murine hepatitis virus and severe acute respiratory syndrome coronavirus are dispensable for viral replication. *J Virol* **79**(21)**,** 13399-411.

Harcourt, B. H., Jukneliene, D., Kanjanahaluethai, A., Bechill, J., Severson, K. M., Smith, C. M., Rota, P. A., and Baker, S. C. (2004). Identification of severe acute respiratory syndrome coronavirus replicase products and characterization of papain-like protease activity. *J Virol* **78**(24)**,** 13600-12.

Hasoksuz, M., Alekseev, K., Vlasova, A., Zhang, X., Spiro, D., Halpin, R., Wang, S., Ghedin, E., and Saif, L. J. (2007). Biologic, antigenic, and full-length genomic characterization of a bovine-like coronavirus isolated from a giraffe. *J Virol* **81**(10)**,** 4981-90.

Helenius, A. (1994). How N-linked oligosaccharides affect glycoprotein folding in the endoplasmic reticulum. *Mol Biol Cell* **5**(3)**,** 253-65.

Helenius, A., and Aebi, M. (2001). Intracellular functions of N-linked glycans. *Science* **291**(5512)**,** 2364-9.

Herold, J., Gorbalenya, A. E., Thiel, V., Schelle, B., and Siddell, S. G. (1998). Proteolytic processing at the amino terminus of human coronavirus 229E gene 1-encoded polyproteins: identification of a papain-like proteinase and its substrate. *J Virol* **72**(2)**,** 910-8.

Herold, J., Siddell, S. G., and Gorbalenya, A. E. (1999). A human RNA viral cysteine proteinase that depends upon a unique Zn2+-binding finger connecting the two domains of a papain-like fold. *J Biol Chem* **274**(21)**,** 14918-25.

Hirano, N., Fujiwara, K., and Matumoto, M. (1976). Mouse hepatitis virus (MHV-2); plaque assay and propagation in mouse cell line DBT cells. *Japan. J. Micro* **20**(3)**,** 219-225.

Horton, R. M., Hunt, H. D., Ho, S. N., Pullen, J. K., and Pease, L. R. (1989). Engineering hybrid genes without the use of restriction enzymes: gene splicing by overlap extension. *Gene* **77**(1)**,** 61-8.

Hughes, S. A., Bonilla, P. J., and Weiss, S. R. (1995). Identification of the murine coronavirus p28 cleavage site. *J Virol* **69**(2)**,** 809-13.

ImageJ 1.40. Bethesda, Maryland: http://rsb.info.nih.gov/ij/

Kamitani, W., Narayanan, K., Huang, C., Lokugamage, K., Ikegami, T., Ito, N., Kubo, H., and Makino, S. (2006). Severe acute respiratory syndrome coronavirus nsp1 protein suppresses host gene expression by promoting host mRNA degradation. *Proc Natl Acad Sci U S A* **103**(34)**,** 12885-90.

Kanjanahaluethai, A., and Baker, S. C. (2000). Identification of mouse hepatitis virus papain-like proteinase 2 activity. *J Virol* **74**(17)**,** 7911-21.

Kanjanahaluethai, A., and Baker, S. C. (2001). Processing of the replicase of murine coronavirus: papain-like proteinase 2 (PLP2) acts to generate p150 and p44. *Adv Exp Med Biol* **494,** 267-73.

Kanjanahaluethai, A., Chen, Z., Jukneliene, D., and Baker, S. C. (2007). Membrane topology of murine coronavirus replicase nonstructural protein 3. *Virology* **361**(2)**,** 391-401.

Kanjanahaluethai, A., Jukneliene, D., and Baker, S. C. (2003). Identification of the murine coronavirus MP1 cleavage site recognized by papain-like proteinase 2. *J Virol* **77**(13)**,** 7376-82.

Kim, J. C., Spence, R. A., Currier, P. F., Lu, X. T., and Denison, M. R. (1995). Coronavirus protein processing and RNA synthesis is inhibited by the cysteine proteinase inhibitor e64dd. *Virology* **208,** 1-8.

Klausner, R. D., and Sitia, R. (1990). Protein degradation in the endoplasmic reticulum. *Cell* **62**(4)**,** 611-4.

Knoops, K., Kikkert, M., Worm, S. H., Zevenhoven-Dobbe, J. C., van der Meer, Y., Koster, A. J., Mommaas, A. M., and Snijder, E. J. (2008). SARS-coronavirus replication is supported by a reticulovesicular network of modified endoplasmic reticulum. *PLoS Biol* **6**(9)**,** e226.

Kooi, C., Cervin, M., and Anderson, R. (1991). Differentiation of acid-pH-dependent and -nondependent entry pathways for mouse hepatitis virus. *Virology* **180**(1)**,** 108-19.

Ksiazek, T. G., Erdman, D., Goldsmith, C. S., Zaki, S. R., Peret, T., Emery, S., Tong, S., Urbani, C., Comer, J. A., Lim, W., Rollin, P. E., Dowell, S. F., Ling, A. E., Humphrey, C. D., Shieh, W. J., Guarner, J., Paddock, C. D., Rota, P., Fields, B., DeRisi, J., Yang, J. Y., Cox, N., Hughes, J. M., LeDuc, J. W., Bellini, W. J., and Anderson, L. J. (2003). A novel coronavirus associated with severe acute respiratory syndrome. *N Engl J Med* **348**(20)**,** 1953-66.

Kuiken, T., Fouchier, R., Rimmelzwaan, G., and Osterhaus, A. (2003a). Emerging viral infections in a rapidly changing world. *Curr Opin Biotechnol* **14**(6)**,** 641-6.

Kuiken, T., Fouchier, R. A., Schutten, M., Rimmelzwaan, G. F., van Amerongen, G., van Riel, D., Laman, J. D., de Jong, T., van Doornum, G., Lim, W., Ling, A. E., Chan, P. K., Tam, J. S., Zambon, M. C., Gopal, R., Drosten, C., van der Werf, S., Escriou, N., Manuguerra, J. C., Stohr, K., Peiris, J. S., and Osterhaus, A. D. (2003b). Newly discovered coronavirus as the primary cause of severe acute respiratory syndrome. *Lancet* **362**(9380)**,** 263-70.

Kuo, L., and Masters, P. S. (2002). Genetic evidence for a structural interaction between the carboxy termini of the membrane and nucleocapsid proteins of mouse hepatitis virus. *J Virol* **76**(10)**,** 4987-99.

Lai, M. M. (2003). SARS virus: the beginning of the unraveling of a new coronavirus. *J Biomed Sci* **10**(6 Pt 2)**,** 664-75.

Lau, S. K., Woo, P. C., Li, K. S., Huang, Y., Tsoi, H. W., Wong, B. H., Wong, S. S., Leung, S. Y., Chan, K. H., and Yuen, K. Y. (2005). Severe acute respiratory syndrome coronavirus-like virus in Chinese horseshoe bats. *Proc Natl Acad Sci U S A* **102**(39)**,** 14040-5.

Lawson, M. A., and Semler, B. L. (1990). Picornavirus protein processing-enzymes, substrates, and genetic regulation. *Curr. Top. Microbiol. Immunol.* **161,** 49-80.

Lee, H.-J., Shieh, C.-K., Gorbalenya, A. E., Koonin, E. V., LaMonica, N., Tuler, J., Bagdzhadhzyan, A., and Lai, M. M. C. (1991). The complete sequence (22 kilobases) of murine coronavirus gene 1 encoding the putative proteases and RNA polymerase. *Virology* **180,** 567-582.

Li, W., Moore, M. J., Vasilieva, N., Sui, J., Wong, S. K., Berne, M. A., Somasundaran, M., Sullivan, J. L., Luzuriaga, K., Greenough, T. C., Choe, H., and Farzan, M. (2003). Angiotensin-converting enzyme 2 is a functional receptor for the SARS coronavirus. *Nature* **426**(6965)**,** 450-4.

Lim, K. P., and Liu, D. X. (1998). Characterization of the two overlapping papain-like proteinase domains encoded in gene 1 of the coronavirus infectious bronchitis virus and determination of the C-terminal cleavage site of an 87-kDa protein. *Virology* **245**(2)**,** 303-12.

Lim, K. P., Ng, L. F., and Liu, D. X. (2000). Identification of a novel cleavage activity of the first papain-like proteinase domain encoded by open reading frame 1a of the coronavirus Avian infectious bronchitis virus and characterization of the cleavage products. *J Virol* **74**(4)**,** 1674-85.

Lindenbach, B. D., and Rice, C. M. (1999). Genetic interaction of flavivirus nonstructural proteins NS1 and NS4A as a determinant of replicase function. *J Virol* **73**(6)**,** 4611-21.

Lindner, H. A., Fotouhi-Ardakani, N., Lytvyn, V., Lachance, P., Sulea, T., and Menard, R. (2005). The papain-like protease from the severe acute respiratory syndrome coronavirus is a deubiquitinating enzyme. *J Virol* **79**(24)**,** 15199-208.

Lu, X., Sims, A., and Denison, M. R. (1998a). Mouse hepatitis virus 3CLpro cleaves a 22 kDa protein from the ORF 1a polyprotein in virus-infected cells and in vitro. *J Virol* **72**(3)**,** 2265-2271.

Lu, X. T., Lu, Y. Q., and Denison, M. R. (1996). Intracellular and in vitro translated 27-kDa proteins contain the 3C-like proteinase activity of the coronavirus MHV-A59. *Virology* **222,** 375-382.

Lu, X. T., Sims, A. C., and Denison, M. R. (1998b). Mouse hepatitis virus 3C-like protease cleaves a 22-kilodalton protein from the open reading frame 1a polyprotein in virus-infected cells and in vitro. *J Virol* **72**(3)**,** 2265-71.

Lu, Y., Lu, X., and Denison, M. R. (1995). Identification and characterization of a serine-like proteinase of the murine coronavirus MHV-A59. *J Virol* **69**(6)**,** 3554-9.

Makela, M. J., Puhakka, T., Ruuskanen, O., Leinonen, M., Saikku, P., Kimpimaki, M., Blomqvist, S., Hyypia, T., and Arstila, P. (1998). Viruses and bacteria in the etiology of the common cold. *J Clin Microbiol* **36**(2)**,** 539-42.

Marra, M. A., Jones, S. J., Astell, C. R., Holt, R. A., Brooks-Wilson, A., Butterfield, Y. S., Khattra, J., Asano, J. K., Barber, S. A., Chan, S. Y., Cloutier, A., Coughlin, S. M., Freeman, D., Girn, N., Griffith, O. L., Leach, S. R., Mayo, M., McDonald, H., Montgomery, S. B., Pandoh, P. K., Petrescu, A. S., Robertson, A. G., Schein, J. E., Siddiqui, A., Smailus, D. E., Stott, J. M., Yang, G. S., Plummer, F., Andonov, A., Artsob, H., Bastien, N., Bernard, K., Booth, T. F., Bowness, D., Czub, M., Drebot, M., Fernando, L., Flick, R., Garbutt, M., Gray, M., Grolla, A., Jones, S., Feldmann, H., Meyers, A., Kabani, A., Li, Y., Normand, S., Stroher, U., Tipples, G. A., Tyler, S., Vogrig, R., Ward, D., Watson, B., Brunham, R. C., Krajden, M., Petric, M., Skowronski, D. M., Upton, C., and Roper, R. L. (2003). The Genome sequence of the SARS-associated coronavirus. *Science* **300**(5624)**,** 1399-404.

Masters, P. S. (2006). The molecular biology of coronaviruses. *Adv Virus Res* **66,** 193-292.

Masters, P. S., Koetzner, C. A., Kerr, C. A., and Heo, Y. (1994). Optimization of targeted RNA recombination and mapping of a novel nucleocapsid gene mutation in the coronavirus mouse hepatitis virus. *J Virol* **68**(1)**,** 328-37.

Mihindukulasuriya, K. A., Wu, G., St Leger, J., Nordhausen, R. W., and Wang, D. (2008). Identification of a novel coronavirus from a beluga whale by using a panviral microarray. *J Virol* **82**(10)**,** 5084-8.

Muylaert, I. R., Chambers, T. J., Galler, R., and Rice, C. M. (1996). Mutagenesis of the N-linked glycosylation sites of the yellow fever virus NS1 protein: effects on virus replication and mouse neurovirulence. *Virology* **222**(1)**,** 159-68.

Narayanan, K., Huang, C., Lokugamage, K., Kamitani, W., Ikegami, T., Tseng, C. T., and Makino, S. (2008). Severe acute respiratory syndrome coronavirus nsp1 suppresses host gene expression, including that of type I interferon, in infected cells. *J Virol* **82**(9)**,** 4471-9.

Narayanan, K., Maeda, A., Maeda, J., and Makino, S. (2000). Characterization of the coronavirus M protein and nucleocapsid interaction in infected cells. *J Virol* **74**(17)**,** 8127-8134.

Normile, D. (2005). Virology. Researchers tie deadly SARS virus to bats. *Science* **309**(5744)**,** 2154-5.

Novoa, R. R., Calderita, G., Arranz, R., Fontana, J., Granzow, H., and Risco, C. (2005). Virus factories: associations of cell organelles for viral replication and morphogenesis. *Biol Cell* **97**(2)**,** 147-72.

Oostra, M., te Lintelo, E. G., Deijs, M., Verheije, M. H., Rottier, P. J., and de Haan, C. A. (2007). Localization and membrane topology of coronavirus nonstructural protein 4: involvement of the early secretory pathway in replication. *J Virol* **81**(22)**,** 12323-36.

Opstelten, D., Horzinek, M., and Rottier, P. (1993). Complex formation between the spike protein and the membrane protein during mouse hepatitis virus assembly. *Adv Exp Med Biol* **342,** 189.

Opstelten, D. J., Raamsman, M. J., Wolfs, K., Horzinek, M. C., and Rottier, P. J. (1995). Envelope glycoprotein interactions in coronavirus assembly. *Journal of Cell Biology* **131**(2)**,** 339-49.

Ortego, J., Escors, D., Laude, H., and Enjuanes, L. (2002). Generation of a replication-competent, propagation-deficient virus vector based on the transmissible gastroenteritis coronavirus genome. *J Virol* **76**(22)**,** 11518-29.

Pachuk, C. J., Breedenbeek, P. J., Zoltick, P. W., Spaan, W. J. M., and Weiss, S. R. (1989). Molecular cloning of the gene encoding the putative polymerase of mouse hepatitis coronavirus, strain A59. *Virology* **171,** 141-148.

Palmenburg, A. C. (1990). Proteolytic processing of picornaviral polyprotein. *Annu. Rev. Microbiol.* **44,** 603-23.

Pasternak, A. O., Spaan, W. J., and Snijder, E. J. (2006). Nidovirus transcription: how to make sense...? *J Gen Virol* **87**(Pt 6)**,** 1403-21.

Paulson, J. C. (1989). Glycoproteins: what are the sugar chains for? *Trends Biochem Sci* **14**(7)**,** 272-6.

Pedersen, K. W., van der Meer, Y., Roos, N., and Snijder, E. J. (1999). Open reading frame 1a-encoded subunits of the arterivirus replicase induce endoplasmic reticulum-derived double-membrane vesicles which carry the viral replication complex. *J Virol* **73**(3)**,** 2016-26.

Perlman, S., and Netland, J. (2009). Coronaviruses post-SARS: update on replication and pathogenesis. *Nat Rev Microbiol* **7**(6)**,** 439-50.

Pinon, J. D., Teng, H., and Weiss, S. R. (1999). Further requirements for cleavage by the murine coronavirus 3C-like proteinase: identification of a cleavage site within ORF1b. *Virology* **263**(2)**,** 471-84.

Posthuma, C. C., Pedersen, K. W., Lu, Z., Joosten, R. G., Roos, N., Zevenhoven-Dobbe, J. C., and Snijder, E. J. (2008). Formation of the arterivirus replication/transcription complex: a key role for nonstructural protein 3 in the remodeling of intracellular membranes. *J Virol* **82**(9)**,** 4480-91.

Prentice, E., Jerome, W. G., Yoshimori, T., Mizushima, N., and Denison, M. R. (2004). Coronavirus replication complex formation utilizes components of cellular autophagy. *J Biol Chem* **279**(11)**,** 10136-41.

Raamsman, M. J., Krijnse Locker, J., de Hooge, A., de Vries, A. F., Griffiths, G., Vennema, H., and Rottier, P. J. (2000). Characterization of the coronavirus mouse hepatitis strain A59 small membrane protein E. *J Virol* **74**(5)**,** 2333-2342.

Ratia, K., Saikatendu, K. S., Santarsiero, B. D., Barretto, N., Baker, S. C., Stevens, R. C., and Mesecar, A. D. (2006). Severe acute respiratory syndrome coronavirus papain-like protease: structure of a viral deubiquitinating enzyme. *Proc Natl Acad Sci U S A* **103**(15)**,** 5717-22.

Restrepo-Hartwig, M. A., and Ahlquist, P. (1996). Brome mosaic virus helicase- and polymerase-like proteins colocalize on the endoplasmic reticulum at sites of viral RNA synthesis. *J Virol* **70**(12)**,** 8908-16.

Risco, C., Anton, I., Enjuanes, L., and Carrascosa, J. (1996). The transmissible gastroenteritis coronavirus contains a spherical core shell consisting of M and N proteins. *J Virol* **70(7)**(Jul)**,** 4773-7.

Ryan, M. D., and Flint, M. (1997). Virus-encoded proteinases of the picornavirus super-group. *J Gen Virol* **78 (Pt 4),** 699-723.

Salonen, A., Ahola, T., and Kaariainen, L. (2005). Viral RNA replication in association with cellular membranes. *Curr Top Microbiol Immunol* **285,** 139-73.

Sawicki, S. G., and Sawicki, D. L. (1990). Coronavirus transcription: subgenomic mouse hepatitis virus replicative intermediates function in RNA synthesis. *J. Virol.* **64**(3)**,** 1050-1056.

Sawicki, S. G., and Sawicki, D. L. (1998). A new model for coronavirus transcription. *Adv Exp Med Biol* **440,** 215-9.

Sawicki, S. G., and Sawicki, D. L. (2005). Coronavirus transcription: a perspective. *Curr Top Microbiol Immunol* **287,** 31-55.

Sawicki, S. G., Sawicki, D. L., and Siddell, S. G. (2007). A contemporary view of coronavirus transcription. *J Virol* **81**(1)**,** 20-9.

Schaad, M. C., Jensen, P. E., and Carrington, J. C. (1997). Formation of plant RNA virus replication complexes on membranes: role of an endoplasmic reticulum-targeted viral protein. *EMBO Journal* **16**(13)**,** 4049-59.

Schiller, J. J., Kanjanahaluethai, A., and Baker, S. C. (1998). Processing of the coronavirus mhv-jhm polymerase polyprotein: identification of precursors and proteolytic products spanning 400 kilodaltons of ORF1a. *Virology* **242,** 288-302.

Schlegel, A., Giddings, T. J., Ladinsky, M. S., and Kirkegaard, K. (1996). Cellular origin and ultrastructure of membranes induced during poliovirus infection. *J Virol* **70**(10)**,** 6576-88.

Sethna, P. B., Hofmann, M. A., and Brian, D. A. (1991). Minus-strand copies of replicating coronavirus mRNAs contain antileaders. *J. Virol* **65**(1)**,** 320-325.

Sethna, T. B., Hung, S. L., and Brian, D. A. (1989). Coronavirus subgenomic minus-strand RNAs and the potential for mRNA replicons. *Proc Natl Acad Sci U S A* **86,** 5626-5630.

Sims, A. C., Ostermann, J., and Denison, M. R. (2000). Mouse hepatitis virus replicase proteins associate with two distinct populations of intracellular membranes. *J Virol* **74**(12)**,** 5647-54.

Snijder, E., Wassenaar, A. L., Den, B. J., and Spaan, W. J. (1995). Proteolytic processing of the arterivirus replicase. [Review] [28 refs]. *Adv Exp Med Biol* **380**(443)**,** 443-51.

Snijder, E. J., Bredenbeek, P. J., Dobbe, J. C., Thiel, V., Ziebuhr, J., Poon, L. L., Guan, Y., Rozanov, M., Spaan, W. J., and Gorbalenya, A. E. (2003). Unique and conserved features of genome and proteome of SARS-coronavirus, an early split-off from the coronavirus group 2 lineage. *J Mol Biol* **331**(5)**,** 991-1004.

Snijder, E. J., van der Meer, Y., Zevenhoven-Dobbe, J., Onderwater, J. J., van der Meulen, J., Koerten, H. K., and Mommaas, A. M. (2006). Ultrastructure and origin of membrane vesicles associated with the severe acute respiratory syndrome coronavirus replication complex. *J Virol* **80**(12)**,** 5927-40.

Snijder, E. J., van Tol, H., Roos, N., and Pedersen, K. W. (2001). Non-structural proteins 2 and 3 interact to modify host cell membranes during the formation of the arterivirus replication complex. *J Gen Virol* **82**(Pt 5)**,** 985-94.

Sola, I., Moreno, J. L., Zuniga, S., Alonso, S., and Enjuanes, L. (2005). Role of nucleotides immediately flanking the transcription-regulating sequence core in coronavirus subgenomic mRNA synthesis. *J Virol* **79**(4)**,** 2506-16.

Sparks, J. S., Lu, X., and Denison, M. R. (2007). Genetic analysis of Murine hepatitis virus nsp4 in virus replication. *J Virol* **81**(22)**,** 12554-63.

Suhy, D. A., Giddings, T. H., and Kirkegaard, K. (2000). Remodeling the endoplasmic reticulum by poliovirus infection and by individual viral proteins: an autophagy-like origin for virus-induced vesicles. *J Virol* **74**(19)**,** 8953-8965.

Sulea, T., Lindner, H. A., Purisima, E. O., and Menard, R. (2006). Binding site-based classification of coronaviral papain-like proteases. *Proteins* **62**(3)**,** 760-75.

Teng, H., Pinon, J. D., and Weiss, S. R. (1999). Expression of murine coronavirus recombinant papain-like proteinase: efficient cleavage is dependent on the lengths of both the substrate and the proteinase polypeptides. *J Virol* **73**(4)**,** 2658-66.

Teng, H., and Weiss, S. R. (2002). Further in vitro characterization of mouse hepatitis virus papain-like proteinase 1: cleavage sequence requirements within pp1a. *J Neurovirol* **8**(2)**,** 143-9.

Thiel, V., Herold, J., Schelle, B., and Siddell, S. G. (2001). Infectious RNA transcribed in vitro from a cDNA copy of the human coronavirus genome cloned in vaccinia virus. *J Gen Virol* **82**(Pt 6)**,** 1273-81.

Thiel, V., Ivanov, K. A., Putics, A., Hertzig, T., Schelle, B., Bayer, S., Weissbrich, B., Snijder, E. J., Rabenau, H., Doerr, H. W., Gorbalenya, A. E., and Ziebuhr, J. (2003). Mechanisms and enzymes involved in SARS coronavirus genome expression. *J Gen Virol* **84**(Pt 9)**,** 2305-15.

Thiel, V., and Siddell, S. G. (2005). Reverse genetics of coronaviruses using vaccinia virus vectors. *Curr Top Microbiol Immunol* **287,** 199-227.

Vasiljeva, L., Merits, A., Golubtsov, A., Sizemskaja, V., Kaariainen, L., and Ahola, T. (2003). Regulation of the sequential processing of Semliki Forest virus replicase polyprotein. *J Biol Chem* **278**(43)**,** 41636-45.

Vennema, H., Godeke, G., Rossen, J., Voorhout, W., Horzinek, M., Opstelten, D., and Rottier, P. (1996). Nucleocapsid-independent association of coronavirus-like particles by co-expression of viral envelope protein genes. *EMBO J* **15(8)**(Apr 15)**,** 2020-8.

Vennema, H., Rijnbrand, R., Heijnen, L., Horzinek, M. C., and Spaan, W. J. M. (1991). Enhancement of the vaccinia virus/phage T7 RNA polymerase expression system using encephalomyocarditis virus 5' -untranslated region sequences. *Gene* **108,** 201-210.

Verheije, M. H., Raaben, M., Mari, M., Te Lintelo, E. G., Reggiori, F., van Kuppeveld, F. J., Rottier, P. J., and de Haan, C. A. (2008). Mouse hepatitis coronavirus RNA replication depends on GBF1-mediated ARF1 activation. *PLoS Pathog* **4**(6)**,** e1000088.

Vijayanand, P., Wilkins, E., and Woodhead, M. (2004). Severe acute respiratory syndrome (SARS): a review. *Clin Med* **4**(2)**,** 152-60.

von Brunn, A., Teepe, C., Simpson, J. C., Pepperkok, R., Friedel, C. C., Zimmer, R., Roberts, R., Baric, R., and Haas, J. (2007). Analysis of intraviral protein-protein interactions of the SARS coronavirus ORFeome. *PLoS One* **2**(5)**,** e459.

Wang, M., Yan, M., Xu, H., Liang, W., Kan, B., Zheng, B., Chen, H., Zheng, H., Xu, Y., Zhang, E., Wang, H., Ye, J., Li, G., Li, M., Cui, Z., Liu, Y. F., Guo, R. T., Liu, X. N., Zhan, L. H., Zhou, D. H., Zhao, A., Hai, R., Yu, D., Guan, Y., and Xu, J. (2005). SARS-CoV infection in a restaurant from palm civet. *Emerg Infect Dis* **11**(12)**,** 1860-5.

Weiss, S. R., Hughes, S. A., Bonilla, P. J., Turner, J. D., Leibowitz, J. L., and Denison, M. R. (1994). Coronavirus polyprotein processing. *Arch Virol* **9[suppl]**(349)**,** 349-58.

Williams, R. K., Jiang, G. S., and Holmes, K. V. (1991). Receptor for mouse hepatitis virus is a member of the carcinoembryonic antigen family of glycoproteins. *Proc Natl Acad Sci U S A* **88**(13)**,** 5533-6.

Woo, P. C., Lau, S. K., Huang, Y., Tsoi, H. W., Chan, K. H., and Yuen, K. Y. (2005). Phylogenetic and recombination analysis of coronavirus HKU1, a novel coronavirus from patients with pneumonia. *Arch Virol* **150**(11)**,** 2299-311.

Youn, S., Leibowitz, J. L., and Collisson, E. W. (2005). In vitro assembled, recombinant infectious bronchitis viruses demonstrate that the 5a open reading frame is not essential for replication. *Virology* **332**(1)**,** 206-15.

Yount, B. (2000). Strategy for systematic assembly of large RNA and DNA genomes: transmissible gastroenteritis virus model. *J Virol* **74**(22)**,** 10600-11.

Yount, B., Curtis, K. M., Fritz, E. A., Hensley, L. E., Jahrling, P. B., Prentice, E., Denison, M. R., Geisbert, T. W., and Baric, R. S. (2003). Reverse genetics with a full-length infectious cDNA of severe acute respiratory syndrome coronavirus. *Proc Natl Acad Sci U S A* **100**(22)**,** 12995-3000.

Yount, B., Denison, M. R., Weiss, S. R., and Baric, R. S. (2002). Systematic assembly of a full-length infectious cDNA of mouse hepatitis virus strain A59. *J Virol* **76**(21)**,** 11065-78.

Zheng, D., Chen, G., Guo, B., Cheng, G., and Tang, H. (2008). PLP2, a potent deubiquitinase from murine hepatitis virus, strongly inhibits cellular type I interferon production. *Cell Res* **18**(11)**,** 1105-13.

Ziebuhr, J., Schelle, B., Karl, N., Minskaia, E., Bayer, S., Siddell, S. G., Gorbalenya, A. E., and Thiel, V. (2007). Human coronavirus 229E papain-like proteases have overlapping specificities but distinct functions in viral replication. *J Virol* **81**(8), 3922-32.

Ziebuhr, J., and Siddell, S. G. (1999). Processing of the human coronavirus 229E replicase polyproteins by the virus-encoded 3C-like proteinase: identification of proteolytic products and cleavage sites common to pp1a and pp1ab. *J Virol* **73**(January)**,** 177-185.

Ziebuhr, J., Snijder, E. J., and Gorbalenya, A. E. (2000). Virus-encoded proteinases and proteolytic processing in the Nidovirales. *J Gen Virol* **81 Pt 4,** 853-79.

Ziebuhr, J., Thiel, V., and Gorbalenya, A. E. (2001). The autocatalytic release of a putative RNA virus transcription factor from its polyprotein precursor involves two paralogous papain-like proteases that cleave the same peptide bond. *J Biol Chem* **276**(35)**,** 33220-32.

Zust, R., Cervantes-Barragan, L., Kuri, T., Blakqori, G., Weber, F., Ludewig, B., and Thiel, V. (2007). Coronavirus non-structural protein 1 is a major pathogenicity factor: implications for the rational design of coronavirus vaccines. *PLoS Pathog* **3**(8)**,** e109.